

UNIVERSITAT POLITÈCNICA DE VALÈNCIA  
DEPARTAMENTO DE MÁQUINAS Y MOTORES TÉRMICOS

---



ASSESSMENT OF FUEL CONSUMPTION  
REDUCTION STRATEGIES ON A GASOLINE  
TURBOCHARGED DIRECT INJECTION ENGINE  
WITH A COOLED EGR SYSTEM

DOCTORAL THESIS

Presented by:

Manuel E. Rivas Perea

Directed by:

Dr. Héctor Climent Puchades

Valencia, June 2016



# DOCTORAL THESIS

## ASSESSMENT OF FUEL CONSUMPTION REDUCTION STRATEGIES ON A GASOLINE TURBOCHARGED DIRECT INJECTION ENGINE WITH A COOLED EGR SYSTEM

Presented by: Manuel E. Rivas Perea  
Directed by: Dr. Héctor Climent Puchades

Examining Board:

President: Dr. José Galindo  
Secretary: Dr. Blanca Giménez  
Vocal: Dr. David Chalet  
Examiners: Dr. Luis Le Moyne  
Dr. Andrés Melgar

Valencia, June 2016



**Resumen.** El objetivo de este trabajo de investigación es estudiar la influencia de un lazo de baja presión de EGR en las prestaciones de un motor de gasolina de encendido provocado turbosobrealimentado e inyección directa, en condiciones de ensayos estacionarios y transitorios, con un proceso de optimización de la calibración original del motor para minimizar el consumo de combustible del motor. La estrategia de “cooled EGR” fue también evaluada operando en sinergia con otras estrategias usadas para reducir el consumo de combustible del motor, entre ellas: mezcla pobre, múltiples inyecciones, operación a alta temperatura del fluido refrigerante del motor y movimiento de “swirl” inducido en el cilindro.

Para cumplir con los objetivos mencionados, se siguió un proceso metódico donde previamente se desarrolló una metodología global para obtener resultados de indudable calidad, basados en el uso de herramientas experimentales que cumplieran con los requerimientos de las condiciones de ensayo, y las apropiadas herramientas teóricas y procedimiento para post-procesar los ensayos realizados. En segundo lugar, se desarrolló una metodología específica para cada etapa del estudio, teniendo en cuenta los procesos de optimización o estudios paramétricos que se pudieran realizar.

Como primera etapa, se presenta un estudio básico del impacto del “cooled EGR” en la combustión, prestaciones, renovación de la carga y emisiones contaminantes del motor. Seguidamente, se procedió a la optimización del centrado de la combustión con la finalidad de minimizar el consumo de combustible del motor y poder analizar el potencial del “cooled EGR” como estrategia de reducción de consumo de combustible. El estudio presentado se realizó para baja, media y alta carga del motor con dos diferentes regímenes de giro del motor. Adicionalmente, se llevó a cabo un estudio del motor operando en condiciones transitorias con “cooled EGR”. Se realizaron una serie de ensayos usando el ciclo NEDC como base y se probaron diferentes estrategias sencillas de control de la apertura de la válvula de EGR para analizar la influencia del “cooled EGR” en condiciones transitorias.

La segunda etapa consiste en el desarrollo de una metodología para optimizar los parámetros del diagrama de distribución (VVT) y el inicio de inyección, para cargas medias del motor, con la finalidad de maximizar el potencial de reducción de consumo de combustible de la estrategia “cooled EGR”. Una vez realizada la optimización, se llevó a cabo un estudio usando la configuración óptima encontrada, operando en sinergia con otras tres estrategias usadas para reducir el consumo de combustible del motor. Estas estrategias fueron evaluadas con la finalidad de incrementar el rango de operación de la estrategia “cooled EGR” para lograr reducir aún más el consumo de combustible del motor. Adicionalmente, se llevó a cabo un estudio básico sobre la influencia de operar con mezcla pobre en la combustión, prestaciones, renovación de la carga y emisiones contaminantes del motor, como introducción al último estudio llevado a cabo sobre la posibilidad de usar la estrategia de mezcla pobre en conjunto con la estrategia de “cooled EGR”, con la finalidad de analizar el potencial de controlar las emisiones contaminantes y reducir el consumo de combustible del motor al mismo tiempo.

**Resum.** L'objectiu d'este treball d'investigació és estudiar la influència d'un llaç de baixa pressió d'EGR en les prestacions d'un motor de gasolina d'encesa provocat turbosobrealimentat i injecció directa, en condicions d'assajos estacionaris i transitoris, amb un procés d'optimització del calibratge original del motor per a minimitzar el consum de combustible del motor. L'estratègia de "cooled EGR" va ser també avaluada operant en sinergia amb altres estratègies usades per a reduir el consum de combustible del motor, entre elles: mescla pobra, múltiples injeccions, operació a alta temperatura del fluid refrigerant del motor i moviment de "swirl" induït en el cilindre.

Per a complir amb els objectius mencionats, es va seguir un procés metòdic on prèviament es va desenrotllar una metodologia global per a obtindre resultats d'indubtable qualitat, basats en l'ús de ferramentes experimentals que compliren amb els requeriments de les condicions d'assaig, i les apropiades ferramentes teòriques i procediment per a post- processar els assajos realitzats. En segon lloc, es va desenrotllar una metodologia específica per a cada etapa de l'estudi, tenint en compte els processos d'optimització o estudis paramètrics que es pogueren realitzar.

Com a primera etapa, es presenta un estudi bàsic de l'impacte del "cooled EGR" en la combustió, prestacions, renovació de la càrrega i emissions contaminants del motor. A continuació, es va procedir a l'optimització del centrat de la combustió amb la finalitat de minimitzar el consum de combustible del motor i poder analitzar el potencial del "cooled EGR" com a estratègia de reducció de consum de combustible. L'estudi presentat es va realitzar per a baixa, mitja i alta càrrega del motor amb dos diferents règims de gir del motor. Addicionalment, es va dur a terme un estudi del motor operant en condicions transitòries amb "cooled EGR". Es van realitzar una sèrie d'assajos usant el cicle NEDC com a base i es van provar diferents estratègies senzilles de control de l'obertura de la vàlvula d'EGR per a analitzar la influència del "cooled EGR" en condicions transitòries.

La segona etapa consistix en el desenrotllament d'una metodologia per a optimitzar els paràmetres del diagrama de distribució (VVT) i l'inici d'injecció, per a càrregues mitges del motor, amb la finalitat de maximitzar el potencial de reducció de consum de combustible de l'estratègia "cooled EGR". Una vegada realitzada l'optimització, es va dur a terme un estudi usant la configuració òptima trobada, operant en sinergia amb altres tres estratègies usades per a reduir el consum de combustible del motor. Estes estratègies van ser avaluades amb la finalitat d'incrementar el rang d'operació de l'estratègia "cooled EGR" per a aconseguir reduir encara més el consum de combustible del motor. Addicionalment, es va dur a terme un estudi bàsic sobre la influència d'operar amb mescla pobra en la combustió, prestacions, renovació de la càrrega i emissions contaminants del motor, com a introducció a l'últim estudi dut a terme sobre la possibilitat d'usar l'estratègia de mescla pobra en conjunt amb l'estratègia de "cooled EGR", amb la finalitat d'analitzar el potencial de controlar les emissions contaminants i reduir el consum de combustible del motor al mateix temps.

**Abstract.** This research work presents the study of a low pressure EGR loop influence on a SI gasoline turbocharged direct injection engine in steady and transient testing conditions, with an optimization process of the original engine calibration in order to minimize the engine fuel consumption when cooled EGR is introduced in steady testing conditions. The cooled EGR strategy was also evaluated operating in synergy with other fuel consumption reduction strategies, such as: lean burn, multi-injection, higher coolant temperature and in-cylinder induced swirl motion.

To fulfill the main objectives of this research work, firstly, a methodical process was followed, where a global methodology was first developed in order to obtain high accuracy engine tests, based on the experimental tools chosen that could comply with the requirements of the testing conditions, and the appropriate theoretical tools and procedure to post-process the tests performed. Secondly, a specific methodology was developed for each stage of the study and testing conditions, taking into account optimization processes or parametric tests in order to study the effect of a single parameter on engine's outputs or optimize an engine parameter in order to minimize the engine fuel consumption.

As a first stage of the study, a basic analysis of the impact of cooled EGR on the engine combustion, performance, air management and exhaust emissions is presented. Afterwards, an optimization of the combustion phasing in order to minimize the fuel consumption was performed, and therefore the potential of cooled EGR in order to reduce the engine fuel consumption was observed for low load, part load and full load engine conditions, for two different engine speeds. In addition, a study in transient conditions of the engine operating with cooled EGR was performed. NEDC cycles were performed with different EGR valve openings and therefore a comparison of different cooled EGR rates influence on the engine performance, air management and accumulated exhaust emissions was presented.

The second stage, consisted in a methodology developed to optimize the VVT setting and injection timing, for part load engine conditions, in order to maximize the cooled EGR potential to reduce engine fuel consumption. After this optimization, a synergy analysis of the optimum engine condition operating with cooled EGR and three other engine fuel consumption reduction strategies was performed. These strategies were tested to investigate and evaluate the potential of increasing the cooled EGR operational range to further decrease the engine fuel consumption. Furthermore, a basic study of the potential to reduce the engine fuel consumption and impact on combustion, air management and exhaust emissions of a lean burn strategy, in part load engine conditions, was presented as introduction of the final study of the cooled EGR strategy operating in synergy with the lean burn strategy in order to investigate the potential to control the exhaust emissions and reduce the engine fuel consumption.





*“Nunca admires al que tiene más dinero sino al que más sabe”  
Candelas Perea*



**Agradecimientos** Esta tesis va dedicada a la memoria de mi abuelo Candelas, uno de mis héroes y ejemplos a seguir. Mi abuelo, es una de las personas que siempre he admirado y que tendré en mi memoria por el resto de mi vida, ha sido el ejemplo más claro de constancia y dedicación que he tenido en mi vida, espero que donde estés puedas sentirte orgulloso de lo que he conseguido, al fin y al cabo, seré el primer doctor de la familia y tu bien sabes que no de los que curan a la gente, te extraño. Me gustaría continuar agradeciendo a mi familia, principalmente a mis padres y a mi hermano, que sin su apoyo y cariño incondicional no hubiera sido posible. Mis padres, gracias a ellos y a su lema “siempre las cosas se pueden hacer mejor”, me ha hecho crecer y siempre dar lo mejor de mí en cualquier aspecto de mi vida profesional y personal, gracias a eso, he logrado ser lo que soy y conseguir lo que he conseguido a lo largo de mi vida, sin duda alguna la variable más importante de porque soy como soy, gracias!, soy afortunado de tener unos padres como los que tengo. Mi hermano, por siempre estar ahí, por soportarme y apoyarme a su manera cómplice desde que éramos muy pequeños, por siempre ayudarme y preocuparse por mí sin importarle su situación personal, porque estemos donde estemos o bajo la condición que sea, nunca podemos parar de reír y de disfrutar de la compañía el uno del otro, gracias Miguelín!. Gracias a mi abuela Miguelina, que esté donde esté ella siempre se preocupa por llamarme, por estar pendiente de mí, por consentirme, espero que salgas adelante de lo que llevas ya combatiendo más de un año y que pueda seguir disfrutando de esa abuela tan maravillosa que eres. Por supuesto gracias también a mi abuela Rosina, a mis primas, a mis tías, que sin duda alguna forman una parte importante de todo ese apoyo que siempre tengo, soy afortunado de tener la familia que tengo!, los quiero a todos!. A Daniela de Lima, por ser mi compañera inseparable durante los últimos 9 años y espero que por el resto de mi vida, por soportarme y apoyarme ciegamente en todo lo que he querido hacer, por darme todo sin esperar nada a cambio, por tener paciencia con respecto a mis acciones o decisiones por muy locas que sean, por quererme y amarme en todos los momentos de nuestra relación, gracias, te amo.

Esta tesis tampoco hubiera sido posible sin el soporte técnico y humano del personal de la CMT-Motores Térmicos. En especial agradecer a mi tutor Héctor Climent, por escucharme, apoyarme, corregirme cuando lo tenía que hacer, pero aún más importante, por haberme dado la responsabilidad y posibilidad de proponer, llevar proyectos y hacer una tesis de la cual no había base en el CMT hasta la fecha, gracias. A mi segundo tutor, José M. Lujan, porque para cualquier problema tenía solución, porque para cualquier pregunta tenía una respuesta, porque no conozco una persona en el CMT con más tacto y noción de motores que él, gracias por siempre tener tiempo para escucharme. A José María Desantes, porque siempre que toqué a su puerta me brindó una ayuda o un consejo, gracias. A Marron (Vicente Esteves), porque no se podía tener mejor técnico de sala ni compañero de ensayos, por ser tan profesional y colega al mismo tiempo, gracias. A Yusep Torner y Valentin, por tenerme tanta paciencia, por haberme enseñado cosas en el taller, porque cuando necesitaba algo siempre tenían una solución mágica, gracias. A Vicente Bermúdez, por confiar en mí y permitirme realizar ensayos que no se habían realizado antes en el CMT, gracias. A Dani Campos, porque sin su ayuda no habría podido medir

partículas en el escape, gracias. A Jorge, por haber tenido tanta paciencia con la gasolina, gracias.

Este doctorado tampoco hubiera sido posible sin la Universidad Politécnica de Valencia, que gracias a ella el CMT-Motores Térmicos es lo que es hoy en día. Por haber apoyado también la idea de crear un equipo de Formula Student desde cero en paralelo a mis estudios de doctorado. Agradecer a Sergio Peña, por haber luchado a mi lado durante dos años para que el equipo esté donde está hoy en día, gracias a los pilares del equipo Lucas Mestre, Javier Catalán, Arturo Prieto, Antonio Hernández, Andrea Puertas, Kevin Goldbach y a toda la junta directiva del FSUPV01, FSUPV02 y FSUPV03, porque siempre se pueden hacer mejor las cosas, porque no hay que dejarlo hasta que sea lo mejor que puede ser, por ser tan pacientes y dedicados al equipo, por haber formado parte del proceso de crecimiento del equipo, por haberme ayudado a disfrutar durante más de 2 años de esto y por seguir incluyéndome en el proyecto como Team Advisor, gracias, las mejores cosas aún están por llegar!.

Obviamente no podía dejar a un lado a mis costillas, JuanPa, Morocho, Colcha, Lucas, Juanma, Mariani, Gaby, Olegario, Edu, Simón, Anton, Arturo, Sebas, Agus, Dani (seguro que me he dejado a alguien por fuera), por haber compartido alguno de los años de doctorado conmigo, por haberme hecho el camino más placentero y divertido, sin ustedes no hubiera sido lo mismo, gracias.

Thanks to University of Bath and the Powertrain and Vehicle Research Centre, for letting me do my research visit among their research group. Special thanks to Richard Burke, my research visit supervisor, for being such a nice person and good professional. Also I would like to thank, Deepak Hari, Andy Lewis and Karl Giles, for bringing me their support and friendship during those months.

Finalmente agradecer al Ministerio de Educación Cultura y Deporte de España por haberme concedido una beca FPU para realizar los estudios de doctorado.

# Table of Contents

<b>1</b>	<b>Introduction</b>	<b>1</b>
1.1	Introduction .....	1
1.2	Thesis context .....	10
1.2.1	Downsizing method .....	10
1.2.2	Variable valve timing strategies .....	11
1.2.2.1	Miller cycle .....	11
1.2.2.2	Atkinson cycle .....	12
1.2.3	Variable compression ratio .....	13
1.2.4	Lean burn strategy .....	13
1.2.5	EGR strategy .....	14
1.3	Objectives and methodology .....	15
1.3.1	Objectives .....	15
1.3.2	Methodology .....	16
	Bibliography .....	17
<b>2</b>	<b>Literature review</b>	<b>19</b>
2.1	Introduction .....	20
2.2	Overview of conventional SI gasoline engine .....	21
2.2.1	Combustion process .....	21
2.2.1.1	Spark and flame initiation .....	22
2.2.1.2	Initial flame kernel development .....	23
2.2.1.3	Turbulent flame propagation .....	24

---

2.2.1.4	Flame termination . . . . .	25
2.2.2	Formation of exhaust emissions . . . . .	26
2.2.2.1	Un-burned hydrocarbon . . . . .	27
2.2.2.2	Nitrogen oxides . . . . .	30
2.2.2.3	Carbon monoxide . . . . .	33
2.2.2.4	Particulate matter . . . . .	34
2.2.3	Air management . . . . .	36
2.2.3.1	Intake system . . . . .	36
2.2.3.2	Exhaust system . . . . .	39
2.2.3.3	Valve actuation system . . . . .	42
2.2.3.4	Supercharging and turbo-charging . . . . .	44
2.3	Strategies to reduce fuel consumption in SI gasoline engines..	45
2.3.1	Downsizing . . . . .	46
2.3.2	Direct injection . . . . .	47
2.3.3	Variable valve timing . . . . .	50
2.3.3.1	Miller cycle . . . . .	51
2.3.3.2	Atkinson cycle . . . . .	52
2.3.4	Variable compression ratio . . . . .	53
2.3.5	Lean burn . . . . .	55
2.3.6	Cooled exhaust gas recirculation . . . . .	57
2.3.6.1	High pressure loop . . . . .	61
2.3.6.2	Low pressure loop . . . . .	64
2.3.6.3	Mixed pressure loop . . . . .	66
2.4	Summary and conclusions . . . . .	68
	Bibliography . . . . .	72
<b>3</b>	<b>Experimental and theoretical tools</b>	<b>79</b>
3.1	Introduction . . . . .	79
3.2	Experimental Tools . . . . .	80
3.2.1	Engine characteristics . . . . .	80

---

3.2.2	Experimental setup . . . . .	85
3.2.2.1	Test bench cell characteristics . . . . .	86
3.2.2.2	Engine dynamometer . . . . .	87
3.2.2.3	Control and acquisition system . . . . .	89
3.2.2.4	Exhaust emissions analysis . . . . .	91
3.2.2.5	Engine testing procedure . . . . .	94
3.2.3	Steady flow test bench . . . . .	96
3.2.4	Turbocharger test bench . . . . .	98
3.3	Theoretical tools . . . . .	100
3.3.1	Combustion diagnosis . . . . .	101
3.3.2	1D Engine modeling . . . . .	104
3.3.3	Design of experiments . . . . .	106
3.4	Summary and conclusions . . . . .	109
	Bibliography . . . . .	110
<b>4</b>	<b>Influence of EGR on a GTDI engine</b>	<b>113</b>
4.1	Introduction . . . . .	113
4.2	Methodology . . . . .	118
4.3	Steady state results and analysis . . . . .	123
4.3.1	Part load tests . . . . .	124
4.3.1.1	Raw effect of cooled EGR on engine performance and exhaust emissions . . . . .	124
4.3.1.2	Spark advance optimization . . . . .	125
4.3.2	Full load tests . . . . .	137
4.3.2.1	Combustion and engine performance . . . . .	139
4.3.2.2	Air management . . . . .	146
4.3.2.3	Exhaust raw emissions . . . . .	148
4.3.3	Low load test . . . . .	152
4.3.3.1	Engine performance and exhaust emissions . . . . .	153
4.4	Transient operation results and analysis . . . . .	157
4.5	Summary and conclusions . . . . .	165
	Bibliography . . . . .	169

---

<b>5</b>	<b>Engine calibration optimization to operate with cooled EGR and additional fuel saving strategies</b>	<b>173</b>
5.1	Introduction	174
5.2	Optimization process and fuel saving strategies	177
5.2.1	Methodology	177
5.2.2	Results and analysis	181
5.2.2.1	VVT parameters optimization	181
5.2.2.2	Injection timing optimization	195
5.2.2.3	Additional strategies to reduce fuel consumption	202
5.3	Lean burn strategy and synergy with cooled EGR	214
5.3.1	Methodology	215
5.3.2	Results and analysis	217
5.3.2.1	Lean burn strategy on a GTDI engine	217
5.3.2.2	Lean burn and cooled EGR synergy influence on a GTDI engine	229
5.4	Summary and conclusions	238
	Bibliography	242
<b>6</b>	<b>Conclusions and future works</b>	<b>245</b>
6.1	Introduction	245
6.2	Conclusions	245
6.3	Future works	257
	<b>Bibliography</b>	<b>261</b>



# Index of Figures

1.1	Benz patent motor car, 1886 . . . . .	2
1.2	Advertisement of the 1962 Oldsmobile Jetfire, first mass production car with a turbocharged gasoline engine . . . . .	3
1.3	Earth Temperature evolution and future predictions . . . . .	6
1.4	Oil price evolution during the last 40 years . . . . .	8
2.1	Gasoline four-stroke processes illustration . . . . .	22
2.2	Combustion image sequence . . . . .	26
2.3	Exhaust emissions in function of the air-fuel . . . . .	28
2.4	Diagram of $NO_x$ and soot formation depending on the equivalence ratio and temperature . . . . .	31
2.5	Temperature representation for different mixture richness with and without $CO_2$ dissociation . . . . .	34
2.6	Flame luminosity images, paired with simultaneous flood laser elastic scattering images. SOI = $-90$ CAD ATDC. Image- capture times are listed between each pair of images . . . . .	36
2.7	LIF from piston-top view for late injections (SOI = $-90$ CAD ATDC) . . . . .	37
2.8	LIF from piston-top view for early injections (SOI = $-320$ CAD ATDC) . . . . .	37
2.9	Planar laser elastic scattering signal from soot recorded at 340 CAD ATDC overlap, for various injection timings . . . . .	37
2.10	Evolution of a soot cloud forming inside a GDI engine . . . . .	38
2.11	Three-way-catalyst conversion efficiency for different air-to-fuel ratios . . . . .	40

2.12	Representation of $NO_x$ trap reactions on lean and rich conditions	41
2.13	Pent-roof cylinder head	42
2.14	VVA systems summary	44
2.15	Turbocharger	45
2.16	Challenges on a boosted downsized engine	47
2.17	Wall-guided combustion method. Fuel spray and piston configuration	49
2.18	Miller cycle representation	51
2.19	Porsche patented variable compression ratio system	54
2.20	EGR rate and equivalence ratio influence over BMEP at full load conditions in a SI gasoline atmospheric engine	57
2.21	EGR rate and equivalence ratio influence on the engine thermal efficiency at part load conditions in a SI gasoline atmospheric engine	58
2.22	EGR rate influence on the maximum possible ignition advance before knocking occurs and the impact on engine BMEP	59
2.23	EGR rate influence on the spark plug temperature with E85 and gasoline as fuels at 3000 rpm and 12.5bar BMEP	60
2.24	Schematic of EGR system	62
2.25	Schematic of EGR system	62
2.26	Schematic of HP EGR system	63
2.27	Intake manifold pressure and exhaust pressure with HP EGR system	63
2.28	Schematic of LP EGR system	65
2.29	CA50, PMEP, BSFC and intake manifold temperature comparison of a HP and LP EGR configuration at 5000 rpm and 15 bar of BMEP	66
2.30	Schematic of Mixed EGR system	67
3.1	Engine torque and power curves at full load	81
3.2	Injection pressure engine map in <i>bar</i>	81
3.3	Cylinder head (left) and piston (right) of the investigated engine	82
3.4	VVT system employed in the GTDI engine	82

---

3.5	Equivalence ratio engine map .....	84
3.6	BSFC engine map in $g/kWh$ .....	85
3.7	Engine tests experimental setup layout .....	86
3.8	Dynamometer assembly layout .....	88
3.9	Torque absorption capacity of the engine dyno Schenck Dynas3 – <i>LI250</i> .....	89
3.10	Dekati FPS-4000 dilution system layout .....	92
3.11	Different stages of exhaust gas sample through the dilution process .....	93
3.12	Schematic of TSI 3090 measurement procedure .....	95
3.13	Coefficient of discharge for the intake valve (top graph) and exhaust valve (bottom graph) .....	97
3.14	Schematic layout of the steady test bench .....	98
3.15	Schematic layout of turbocharger test bench .....	99
3.16	Turbocharger compressor map with the engine operating points for 100%, 75% and 50% of engine load .....	100
3.17	1D engine model representation on the interface of the <i>OpenWAM<sup>TM</sup></i> software .....	105
3.18	Intake (top) and exhaust (bottom) manifold instantaneous pres- sure comparison between measured (solid line) and calculated (dashed line) results at full load and 2500 rpm .....	106
3.19	Volumetric efficiency comparison at full load engine conditions	107
3.20	Comparison between measured and simulated cylinder pressure for 2000 rpm - 10 bar BMEP (top) and 3000 rpm - 10 bar BMEP (bottom) .....	108
4.1	Engine torque for the original engine configuration, with a LP EGR loop and with a mixed EGR loop .....	115
4.2	Intake pressure influence for different EGR rates using a mixed and LP EGR loop .....	116
4.3	BSFC engine map in $g/kWh$ with the tested operating points using EGR .....	119
4.4	NEDC cycle speed trace and calculated torque trace to follow in the engine test bench .....	121

4.5	NEDC cycle speed trace and EGR rate when a 25% of opening is used on the EGR valve . . . . .	122
4.6	NEDC cycle speed trace and EGR rate when a 40% of opening is used on the EGR valve . . . . .	122
4.7	NEDC cycle speed trace and EGR rate when a 25% of opening is used on the EGR valve during the extra-urban part of the cycle . . . . .	123
4.8	Engine BSFC at 2000 rpm and 50% load (left graph) and at 3000 rpm and 50% (right graph) for different EGR rates . . . .	125
4.9	Exhaust manifold temperature (upper left graph) and intake manifold pressure (upper right graph) at 2000 rpm and 50% load and exhaust manifold temperature (bottom left graph) and intake manifold pressure (bottom right graph) at 3000 rpm and 50% for different EGR rates . . . . .	126
4.10	$CO$ (upper left graph), $NO_x$ and $HC$ emissions (upper right graph) at 2000 rpm and 50% load and $CO$ (bottom left graph), $NO_x$ and $HC$ emissions (bottom right graph) at 3000 rpm and 50% load for different EGR rates . . . . .	127
4.11	Engine BSFC and indicated efficiency at 2000 rpm and 50% load (left graph) and at 3000 rpm and 50% (right graph) for different EGR rates . . . . .	128
4.12	Exhaust manifold temperature at 2000 rpm and 50% load (left graph) and at 3000 rpm and 50% (right graph) for different EGR rates . . . . .	128
4.13	CA50 and spark advance at 2000 rpm and 50% load (left graph) and at 3000 rpm and 50% (right graph) for different EGR rates	129
4.14	Combustion duration at 2000 rpm and 50% load (left graph) and at 3000 rpm and 50% (right graph) for different EGR rates	130
4.15	Combustion temperature and heat losses at 2000 rpm and 50% load (left graph) and at 3000 rpm and 50% (right graph) for different EGR rates . . . . .	131
4.16	Coefficient of variation of the IMEP at 2000 rpm and 50% load (left graph) and at 3000 rpm and 50% (right graph) for different EGR rates . . . . .	131
4.17	Intake manifold pressure at 2000 rpm and 50% load (left graph) and at 3000 rpm and 50% (right graph) for different EGR rates	132

---

4.18	Compressor map operating points (left graph) and turbocharger speed (right graph) at 2000 rpm and 50% load and at 3000 rpm and 50% for different EGR rates .....	133
4.19	Compressor inlet temperature (top graphs), temperature ambient and EGR valve outlet temperature (bottom graphs) at 2000 rpm and 50% load (left graph) and at 3000 rpm and 50% (right graph) for different EGR rates .....	134
4.20	Exhaust manifold pressure at 2000 rpm and 50% load (left graph) and at 3000 rpm and 50% (right graph) for different EGR rates.....	135
4.21	Pumping losses at 2000 rpm and 50% load (left graph) and at 3000 rpm and 50% (right graph) for different EGR rates ....	136
4.22	Exhaust raw emissions at 2000 rpm and 50% load for different EGR rates. <i>HC</i> emissions (top left graph), <i>CO</i> emissions (top right graph), <i>NO<sub>x</sub></i> emissions (bottom left graph) and <i>PM</i> emissions (bottom right graph) .....	137
4.23	Exhaust raw emissions at 3000 rpm and 50% load for different EGR rates. <i>HC</i> emissions (top left graph), <i>CO</i> emissions (top right graph), <i>NO<sub>x</sub></i> emissions (bottom left graph) and <i>PM</i> emissions (bottom right graph) .....	138
4.24	BSFC (top left graph) and indicated efficiency (bottom left graph) for EGR rates at 2000 rpm and 100% of engine load and BSFC (top right graph) and indicated efficiency (bottom right graph) for EGR rates at 3000 rpm and 100% of engine load .....	140
4.25	Exhaust manifold temperature for EGR rates at 2000 rpm and 100% of engine load (left graph) and at 3000 rpm and 100% of engine load (right graph) .....	141
4.26	Combustion temperature for EGR rates at 2000 rpm and 100% of engine load (left graph) and at 3000 rpm and 100% of engine load (right graph) .....	142
4.27	CA50 (top left graph) and combustion duration (bottom left graph) for EGR rates at 2000 rpm and 100% of engine load and CA50 (top right graph) and combustion duration (bottom right graph) for EGR rates at 3000 rpm and 100% of engine load ..	143

4.28	CoV of the IMEP for different EGR rates at 2000 rpm and 100% of engine load (left graph) and at 3000 rpm and 100% of engine load (right graph) .....	144
4.29	Heat losses for different EGR rates at 2000 rpm and 100% of engine load (left graph) and at 3000 rpm and 100% of engine load (right graph) .....	145
4.30	Intake manifold pressure (top left graph) and turbocharger compression ratio (bottom left graph) for different EGR rates at 2000 rpm and 100% of engine load and intake manifold pressure (top right graph) and turbocharger compression ratio (bottom right graph) for different EGR rates at 3000 rpm and 100% of engine load .....	147
4.31	Compressor map (left graph) and turbocharger speed (right graph) for different EGR rates at 2000 rpm and 100% of engine load and 3000 rpm and 100% of engine load .....	148
4.32	Temperature at compressor inlet in three different positions placed in the same virtual diameter, each of them separated by 120°, for different EGR rates at 2000 rpm and 100% of engine load (left graph) and at 3000 rpm and 100% of engine load (right graph) .....	148
4.33	Pumping losses (top left graph) and exhaust manifold pressure (bottom left graph) for different EGR rates at 2000 rpm and 100% of engine load and pumping losses (top right graph) and exhaust manifold pressure (bottom right graph) for different EGR rates at 3000 rpm and 100% of engine load .....	149
4.34	Exhaust raw emissions with optimized SA at 2000 rpm and 100% load. $NO_x$ emissions (top left graph), $HC$ emissions (top right graph), $CO$ emissions (bottom left graph) and $PM$ emissions (bottom right graph) .....	150
4.35	Exhaust raw emissions with optimized SA at 3000 rpm and 100% load. $NO_x$ emissions (top left graph), $HC$ emissions (top right graph), $CO$ emissions (bottom left graph) and $PM$ emissions (bottom right graph) .....	151
4.36	Tests A, B and C: BSFC at 2000 rpm and 25% load for different EGR rates .....	154
4.37	Tests A, B and C: exhaust manifold temperature at 2000 rpm and 25% load for different EGR rates .....	154

4.38 Tests A, B and C: $NO_x$ emissions at 2000 rpm and 25% load for different EGR rates . . . . .	155
4.39 Tests A, B and C: intake manifold pressure at 2000 rpm and 25% load for different EGR rates . . . . .	156
4.40 Tests A, B and C: $HC$ (top graph) and $CO$ (bottom graph) emissions at 2000 rpm and 25% load for different EGR rates . . . . .	157
4.41 NEDC cycle engine speed based graphs presenting the intake pressure for 25% EGR valve opening setup compared to the original setup in the left graph and the 40% EGR valve opening setup compared to the original setup in the right graph . . . . .	159
4.42 NEDC cycle engine speed based graphs presenting the compressor map (bottom graphs) and turbocharger speed (top graphs) for 25% EGR valve opening setup compared to the original setup (left graphs) and the 40% EGR valve opening setup compared to the original setup (right graphs) . . . . .	160
4.43 NEDC cycle engine speed based graphs presenting the turbine outlet temperature for 25% EGR valve opening setup compared to the original setup in the left graph and the 40% EGR valve opening setup compared to the original setup in the right graph . . . . .	161
4.44 NEDC cycle engine speed based graphs presenting the exhaust manifold pressure for 25% EGR valve opening setup compared to the original setup in the left graph and the 40% EGR valve opening setup compared to the original setup in the right graph . . . . .	162
4.45 NEDC cycle $NO_x$ accumulative raw emissions for 25%, 40% and 25% extra-urban EGR valve opening setup compared to the original setup . . . . .	163
4.46 NEDC cycle $HC$ accumulative raw emissions for 25%, 40% and 25% extra-urban EGR valve opening setup compared to the original setup . . . . .	164
4.47 NEDC cycle $CO$ accumulative raw emissions for 25%, 40% and 25% extra-urban EGR valve opening setup compared to the original setup . . . . .	164
4.48 NEDC cycle $CO_2$ accumulative raw emissions for 25%, 40% and 25% extra-urban EGR valve opening setup compared to the original setup . . . . .	165
5.1 DoE inputs, quadratic model and outputs . . . . .	179

5.2	Optimization process flow-chart . . . . .	181
5.3	IGR in % at 2000 rpm and 50% load (left graph) and at 3000 rpm and 50% (right graph) for different IVO and EVC values at the maximum EGR rate conditions . . . . .	182
5.4	Pumping losses in $J$ at 2000 rpm and 50% load (left graph) and at 3000 rpm and 50% (right graph) for different IVO and EVC values at the maximum EGR rate conditions . . . . .	183
5.5	Heat losses in $J$ at 2000 rpm and 50% load (left graph) and at 3000 rpm and 50% (right graph) for different IVO and EVC values at the maximum EGR rate conditions . . . . .	183
5.6	Indicated efficiency in % at 2000 rpm and 50% load (left graph) and at 3000 rpm and 50% (right graph) for different IVO and EVC values at the maximum EGR rate conditions . . . . .	184
5.7	BSFC in $g/kWh$ at 2000 rpm and 50% load (left graph) and at 3000 rpm and 50% (right graph) for different IVO and EVC values at the maximum EGR rate conditions . . . . .	185
5.8	Engine BSFC with SA and VVT settings optimized at 2000 rpm and 50% load (left graph) and at 3000 rpm and 50% (right graph) for different EGR rates . . . . .	186
5.9	Combustion duration with optimized SA and optimized VVT settings and SA at 2000 rpm and 50% load (left graph) and at 3000 rpm and 50% (right graph) for different EGR rates . . . . .	187
5.10	CA50 with optimized SA and optimized VVT settings and SA at 2000 rpm and 50% load (left graph) and at 3000 rpm and 50% (right graph) for different EGR rates . . . . .	187
5.11	Combustion temperature with optimized SA and optimized VVT setting and SA at 2000 rpm and 50% load (left graph) and at 3000 rpm and 50% (right graph) for different EGR rates . . . . .	188
5.12	CoV of the IMEP with optimized SA and optimized VVT setting and SA at 2000 rpm and 50% load (left graph) and at 3000 rpm and 50% (right graph) for different EGR rates . . . . .	189
5.13	Intake manifold pressure with optimized SA and optimized VVT setting and SA at 2000 rpm and 50% load (left graph) and at 3000 rpm and 50% (right graph) for different EGR rates . . . . .	190



---

5.14	Intake and exhaust instantaneous mass flows with original VVT setting and optimized VVT setting at 2000 rpm and 50% load (top graph) and at 3000 rpm and 50% (bottom graph) for 15% of EGR rate .....	191
5.15	Exhaust manifold pressure with optimized SA and optimized VVT setting and SA at 2000 rpm and 50% load (left graph) and at 3000 rpm and 50% (right graph) for different EGR rates ..	192
5.16	Exhaust manifold temperature with optimized SA and optimized VVT setting and SA at 2000 rpm and 50% load (left graph) and at 3000 rpm and 50% (right graph) for different EGR rates.....	192
5.17	Pumping losses with optimized SA and optimized VVT setting and SA at 2000 rpm and 50% load (left graph) and at 3000 rpm and 50% (right graph) for different EGR rates .....	193
5.18	Exhaust emissions with optimized SA and optimized VVT setting and SA at 2000 rpm and 50% load (left graphs) and at 3000 rpm and 50% (right graphs) for different EGR rates. $NO_x$ emissions (top graphs), $HC$ emissions (middle graphs) and $CO$ emissions (bottom graphs) .....	194
5.19	BSFC (left graph) and indicated efficiency (right graph) for different start of injection values at 2000 rpm and 50% of engine load .....	197
5.20	Spark advance (left graph) and CA50 (right graph) for different start of injection values at 2000 rpm and 50% of engine load .	197
5.21	CoV of the IMEP (left graph) and combustion duration (right graph) for different start of injection values at 2000 rpm and 50% of engine load .....	198
5.22	Combustion temperature (left graph) and heat losses (right graph) for different start of injection values at 2000 rpm and 50% of engine load .....	199
5.23	Intake manifold pressure (left graph) and exhaust manifold pressure (right graph) for different start of injection values at 2000 rpm and 50% of engine load.....	200
5.24	Pumping losses (left graph) and exhaust manifold temperature (right graph) for different start of injection values at 2000 rpm and 50% of engine load.....	200

5.25 Exhaust raw emissions and combustion efficiency for different start of injection values at 2000 rpm and 50% of engine load. $NO_x$ (top left graph), $HC$ (top right graph), $CO$ (bottom left graph) raw emissions and combustion efficiency (bottom right graph) .....	201
5.26 BSFC (left graph) and indicated efficiency (right graph) for different EGR rates at 2000 rpm and 50% of engine load with different setting setups .....	203
5.27 BSFC (left graph) and CoV of the IMEP (right graph) for different engine coolant temperature at 2000 rpm and 50% of engine load .....	207
5.28 Combustion temperature (left graph) and heat losses (right graph) for different engine coolant temperature at 2000 rpm and 50% of engine load .....	208
5.29 CA50 (left graph) and combustion duration (right graph) for different engine coolant temperature at 2000 rpm and 50% of engine load .....	208
5.30 Intake manifold pressure (left graph) and pumping losses (right graph) for different engine coolant temperature at 2000 rpm and 50% of engine load .....	209
5.31 Exhaust manifold temperature (left graph) and exhaust manifold pressure (right graph) for different engine coolant temperature at 2000 rpm and 50% of engine load .....	210
5.32 $NO_x$ raw emissions (top left graph), $HC$ emissions (top right graph), $CO$ emissions (bottom left graph) and $CO_2$ emissions (bottom right graph) for different engine coolant temperature at 2000 rpm and 50% of engine load .....	211
5.33 Coefficient of discharge of the original cylinder head (left graph) and with a 10 mm and 24 mm of diameter restriction in one of the intake ports for different valve lift values .....	212
5.34 Swirl torque measured in the flow bench for three different cylinder head setups and for different valve lift positions.....	213
5.35 Engine BSFC (top graphs) and indicated efficiency (bottom graphs) at 2000 rpm and 50% load (left graphs) and at 3000 rpm and 50% (right graphs) for lambda values .....	218
5.36 CA50 at 2000 rpm and 50% load (left graph) and at 3000 rpm and 50% (right graph) for different lambda values .....	219

5.37	CoV of the IMEP at 2000 rpm and 50% load (left graph) and at 3000 rpm and 50% (right graph) for different lambda values	220
5.38	Combustion duration at 2000 rpm and 50% load (left graph) and at 3000 rpm and 50% (right graph) for different lambda values	220
5.39	Combustion temperature at 2000 rpm and 50% load (left graph) and at 3000 rpm and 50% (right graph) for different lambda values	221
5.40	Heat losses at 2000 rpm and 50% load (left graph) and at 3000 rpm and 50% (right graph) for different lambda values	222
5.41	Exhaust manifold temperature at 2000 rpm and 50% load (left graph) and at 3000 rpm and 50% (right graph) for different lambda values	223
5.42	Compressor outlet pressure and intake manifold pressure at 2000 rpm and 50% load (left graph) and at 3000 rpm and 50% (right graph) for different lambda values	224
5.43	Evolution of compressor operating point in the compressor map (left graph) and turbocharger speed (right graph) at 2000 rpm and 50% load and at 3000 rpm and 50% for different lambda values	225
5.44	Pumping losses at 2000 rpm and 50% load (left graph) and at 3000 rpm and 50% (right graph) for different lambda values	225
5.45	Exhaust raw emissions and combustion efficiency (bottom right graph) at 2000 rpm and 50% load for different lambda values. $NO_x$ (top left graph), $HC$ (top right graph), $CO$ (bottom left graph) and combustion efficiency (bottom right graph)	226
5.46	Exhaust raw emissions and combustion efficiency (bottom right graph) at 3000 rpm and 50% load for different lambda values. $NO_x$ (top left graph), $HC$ (top right graph), $CO$ (bottom left graph) and combustion efficiency (bottom right graph)	228
5.47	Dilution factor in % at 2000 rpm and 50% load (left graph) and at 3000 rpm and 50% (right graph) for different lambda and EGR values	230
5.48	BSFC in $g/kWh$ at 2000 rpm and 50% load (left graph) and at 3000 rpm and 50% (right graph) for different lambda and EGR values	231

5.49	Indicated efficiency in % at 2000 rpm and 50% load (left graph) and at 3000 rpm and 50% (right graph) for different lambda and EGR values.....	232
5.50	Combustion duration in <i>CAD</i> at 2000 rpm and 50% load (left graph) and at 3000 rpm and 50% (right graph) for different lambda and EGR values.....	232
5.51	Ignition advance in <i>CADBTD</i> at 2000 rpm and 50% load (left graph) and at 3000 rpm and 50% (right graph) for different lambda and EGR values.....	233
5.52	Pumping losses in <i>J</i> at 2000 rpm and 50% load (left graph) and at 3000 rpm and 50% (right graph) for different lambda and EGR values.....	233
5.53	Intake manifold pressure in <i>bar</i> at 2000 rpm and 50% load (left graph) and at 3000 rpm and 50% (right graph) for different lambda and EGR values.....	234
5.54	Combustion temperature in °C at 2000 rpm and 50% load (left graph) and at 3000 rpm and 50% (right graph) for different lambda and EGR values.....	235
5.55	Exhaust manifold temperature in °C at 2000 rpm and 50% load (left graph) and at 3000 rpm and 50% (right graph) for different lambda and EGR values.....	235
5.56	<i>NO<sub>x</sub></i> raw exhaust emissions in <i>ppm</i> at 2000 rpm and 50% load (left graph) and at 3000 rpm and 50% (right graph) for different lambda and EGR values.....	236
5.57	<i>CO</i> raw exhaust emissions in <i>ppm</i> at 2000 rpm and 50% load (left graph) and at 3000 rpm and 50% (right graph) for different lambda and EGR values.....	237
5.58	<i>HC</i> raw exhaust emissions in <i>ppm</i> at 2000 rpm and 50% load (left graph) and at 3000 rpm and 50% (right graph) for different lambda and EGR values.....	237
5.59	Three way catalyst exhaust emissions conversion efficiency at 2000 rpm and 50% load for different lambda values and EGR values.....	238

# Index of Tables

1.1 Emissions regulations for SI gasoline engines (top table) and CI diesel engines (bottom table) in Europe. *Direct injection engines. ....	5
2.1 EGR configuration comparison .....	68
3.1 Engine characteristics .....	83
3.2 Injector characteristics .....	83
3.3 Fuel characteristics .....	87
3.4 Fuel balance characteristics .....	91
3.5 Sensors accuracy .....	91
3.6 Sensor characteristics in turbocharger test bench facility (*Only for compressor inlet) .....	100
4.1 Selected operating conditions .....	119
4.2 Ford Mondeo vehicle data .....	120
4.3 Ford Explorer data .....	158
5.1 Selected operating conditions .....	178
5.2 DoE test plan for 2000 rpm and 10 bar BMEP engine conditions	178
5.3 DoE test plan for 3000 rpm and 10 bar BMEP engine conditions	179
5.4 Engine operating conditions .....	204
5.5 Engine performance results .....	204
5.6 Engine combustion results .....	205
5.7 Engine exhaust raw emissions results .....	206

5.8	Engine performance results .....	213
5.9	Engine combustion results .....	214
5.10	Engine exhaust raw emissions .....	214
5.11	Selected operating conditions .....	215
5.12	DoE test plan for 2000 rpm and 10 bar BMEP engine conditions	216
5.13	DoE test plan for 3000 rpm and 10 bar BMEP engine conditions	216

# Nomenclature

## *Latin*

$A$	Area
$C_p$	Specific heat capacity at constant pressure
$C_v$	Specific heat capacity at constant pressure
$D$	Diffusivity
$h$	Specific enthalpy per unit of mass
$l$	Length scale
$m$	Mass
$\dot{m}$	Mass flow rate
$P$	Pressure
$Q$	Heat transfer
$r$	Compression ratio
$R$	Universal gas constant
$S$	Flame speed
$t$	Time
$T$	Temperature
$U$	Velocity
$u$	Internal energy
$V$	Volume

## *Greek*

$\alpha$	Dilution factor
$\beta$	Fraction of $CO_2$ dissociated
$\Delta$	Variation/Increment
$\Delta P$	Difference between EGR cooler inlet and compressor inlet
$\eta$	Efficiency

---

$\mu$	mass of un-burned gas
$\Phi$	Equivalence ratio
$\rho$	Density
$\sigma$	Standard deviation
$\gamma$	Ratio of specific heats
$\lambda$	Ratio of specific heats

**Subscripts**

<i>air</i>	Relative to fresh intake air conditions
<i>atm</i>	Relative to atmospheric conditions
<i>b</i>	Relative to the conditions of the burnt mixture
<i>bb</i>	Relative to the blow-by flow
<i>cyl</i>	Relative to the conditions in the interior of the cylinder
<i>evap</i>	Relative to evaporative conditions
<i>exh</i>	Relative to the exhaust manifold conditions
<i>f</i>	Referred to the front flame
<i>fuel</i>	Relative to the fuel
<i>g</i>	Relative to the gas
<i>in</i>	Referred to the inlet flow
<i>ind</i>	Referred to indicated efficiency
<i>inj</i>	Relative to the injected fuel
<i>int</i>	Relative to the intake manifold conditions
<i>isen</i>	Referred to isentropic conditions
<i>L</i>	Referred to the laminar phase of the combustion
<i>o</i>	Relative to the conditions at the outlet of the injector nozzle
<i>out</i>	Referred to the outlet flow
<i>rate</i>	Referred EGR rate conditions
<i>ref</i>	Referred to the reference conditions
<i>t</i>	Referred to the turbulent phase of the combustion
<i>u</i>	Relative to the conditions of the unburnt mixture
<i>w</i>	Referred to the cylinder walls

**Acronyms**

AFR	Air/fuel ratio
ATDC	Crankangle after top-dead-center
BTDC	Crankangle before top-dead-center



---

BMEP	Brake mean effective pressure
BSFC	Brake specific fuel consumption
CA10, CA50, CA90	Referred to the crank-angle where 10 %, 50 % and 90 % of the fuel injected mass has been burnt
$C_D$	Coefficient of discharge
CCV	Cycle-to-cycle variation
CFD	Computational fluid dynamics
<i>CHO</i>	Carbohydrate (aldehyde)
CI	Compression ignition
CR	Compression ratio
<i>CO</i>	Carbon monoxide emissions
<i>CO<sub>2</sub></i>	Carbon dioxide emissions
EPA	Environmental protection agency
D	Diffusivity
DoE	Design of experiments
DPF	Diesel particulate filter
EGR	Exhaust gas recirculation
E5,E10	Referred to gasoline with 5% and 10% of ethanol
EEVC	Early exhaust valve closing
EIVC	Early intake valve closing
EoC	End of combustion
EVC	Exhaust valve closing
EVO	Exhaust valve opening
EU5,EU6	Referred to the Euro 5 and Euro 6 emissions regulations
FMEP	Friction Mean Effective Pressure
GDI	Gasoline direct injection
GPF	Gasoline particulate filter
GTDI	Gasoline turbocharged direct injection
<i>H</i>	Hydrogen
<i>HC</i>	Unburnt hydrocarbon emissions
HP	High pressure
HRL	Heat release law
ICE	Internal combustion engine
ID	Ignition delay
IGR	Internal gas recirculation

---

IGR	Internal gas recirculation fraction
IMEP	Indicated mean effective pressure
IVC	Intake valve closing
IVO	Intake valve opening
ISFC	Indicated specific fuel consumption
LIF	Laser induced fluorescence
LIVC	Late intake valve closing
LPG	Low pressure
LPG	Referred to liquefied petroleum gas engines
LNT	Lean $NO_x$ trap after-treatment system
MBC	Model based calibration
NEDC	New European driving cycle
$NO_x$	Nitrogen oxides ( $NO$ y $NO_2$ )
$O_2$	Oxygen
PFI	Port fuel injection
$PM$	Particulate matter emissions
PMEP	Pumping mean effective pressure
PRESS	Predicted error sum of squares
R&D	Research and development
RAD	Radical
RMSE	Root mean squared error
RoHR	Rate of heat release
SCR	Selective catalytic reduction after-treatment system
SI	Spark ignition
SoC	Start of combustion
SoI	Start of injection
TDC	Top-dead-center
THC	Total hydrocarbon emissions
TWC	Three-way catalyst
U.S.	United States
VVA	Variable valve actuation systems
VVT	Variable valve timing

# Chapter 1

## Introduction

### Contents

---

<b>1.1</b>	<b>Introduction</b> .....	<b>1</b>
<b>1.2</b>	<b>Thesis context</b> .....	<b>10</b>
1.2.1	Downsizing method .....	10
1.2.2	Variable valve timing strategies .....	11
1.2.2.1	Miller cycle .....	11
1.2.2.2	Atkinson cycle .....	12
1.2.3	Variable compression ratio .....	13
1.2.4	Lean burn strategy .....	13
1.2.5	EGR strategy .....	14
<b>1.3</b>	<b>Objectives and methodology</b> .....	<b>15</b>
1.3.1	Objectives .....	15
1.3.2	Methodology .....	16
	<b>Bibliography</b> .....	<b>17</b>

---

### 1.1 Introduction

The gasoline engine has been around for more than a century. The four-stroke SI gasoline engine was invented by a German inventor Nikolaus August Otto in 1876, in collaboration with Gottlieb and Wilhelm Mayback. Two years later, in 1878, Dugald Clerk designed the first two-stroke SI gasoline engine and in 1886 the first automobiles as the one shown in Figure 1.1, using a four-stroke gasoline engine, were in production thanks to Karl Benz.

At the beginning of the 20<sup>th</sup> century, a Swiss engineer, called Alfred Buchi, patents de turbocharger and starts producing the first examples. In 1902 the French inventor Leon Levavasseur invented the mechanical injection for gasoline powered aviation engines and by 1907 he had already installed the system in a SI gasoline engine, producing 100 hp.

The gasoline engine was spread everywhere at that time and was used in airplanes, trucks and some railway locomotives. It was between 1910 and 1920 when CI diesel engines started to replace the SI gasoline engines in trucks, locomotives and heavy equipment.

During the World War I, a French engineer named Auguste Rateau, fitted the first turbochargers to a Renault SI gasoline engine to power some airplane French fighters. Later in 1925, the Swedish engineer, Jonas Hesselman, introduced the Hesselman engine, which had the first use of direct injection on a SI gasoline engine. Moreover, in the same year, the first variable valve system was patented by the U.S. for a gasoline aviation engine.

It was 35 years later when Fiat patented the first functional automotive variable valve timing, which also included variable lift. And then 55 years later, in 1980, Alfa Romeo used the first variable valve timing system in a production passenger car powered by a SI gasoline engine.



*Figure 1.1. Benz patent motor car, 1886.*

During the World War II it was common to use turbocharged SI gasoline engines equipped with mechanical direct injection in the aviation, and some U.S. airplane engines were also equipped with variable valve timing. After the

war, all this development of new technologies for aviation engines were taken into account by car manufacturers for mass production vehicles.

The first automotive direct injection system to run on gasoline was developed by Bosch and was introduced by Goliath in 1952. It was basically a high-pressure diesel direct-injection pump with an intake throttle valve. Then, in 1954 Mercedes used a Bosch mechanical direct injection system, derived from wartime airplane engines, in their F1 car. Three years later in 1957, the first commercial electronic fuel injection system was developed by the Benxi Corporation and was offered by the American Motors Corporation.

In 1962, General Motors manufactured the first mass production passenger car equipped with a turbocharged SI gasoline engine, the Oldsmobile Jetfire, whose advertisement is presented in Figure 1.2. The turbocharger was then used from 1966 in Motorsport competitions until today.



*Figure 1.2.* Advertisement of the 1962 Oldsmobile Jetfire, first mass production car with a turbocharged gasoline engine.

Between 1970 and 1980 in U.S. and Japan, the respective federal governments imposed the firsts exhaust emissions regulations. Before that time period, the vast majority of gasoline-fueled automobile and light truck engines did not use fuel injection or any after-treatment system. To more

easily comply with emissions regulations, automobile manufacturers began installing fuel injection systems in more SI gasoline engines during the late 70's. Electronic fuel injection was increasing its popularity through the late 70's and 80's with the German, French, Japan and U.S markets leading and the UK and Commonwealth markets lagging somewhat. Then the first after-treatment system arrived in 1975, and it was a two-way catalyst used to convert  $HC$  and  $CO$  emissions into  $CO_2$ . Later in 1981 it was replaced by the three way catalyst (TWC) that also reduced the  $NO_x$  emissions. Since the early 90's, almost all the gasoline passenger cars sold in first world markets were equipped with electronic fuel injection and a TWC. It was between 1970 and 1980 when CI diesel engines started to be more popular, in Europe, for production cars because of their reliability, life-span and lower fuel consumption. In U.S. the use of CI diesel engines increased in the larger on-road and off-road vehicles. In the case of Europe, the first exhaust emissions regulations were imposed in 1993, called Euro I.

The CI diesel engine had gained more popularity in the last 20 years for mass production cars in Europe than in the rest of the world due to the lighter pollutant emissions regulations and the stimulus provided by some European countries, this lead to increase the percentage of diesel powered cars [1]. Nowadays in Europe, 50% of the total car population are using CI diesel engine.

Regarding Japan, in 1990, CI diesel engines powered 6% of all new cars sold. However, in 1992, a law concerning special measures to reduce the total amount of Nitrogen Oxides ( $NO_x$ ) emitted from motor vehicles in specified areas and a tax change, narrowed the cost advantage of CI diesel engines powered cars and made them more expensive. Later, in 1999 a campaign lead by the governor of Tokyo, Shintaro Ishihara, against the soot produced by CI diesel engines, devastated all the CI diesel engine popularity in Japan.

Concerning the case of U.S., the emissions regulations are being more stringent than the European's since the early 90's. This, mixed with the low pump fuel prices and the low availability for diesel powered passenger cars offered by the manufacturers, formed a difficult market for diesel engines to grow in passenger cars. Because of the pump fuel price difference between Europe and U.S, American car buyers are less concerned about fuel economy. For this reason, the American companies, as Ford or General Motors, had develop efficient gasoline engines for the European market to introduce them slowly in the future on the U.S. market.

Vijayaraghavan had evaluated the benefits of the introduction of new emissions standards, as Tier II in the case of U.S., and certifies a big positive

	Valid from	$CO$ [g/km]	$HC$ [g/km]	$NO_x$ [g/km]	$HC+NO_x$ [g/km]	$PM$
Euro I	07/92	2.72	-	-	0.97	-
Euro II	01/96	2.20	-	-	0.5	-
Euro III	01/00	2.30	0.20	0.15	-	-
Euro IV	01/05	1.00	0.10	0.08	-	-
Euro V	09/09	1.00	0.10	0.06	-	0.005*
Euro VI	09/14	1.00	0.10	0.06	-	0.005*

	Valid from	$CO$ [g/km]	$HC$ [g/km]	$NO_x$ [g/km]	$HC+NO_x$ [g/km]	$PM$
Euro I	07/92	3.16	-	-	1.13	0.14
Euro II	01/96	1.00	-	-	0.70	0.08
Euro III	01/00	0.64	-	0.50	0.56	0.05
Euro IV	01/05	0.50	-	0.25	0.30	-
Euro V	09/09	0.50	-	0.18	0.23	0.005
Euro VI	09/14	0.50	-	0.08	0.17	0.005

**Table 1.1.** Emissions regulations for SI gasoline engines (top table) and CI diesel engines (bottom table) in Europe. \*Direct injection engines..

impact in the atmosphere [2]. He also explains that in the future, when a certain amount of reduction in engine exhaust emissions is achieved, the impact on the atmosphere is going to be negligible at certain point and this is something that future emissions regulations standards have to take into account.

Currently in Europe, nitrogen oxides ( $NO_x$ ), total hydrocarbon ( $THC$ ), non-methane hydrocarbons ( $NMHC$ ), carbon monoxide ( $CO$ ) and particulate matter ( $PM$ ) are regulated for most vehicles, including cars, lorries, trains, tractors and similar machinery, barges, but excluding seagoing ships and airplanes. For each vehicle type, different standards apply. Compliance is determined by running the engine at a standardized test cycle. SI gasoline engines are gaining attention lately since CI diesel engines are struggling with the upcoming pollutant emission regulations, and because of this, more car manufacturers are investing more resources in the research and development of the new gasoline engines. In Table 1.1 the emissions standard regulations for CI diesel and SI gasoline engines in Europe are presented.





correlation between the estimates of  $CO_2$  levels in the atmosphere and the estimates of the earth's temperature over the past 550 million years (the phanerozoic period). The message is clear that several factors must influence the earth's temperature, and that while  $CO_2$  is one of these factors, it is seldom the dominant one. Other factors that influence the earth's temperature are spontaneous variations of the complicated fluid flow patterns in the oceans and atmosphere of the earth (perhaps influenced by continental drift), volcanoes, variations of the earth's orbital parameters (ellipticity, spin-axis orientation, etc.), asteroid and comet impacts, variations in the sun's output (not only the visible radiation but the amount of ultraviolet light, and the solar wind with its magnetic field), variations in cosmic rays leading to variations in cloud cover, and other causes [3].

On the other hand, the  $CO_2$  is a major source of ocean acidification since it dissolves in water to form carbonic acid [4]. Projected acidification is likely to be stronger than has been experienced for tens of millions of years, and its rate of change is more than 100 times that found at any time during this period [5]. If  $CO_2$  emissions continue to rise at current rates, by the end of this century the resulting changes in seawater chemistry will expose many marine organisms to conditions that they may not have experienced during their entire evolutionary history [6].

For these main reasons stated before, great research and development efforts are being carried out to design more efficient SI gasoline engines in terms of fuel consumption and production costs since the  $CO_2$  concentration in the atmosphere and oil price has been rising through the last years. In Figure 1.4 the oil price history is presented. It can be seen that the oil price decreased during the last year, this is a similar behavior that can be also seen in the 80's and 2008, but sooner or later, since the oil is a limited resource, its price is going to increase again and more efficient engines will be demanded.

A very popular and attractive strategy used to reduce fuel consumption on SI gasoline engines, during the last decade, consists of using a downsizing concept, where the displacement of the engine is decreased and a turbocharging system compensates this loss of engine size, so the new engine configuration delivers the same torque and power as the reference engine [7]. In the late 2000's, Volkswagen was the first manufacturer to launch a downsized engine in a mass production passenger car. It was a 1.4 l engine with a turbocharger and a mechanical compressor, to replace their 1.6 l and 2.0 l atmospheric.

As mentioned, the engine downsize era is using turbochargers, but also electronic direct injection and variable valve timing to achieve the objectives of performance, fuel consumption and pollutant exhaust emissions. These

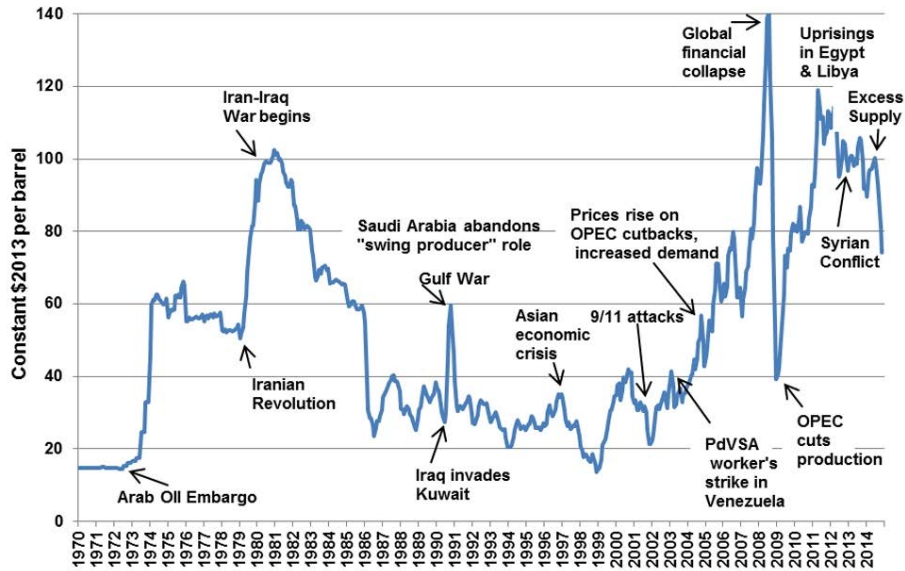


Figure 1.4. Oil price evolution during the last 40 years.

technologies were invented in the early 1900's for gasoline powered aviation engines and after almost a century of development, these technologies are a must for actual gasoline powered production cars engines.

The manufacturers also tend to develop technologies to comply with the upcoming pollutant emissions regulations. In modern direct injection gasoline engines a new pollutant emission is going to be regulated in EURO VI, the particle ( $PM$ ) emissions, as observed in Table 1.1 . Direct injection gasoline engines tend to produce particles as diesel engines, but in less quantity [8, 9]. These particles are a potential harm to the human health, as some studies have revealed it is a carcinogen element that could produce lung cancer [10] and should be regulated.

Passive and active solutions have been developed in order to reduce the tailpipe exhaust emissions. The passive solutions treat the pollutant emissions after the combustion and they are usually called as after-treatment system installed in the exhaust line. In the case of gasoline engines is the TWC, usually installed close to the head of the engine or, in case of a turbocharged engine, close to the turbine exit. The TWC converter has three simultaneous tasks: reduction of nitrogen oxides ( $NO_x$ ) to nitrogen ( $N_2$ ) and oxygen ( $O_2$ ), oxidation of carbon monoxide ( $CO$ ) to carbon dioxide ( $CO_2$ ) and oxidation of unburnt hydrocarbons ( $HC$ ) to carbon dioxide ( $CO_2$ ) and water ( $H_2O$ ).

TWC are effective when the engine is operated within a narrow band [11] of air-fuel ratios near stoichiometry, however, conversion efficiency falls very rapidly when the engine is operated outside of the stoichiometric mixture. Under lean mixture engine operation, there is excess oxygen and the reduction of  $NO_x$  is not favored. Under rich conditions, the excess fuel consumes all the available oxygen before the catalyst, thus only stored oxygen is available for the oxidation function.

The active solutions are based on the reduction of the emissions inside the cylinder. The research in this area has led to improvements some as the electronic direct injection systems, variable valve timing, combustion chamber, pistons and spark plug designs. In general this solutions are attractive from the point of view of production and implementation cost compared to the passive solutions.

As an example, the firsts SI gasoline direct injection (GDI) engines used a wall spray guided injector configuration [12], with this configuration is difficult to reduce the  $PM$  emissions to the new Euro VI  $PM$  regulations. In most of the cases, the only solution to reduce the  $PM$  formation in this case is to change the configuration of the injector and injector specifications to reduce the wall wetting [13]. But this implies the redesign of the engine head and the modification of the manufacturing process, followed by an optimization of the chamber, piston and injector. Honda, Volkswagen and other manufacturers decided not to follow this path and used the port fuel injection (PFI) system, developed for early models, for low and part load operating conditions (usually the zone used for the homologation cycle in Europe) and the direct injection for full load operating conditions. With this active solution modern GDI engines would comply with new Euro VI regulations with the same, or better, efficiency using the same after-treatment as gasoline engines on the 80's, if they operate in stoichiometric conditions. On the other hand, there are some car manufacturers that prefer passive solutions. Particle filters are being developed for gasoline engines, since it is supposed that the actual active solutions development are not going to be enough to comply with the stringent future  $PM$  pollutant emissions regulation.

In the gasoline engine research area during the last decade, the cooled exhaust gas recirculation and lean burn strategies are being studied and developed to further reduce the fuel consumption of future SI gasoline engines. The exhaust gas recirculation (EGR) is a technology that was already used in gasoline engines during the 70's but it was until the last decade when showed the real potential in synergy with turbochargers, direct injection and better control systems. This technology has been used for the last decade on diesel

engines to reduce the  $NO_x$  exhaust emissions, but the EGR in SI gasoline turbocharged engines is still not used in mass production cars.

On the other hand the lean burn is also used to reduce the fuel consumption, by reducing the throttled area of the engine map but at the cost of not being able to use a TWC as a after-treatment system, increasing the complexity and cost of the after-treatment system. Some cars on the last decade have been using lean mixture conditions for low loads and a TWC and  $NO_x$  trap as a after-treatment system.

This PhD-Thesis is mainly focused on the understanding and potential of these two fuel consumption reduction strategies, cooled EGR and lean burn, on a modern gasoline turbocharged direct injection engine (GTDI). The work should lead to clear and valuable conclusions for the path that SI gasoline engines are going to be following for the next years to come.

## 1.2 Thesis context

In last Section 1.1 a chronological history of technologies invention and pollutant exhaust emissions regulations in the principal countries of the world was presented. As it was stated before, the last decade SI gasoline engines have been gaining attention since diesel engines are struggling to comply with new upcoming pollutant exhaust emissions regulations. Furthermore the increase of the fuel price in the last decade has led to design and develop more efficient engines in terms of thermal efficiency. To develop a more efficient gasoline engine active solutions must be implemented, the most popular and used in the last decade is called downsizing.

### 1.2.1 Downsizing method

Downsizing, as explained briefly in Section 1.1, consists in reducing the engine displacement and add a force induction system as a turbocharger or supercharger, that compensates the loss of engine size, so the new engine configuration delivers the same torque and power as the replaced natural aspirated engine or bigger turbocharged engine in the case of heavy downsizing. This reduction in engine size leads to a reduction in fuel consumption mainly by reducing the pumping losses, friction losses and weight of the powertrain assembly.

The reduction of the engine size leads to new problems and new technologies are been developed because of it. Reducing the engine

displacement increases the load of the engine, which at low engine speeds leads to more knocking problems [14] and at high engine speeds leads to high exhaust gas temperature [15]. The high exhaust gas temperature should be controlled to guarantee the proper reliability of the turbocharger. Because of this, an enrichment strategy is used to control this problem, increasing the fuel consumption at high engine speed and high load operating conditions. Furthermore a recent technology, the integrated exhaust manifold in the cylinder head [16], has been developed to mitigate the high exhaust gas temperature, reducing the needed fuel to control the exhaust gas temperature leading to a reduction in the fuel consumption under these operating conditions.

The knocking problems could be solved by lowering the compression ratio of the engine, but this would hurt the fuel consumption. On the other hand, the electronic direct injection helped mitigate this problem by decreasing the cylinder temperature before the compression stroke [17]. The cylinder temperature reduction is consequence of the fuel being injected and evaporated inside the cylinder. This also leads to an increase in the compression ratio of the engines, increasing the thermal efficiency and decreasing the fuel consumption of the downsized engines. Furthermore the variable valve timing strategy also helps mitigate the knocking problems at low engine speeds and high load operating conditions by reducing the amount of internal exhaust gases and by using a late intake valve closing (LIVC), this would increase the thermal efficiency of the engine by allowing more compression ratio or better combustion phasing.

As it was explained, the downsizing led to new technology development to solve certain problems that came with the engine size reduction method to reduce fuel consumption. These new technologies had increased the thermal efficiency of downsized gasoline engines.

### 1.2.2 Variable valve timing strategies

The most popular strategies to reduce the fuel consumption using a variable valve timing (VVT) technology are the Miller and Atkinson cycles.

#### 1.2.2.1 Miller cycle

The Miller cycle was patented by Ralph Miller, an American engineer, in 1957. A traditional reciprocating internal combustion engine uses four strokes, of which two can be considered high-power: the compression stroke

and expansion stroke. In the Miller cycle, the intake valve is left open longer than it would be in an Otto cycle engine. In effect, the compression stroke is two discrete cycles: the initial portion when the intake valve is open and final portion when the intake valve is closed. This two-stage intake stroke creates the so-called "fifth" stroke that the Miller cycle introduces. As the piston initially moves upwards in what is traditionally the compression stroke, the charge is partially expelled back out through the still-open intake valve. Typically this loss of charge air would result in a loss of power. However, in the Miller cycle, this is compensated by the use of a turbocharger, a supercharger or an electrical turbocharger.

Recently the term Miller cycle has been used to describe a LIVC on the boosted zone of the engine map. This decreases the pumping losses and the dynamic compression ratio reducing the fuel consumption and the risk of knocking.

#### **1.2.2.2 Atkinson cycle**

The Atkinson cycle is a type of internal combustion engine invented by James Atkinson in 1882 which consists in a piston engine that allows the intake, compression, power, and exhaust strokes of the four-stroke cycle to occur in a single turn of the crankshaft. Due to the unique crankshaft design of the Atkinson engine, its expansion ratio can differ from its compression ratio and, with a power stroke longer than its compression stroke, the engine can achieve greater thermal efficiency than a traditional piston engine. While Atkinson's original design is no more than a historical curiosity, many modern engines use unconventional valve timing to produce the effect of a shorter compression stroke/longer power stroke, thus realizing the fuel economy improvements the Atkinson cycle can provide.

Recently, the term "Atkinson cycle" has been used to describe a modified Otto cycle engine in which the intake valve is held open longer than normal to allow a reverse flow of intake air into the intake manifold, generally on atmospheric engines or the throttle area of a turbocharged engine map. The effective compression ratio is reduced (for a time the air is escaping the cylinder freely rather than being compressed) but the expansion ratio is unchanged. This means the compression ratio is smaller than the expansion ratio. Heat gained from burning fuel increases the pressure, thereby forcing the piston to move, expanding the air volume beyond the volume when compression began. The goal of the modern Atkinson cycle is to allow the pressure in the combustion chamber at the end of the power stroke to be equal to atmospheric

pressure; when this occurs, all the available energy has been obtained from the combustion process.

The disadvantage of the four-stroke Atkinson cycle engine versus the more common Otto cycle engine is reduced power density, that is the main reason for the compression ratio increase in the engines that run with a Atkinson cycle, a good example is the Toyota Prius with a 13:1 of compression ratio.

### 1.2.3 Variable compression ratio

Variable compression ratio is a technology used to adjust the compression ratio of an internal combustion engine while the engine is in operation. Higher loads require lower compression ratio to be more efficient and vice versa. For automotive use this needs to be done dynamically in response to the load and driving demands.

SI gasoline engines have a limit on the maximum pressure during the compression stroke, after which the fuel/air mixture starts to present autoignition symptoms. For downsized engines, using turbochargers or superchargers to increase the performance of the engine leads to knocking problems unless the compression ratio is decreased, the disadvantage is that under light load, the engine is not as efficient as it should be. The solution is to be able to vary the inlet pressure and adjust the compression ratio to fulfill the requirements of the engine. This gives the best of both worlds, a small efficient engine that behaves exactly like a modern family car engine but with high torque and power outputs.

### 1.2.4 Lean burn strategy

The lean burn strategy consists of burning a lean mixture instead of a stoichiometric mixture at low and part load operating conditions. In order to make it worthwhile, a fuel direct injection system, and a piston bowl and injector matching should be designed to ensure the correct combustion stability in synergy with the head design [18]. After the design, the engine can run on lean mixtures with better or the same cycle to cycle combustion dispersion than the usual stoichiometric mixture. This strategy leads to a reduction of fuel consumption mainly by reducing the pumping losses, heat losses and increase of the combustion efficiency [19].

The principal problem of this strategy is the  $NO_x$  exhaust emissions, as stated before in Section 1.1. Since the TWC works under stoichiometric conditions, while the engine is operating with a lean mixture the  $NO_x$  exhaust

emissions cannot be catalyzed. The typical solution is to add an additional after treatment component to treat the  $NO_x$  emissions. There are two different technologies to treat the  $NO_x$  exhaust emissions: the first one is a  $NO_x$  trap and it usually works as a filter of particles by trapping the  $NO_x$  and releasing it as  $CO_2$  when the engine operates in stoichiometric mixture. The second one is a selective catalytic reduction (SCR) system that uses typically urea to catalyze the  $NO_x$  emissions.

As in the case of the downsizing technology, the lean burn strategy is also leading to new technology development to solve the problems that appear when operating in lean conditions. These new technologies would make possible the existence of SI gasoline engines that could operate with lean mixture at low load conditions to further reduce the fuel consumption.

### 1.2.5 EGR strategy

Exhaust gas recirculation (EGR) is an emission control technology allowing significant  $NO_x$  emission reductions from most types of diesel engines: from light-duty engines through medium- and heavy-duty engine applications right up to low-speed, two-stroke marine engines. While the application of EGR for  $NO_x$  reduction is the most common reason for applying EGR to modern commercial diesel engines, its potential application extends to other purposes as well. Some of these include: imparting knock resistance, reducing the need for high load fuel enrichment in SI engines and reducing fuel consumption.

From 1972 to the late 80's EGR was commonly used for  $NO_x$  control in gasoline fueled passenger car and light-duty truck engines in North America. After the early 1990's, some gasoline fueled applications were able to dispense with EGR. Following the early gasoline application, EGR was also introduced to diesel passenger cars and light-duty trucks and then heavy-duty diesel engines.

This strategy consists in re-introducing exhaust gas into the intake of the engine. In the case of turbocharged gasoline engines, the exhaust gas is cooled to maximize its fuel consumption reduction effect and to ensure intake system components reliability such as the compressor, plastic intake manifolds and so on.

The cooled EGR reduces the knocking tendency, the pumping losses, the exhaust gas temperature and the heat losses through the cylinder walls [20]. It has been reported how introducing in some cases just 5% to 10% of cooled EGR at high loads avoids the need of operating the engine in rich air-fuel-ratio (AFR) ratio conditions (over-fuelling or enrichment strategy) to control the



exhaust gas temperature as observed by Bandel et al. in their research work [21]. This technology is the perfect complement for new downsized gasoline engines.

There are different EGR configurations for turbocharged SI gasoline engines such as low pressure, high pressure and mixed pressure. The low pressure EGR configuration extracts the exhaust gas after the turbine and catalyst to be introduced before the compressor. On the other hand high pressure takes the exhaust gas before the turbine to be introduced after the compressor. And the mixed configuration is a mix between a low pressure and high pressure configuration, it takes the exhaust gas before the turbine to introduce it before the compressor. The advantages and disadvantages of each configuration are going to be explained on the literature review in Chapter 2.

In this technological-scientific context, this PhD-Thesis studies the cooled EGR strategy to reduce fuel consumption and its influence on the optimization of different engine parameters, as variable valve timing and injection timing. Furthermore a lean burn strategy was also studied to reduce the fuel consumption and a synergy using lean burn and cooled EGR at the same time was also performed. The effects on the combustion, air management and gas exhaust emissions were analyzed in each stage of this research work.

## 1.3 Objectives and methodology

### 1.3.1 Objectives

The main objective of this PhD-Thesis is to analyze the potential of the cooled EGR strategy to reduce fuel consumption, its synergy with other possible strategies, as lean burn, and the influence on the engine performance, combustion, air management and exhaust emissions.

Furthermore, other specific objectives were imposed during the development of the investigation:

- The study of the cooled EGR influence over the performance and exhaust emissions of the engine using the original VVT and injection timing parameters, in steady and transient operating conditions.
- A development of a methodology that could optimize VVT, to maximize the fuel consumption reduction when operating with cooled EGR, using 1D simulations and design of experiments (DoE) to reduce engine testing.

- Analysis of the injection timing effect on the engine performance and exhaust emissions when using cooled EGR.
- Analysis of different strategies to increase the EGR range in part load conditions such as multiple injections, higher engine coolant temperature operation and induced swirl motion.
- The study of the lean burn strategy in conjunction with cooled EGR to minimize  $NO_x$  emissions and maximize fuel consumption reduction.

Finally the fuel consumption reduction obtained after the investigation using cooled EGR, lean burn and both at the same time would determine the advantages and disadvantages of each strategy for the near future. It is important to remark that the comparison is made using the original conditions of an engine that was homologated for Euro *V* regulations.

### 1.3.2 Methodology

An exhaustive literature review is presented in Chapter 2, starting with the basis of the gasoline engine up to the complicated phenomena that occur in the new implemented fuel consumption reduction strategies.

Before starting with the engine testing it was necessary to review the theoretical and experimental tools to understand the limitations of the research and the possible analysis that could be performed. These tools are presented and described in Chapter 3.

In the first stage of this research work, the main objective was to establish the methodology that should be followed in order to reduce the fuel consumption. Once the main methodology was assessed, in the second stage, the influence of the cooled EGR over the GTDI engine using the original parameters was studied for steady and transient operating conditions. This study is presented in Chapter 4 where an analysis of the engine performance, combustion, air management and exhaust emissions of the engine is performed for low, partial and full load conditions at two different engine speeds for steady and transient operating conditions. In the case of transient operating conditions, NEDC cycles were performed using different opening setups of the EGR valve, using a Ford Modeo as base vehicle in order to analyze the effect of EGR on the engine performance, air management and accumulated exhaust emissions.

The third stage of this research was to optimize the VVT setting and injection timing to minimize the fuel consumption when using cooled EGR

and the exploration of EGR misfire range extender strategies. A methodology using 1D simulations and a DoE was developed in order to optimize and study the influence of the VVT parameters using cooled EGR on the GTDI engine. Furthermore, an injection timing optimization was also carried out following a parametric study methodology. In addition, the explanation and analysis of different EGR misfire range extender strategies is presented, such as multiple sparks, swirl motion and multiple injections. These studies are presented on Chapter 5 where an analysis of the performance, combustion, air management and exhaust emissions of the GTDI engine is performed for partial load conditions at two different engine speeds.

Finally, the lean burn strategy and its operation in synergy with cooled EGR was studied. This study was performed using a DoE and a normal parametric study methodology. At the final part of Chapter 5, an analysis of the performance, combustion, air management and exhaust emissions of the engine is presented for partial load conditions at two different engine speeds.

And finally the Chapter 6 presents the main conclusions of this research work and the future works that can be explored in the near future in the SI gasoline turbocharged direct injection engines research and development area.

## Bibliography

- [1] Michel C. and Eckard H. "Critical evaluation of the European diesel car boom - global comparison, environmental effects and various national strategies". In *Environmental Sciences Europe*, 2013.
- [2] Vijayaraghavan K., Lindhjem C., DenBleyker A., Nopmongcol U., Grant J., Tai E. and Yarwood G. "Effects of light duty gasoline vehicle emission standards in the United States on ozone and particulate matter". *Atmospheric Environment*, Vol. 60, pp. 109–120, 2012.
- [3] Happer W. "The Truth About Greenhouse Gases". In *The Global Warming Policy Foundation*, pp. 57–61, 2011. Briefing Paper No 3.
- [4] Makarow M., Ceulemans R. and Horn L. "Impacts of Ocean Acidification". In Foundation European Science, editor, *Science Policy Briefing*, 2009.
- [5] Hoegh-Guldberg O., Mumby P. J., Hooten A. J., Steneck R. S., Greenfield P., Gomez E., Harvell C. D. and Sale P. F. "Coral Reefs Under Rapid Climate Change and Ocean Acidification". *Science*, Vol. 318 n° 5857, pp. 1737–1742, 2007.
- [6] Ridgwell A. and Zeebe R. E. "The role of the global carbonate cycle in the regulation and evolution of the Earth system". *Earth Planet. Sci. Lett.*, Vol. 234, pp. 299–315, 2005.
- [7] Coltman D., Turner J. W. G., Curtis R., Blake D., Holland B., Pearson R. J., Arden A. and Nuglisch H. "Project Sabre: A Close-Spaced Direct Injection 3-Cylinder Engine with Synergistic Technologies to Achieve Low CO<sub>2</sub> Output". *SAE Int. J. Engines*, Vol. 1 n° 1, pp. 129–146, 2008. 2008-01-0138.

- [8] Bermudez V., Lujan J. M., Climent H. and Campos D. “Assessment of pollutants emission and aftertreatment efficiency in a GTDi engine including cooled LP-EGR system under different steady-state operating conditions”. *Applied Energy*, Vol. 158, pp. 459–473, 2015.
- [9] Ntziachristos L., Amanatidis S., Samaras Z., Janka K. and Tikkanen J. “Application of the Pegasor Particle Sensor for the Measurement of Mass and Particle Number Emissions”. *SAE Int. J. Fuels Lubr.*, Vol. 6 n° 2, pp. 521–531, 2013. 2013-01-1561.
- [10] Werner S. and Ulrich A. “Lung cancer due to diesel soot particles in ambient air”. *International Archives of Occupational and Environmental Health*, Vol. 68 n° 1, pp. S3–S61, 1996.
- [11] Hepburn J., Patel K., Meneghel M. and Gandhi H. “Development of Pd-only Three Way Catalyst Technology”. In *SAE Technical Paper*, 1994. 941058.
- [12] Kawamoto M., Honda T., Katashiba H., Sumida M., Fukutomi N. and Kawajiri K. “A Study of Center and Side Injection in Spray Guided DISI Concept”. In *SAE Technical Paper*, 2005. 2005-01-0106.
- [13] Warey A., Huang Y., Matthews R., Hall M. and Ng H. “Effects of Piston Wetting on Size and Mass of Particulate Matter Emissions in a DISI Engine”. In *SAE Technical Paper*, 2002. 2002-01-1140.
- [14] Hettlinger A. and Kulzer A. “A New Method to Detect Knocking Zones”. *SAE Int. J. Engines*, Vol. 2 n° 1, pp. 645–665, 2009.
- [15] Thirouard M. and Pacaud P. “Increasing Power Density in HSDI Engines as an Approach for Engine Downsizing”. *SAE Int. J. Engines*, Vol. 3 n° 2, pp. 56–71, 2010.
- [16] Watanabe I., Kawai T., Yonezawa K and Ogawa T. “The New Toyota 2.0-Liter Inline 4-Cylinder ESTEC D-4ST Engine - Turbocharged Direct Injection Gasoline Engine -”. In *23rd Aachen Colloquium Automobile and Engine Technology*, 2014.
- [17] Lecointe B. and Monnier G. “Downsizing a Gasoline Engine Using Turbocharging with Direct Injection”. In *SAE Technical Paper*, 2003. 2003-01-0542.
- [18] Raimann J., Arndt S., Grzeszik R., Ruthenberg and Worner P. “Optical Investigations in Stratified Gasoline Combustion Systems with Central Injector Position Leading to Optimized Spark Locations for Different Injector Designs”. In *SAE Technical Paper*, 2003. 2003-01-3152.
- [19] Gomez A. and Reinke P. “Lean burn: A Review of Incentives, Methods, and Tradeoffs”. In *SAE Technical Paper*, 1988. 880291.
- [20] Potteau S., Lutz P., Leroux S., Moroz S. and Tomas E. “Cooled EGR for a Turbo SI Engine to Reduce Knocking and Fuel Consumption”. In *SAE Technical Paper*, 2007. 2007-01-3978.
- [21] Bandel W., Fraidl G. K., Kapus P. E., Sikinger H. and Cowland C. N. “The Turbocharged GDI Engine: Boosted Synergies for High Fuel Economy Plus Ultra-low Emission”. In *SAE Technical Paper*, 2006. 2006-01-1266.

# Chapter 2

## Literature review

### Contents

---

<b>2.1</b>	<b>Introduction</b> .....	<b>20</b>
<b>2.2</b>	<b>Overview of conventional SI gasoline engine</b> .....	<b>21</b>
2.2.1	Combustion process .....	21
2.2.1.1	Spark and flame initiation .....	22
2.2.1.2	Initial flame kernel development .....	23
2.2.1.3	Turbulent flame propagation .....	24
2.2.1.4	Flame termination .....	25
2.2.2	Formation of exhaust emissions .....	26
2.2.2.1	Un-burned hydrocarbon .....	27
2.2.2.2	Nitrogen oxides .....	30
2.2.2.3	Carbon monoxide .....	33
2.2.2.4	Particulate matter .....	34
2.2.3	Air management .....	36
2.2.3.1	Intake system .....	36
2.2.3.2	Exhaust system .....	39
2.2.3.3	Valve actuation system .....	42
2.2.3.4	Supercharging and turbo-charging .....	44
<b>2.3</b>	<b>Strategies to reduce fuel consumption in SI gasoline engines</b> .....	<b>45</b>
2.3.1	Downsizing .....	46
2.3.2	Direct injection .....	47
2.3.3	Variable valve timing .....	50
2.3.3.1	Miller cycle .....	51

---

2.3.3.2	Atkinson cycle.....	52
2.3.4	Variable compression ratio .....	53
2.3.5	Lean burn .....	55
2.3.6	Cooled exhaust gas recirculation .....	57
2.3.6.1	High pressure loop .....	61
2.3.6.2	Low pressure loop .....	64
2.3.6.3	Mixed pressure loop.....	66
<b>2.4</b>	<b>Summary and conclusions .....</b>	<b>68</b>
	<b>Bibliography .....</b>	<b>72</b>

---

## 2.1 Introduction

SI gasoline engines have been the main choice for passenger cars around the world [1], since the invention of the car, until the late 90's when CI diesel engines development in Europe started to gain popularity thanks to their lower fuel consumption, the increase in fuel prices and the government aids [2]. On the other hand, the situation in Japan was undergoing the same path until the Japanese government restricted in a harder manner the emissions targets for diesel engines in passenger cars [2] and they considered diesels to be a dead-end technology environmentally: "When equipped with all future after-treatment equipment, diesel cars will become as expensive as hybrid cars", says Katsuhiko Hirose, hybrid project general manager for Toyota [3]. In the U.S. the fuel prices did not increased in the same way as in Europe and the stringent emissions regulations restricted the introduction of diesel engines for passenger cars in the U.S. market.

Lately the popularity in Europe of new passenger cars powered by gasoline engines had increased, after the introduction of Euro *V* and Euro *VI*. The development of new SI gasoline engines, which helped to reduce the fuel consumption, and the more stringent emissions regulations for diesel powered passenger cars, also played a big role.

From 2000 to 2012 the development of SI gasoline engines has been focused on the reduction of fuel consumption. Lately the development it is been also on the exhaust gas emissions area to comply with the Euro *VI* that it is going to be introduced in 2016. The main problem is in the area of *PM* emissions, thus injection, injector placement, combustion chamber and piston bowl design in the active solutions side and obviously Gasoline Particle Filter (GPF) on the passive solution side are being developed.

This chapter is structured in two main sections. The first section focuses in the conventional gasoline engines advantages and disadvantages, and aims to provide the reader with an overview of the combustion process, describing the type of combustion, its drawbacks and the formation of exhaust emissions. And the air management, describing the load regulation, boosting solutions and its drawbacks.

In the second section, the state of the art, most recent and important of strategies and methodologies used in SI gasoline engines to reduce the fuel consumption are summarized, focused on the combustion, performance, air management and exhaust emissions outputs. For the purposes of the discussion presented in this PhD-Thesis, the literature review makes special emphasis in the strategy using cooled EGR as the main factor to reduce the fuel consumption.

## 2.2 Overview of conventional SI gasoline engine

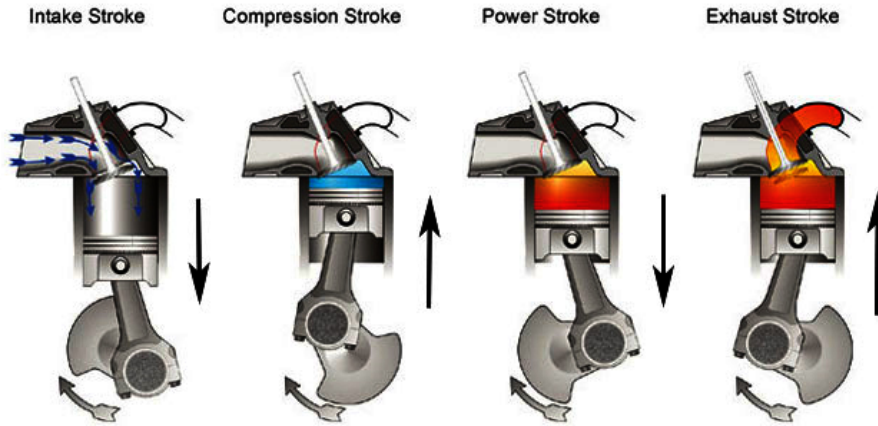
Gasoline engine is a class of internal-combustion engine that generates power by burning a volatile liquid fuel (gasoline or a gasoline mixture such as E10 or E5) with ignition initiated by an electric spark. In this PhD-Thesis, the literature review is only based on four-stroke gasoline engines. These gasoline engines power the vast majority of automobiles, light trucks, medium-to-large motorcycles, and lawn mowers. In the four-stroke SI gasoline engines there is a sequence of processes based on the Otto cycle: compression, power, exhaust and intake stroke as it is showed in Figure 2.1.

This section is structured in two main sub-sections. The first subsection explains and describes the combustion process, its drawbacks and the formation of exhaust emissions. And the second subsection describes the air management process and load regulation, boosting systems and exhaust after-treatment.

### 2.2.1 Combustion process

The combustion process in SI engines can be divided into four main stages [4]: spark and flame initiation, initial flame kernel development, turbulent flame propagation and flame termination.

Basically, the first 5% of the air-fuel mixture process is labeled as the flame development process, the first two stages. During this period, ignition occurs and the combustion process starts, however very little in-cylinder pressure rise



*Figure 2.1. Gasoline four-stroke processes illustration.*

hence there is no useful work done. At 80% to 90% of the process, the work is produced in the engine because of the turbulent flame propagation stage of the combustion process, where the bulk of the fuel and air mass is burned. During this time, the pressure inside the cylinder is greatly increased thus provides the force to produce the work in the expansion stroke. Then, for the final 5% of the process, the flame termination, the pressure quickly decreases and the combustion stops [5].

### 2.2.1.1 Spark and flame initiation

An excellent overview of the physics and effects of spark ignition on internal combustion engines has been given by Maly et al. [6]. The spark is initiated by a voltage rise between the electrodes of the spark plug, which produces an electrical breakdown in the spark-plug gap. This first stage is characterized by very high peak values of voltage ( $\approx 10$  kV) and current ( $\approx 200$  A) and occurs in an extremely short time ( $\approx 1$ -10ns). The energy supplied at this stage is transferred with almost 95% efficiency to the plasma [7]. The breakdown phase is followed by the arc phase that lasts for some hundreds of microseconds [8]. The voltage falls down to levels of 50 – 100 V but the current is still relatively high.

The final stage of the spark event is the glow phase. During this stage the voltage grows up to about 500 V and the current is of the order of 0.1 A. Although this stage of discharge is associated with low power, the energy



release is more than 90% of the total energy supplied by the spark [9]. The efficiency of the energy transfer to the mixture during the arc and glow phases can be up to 60% under typical in-cylinder conditions [10]. It is actually during the glow phase that self-sustained propagation is established and, eventually, there is no distinct boundary between this last phase of the spark event and the initial flame kernel development stage.

### 2.2.1.2 Initial flame kernel development

A flame kernel is a small volume of combustion products in unburned flame mixture where a thin layer of reactions occurs on the surface. Optical observation results showed that spark ignited flame kernel often keeps a spherical shape under quiescent conditions unless heat transfer occurs between the kernel and spark plug electrodes and chamber walls. It is reported that the flame kernel needs to reach a certain critical size to ensure self-sustained propagation against various types of heat losses [11] which propagates in a laminar manner with a smooth flame front. The initial flame kernel size is typically compared with the gap size between that spark plug electrodes, thus a large spark plug gap size is relatively beneficial to ignition as long as it allows breakdown to happen.

The ability of the spark-generated kernel to continue to grow into a fully developed self-sustaining flame depends upon the hydrodynamics of the local strain field, as well as thermo-physical and chemical parameters such as the rate of heat loss and equivalence ratio. For unstrained or lightly strained kernels without heat loss, the combustion wave continues to propagate until all reactants are consumed. As the hydrodynamic strain rate is increased, the flame front may be quenched and reactant consumption rate fall to zero. Well-controlled laminar vortex has been applied to study the flow effect on flame propagation [12, 13]. Vortex strength, which indicates the flow speed of the vortex, is a dominant factor in quenching a flame kernel. In addition, vortex with larger length scales would require lower strength to quench a flame kernel. Quenching of flame kernel usually occurs when reacting front of flame kernel becomes stretched by strong flow and several local reacting fronts are propagating towards each other. This quenching may occur only locally, allowing the kernel to recover and consume the reactant charge, or if the strain rate is high enough, the entire kernel may quench.

The initial flame kernel formation and kernel growth are mainly affected by characteristics of ignition system, in-cylinder temperature, turbulence, spark plug configurations, the shape of the combustion chamber, fuel distribution,

and mixture flow. This obviously affects the cycle-by-cycle variations (CCV) in combustion and, consequently, in torque level, a fundamental problem of SI gasoline engines [14].

### 2.2.1.3 Turbulent flame propagation

Premixed turbulent combustion can be classified into different regimes [15, 16], depending on the Karlovitz number, the Damkohler number and the Reynolds number. The two regimes of interest in internal combustion engines are the flamelet regime and the distributed reaction zone. The border between these two regimes is postulated to occur at Karlovitz number of unity, which represents the condition where the flame thickness is on the order of the Kolmogorov length scale, also known as the Klimov-Williams criterion [17]. On one side of this border, the flamelet regime, combustion occurs as a series of one or more continuous flame fronts. In contrast, the distributed reaction regime is characterized by local quenching which leads to discontinuities in the flame front, and allows products and reactants to mix. Where this border lies is of great interest to the engine designer because it is very beneficial to operate as close as possible to the border between these two regimes, where the turbulent burning velocity is high, with the flame front remaining intact, thus minimizing combustion inefficiencies and emissions.

The process can be described by a simple entrainment-and-burn-model suggested by Keck et al. [18]. The flame front, with nominal front area of  $A_f$  takes in unburned gas of density  $\rho_u$  with an entrainment velocity  $U_t$  which is equal to the local turbulent velocity fluctuation. This entrained gas is then consumed in a time scale by  $\frac{\ell_t}{S_L}$ , where  $\ell_t$  is the turbulent length scale and  $S_L$  is the laminar flame speed.

$$\frac{d\mu}{dt} = \rho_u A_f U_t - \frac{\mu}{\frac{\ell_t}{S_L}} \quad (2.1)$$

In the equation 2.1  $\mu$  is the mass of unburned gas which is entrained but not burned yet. Then the mass burn rate  $m_b$  is the sum of the laminar burning at the nominal front and that of the entrained unburned mixtures.

$$\frac{dm_b}{dt} = \rho_u A_f S_L + \frac{\mu}{\frac{\ell_t}{S_L}} \quad (2.2)$$

From equation 2.1 and 2.2, the quasi-steady (i.e when  $\frac{d\mu}{dt} = 0$ ) burn rate is:

$$\frac{dm_b}{dt} = \rho_u A_f (S_L + U_t) \quad (2.3)$$

The quasi-steady burning velocity is, therefore,  $S_L + U_t$ . Thus the turbulent velocity augments the laminar flame speed after the flame front transforms from a smooth surface to a wrinkle one. Under conditions for which the laminar speed is too low, however, the burn out time  $\frac{\ell_t}{S_L}$  will be comparable or longer than the diffusion time  $\frac{\ell_t^2}{D}$  (where  $D$  is the mass diffusivity), and the wrinkle laminar flame model will no longer be valid. Then the combustion progresses slowly in distributed manner.

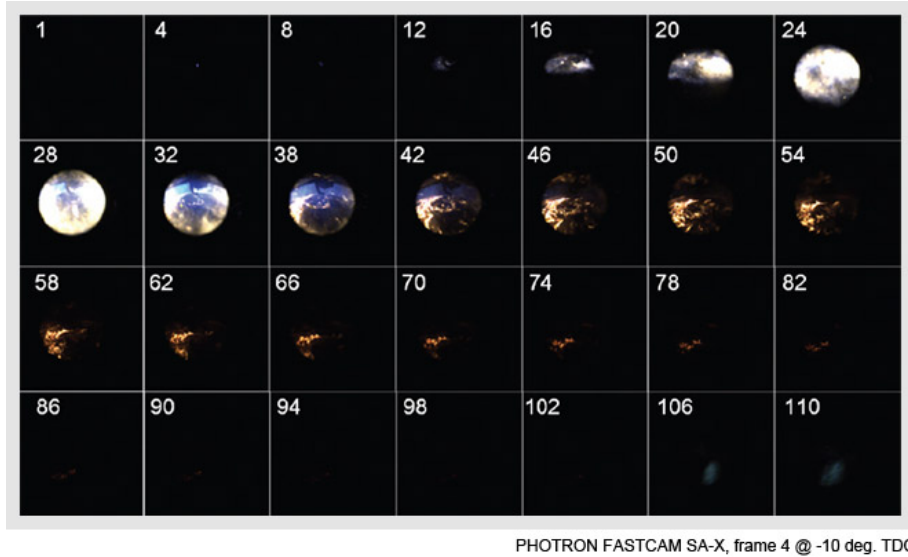
The relationship between charge motion and the local turbulence that enhances flame propagation is not straight forward [19]. Only small eddies are effective in wrinkling the flame front. It has been established that the small scale turbulence generated in the intake process are mostly dissipated in the compression process. The turbulence that matters is produced by the breakup of organized charge motion such as the swirl and tumble motion generated by the induction process. Thus the breakup details affect the burn rate.

#### 2.2.1.4 Flame termination

At a range about 15 to 20 CAD ATDC in atmospheric engines and 30 to 40 CAD ATDC depending of the load in a turbocharged engine, 90-95% of the air-fuel mass has been combusted while the flame front already reached the extreme corners of the combustion chamber. Although at this point the piston has already moved away from TDC, the combustion chamber volume has only increased about 10-20% from the very small clearance volume. This means that the last mass of fuel-air reacts in very small volume in the corner of the combustion chamber as well at the wall of the combustion chamber, piston and cylinder.

Because of the closeness of the combustion chamber walls, the last end gas reacts at a very reduce rate. In addition, the large mass of the metal walls acts as a heat sink and conducts away the energy in the reaction flame. Both of these mechanisms reduce the reaction rate and flame speed and the combustion finally ends.

Although the additional works delivered by the piston are very little, it is still important because the force transmitted to the piston taper off slowly resulting in smooth engine operation. Usually, during the flame termination period, self-ignition will occur causing the phenomena called engine knock. However, the resulting knock is usually unnoticeable. This is because the



*Figure 2.2. Combustion image sequence.*

amount of air-fuel mixture left in the combustion chamber is very little and it can only cause slight pressure pulses [5].

In Figure 2.2 a complete combustion process can be observed, is a SA-X combustion image sequence shot at 5000 frames per second with a shutter of  $1/5070$  or  $197 \mu\text{s}$  and a resolution of  $512 \times 512$  pixels. The sequence starts at the upper left corner. Every 4th frame thereafter is shown below for illustration purposes only with text numbers added to the image. It can be seen the spark on frame 4 and clearly the flame front propagating. Frame 106 and 110 show an after burn as a faint blue flame called pool fires [20] just after the flame termination. The actual firing of the spark normally occurs BTDC by several degrees ( $-10^\circ$  TDC) in a normal combustion cycle, but in some high load and low engine speed operating conditions of a turbocharged engine the spark can occur ATDC.

### 2.2.2 Formation of exhaust emissions

The gasoline or other fuels used in SI engines as natural gas or ethanol, are mixtures of hydrocarbons, compounds that contain hydrogen and carbon atoms. In a perfect combustion, oxygen in the air would convert all of the hydrogen in fuel to water and all the carbon into carbon dioxide. Nitrogen

in the air would remain unaffected. In reality, the combustion process is not perfect, and automotive engines emit several types of pollutants. The principal exhaust pollutants that are going to be analyzed in this PhD-Thesis and that are actually been regulated are: nitrogen oxides ( $NO_x$ ), unburned hydrocarbons ( $HC$ ), carbon monoxide ( $CO$ ), particle matter ( $PM$ ) and carbon dioxide ( $CO_2$ ).

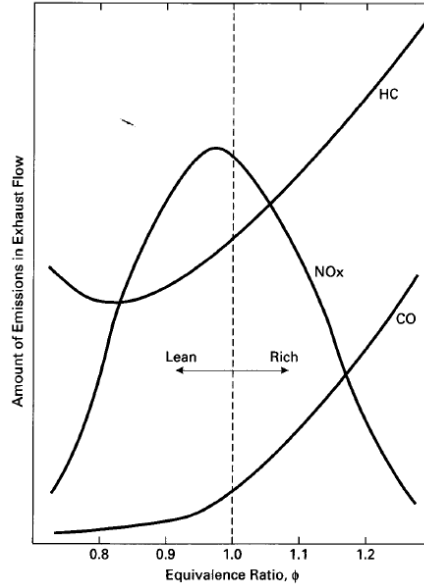
### 2.2.2.1 Un-burned hydrocarbon

Hydrocarbon emissions result when fuel molecules in the engine do not burn or burn only partially. The makeup of  $HC$  emissions will be different for each gasoline blend, depending on the original fuel components. Combustion chamber geometry and engine operating parameters also influence the  $HC$  component spectrum.

When hydrocarbons emissions get into the atmosphere react in the presence of nitrogen oxides and sunlight to form ground-level ozone, a major component of smog. Ozone can irritate the eyes, damage lungs, and aggravate respiratory problems. It is our most widespread urban air pollution problem. Some kinds of exhaust hydrocarbons are also toxic, with the potential to cause cancer.

The causes of  $HC$  emissions are:

- Non-stoichiometric air-fuel ratio: Figure 2.3 shows that  $HC$  emissions levels are a strong function of air-fuel ratio. With a fuel-rich mixture there is not enough oxygen to react with all the carbon, resulting in high levels of  $HC$  and  $CO$  at the exhaust. This is particularly true in engine start-up, when air-fuel mixture is purposely made rich. It is also true to a lesser extent during rapid acceleration under load. If the air-fuel ratio is too lean, poorer combustion occurs, again resulting in  $HC$  emissions. The extreme of poor combustion for a cycle is total misfire.
- Incomplete combustion: even when the fuel and air entering an engine are at the ideal stoichiometric mixture, perfect combustion does not occur and some  $HC$  ends up in the exhaust. There are several causes of this. Incomplete mixing of the air and fuel results in some fuel particles not finding oxygen to react with. Flame quenching at the walls leaves a small volume of unreacted air-and-fuel mixture. The thickness of this unburned layer is on the order of tenths of a mm. Some of this mixture, near the wall that does not originally get burned as the flame front



*Figure 2.3. Exhaust emissions in function of the air-fuel.*

passes, will burn later in the combustion process as additional mixing occurs due to turbulence.

Another cause of flame quenching is the expansion which occurs during combustion and power stroke. As the piston moves away from TDC, expansion of the gases lowers both temperature and pressure within the cylinder. This slows combustion and finally quenches the flame somewhere late in the power stroke. This leaves some fuel particles unreacted.

High exhaust residual causes poor combustion and a greater likelihood of expansion quenching. This is experienced at low load and idle conditions. High levels of EGR will also cause this.

- Crevice volumes: during the compression stroke and early part of the combustion process, air and fuel are compressed into the crevice volume of the combustion chamber at high pressure. As much as 3% of the fuel in the chamber can be forced into this crevice volume, depending on the tolerance of the piston/cylinder and the height from the top of the piston to the first compression ring. Later in the cycle during the expansion stroke, pressure in the cylinder is reduced below crevice volume pressure,

and reverse blow-by occurs. Fuel and air flow back into the combustion chamber, where most of the mixture is consumed in the flame reaction. However, by the time the last elements of reverse blow-by flow occur, flame reaction has been quenched and unreacted fuel particles remain in the exhaust. Location of the spark plug relative to the top compression ring gap will affect the amount of HC in engine exhaust, the ring gap being a large percent of crevice volume. The farther the spark plug is from the ring gap, the greater is the HC in the exhaust. This is because more fuel will be forced into the gap before the flame front passes.

Crevice volume around the piston rings is greatest when the engine is cold, due to the differences in thermal expansion of the various materials. Up to 80% of all HC emissions can come from this source, depending on the piston alloy composition and the piston/cylinder tolerance.

- Leak past the exhaust valve: as pressure increases during compression and combustion, some air-fuel is forced into the crevice volume around the edges of the exhaust valve and between the valve and valve seat. A small amount even leaks past the valve into the exhaust manifold. When the exhaust valve opens, the air-fuel which is still in this crevice volume gets carried into the exhaust manifold, and there is a momentary peak in HC concentration at the start of the blow-down.
- Valve overlap: during valve overlap, both the exhaust and intake valves are open, creating a path where air-fuel intake can flow directly into the exhaust manifold. A well-designed engine minimizes this phenomena, using a VVT system gives more freedom to the design limiting at the same time the amount of fresh mixture that can flow directly into the exhaust manifold. This problem is solved when the fuel is injected directly into the cylinder after the EVC, as in the case of GDI engines.
- Deposits on combustion chamber walls: gas particles, including those of fuel vapor, are absorbed by the deposits on the walls of the combustion chamber. The amount of absorption is a function of gas pressure, so the maximum occurs during compression and combustion. Later in the cycle, when the exhaust valve opens and cylinder pressure is reduced, absorption capacity of the deposit material is lowered and gas particles are released back into the cylinder. These particles, including some HC, are then expelled from the cylinder during the exhaust stroke. This problem is greater in engines with higher compression ratios or turbocharged, due to the higher pressure these engines generate. More gas absorption occurs as pressure goes up. Clean combustion chamber

walls with minimum deposits will reduce *HC* emissions in the exhaust. Most gasoline blends include additives to reduce deposit buildup in engines.

Older engines will typically have a greater amount of wall deposit buildup and a corresponding increase of *HC* emissions. This is due both to age and to less charge motion that was generally found in earlier engine design. High charge motion helps to keep wall deposits to a minimum. When lead was eliminated as a gasoline additive, *HC* emissions from wall deposits became more severe. When leaded gasoline is burned the lead treats the metal wall surfaces, making them harder and less porous to gas absorption.

- Oil on combustion chamber walls: a very thin layer of oil is deposited on the cylinder walls of an engine to provide lubrication between them and the moving piston. During the intake and compression strokes, the incoming air and fuel comes in contact with this oil film. In much the same way as wall deposits, this oil film absorbs and desorbs gas particles, depending on gas pressure. During compression and combustion, when cylinder pressure is high, gas particles, including fuel vapor, are absorbed into the oil film. When pressure is later reduced during expansion and blow-down, the absorption capability of the oil is reduced and fuel particles are released back into the cylinder. Some of this fuel ends up in the exhaust.

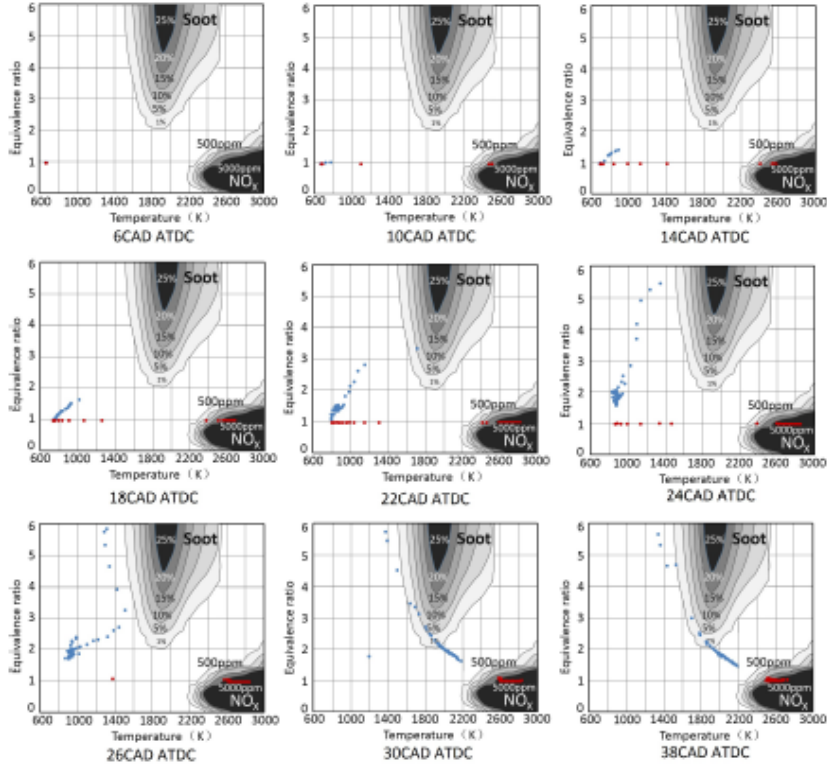
Propane is not soluble in oil, so in propane-fueled engines the absorption-desorption mechanism adds very little to *HC* emissions.

As an engine ages, the clearance between piston rings and cylinder walls becomes greater, and a thicker film of oil is left on the walls. Some of this oil film is scraped off the walls during the compression stroke and ends up being burned during combustion. Oil is a high-molecular-weight hydrocarbon compound that does not burn as readily as gasoline. Some of it ends up as *HC* emissions. This happens at a very slow rate with a new engine but increases with engine age and wear. The blow-by gases that are recirculated, have to also be taken into account for turbocharged engines especially at high loads.

#### 2.2.2.2 Nitrogen oxides

The nitrogen oxides ( $NO_x$ ) are formed by the stabilization of atmospheric nitrogen in oxidizing atmospheres at high flame temperature exceeding  $2200K$  as can be seen in Figure 2.4, where a normal exhaust emissions formation of





**Figure 2.4.** Diagram of  $NO_x$  and soot formation depending on the equivalence ratio and temperature. Source: Wang et al. [22].

a GDI engine is represented. It is observed in the red point the premixed combustion at high temperature, forming  $NO_x$ , and it is followed by the combustion extinction, in blue points, where the combustion flame ignites the fuel accumulated in the piston and cylinder walls, at lower temperature producing soot emissions. Thermal  $NO_x$  is generally produced during the combustion of both gases and fuel at high temperature [21] as mentioned before.

High activation energies are required for the dissociation of oxygen molecules and the disengagement of the triple bond of nitrogen. This phenomenon causes the formation of thermal  $NO_x$  to be largely dependent on the temperature, the degree of air to fuel mixing, the concentration of oxygen and nitrogen in the flame and duration of reaction occurred [23].

There are several factors which affect the formation of  $NO_x$  in the engine and they are listed below:

- The air-fuel ratio: it plays a major role in determining the amount of emission of  $NO_x$  as oxides of nitrogen are formed by the reaction of nitrogen in the fuel with oxygen in the combustion air. When the equivalence ratio is lower than one, which indicates that the combustion is in the lean condition, the fuel mixture has considerably less amount of fuel and excess of air. SI gasoline engines designed for lean burning can achieve higher compression ratios and hence produce better performance. However, it will generate high amount of  $NO_x$  due to the excess oxygen present in the mixture [24]. On the other hand when the combustion is in fuel-rich conditions (with excess of fuel) the oxidation reaction involve the  $OH$  and  $H$  radicals [25] and the  $NO_x$  formation is lower as can be seen in the Figure 2.3.
- Combustion temperature: it is also one of the primary factors that influence the formation of  $NO_x$ , as stated before. The formation of  $NO_x$  is directly proportional to the peak combustion temperature, with higher temperatures producing higher  $NO_x$  emissions [26]. The firing and quenching rates also influence the rate of  $NO_x$  formation where a high firing rate is associated with the higher peak temperatures and thus increases the  $NO_x$  emission. On the other hand, high rates of thermal quenching result in lower peak temperatures and contribute to the reduction of  $NO_x$  emission [27].

The environmental problems caused by  $NO_x$  are now worldwide issues due to the seriousness of ozone reactivity and the amount of formation of smog.  $NO_x$  combines with water vapor in clouds to produce acid rain which pollutes clean water sources and corrodes metals used in our daily life. Acid rain also harms the growth of organisms in the lake and disturbs the balance of the ecosystem both on land and at sea. Apart from that, acidified soil is also the result of acid rain and it causes damage to the root system of trees, disabling the nutrient absorption process and disrupting the natural process of photosynthesis [28].

When  $NO_x$  react chemically with other atmospheric gaseous compounds such as volatile organic compounds under the sunlight, it will form smog. Smog is forefront to our environmental concerns as it reduces the visibility of surroundings and poses a health hazard to humans which includes irritation of eyes, respiratory and cardiovascular problems such as asthma and headaches [29].

### 2.2.2.3 Carbon monoxide

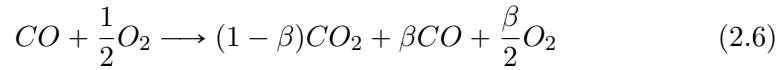
The carbon monoxide is a colorless, odorless, poisonous gas, that is generated in an engine when it is operated with a rich fuel-air equivalence ratio, as shown in Figure 2.3. When there is not enough oxygen to convert all carbon to  $CO_2$ , some fuel does not get burned and some carbon ends up as  $CO$ . The  $CO$  formation is an important combustion mechanism of hydrocarbons:



where  $Rad$  is a radical. Not only is  $CO$  considered an undesirable emission, but it also represents lost chemical energy that was not fully utilized in the engine.  $CO$  is a fuel that can be combusted to supply additional thermal energy [30]:

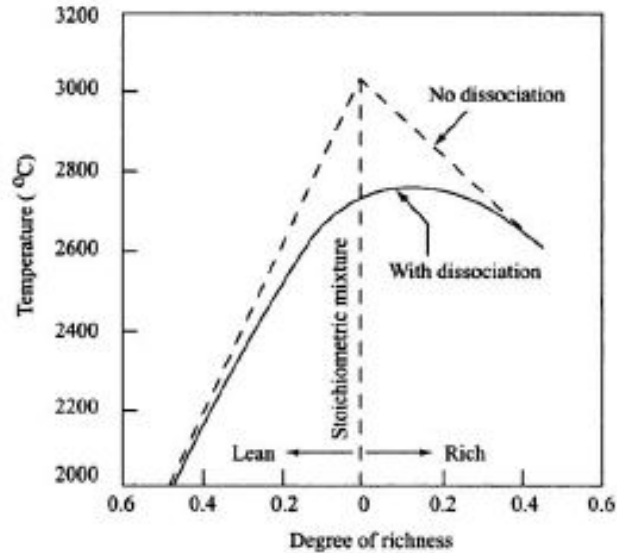


If the final temperature is high enough, the  $CO_2$  will dissociate:



where  $\beta$  is the fraction of  $CO_2$  dissociated. The temperature is a function of the dissociation fraction. If  $\beta = 1$ , the reaction remains unchanged and there is not heat released. On the other hand, if  $\beta = 0$ , the maximum amount of heat release occurs and the temperature and pressure would be the highest possible allowed by the first law of thermodynamics [30], as it can be seen in Figure 2.5 where the temperature is represented for different mixture richness with and without  $CO_2$  dissociation. It can be observed, how the temperature is higher when the dissociation does not happen because of the heat release obtained by the reaction presented in Equation 2.5.

Maximum  $CO$  is generated when an engine runs rich, such as when starting or accelerating under load. Even when the intake air-fuel mixture is stoichiometric or lean, some  $CO$  will be generated in the engine. Poor mixing, local rich regions, and incomplete combustion will create some  $CO$ . All the reasons mentioned before for  $HC$  formation also apply for  $CO$ . But that does not mean that if the  $HC$  increase the  $CO$  has also to increase, because the amount of dissociated  $CO_2$  can decrease because of lower combustion temperatures, reducing the total  $CO$  emissions. For example, this occurs



**Figure 2.5.** Temperature representation for different mixture richness with and without  $CO_2$  dissociation.

when cooled EGR is introduced into the engine, lowering the combustion temperatures, increasing the  $HC$  emissions and decreasing  $CO$  emissions [31].

#### 2.2.2.4 Particulate matter

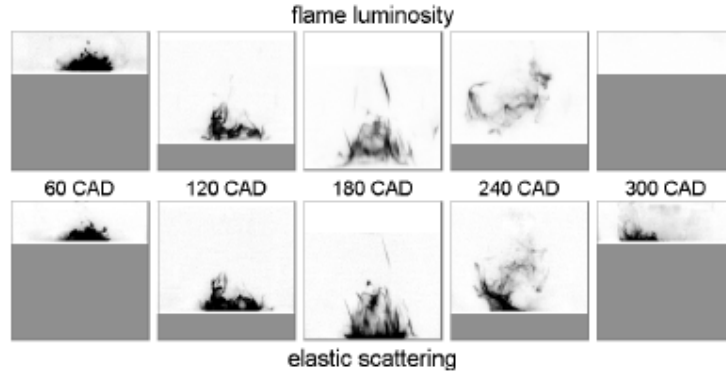
Particulate matter ( $PM$ ) or soot emissions have long been a concern of those involved with regulating the diesel industry, as  $PM$  emissions from diesel engines have been shown to be significant and are believed to be a health hazard, but nowadays this concern is also on the gasoline engine side. However, the knowledge related to gasoline engines exhaust particles is not at the same level as the knowledge of diesel exhaust particles. The disadvantage of GDI technologies is an increase in particle number emission compared to the PFI technology, as it is demonstrated by Aakko and Nylund [32], Mohr et al. [33], and Braisher et al. [34] in their research works. If compared to diesel exhaust particle number concentrations, the GDI exhaust number concentrations are significantly lower than the concentration of diesel engine exhaust particles without a diesel particulate filter (DPF) but higher than concentrations with a DPF [35].

Soot particles are clusters of solid carbon spheres. These spheres have diameter from 10 nm to 80 nm, with most within the range of 15 - 30 nm. The spheres are solid carbon with HC and traces of other components absorbed on the surface. A single soot particle will contain up to 4000 carbon spheres [36]. Carbon spheres are generated in the combustion chamber in the fuel-rich zones where there is not enough oxygen to convert all carbon to  $CO_2$ . Then, in lean operation, turbulence and mass motion continue to mix the components in the combustion chamber, most of these carbon particles find sufficient oxygen to further react and are consumed to  $CO_2$ .

In SI GDI engines, fuel is injected directly into the cylinder, increasing the likelihood of spray impingement on piston and cylinder surfaces. In fact, many stratified-charge strategies rely on shaped pistons to direct the fuel spray to the vicinity of the spark plugs [37]. Under these conditions, as well as in the case of unintentional fuel impingement during homogeneous charge operation, fuel films can form on the piston, with significant implications for combustion performance. If such films persist until combustion of the premixed charge in the cylinder, they may ignite and burn as diffusion flames. In an optical engine, they are prominently visible as bright yellow flames often persisting through the expansion stroke.

Using an optical piston, Witze, et al. [20] presented visible-light images of burning films in a PFI engine that were assigned the label pool fires. These pool fires can be observed in Figure 2.6 for a GDI engine. The  $PM$  is generated during burning of these pool fires where temperature is between  $1600K$  and  $2200K$ , and local equivalence ratio of fuel above 2 as it was presented in Figure 2.4 following the evolution of the blue points. Figure 2.6 shows a strong correlation between pool fires and  $PM$  formation, since pool fire luminosity is primarily due to incandescent particles, and these same particles are responsible for laser elastic scattering. At later times in the cycle, however, some differences in the images are apparent. At 180 and 240 CAD ATDC (TDC combustion), the pool fire has begun to lift from the piston top while the soot scattering signal remains attached to the piston surface. At 300 CAD ATDC, the pool fire has extinguished while some soot signal remains. Based on these observations, we conclude that significant soot is produced during the pool fire burn, with a portion of it remaining close to the piston top even after the flames have apparently extinguished [38].

Stevens et al. [38] studied the formation of  $PM$ , observing the fuel film and pool fires in a optical GDI engine for different injection timings and how this parameter could affect the  $PM$  formation. In Figures 2.7 and 2.8, a laser-induced fluorescence (LIF) image is presented. The fuel film formed



**Figure 2.6.** Flame luminosity images, paired with simultaneous flood laser elastic scattering images.  $SOI = -90$  CAD ATDC. Image-capture times are listed between each pair of images. Source: Stevens et al. [38].

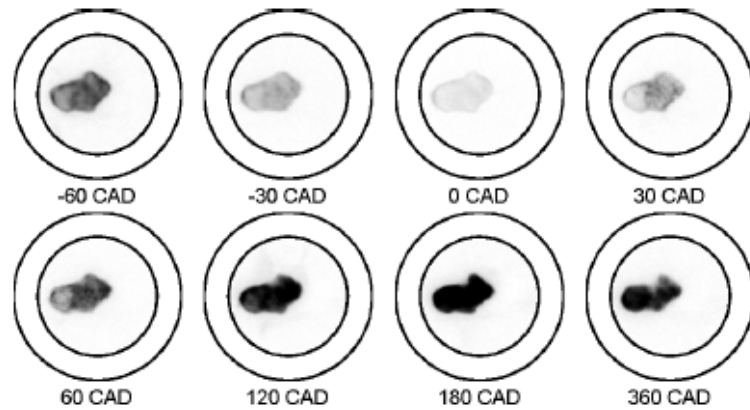
in the piston can be observed for a late start of injection (SOI)  $-90$  CAD ATDC and an early SOI  $-320$  CAD ATDC. Early injections tend to form less fuel film in the piston, therefore a lower generation of  $PM$  as Stevens et al. [38] demonstrated with Figure 2.9 where soot is recorded at 340 CAD ATDC, for different injection timings. This study correlates in a direct manner the quantity of fuel film in the piston with the quantity of  $PM$  formed. In Figure 2.10 a more representative plot of soot formation can be observed from a CFD simulation performed by Reaction Design, who develops and sells the ChemKin software package for modeling gas- and surface-phase chemistry, and cited in Stevens article [39].

### 2.2.3 Air management

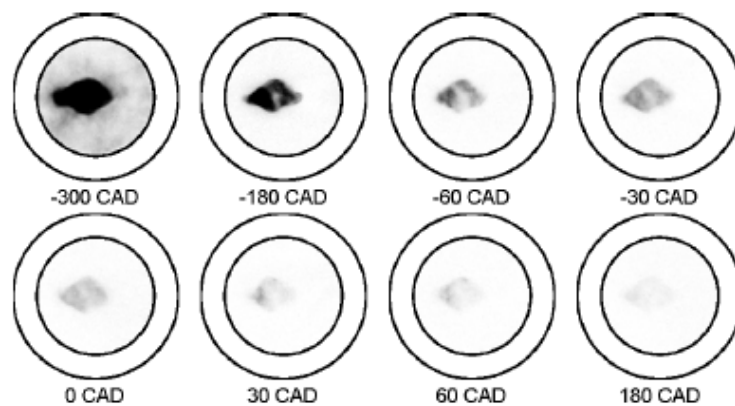
The air management in a SI gasoline engine implies the intake and exhaust systems, the exhaust gas recirculation system, the valve actuation system, and the boosting system in the case that the engine has forced induction.

#### 2.2.3.1 Intake system

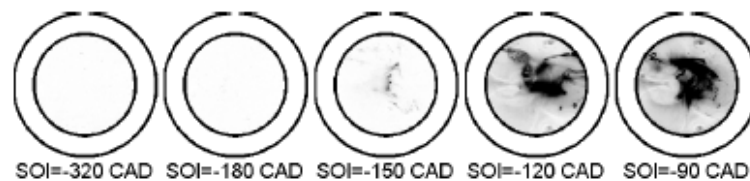
The intake manifold: it is a system designed to deliver air to the engine through pipes to each cylinder, called runners. On a SI gasoline engine, air flow rate through the intake manifold is controlled by a throttle plate (butterfly valve) usually located at the upstream end of the intake system. The throttle



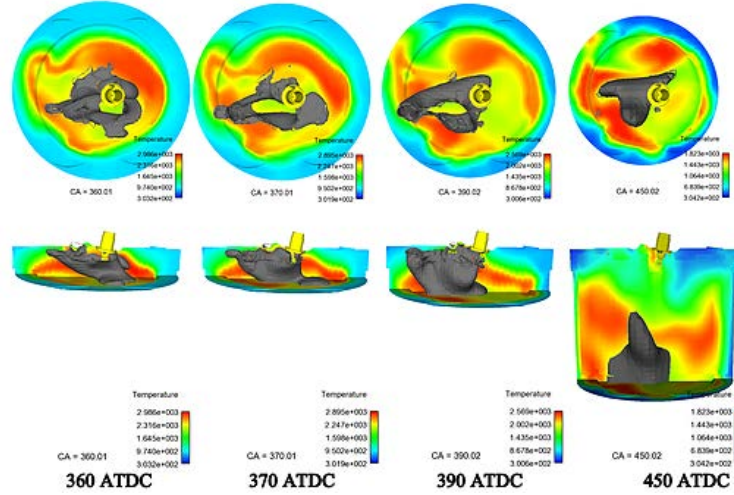
**Figure 2.7.** LIF from piston-top view for late injections ( $SOI = -90$  CAD ATDC). Source: Stevens et al. [38].



**Figure 2.8.** LIF from piston-top view for late injections ( $SOI = -90$  CAD ATDC). Source: Stevens et al. [38].



**Figure 2.9.** Planar laser elastic scattering signal from soot recorded at 340 CAD ATDC for various injection timings. Source: Stevens et al. [38].



**Figure 2.10.** Evolution of a soot cloud forming inside a GDI engine. Source: Steven [39].

plays a big role in the volumetric efficiency and thus the engine load and torque. The design and tuning of the intake manifold has a big influence on the volumetric efficiency curve of the engine. Depending of the engine goals, torque and power, the design of the intake manifold is focused in a different way. For example, in gasoline turbocharged engines a limited factor is the low end torque, which is a challenging task using turbines with fixed geometry. In this case the intake manifold is designed to increase the volumetric efficiency around the engine speed where the low end maximum torque should be. The engine used to perform the experiments of this thesis has an intake manifold tuned for 1750 – 2000 rpm where it has the maximum low end torque. On the other hand, if the engine torque and power goals are different the intake manifold should be designed to fulfill these goals.

Inter-cooler: in the case of having a gasoline engine with a turbocharger or supercharger, the air pressurized is heated during the process and it is mandatory to cool it down in order to reduce the knocking risks and increase the volumetric efficiency. Normally an air-to-air heat exchanger is used to reduce the intake temperature. In heavily downsized engines, water-to-air heat exchanger are being used, to further increase the inter-cooler efficiency and better control the intake temperature. These water-to-air inter-coolers usually use a low temperature water cooling system in order to control the intake



temperature [40]. The inter-cooler is usually placed between the turbocharger or supercharger and the throttle body.

Some gasoline and diesel applications are starting to use an integrated inter-cooler into the intake manifold, to reduce lag and improve packaging. In the research work of Lujan et al. [41] an integrated inter-cooler into the intake manifold is used for a diesel engine application.

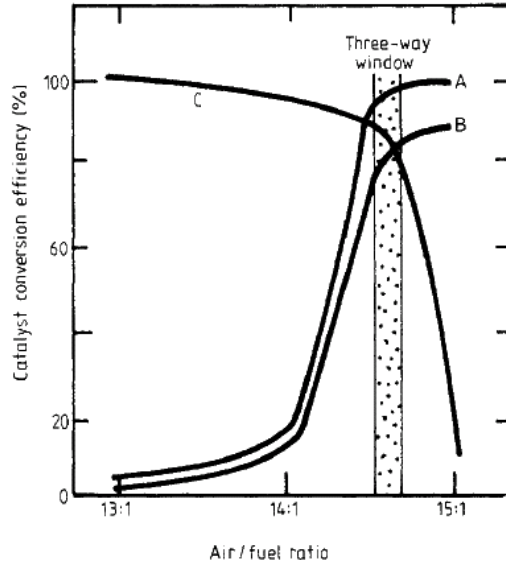
The inter-cooler used in this PhD-Thesis, it is a water-to-air exchanger, with a parallel low temperature water cooling system that it is going to be explained in Chapter 3, in order to control more precisely the intake air temperature to compare different conditions at the same intake temperature.

### 2.2.3.2 Exhaust system

The exhaust manifold: the exhaust gases created during the combustion leave the cylinder through the exhaust valves and the exhaust manifold, a piping system that directs the flow into one or more exhaust pipes. From the exhaust manifold, the gases flow through an exhaust pipe to the after-treatment system of the engine, which consists of a TWC, in some cases also  $NO_x$  trap, and in a near future a possible gasoline particle filter (GPF). The influence of the exhaust manifold design and tuning on the volumetric efficiency, and the shape of the engine torque is lower than in the case of the intake manifold but it is well known that it complements the design of the intake manifold.

In the case of a gasoline turbocharged engine, the design of the exhaust manifold depends on the turbine and the number of cylinders. In certain applications the exhaust manifold is integrated in the cylinder head, to help the cooling of the exhaust gases and reduce the enrichment strategy, in order to limit the temperature of the gases at the inlet of the turbine. For example, the exhaust manifold of the engine used in this PhD-Thesis, has a double metal sheet with air between them to isolate the exhaust gases, but the improved version of the engine has the exhaust manifold integrated into the cylinder head to help cooling the exhaust gases before the turbine.

After-treatment: the first and only after-treatment used in SI gasoline engines since 1975 is the catalytic converter. Started as a two-way catalyst that reduced  $CO$  and  $HC$  emissions, and in 1981 evolved into the three-way catalyst (TWC) that also reduce  $NO_x$  emissions. The TWC has been utilized for a long time because of its packaging, low cost and high conversion efficiency of  $NO_x$ ,  $CO$  and  $HC$  emissions. The TWC operates in an oscillating rich and lean mixture range around stoichiometric mixture conditions. When the

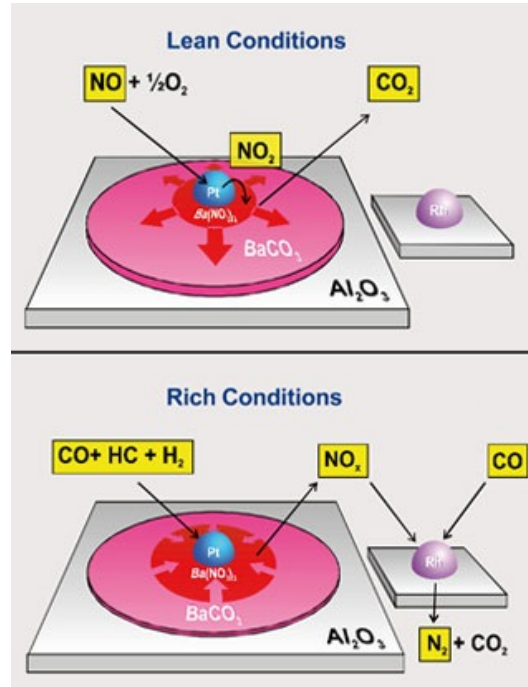


**Figure 2.11.** Three-way-catalyst conversion efficiency for different air-to-fuel ratios.

mixture is in rich conditions the  $NO_x$  is catalyzed and when the mixture is in lean conditions the  $HC$  and  $CO$  are catalyzed as it can be observed in Figure 2.11.

In the case of GDI engines that could operate with lean mixtures in certain area of the engine map, a two-way catalyst is used to catalyzed  $HC$  and  $CO$  emissions, and for the  $NO_x$  emissions treatment a  $NO_x$  trap has been mainly used for the past decade as it is a more cost effective solution for these vehicles than SCR system for  $NO_x$  [42]. In a  $NO_x$  trap, a  $NO_x$  storage component, usually an alkali or alkaline earth metal oxide, for example barium oxide, is added to the platinum and rhodium catalyst. Under normal lean conditions this stores  $NO_x$  as nitrate, as can be seen in the top picture of Figure 2.12. Then, every 60 – 120 seconds the nitrate regenerates when the engine runs on rich conditions in the stoichiometric range, so that some  $CO$  and  $HC$  can reduce the nitrate to harmless nitrogen as it is represented in the bottom picture of Figure 2.12.

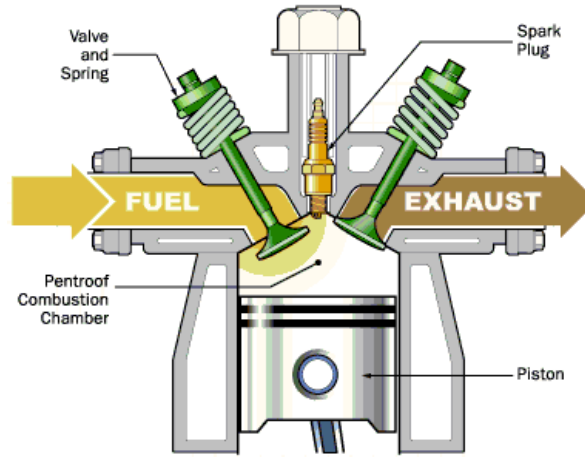
On the other hand, the new gasoline engine emissions regulations for the upcoming years, regulates more strictly the  $PM$  emissions, and for GDI engines this could be a major problem if a particle filter is not used as after-treatment. GPF are being developed for GDI engines, to be used in the near



**Figure 2.12.** Representation of  $\text{NO}_x$  trap reactions on lean and rich conditions.

future [43]. With current market technology the filtration efficiency is between 76% and 82%, depending of the homologation cycle. This values have been reported by Chan et al [44] in their research work.

Exhaust gas recirculation system: in many automobile atmospheric engines, some exhaust gas is recycled into the intake system to dilute the incoming air. Up to 20% to 30% of the exhaust gases will be diverted back into the intake manifold, depending on how the engine is being operated. Not only does this exhaust gas displace some incoming air, but it also heats the incoming air and lowers its density, both of these interactions lower the volumetric efficiency of the engine. On the other hand, on turbocharged gasoline engines the EGR is a technology that has not arrived yet to commercial vehicles; it is still in development. For this reason, the gasoline turbocharged engine used in this PhD-Thesis has a custom made low pressure cooled EGR loop. This system is composed normally by a heat exchanger and a valve that regulates the EGR flow. One of the main challenges of implementing a EGR loop, is the packaging and the interaction with other engine components. A more detailed



*Figure 2.13. Pent-roof cylinder head.*

explanation of the different configurations and benefits of the EGR are going to be explained later in Section 2.3.6.

### 2.2.3.3 Valve actuation system

In SI gasoline engines is common to use a bend roof architecture on the cylinder head chamber and thus the intake and exhaust valves are commonly in a certain angle respect to the vertical plane of the cylinder head as it can be seen in Figure 2.13. There have been different technologies on the last few years with the main purpose of changing de duration and lift of the valve profile, in order to optimize the engine thermal efficiency and exhaust emissions in different engine speed and load conditions.

Some of the important and commercial methods to implement a variable valve control are mentioned below:

- **Cam switching:** This method uses two cam profiles, with an actuator to swap between the profiles (usually at a specific engine speed). Cam switching can also provide variable valve lift and variable duration, however the adjustment is discrete rather than continuous.

The first production use of this system was Honda's VTEC system. VTEC changes hydraulic pressure to actuate a pin that locks the high

lift, high duration rocker arm to an adjacent low lift, low duration rocker arm(s) [45].

- Cam phasing: Many production VVT systems use this method, using a device known as a variator. This allows continuous adjustment of the cam timing (although many early systems only used discrete adjustment), however the duration and lift cannot be adjusted. This type of method is the one used in the engine that was used for the test of this PhD-Thesis and in the research work of Watanabe et al. [46] .
- Oscillating cam: These designs use an oscillating or rocking motion in a part cam lobe, which acts on a follower. This follower then opens and closes the valve. Some oscillating cam systems use a conventional cam lobe, while others use an eccentric cam lobe and a connecting rod. The principle is similar to steam engines, where the amount of steam entering the cylinder was regulated by the steam “cut-off” point.


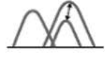

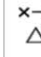
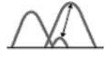
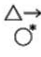

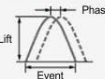
The advantage of this design is that adjustment of lift and duration is continuous. However in these systems, lift is proportional to duration, so lift and duration cannot be separately adjusted. The BMW (valvetronic) [47], Nissan (VVEL) [48], and Toyota (valvematic) [49] oscillating cam systems act on the intake valves only.

- Eccentric cam drive: this system operates through an eccentric disc mechanism which slows and speeds up the angular speed of the cam lobe during its rotation. Arranging the lobe to slow during its open period is equivalent to lengthening its duration.

The advantage of this system is that duration can be varied independent of lift [50] (however this system does not vary lift). The drawback is two eccentric drives and controllers are needed for each cylinder (one for the intake valves and one for the exhaust valves), which increases complexity and cost. MG Rover is the only manufacturer that has released engines using this system.

- Cam-less: Engine designs which do not rely on a camshaft to operate the valves have greater flexibility in achieving variable valve timing and variable valve lift. However, there has not been a production cam-less engine released for road vehicles as yet, but there are quite a few research studies using a cam-less engine [51, 52].

In Figure 2.14 a summary of the variable valve actuation systems is presented, in order to fully understand the advantages and disadvantage of each system.

Type		Valve lift characteristics	Phase	Lift	Event	Deactivation	Continuous control	Engine performance	Installation	Cost
With cam	Valve timing control		○	×	×	×	○	Low	Good	Low
	Cam switching			○	○	○		↓	↑	↑
	Variable valve event and lift control			○	○	○	○			
Without cam	Hydraulic or electromagnetic drive		○	○	○	○	High			
* Additional functions made possible by combining with valve timing control.										
<b>Legend:</b> ○ Possible △ Partially possible × Not possible										
										

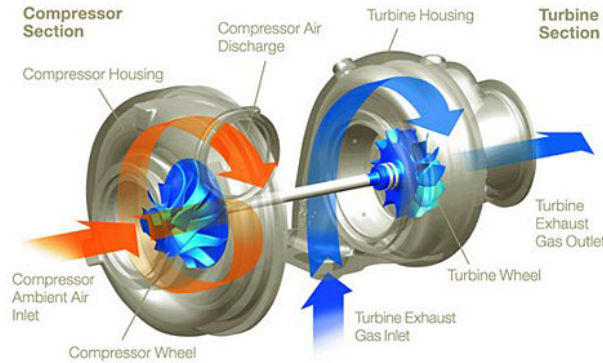
**Figure 2.14.** VVA systems summary. Source: Hara et al. [53].

#### 2.2.3.4 Supercharging and turbo-charging

Superchargers and turbochargers are compressors mounted in the intake system and used to raise the pressure of the incoming air. The turbocharger uses the exhaust gases energy to conduct a turbine, placed into the exhaust manifold, that connected with an axle to a compressor, placed upstream the throttle valve on the intake system, increases the pressure of the incoming air, as can be pictured in Figure 2.15. On the other hand superchargers are mechanically driven by the engine using belts, chains, shafts or gears in order to increase the intake air pressure.

Turbochargers are widely used in car and commercial vehicles because it allows smaller-capacity engine with improved fuel economy, reduce emissions and higher power and torque compared to superchargers which uses the engine power to pressurize the intake air, increasing the fuel consumption and the exhaust emissions. Although there are some commercial gasoline engines that use both components in order to provide a good throttle response and low end torque (advantages of supercharger) without compromising the power at high engine speed (bigger turbocharger), a clear example is the 1.4 l TFSI engine of Volkswagen, also mentioned before on the introduction.

In the case of new heavily downsized engines, some applications in the research and development area have been using electrical compressors to be



*Figure 2.15. Turbocharger.*

able to use a bigger turbocharger for high power and compensate at low engine speeds and transients.

The turbochargers are usually used in a single configuration in the majority of the engines, although in some applications a twin-turbo configuration is required to fulfill the torque and power goals of the engine, as for example the new Nissan GTR V6 bi-turbo or the new Porsche 911 Carrera twin-turbo. In the case of a twin-turbo, both turbochargers are in parallel, both fed one-half of the engine's exhaust and operate at the same time. And in the case of a two-stage turbocharging system, both turbochargers are in sequence, one turbocharger operates at low engine speeds and the second operates at a predetermined higher engine speed and load.

The engine that was used to perform the tests of the presented PhD-Thesis uses a single stage turbo-charging configuration. Further detail for better understanding of the background on turbocharger configurations and literature review can be found in Varnier PhD-Thesis [54].

## 2.3 Strategies to reduce fuel consumption in SI gasoline engines

Since the last decade, one of the main concerns of automotive industry is to reduce the fuel consumption of their engines. More specifically, in gasoline engines has been one of the main goals since exhaust emissions are been controlled by the well-known and mentioned TWC.

Several strategies and methodologies have been developed on the last years in order to reduce the fuel consumption of gasoline engines. Some of them are going to be involved in this PhD-Thesis and are going to be explained in more detail in the following sub-sections.

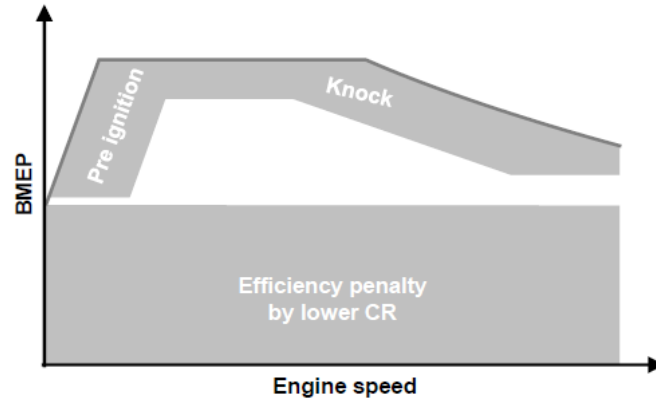
### 2.3.1 Downsizing

Engine downsizing is the use of a smaller displacement engine that provides similar torque and power of a larger one. Many manufacturers are reducing the number of cylinders, and by adding a boosting system, they compensate the loss in engine size. This strategy is being applied since the early 2000's when Volkswagen replace the 1.6 l and 2.0 l atmospheric engines with the 1.4 TFSI engine already mentioned before. Recently Ford launched the three-cylinder 1.0 l EcoBoost engine to replace the 1.6 l atmospheric engine. Also the 2.0 l engine used in this PhD-Thesis is a replacement of a V6 3.5 l atmospheric engine.

The fuel consumption reduction achieved by using this strategy depends of the downsizing magnitude. There have been some studies comparing a downsized engine with the replaced engine. In the case of the research work performed by Turner et al. [55] they claimed to achieve almost 35% of reduction in engine fuel consumption in a NEDC cycle. Turner et al. replaced a 5.0 l V8 engine with a 4 cylinder 2.0 l turbocharged engine. In other cases the reduction in engine fuel consumption is lower since it depends on the downsizing magnitude as mentioned before. In the research work of Coltman et al. [56] they replace a 2.2 l 4 cylinder naturally aspirated engine with a 1.5 l 3 cylinder turbocharged engine. They managed to reduce in 20% the engine fuel consumption in a NEDC cycle and improved the 0 – 100 km/h time by more than 1 second.

Low  $CO_2$  emissions can be achieved by downsizing, which is a clear industry direction with increasing degrees of downsizing being implemented as mentioned before. However, extreme downsizing requires operation at relatively high engine load to be effective, and this brings issues with driveability, combustion variability and fuel enrichment for component protection. Furthermore, if the number of cylinders is not reduced, the architecture potentially forms a type of barrier to the engine (since the bore size and thus the valve and injector packaging may become a challenging task). In Figure 2.16 a basic engine map representation with simplified areas for the downsizing main challenges is presented.





*Figure 2.16. Challenges on a boosted downsized engine. Source: Glahn et al. [40].*

The drive-ability issues can be addressed by advanced charging strategies, for example, sequential turbocharging or supercharger with a turbocharger, as it was explained before in the turbocharger section, variable geometry compressors [57] or turbines [58], or electrically driven compressors [59, 60]. But all these adds cost and complexity of the overall powertrain system. Against this, a fixed geometry turbocharger offers significant advantages in terms of bill of materials and control issues.

The knocking problems and high exhaust temperature can be mitigated by using direct injection, cooled EGR, variable compression ratio (VCR), VVT systems and many other strategies and methodologies that are being developed nowadays.

### 2.3.2 Direct injection

Direct injection (DI), as it was stated in the introduction, was used in the early airplane engines during the world war. In automotive SI gasoline engines, it is being used since the late 90's and early 2000's. It was in the Japanese market that appeared the first passenger car using an electronic direct injection gasoline engine, produced by Mitsubishi in 1996, followed then by Nissan, Toyota and some other companies in the early 2000's.

When the fuel is injected directly into the cylinder, it decreases the cylinder temperature by absorbing the heat inside the cylinder needed to evaporate the fuel. The effect of reducing the cylinder temperature is higher in a DI system

than a PFI system where the fuel is injected in the port of the intake manifold and it absorbs the heat of the cylinder head port and intake manifold.

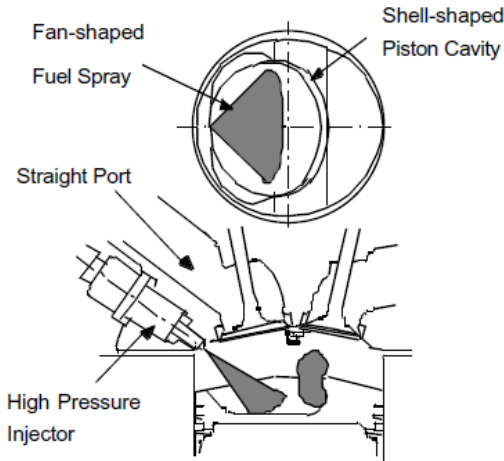
By reducing the cylinder temperature with a DI system, the compression ratio of the engine can be increased with less knocking risks than in the PFI version. There are some good examples on modern GDI or GTDI engines that are nowadays on the market, where it can be seen that all of them have higher compression ratio than the SI gasoline engines of the PFI era. Toyota has reported 13 : 1 compressions ratio in 2010 on their Prius engine [61] and Mazda recently declared a 14 : 1 compression ratio in their SkyActiv-G engines series; both of them are atmospheric engines. In the case of turbocharged DI engines the compression ratio is lower than an atmospheric engine but with DI systems also installed in these engines the compression ratios are higher than 10 : 1 in most of the applications [46].

Another unique advantage when using DI systems is the possibility to operate with a stratified charge. Normally in PFI systems the injection is performed before the IVO or during the intake stroke, in DI systems the normal injection timing is during the intake stroke, to maximize the effect of cylinder cooling and increase the volumetric efficiency of the engine [62]. In the case of the PFI the mixture will be homogeneous and in DI is not fully homogeneous as Knop et al. [62] could described in their work, where they observed the mixture heterogeneity even when early injection strategies and fluid motion was fully optimized.

The concept of stratified charge is based on the so-called wall-guide combustion method, in which fuel is directly injected during the compression stroke from a fan-spray- type, high-pressure injector into the cylinder, and the resultant combustible mixture is condensed around the spark plug [63], as can be seen in Figure 2.17. This concept is basically used to increase the lean misfire range of the engine when operates with lean mixtures at low loads.

In terms of exhaust emissions DI has some disadvantages compared to PFI. Knop et al. [62] compared a PFI and DI system in a turbocharged engine, obtaining more *CO* emissions for the DI system, due to the mixture heterogeneity mentioned before an the piston and cylinder wall wetting. Other studies have also confirmed the higher formation of *PM* emissions when using DI [64, 65] since PFI uses a pre-mixed combustion process which produces negligible levels of *PM*, particularly with modern PFI engines which provide excellent mixture quality.

Vehicle technology development and upcoming *PM* emission limits have increased the need for detailed analyses of *PM* emissions of vehicles using GDI techniques, and in general modern gasoline vehicles can emit four distinctive



**Figure 2.17.** Wall-guided combustion method. Fuel spray and piston configuration. Source: Mori et al. [63].

types of exhaust particles. The differences in particle characteristics and formation should be taken into account in the development of emission control strategies and technologies and, on the other hand, in the assessment of the impact of particle emissions on environment and human health [66]. Future European (Euro 6) and US emissions standards, that were mentioned in the introduction, will include more stringent *PM* limits for gasoline engines to protect against increases in airborne particulate levels due to the more widespread use of GDI engines.

There have been some studies in the recent years to reduce the *PM* emissions in GDI engines. Whitaker et al. [64] proposed a multiple injection strategy to avoid the wall wetting as much as possible, and reduce the amount of *PM* formed and the potential for a turbocharged GTDI engine to meet the proposed Euro 6 *PM* standard without using a particulate filter is demonstrated. Price et al. [65] showed a methodology to measure the *PM* emissions during cold starts in the new generation of GDI engines and the parameters that influence the formation of *PM*. They claimed to reduce the number of *PM* emissions by an order of magnitude during a  $-10^{\circ}\text{C}$  cold start by increasing the temperature of the cooling system.

GDI engines are a key enabler to reducing  $\text{CO}_2$  emissions and improving the fuel economy of light-duty vehicles, but *PM* emissions have to be reduced in order to limit the impact to the human health and environment.

### 2.3.3 Variable valve timing

This technology permits the SI gasoline engines to be more versatile in all the different operating conditions. Nowadays it is a must for the downsized engines to have a VVT system in order to fully optimize the fuel consumption in all the different areas of the operating map, for example:

- High load and low engine speed: the VVT system is used to increase the scavenging of the engine, increasing the overlap of the valves, to increase the volumetric efficiency of the engine and reduce the internal gas recirculation (IGR) reducing the risk of knocking, allowing the combustion to be phased in a more optimum crank angle, also reducing the fuel consumption. In addition to the increase of the overlap, the intake valve can be retarded to decrease the engine dynamic compression ratio, reduce the risk of knocking and helps the turbocharger to spool.
- High load and high engine speed: since the downsized engines are generally using turbochargers with fixed geometry turbines, the turbocharger is designed to deliver good boost pressure at low engine speed (1600–1750 *rpm*) and therefore the turbine is too small to achieve good efficiency at high engine speeds producing a high back pressure. In this case the overlap it is completely reduced to limit any back-flow of the exhaust to the intake port or cylinder and minimize the amount of IGR to reduce risk of knocking and improve the phasing of the combustion. That also decreases the amount of enrichment needed to control the exhaust gas temperature at the turbine inlet.
- Part load: in this operating range the VVT settings depend on the engine downsizing level. As a general approach this range is around the atmospheric full load curve of the engine. In this case the VVT system it is used to optimize the fuel consumption, engine response and engine warm-up. In cases of high downsizing level, this range is still on the boosted zone, and a similar approach, as explained before on the high load and low engine speed operating range, is taken.
- Low load: as it was mentioned in part load, the main objective is to optimize the fuel consumption, the engine response and the engine warm-up. But in these operating conditions, the SI gasoline engines still have some disadvantages in fuel consumption compared to diesel engines, because of the throttling methodology implemented to control the air mass flow, reducing the intake pressure and therefore increasing the pumping losses. This can be mitigated by using different strategy

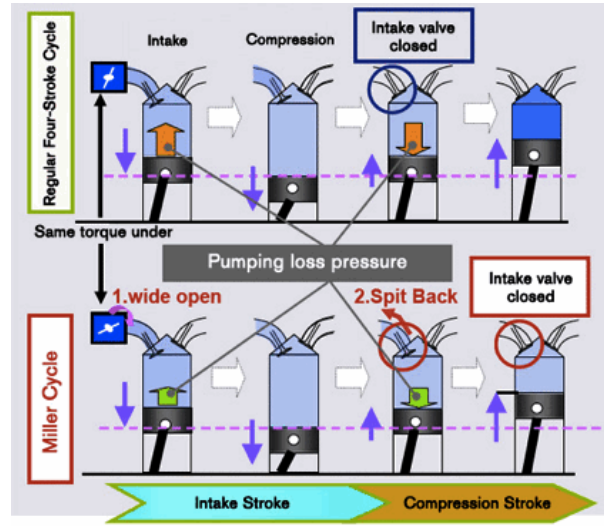


Figure 2.18. Miller cycle representation.

known as Atkinson and Miller cycle, which is going to be explained the next two sub-sections, taking advantage of a VVT system.

### 2.3.3.1 Miller cycle

A traditional SI gasoline engine has 4-strokes. When Miller cycle is adopted, it splits the compression stroke into two parts with a LIVC. In effect, the compression stroke is performed in two discrete phases: the initial portion when the intake valve is open and final portion when the intake valve is closed. This two-stage intake stroke creates the so-called 5<sup>th</sup> stroke that the Miller cycle introduces; a detailed representation can be seen in Figure 2.18

As the piston initially moves upwards in what is traditionally the compression stroke, the charge is partially expelled back out through the still-open intake valve. Typically this loss of charge air would result in a loss of power. However, in the Miller cycle, this is compensated by opening the throttle or increasing the pressure of the intake manifold using a compressor, a turbocharger or tuning the pressure waves to have resonance at this part of the cycle at high engine speeds. In recent years the EIVC is also called Miller cycle, because the intake stroke is split into two parts, having two discrete phases: the initial portion when the intake valve is open and the final portion

when the intake valve is closed. In some studies the definition of “Miller cycle” is not well used and it is confused with the Atkinson cycle.

Nowadays in the downsizing era of the SI gasoline engines, where the engines are typically equipped with VVT systems on the intake and exhaust valves, Miller cycle can be implemented to further minimize the fuel consumption. Several studies have been performed in this area, showing a reduction of fuel consumption of 7% to 11%, depending on the engine and operating conditions tested. Li et al. [67] studied the potential of using a Miller cycle at high load with the EIVC and the LIVC strategy, obtaining a reduction of 11% on the indicated specific fuel consumption of the engine using the EIVC strategy. In the case of Miklanek et al. [68], they compared the reduction in fuel consumption using a Miller Cycle via 1D simulation, observing a significant fuel economy improvement compared to the Otto cycle, especially due to the application of the Miller cycle.

In this PhD-Thesis, a LIVC strategy was used at part load together with an EEVC, to further minimize the fuel consumption when introducing cooled EGR to the engine.

### 2.3.3.2 Atkinson cycle

The original Atkinson cycle was based in an engine invented by James Atkinson in 1882. The Atkinson cycle is designed to provide efficiency at the expense of power density. The original Atkinson cycle piston engine allowed the intake, compression, power, and exhaust strokes of the four-stroke cycle to occur in a single turn of the crankshaft. Due to the unique crankshaft design of the Atkinson, its expansion ratio can differ from its compression ratio and, with a power stroke longer than its compression stroke, the engine can achieve greater thermal efficiency than a traditional piston engine. While Atkinson’s original design is no more than a historical curiosity, many modern engines use unconventional valve timing to produce the effect of a shorter compression stroke/longer power stroke, thus realizing the fuel economy improvements the Atkinson cycle can provide. In SI gasoline engines the Atkinson cycle has the same roots as the Miller cycle but at intake conditions below the atmospheric pressure.

In the last years some studies have been performed in order to fully understand the Atkinson cycle potential in SI gasoline engines. Many of these studies make reference to a Miller cycle when it is really an Atkinson cycle because the LIVC is used to optimize the engine efficiency between low and part load. França [69], studied a LIVC strategy at low load and observed

an improvement of 2% on the thermal efficiency of the engine compared to the original setup in a 4 cylinder gasoline engine. Wang et al. [70] studied the potential of using a LIVC strategy at low loads with three different fuels, obtaining 6.9% of fuel consumption reduction at 7.5 bar of IMEP at 1500 rpm with gasoline, but when using 2.5-Dimethylfuran or bio-ethanol the improvement was not evident.

In some operating conditions at low load, it is a balance between the fuel consumption optimization and the engine warm-up time. In recent SI gasoline engines a different VVT settings are used depending on the engine coolant temperature, in order to warm-up the engine fast and minimize the fuel consumption while operating in cold and hot conditions.

#### 2.3.4 Variable compression ratio

The VCR technology is indeed used to modify the compression ratio of the engine while it is running. This is done to increase the thermal efficiency of the engine; at high loads the compression ratio needed is lower than at part and low loads in order to fully minimize the fuel consumption of the engine.

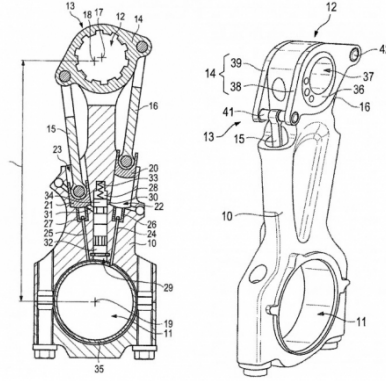
For an ideal Otto-cycle, the theoretical efficiency is given by,

$$\eta = 1 - \left(\frac{1}{r^{(\gamma-1)}}\right) \quad (2.7)$$

where  $r$  is the compression ratio and  $\gamma$  is the ratio of specific heats. Theoretically, increasing the compression ratio of an engine can improve the thermal efficiency, as said before. But the compression ratio cannot be increased without taking into account the knocking risks of the engine at the different operating loads.

Harry Ricardo built and tested the first engine with a VCR system in 1920. After this invention many automotive companies have been doing their own research with no public results yet. Despite of that, there has been some companies that have published some results and performed some patents, in which Waulis Motor Ltd, Peugeot, Saab, Nissan, Porsche, FEV, and Gomecsys can be mentioned.

There are many different invented systems that can achieve the compression ratio variation during the engine operation. On the first group, the design is focused on changing the length of the rod or the height of the piston, as Porsche patent, the mechanism can be seen in Figure 2.19. In the second group, the main focus is to change the volume of the chamber, as the



**Figure 2.19.** Porsche patented variable compression ratio system.

Saab with their SVC engine presented in Genova motor show in 2000, that never reached the production line due to the company's bankruptcy. And on the third group, the VCR system design focus on changing the crankshaft geometry instead of the rod length.

During the past decades there have been several studies about the feasibility of a VCR system and the potential improvements on the engine thermal efficiency. De Bortoli Cassiani et al. [71] studied the different VCR systems until that year and evaluated the VCR potential via simulation. In the case of Roberts et al [72], they tested the potential of a VCR system at low loads and high loads, concluding that the fuel economy improvement was higher than other technologies such as cylinder deactivation, cam-less valve operation and GDI. A two stage VCR system was evaluated and compared with a fully VCR system by Kleeberg et al. [73], proving that an important reduction of fuel consumption can be achieved using this simplified 2-stage VCR system, between 5 – 7% depending on the driving cycle. And there is also more specific studies of new VCR systems design, as the work performed by Schwaderlapp et al. [74], where they design a variable compression ratio solution, featuring an eccentric movement of the crankshaft.

The VCR engines have great potential to increase engine power output and reduce fuel consumption, and when coupled with technologies such as turbocharging, VVT systems and direct injection, the effectiveness of the system is further increased. Once established, this technology will bring the SI gasoline engine into a new phase of development and thermal efficiency.



### 2.3.5 Lean burn

This strategy consists in using lean combustion operating conditions in a SI gasoline engine, instead of stoichiometric combustion conditions. This strategy has been in development for the last few decades. It was implemented in the late 70's and early 80's but with stringent emissions regulations some of these applications started to disappear because it was not a profitable technology since an oxidizer catalyst and a  $NO_x$  reduction system had to be used. It was in Japan that still existed some applications on the market until the late 90's and beginning of the 2000's. It was on the beginning of the 2000's when some application started to appear in Europe due to the introduction of the direct injection and therefore the stratified lean burn strategy, using a oxidizer catalyst and a  $NO_x$  reduction system on the exhaust as after-treatment.

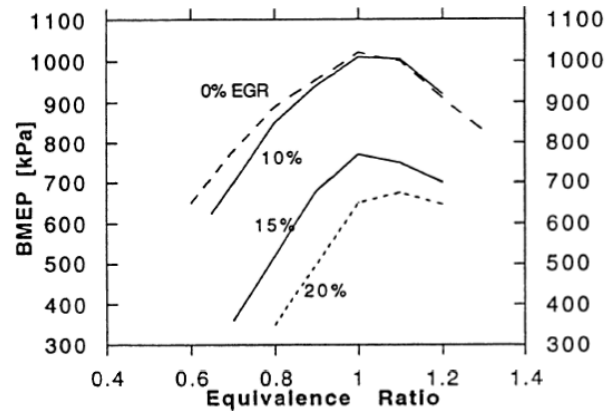
The lean burn strategy has a big difficulty to meet the emissions regulations without a proper after-treatment system. Since the engine operates in lean mixtures a TWC cannot be used, because as it is known, the TWC operates in a cyclic manner around the stoichiometric mixture, as explained before, decreasing its efficiency in a drastic way for the  $NO_x$  conversion if the mixture has excess of oxygen (lean mixtures), as it can be seen in Figure 2.11. Instead of using a TWC, a  $HC/CO$  oxidizer catalyst and a  $NO_x$  trap or SCR system of  $NO_x$  have to be used in order to comply with the emissions regulations.

There was an era where the emissions regulations were not as strict as nowadays and there were studies that analyzed the use of lean burn to meet  $HC$  and  $CO$  emissions regulations without using a oxidizer catalyst. One of those studies was performed by John J. [75] in 1975, where he analyzes the improvements of fuel economy using a lean burn strategy and declares that the use of this technology was dependent on federally regulated auto emissions standards of that era. As years passed and the emissions regulations were starting to restrict more the exhaust emissions of the engines, the trade-off started to happen and studies of advantages and disadvantages of the lean burn technology started to appear on the 80's. Among them, the work of Gomez and Reinke [76], where a summary of theoretical considerations that motivate the development of the lean burn strategy is presented along with a review of the most common approaches used to implement this technique at that time. The development continued. Hiroyuki et al. [77] in 1988 studied a high compression lean burn engine concept, observing a reduction in fuel consumption at that time of 10.5% on the Japanese 10-mode cycle, 8.3% on the ECE mode cycle, and 6.3% on the U.S. EPA test mode cycle while meeting respective emission standards.

In the 90's there were still multiple studies around the lean burn concept. In the case of Yu et al. [78] in 1995, they were already searching to expand the limits of lean misfire, in order to further decrease the fuel consumption and  $NO_x$  emissions, they managed to expand the lean burn misfire limit until 23 air-to-fuel ratio, achieving a reduction of 60.6% in  $NO_x$  emissions and a reduction of 10.6% on fuel consumption. In the late 90's a study of lean burn concept in SI gasoline turbocharged engines started to appear, and also its comparison with other popular strategy to reduce fuel consumption, the exhaust gas recirculation. Grandin and Angstrom [79] studied the potential of using a lean mixture to reduce the risks of knocking and the exhaust gas temperature, and compared it with the EGR strategy in a SI gasoline turbocharged engine. They found that the lean burn strategy reduced the  $HC$  and  $CO$  compared to the EGR strategy but with a disadvantage, because it is not possible to use the TWC on lean burn conditions and this penalizes the  $NO_x$  emissions on the tailpipe compared to an EGR strategy. So a reduction of  $HC$  and  $CO$  emissions for the cost of adding an extra after-treatment system that can reduce the  $NO_x$  emissions. Research work is still performed to further develop this strategy, Saito et al. [80] studied the expansion of the lean burn strategy range by increasing the tumble intensity in 2013, this generated a fuel consumption reduction of 5.7% compared to the base model.

As stated before the lean burn strategy offers a big advantage in the fuel consumption reduction of the engine. This reduction in fuel consumption is achieved by reducing the pumping losses and the heat transfer, and increasing the combustion efficiency, as some of these authors confirm [78, 80, 81]. It also reduces the  $HC$  and  $CO$  emissions as Grandin and Angstrom [79] described in their research work, but it is an important disadvantage that this strategy cannot use the TWC as an after-treatment system for the reasons explained before. On the near future,  $PM$  emissions regulation is going to force the implementation of a particle filter as an after-treatment system in some applications. In this case if the engine is going to be run with a lean burn strategy, it would certainly need a  $NO_x$  reduction system and this would probably complicate in a higher level the implementation of this strategy in future non-hybrid application.

In this PhD-Thesis a quick review of a lean burn strategy was performed, in order to compare the advantages and disadvantages to the EGR strategy and also analyzed the misfire range limits of the engine using lean burn and high diluted conditions. A deep analysis is going to be performed in order to fully understand the reasons of all the benefits that this strategy provides and its future potential.



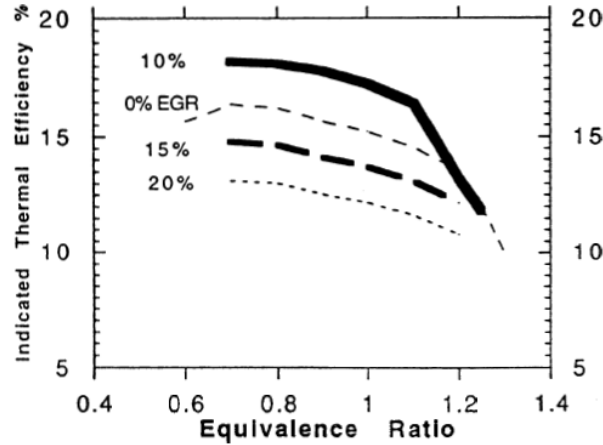
**Figure 2.20.** EGR rate and equivalence ratio influence over BMEP at full load conditions in a SI gasoline atmospheric engine. Source: Hacothen et al [82].

### 2.3.6 Cooled exhaust gas recirculation

This strategy consists in taking some amount of the exhaust gases and re-introduce them to the intake system together with the fresh air. This strategy has been very popular in diesel engines for many years to reduce  $NO_x$  emissions. In the case of the SI gasoline engine application, it offers more benefits than just the  $NO_x$  emissions reduction and therefore the interest of automotive companies in the implementation of this technology.

The EGR started to be used in SI gasoline engines in the 90's, and it was basically used to improve fuel consumption at low loads and reduce exhaust emissions. The EGR was not used at full load on atmospheric engines because it replaced part of the air mass in the cylinder, reducing the performance of the engine as Hacothen et al. [82] observed in their study. This can be observed in the Figure 2.20, where the brake mean effective pressure is plotted for different EGR rates with different equivalence ratio conditions. On the other hand, as mentioned before, the EGR was used to improve the fuel economy of the engine at low and part loads in atmospheric SI gasoline engines.

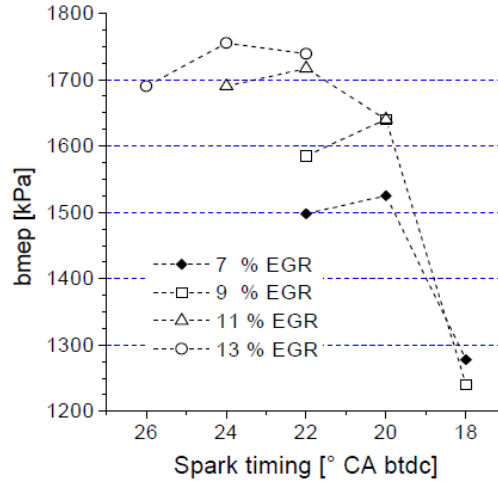
Hacothen et al. [82] also observed an important increase on the engine thermal efficiency when using 10% of EGR. The engine efficiency increased from 15% to more than 17% using stoichiometric conditions in the mixture and also with other equivalence ratio conditions. In Figure 2.21 it can be seen the engine thermal efficiency for different EGR rates and different equivalence ratio conditions. The improvement on the engine thermal efficiency at part



**Figure 2.21.** EGR rate and equivalence ratio influence the engine thermal efficiency at part load conditions in a SI gasoline atmospheric engine. Source: Hacothen et al [82]..

load conditions is due to the reduction of pumping losses and the increase of initial temperature at the closing of the intake valve. This leads to an increase of the reactivity of the mixture, improving the cycle-to-cycle variation and the combustion efficiency despite the dilution effect.

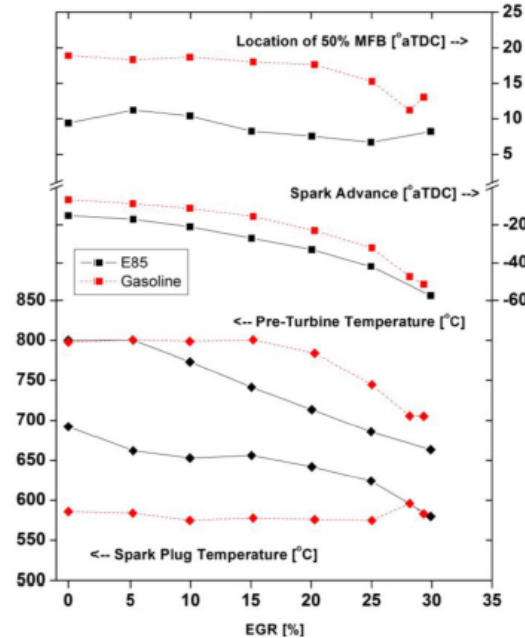
In the late 90's, EGR was starting to be used in turbocharged SI gasoline engines. In the early studies the EGR was cooled in order to reduce the mixture reactivity and the knocking risk of the engine. Grandin et al. [83] studied the effect of various amounts of EGR at different temperatures and ignition timings. They found considerable knock suppression using EGR at maximum power output comparable with what was achieved with fuel enrichment. In Figure 2.22 BMEP is plotted against ignition timing for different EGR rates at 4000 rpm and high load. It can be seen how increasing the EGR rate, the ignition timing could be advanced, due to the partial suppression of knocking, increasing the BMEP of the engine for the same conditions. The knocking risk reduction is based on the dilution effect of the EGR, which decreases the mixture reactivity and therefore the combustion temperature and the end gas temperature. Grandin et al. [83] also calculated the end gas temperature for different EGR rates showing that when the EGR rate is increased the end gas temperature decreases which reduces the risk of knocking.



**Figure 2.22.** EGR rate influence on the maximum possible ignition advance before knocking occurs and the impact on engine BMEP. Source: Grandin et al [83].

Turbocharged engines have been operated at rich air/fuel-ratios during high load conditions due to inherent high thermal loads. In most of the turbocharged engines the exhaust gas temperature is limited between  $930^{\circ}\text{C}$  and  $960^{\circ}\text{C}$ , this leads to enrich the mixture to reduce the exhaust gas temperature in the operating conditions that surpass limits at stoichiometric conditions. Grandin et al. [79, 83] demonstrated that adding cooled EGR, the exhaust temperature can be reduced and therefore the enrichment. The combustion temperature is reduced when EGR is added, as mentioned before, combined with the improved combustion phasing due to the partial suppression of knocking, leads to a reduction on the exhaust gas temperature. These results were also confirmed years later by different investigations reported in the literature [31, 84–87], where a reduction of knocking problems, enrichment strategies and fuel consumption was also observed when adding cooled EGR to a turbocharged SI gasoline engine.

The benefits of EGR are also present in the exhaust gas emissions. As Alger et al. [31] observed that using EGR helped reduce  $CO$ ,  $NO_x$  and  $PM$  while increasing  $HC$  emissions. Taking into account that the TWC efficiency is near the 99% conversion efficiency for  $HC$  emissions [88], the increase in  $HC$  emissions before the TWC are negligible at the tailpipe. The increase of  $HC$  emissions and the reduction of  $CO$ ,  $NO_x$  and  $PM$  emissions while adding EGR to the engine is related to the reduction of the combustion



**Figure 2.23.** EGR rate influence on the spark plug temperature with E85 and gasoline as fuels at 3000 rpm and 12.5bar BMEP. Source: Gukelberger et al. [93].

temperature, this was observed by Alger et al. [31, 89], Lujan et al. [90] and Kumano et al. [91] in their studies. This trend is obvious when the original operating conditions without EGR is at stoichiometric conditions but if the engine is using the enrichment strategy to control the exhaust gas temperature, adding EGR to eliminate the enrichment strategy permits to use the maximum conversion efficiency of the TWC reducing all emissions at the tailpipe [83, 86, 90].

Depending on the engine and the design of the cylinder head, ignition system, piston geometry, and injector position (in the case of the GDI engines), the operating range of EGR limit is different. In most of the studies the engine cannot withstand more than 20% to 25% of EGR [90, 92], in the other cases where the engine can withstand more than 35% of EGR an upgraded ignition system is needed [89]. Several studies have been performed to optimize the head cylinder design, compression ratio or piston geometry obtaining little to none improvement on the EGR misfire limit range [92].

As with lean mixtures, the engine operates in different in-cylinder temperature and pressure conditions when EGR is added, with more advance

combustion and higher compression ratios due to the increase on the knock tolerance. The spark plug temperature will also change and thus its optimum heat range compared to an engine without EGR. Gukelberger et al. [93] studied the influence of EGR rate on the temperature of the spark plug, reporting that engines with added EGR tend to increase the spark plug temperature in the operating condition where an enrichment strategy is eliminated. On the other hand, in engine conditions where the combustion is limited by knocking and the EGR permits to optimize the phasing of the combustion, the temperature of the spark plug tends to stay at the same value while increasing the EGR rate and the ignition advance. In this case there is the effect of increasing the spark plug temperature by advancing the combustion and the dilution effect of the EGR that decreases the spark temperature at the same time, balancing each other and maintaining the spark plug temperature at the same value as in non-diluted conditions. This behavior can be seen in Figure 2.23 for different EGR rates at 3000 rpm and 12.5 BMEP [93].

Figure 2.25 shows a summary of the principal reasons for the fuel consumption reduction when cooled EGR is used. These reasons were already explained above but it is presented in a schematic form so it can be better understood.

The EGR configuration used in the 90's and beginning of 2000's in atmospheric engines was an EGR loop that extracted the exhaust gas after or before the catalyst to reintroduce it in the intake manifold, as can be seen in Figure 2.24. With the introduction of turbocharged engine, the EGR loop configuration can have its advantages and disadvantages due to the three possible arrangements. The EGR can be performed with three different configurations in turbocharged engines: high pressure loop, low pressure loop and mixed pressure loop. In this PhD-Thesis a mixed and low pressure loop were analyzed to finally use a low pressure loop to perform the research work tests. In the following subsections the three different EGR loops configurations are going to be reviewed in order to have a solid base to support results that are going to be presented in the PhD-Thesis.

### 2.3.6.1 High pressure loop

This configuration has been very popular in the past decade thanks to the diesel engines. This configuration extracts the exhaust gas flow upstream the turbine inlet and introduces it at the intake manifold or upstream the throttle body but downstream the compressor outlet as it can be seen in the simplified Figure 2.26.

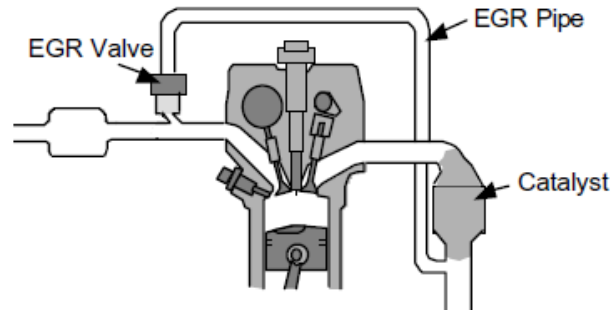


Figure 2.24. Schematic of EGR system. Source: Mori et al. [63].

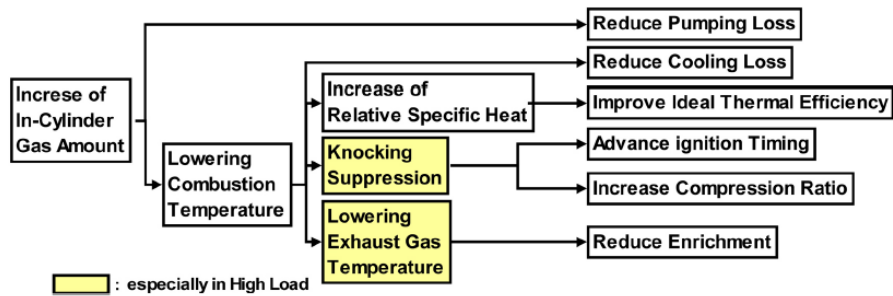


Figure 2.25. Schematic of EGR system. Source: Takaki et al. [94].

In order to supply sufficient EGR to an engine, a pressure difference is required at the EGR system junction between the exhaust and intake systems. Nowadays, turbocharger manufacturers are focused on improving the efficiency of both turbines and compressors. This is geared at making a HP EGR system feasible in a power-train system where the post-compressor pressure is close to or even greater than the pre-turbine pressure. These conditions can be achieved at low engine speeds and high load. In Figure 2.27 intake and exhaust pressure variations during one engine cycle are represented. At certain crank angle degrees, the intake pressure is higher than the exhaust pressure while the opposite is true at other crank angle degrees. In this case, it is difficult to provide an adequate EGR rate to an engine with HP EGR system even though the averaged exhaust pressure is barely or even slightly higher than the intake pressure.

This configuration reduces the flow through the turbine, reducing the turbine power. This also damages the low end torque that the engine can



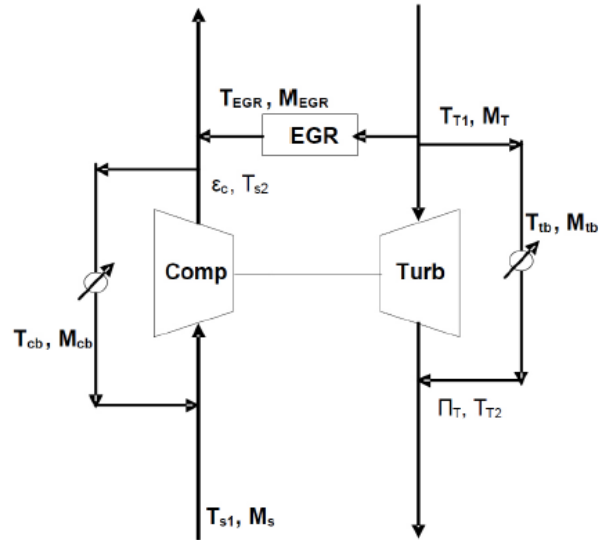


Figure 2.26. Schematic of HP EGR system. Source: Zhong et al. [95].

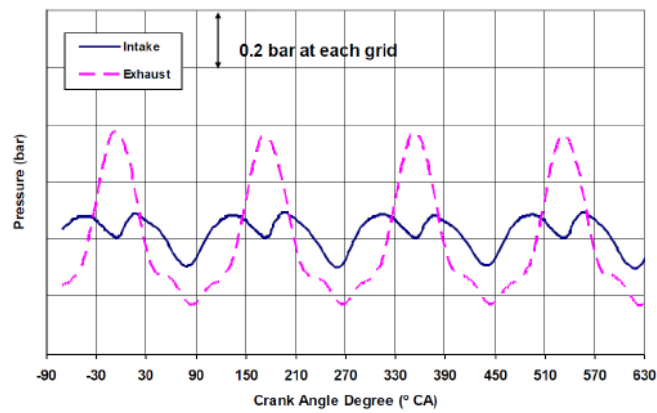


Figure 2.27. Intake manifold pressure and exhaust pressure with HP EGR system. Source: Zhong et al. [95].

produce due to the reduction of mass flow that passes through the turbine, reducing the amount of pressure that the turbocharger can produce. But at high engine speeds and high load the HP EGR loop reduces the pumping losses, compared to other configurations, by reducing the pressure on the exhaust manifold, as Glahn et al. observed in their research work [40].

This configuration compared to the other EGR configurations could have the most compact design. This also has an advantage on transient conditions, where the HP EGR configuration is the fastest to respond to engine load variations. Glahn et al. [40] observed a clear improvement on EGR response, compared to other configurations, when a HP EGR loop was used.

On the other hand, HP EGR configuration requires a high cooling power to reduce the EGR gas temperature, in some cases from 900 °C, to around 100 – 200 °C to avoid melting the intake manifold or the EGR valve. In SI downsized turbocharged gasoline engines, high intake temperatures need to be avoided in order to control the knocking, that is the main reason of using a low temperature cooling system for the EGR cooler when a HP EGR loop is used as Glahn et al. demonstrated in their research work [40].

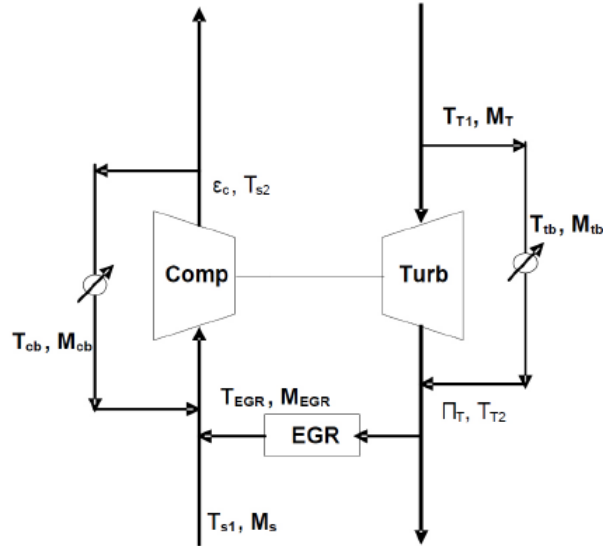
### 2.3.6.2 Low pressure loop

The LP EGR configuration has been also used lately by recent diesel engines and it has been in development for turbocharged SI gasoline engines. In this configuration the exhaust gas is extracted downstream the turbine, typically also downstream the catalyst outlet, and reintroduced upstream the compressor inlet, as it is represented in Figure 2.28.

The pressure difference that can be found in LP EGR configurations, between the exhaust system and the intake system, is lower than in HP configurations but enough to perform the necessary EGR rate, as it is stated in the work of Lujan et al. [90]. This configuration has the advantages over a HP configuration, because it can deliver EGR at low engine speeds and high loads, where the intake pressure is higher than the exhaust pressure, and reduce the fuel consumption. This advantage turns into a disadvantage during transient conditions because the EGR response is slower, and therefore the torque build up, than with a HP configuration [40].

Introducing the exhaust gas upstream the compressor has a big advantage on cooling power needed over the HP configuration, because it is enough to cool down the gas to 150 – 100 °C in order to protect the EGR valve and compressor. It is important to remark that the temperature of the exhaust gases at the inlet of the EGR line is significantly lower in the LP than in the HP configuration. The temperature of the mixture air/EGR downstream the inter-cooler is controlled. Therefore a LT cooling system is not necessary as in the case of a HP EGR configuration.

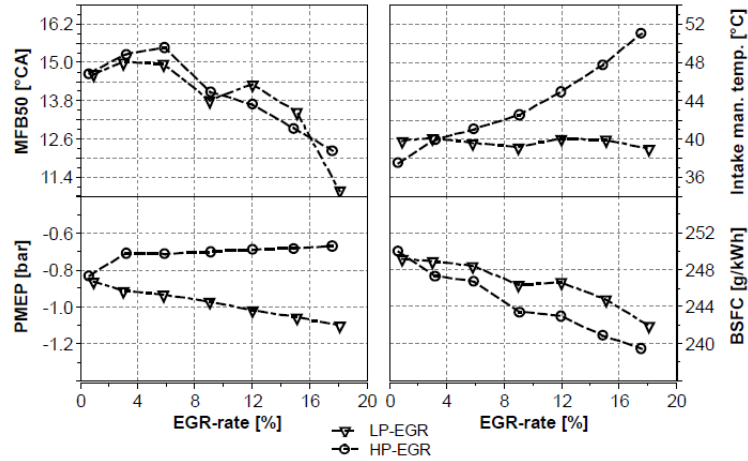
In this configuration the compressor has to compress the air plus the EGR, and in order to maintain the same amount of air mass flow than without EGR



**Figure 2.28.** Schematic of LP EGR system. Source: Zhong et al. [95].

the compressor has to increase the boost pressure, increasing the expansion pressure ratio in the turbine and therefore increasing the exhaust manifold pressure and pumping losses. In the case of the HP EGR configuration the compressor also needs to compensate by increasing the boost pressure to maintain the same air mass flow, but the quantity of exhaust gas that passes through the turbine are less than in the LP EGR configuration, due to the HP EGR recirculation, so the turbine pressure ratio is lower, decreasing the exhaust manifold pressure and pumping losses. This is explained in the research work of Glahn et al. [40], Zhong et al. [95] and Cairns et al. [84], and it can be seen in Figure 2.29, where it can be observed a comparison of the pumping losses (PMEP), crank angle of the 50% burned mass fraction (CA50), brake specific fuel consumption (BSFC) and intake manifold temperature of a HP and LP EGR configuration at 5000 rpm and 15 bar of BMEP, which corresponds to a high engine speed and high load.

In the case of the exhaust gas pick-up point for the LP configuration, it is also important, because it can be placed upstream or downstream the catalyst. There has been some confirmations in the research work of Takaki et al. [94], about preferably using the exhaust gas already treated, downstream the TWC, because the  $NO_x$  composition on the exhaust gas has a negative impact on the knocking limits of the engine. This is also an advantage of using LP EGR



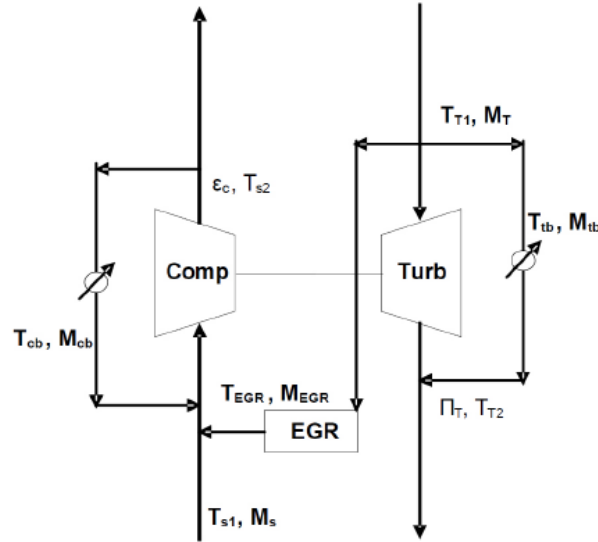
**Figure 2.29.** CA50, PMEP, BSFC and intake manifold temperature comparison of a HP and LP EGR configuration at 50000 rpm and 15 bar of BMEP. Source: Glahn et al. [40].

configurations compared to a HP configuration, because the exhaust gas can be picked downstream the catalyst with less  $NO_x$  concentration than in the HP configuration.

### 2.3.6.3 Mixed pressure loop

The mixed EGR configuration is a combination of the LP and HP EGR configurations. Some authors like to also name it as middle pressure EGR loop, because the exhaust gas is extracted upstream the turbine (as the HP configuration) and reintroduced upstream the compressor (as the LP configuration), this can be seen in Figure 2.30. As first approach it seems that this configuration could be the best trade-off between the HP and LP EGR configuration but it also has some disadvantages of the HP configuration and some of the LP configuration.

The problem of HP configuration exhaust/intake pressure difference at low engine speed and high load is solved reintroducing the exhaust gas upstream the compressor. But it will still have a limited operating range at low engine speed and high load because a portion of the exhaust gas is extracted before the turbine, leaving the turbine with less energy available, decreasing the maximum possible torque at low engine speed, as Takaki et al. also observed in their research work [94]. In terms of cooling power, it is between the



**Figure 2.30.** Schematic of Mixed EGR system. Source: Zhong et al. [95].

HP and LP configuration because the final exhaust gas temperature has to be the same as in the LP configuration but the extracted exhaust gas in the mixed configuration are hotter than the LP configuration, increasing the cooling power needed. But since the final exhaust gas temperature can be higher than with the HP configuration, the needed cooling power of the mixed configuration is lower than the HP configuration.

It presents, at high speed and high load, the same advantage as the HP configuration in terms of pumping losses, as it is mentioned by Glahn et al [40]. In the case of the exhaust composition, it has the same disadvantages as the HP configuration, compared to the LP configuration, because the exhaust gas is not treated before reintroducing it to the engine. At the same time the mixed configuration has the same disadvantage as the LP configuration in transient conditions (it will hardly depend on the packaging) which has more EGR retard as the HP configuration as explained before. In the Table 2.1 a brief summary is presented of the different EGR configuration advantages and disadvantages.

Taking into account all these factors described before, there is non optimum or best EGR configuration. It depends on the application, the main target and the limitations that the application could have. In this case, for this Phd-thesis, a LP EGR configuration was chosen to maximize the EGR operating

Conditions	HP loop	LP loop	Mixed loop
Operating Range	-	++	+
Transient Response	-	--	--
Pumping Losses Reduction	++	+	++
Colling Power	---	-	--
Knocking Mitigation	+	++	+
Exhaust Gas Temperature Reduction	+	++	+
BSFC Low rpm	+	++	+
BSFC High rpm	++	+	++

**Table 2.1.** EGR configuration comparison.

range on the engine map at low engine speed and high load, and because the main target was steady state tests and optimization before 3000 rpm. These conditions suited perfectly the LP configuration main advantages over the other two configurations.

## 2.4 Summary and conclusions

In the Chapter 2, a literature review of 4-stroke gasoline engines state of the art was presented and how new strategies and technologies are being applied to reduce fuel consumption. At the same time an analysis of these new technologies has been performed to classify them and identify the main strategies in which the effort and resources must be concentrated in the near future.

The gasoline engine is going through a complex process of development and optimization. As it was stated, new exhaust emission regulations,  $CO_2$  atmosphere concentrations and oil future prices are the main reasons for this high rate evolution of gasoline engines.

The combustion process for these engines has not changed since the invention of these engines. The main phases are the ignition, propagation and flame termination. The ignition process is affected by the mixture reactivity around the spark plug (that implies: temperature, density and oxygen concentration), the energy of the ignition system and the gap of the spark plug. If one of these mentioned factors is affected, the first phase of the combustion is going to be worst, which could lead to more cycle to cycle variation and even misfire.

The turbulent propagation is also affected by the mixture reactivity, kernel size (the first phase of the combustion), and turbulence inside the cylinder. Decreasing either one of these factors would reduce the combustion flame speed thus the combustion duration would be longer and depending on the operating conditions this could be an advantage or a disadvantage.

Finally, on the flame termination, the previous two combustion phases play a big role in this phase, but also the mixture reactivity, the fuel film on the piston and cylinder walls, and the wall temperature of the piston, cylinder wall and chamber. This phase of the combustion could determine the production of *HC*, *CO* and *PM* emissions. These main combustion phases must be understood in order to explore further the development of gasoline engines and understand the trade-off with the exhaust emissions.

The understanding of the formation of exhaust emissions is also important in order to understand the meaning and reason of exhaust emission outputs, when different strategies or technologies are applied to optimize the thermal efficiency of gasoline engines. The formation of un-burned *HC* are mainly driven by combustion temperatures and mixture oxygen concentration, so the strategies or technologies that affect these main parameters are going to increase or decrease the production of *HC* emissions. In the case of *CO* emissions, the main factors are the same as in *HC* emissions.

Concerning *NO<sub>x</sub>* emissions the main influence for its production is combustion temperature and also oxygen concentration. High combustion temperatures produce high amounts of *NO<sub>x</sub>* emissions and the same as high oxygen concentrations. In Section 2.2.2.2 and Figure 2.4, it can be observed the combustion temperature region and equivalence ratio of the mixture where *NO<sub>x</sub>* emissions are formed. Using the same diagram, the region of combustion temperature and equivalence ratio of the mixture where *PM* emissions are formed is also observed. The main reason for *PM* formation in GDI engines is the piston and cylinder wall wetting.

Taking into account the basic information of the combustion process and exhaust emissions formation a simply analysis can be performed on the different strategies and technologies that are being developed nowadays to increase the thermal efficiency of gasoline engines. A review of the most important and potentially superior technologies and methodologies to reduce the fuel consumption on gasoline engines was presented in Section 2.3.

The downsizing is the main strategy that is driving the development process of the gasoline engine and because of it, other strategies and technologies are being developed to work in synergy with downsized engines or to solve limitations of these new gasoline engines. The downsizing basically

consists in reducing the engine displacement and compensating this loss in displacement by adding a forced induction system. This leads in general to smaller engines, less cylinders, and more complex designs. The main factors that help reduce the fuel consumption are the reduction in friction losses and pumping losses. But since the engine is smaller, the amount of load is higher to produce the same performance as the larger engine that it is replaced, and because of the type of combustion and the restricted octane number of the fuel, these engines cylinder head, geometry, piston and turbulence have to be optimized in order to avoid autoignition at high engine loads. This would obviously limit the compression ratio of the engine and therefore the fuel consumption reduction at low/part load is a compromise with high load performance. This was also a problem in the last gasoline engines, but when a downsizing strategy is applied, the problems at high load are maximized. Other technologies as direct injection or variable valve timing can give more degrees of freedom to these mentioned problems at high load, and further optimize all engine map conditions.

In the case of the DI, the fuel can now evaporate inside the cylinder, absorbing heat from the cylinder and reducing the risk of knocking. This technology has been developed for the past decade to improve CCV, increase the dilution misfire range of gasoline engines and improve the mixture ignitability under lean conditions. Nowadays this technology is also the first cause of *PM* emissions in gasoline engines, because of the wall wetting effect that these in-cylinder injections produce.

On the other hand, VVT systems are more complex, because they permit the optimization of the gas exchange of the engine in all areas of the engine map. There are two main strategies used to reduce the fuel consumption at low/part load and high load, the Miller cycle and the Atkinson cycle. These main strategies optimize the IVC to help reduce the fuel consumption of the engine by excessively retarding the closure or by advancing the closure before bottom dead center. The most popular is the excessive retarded IVC, in the case of non boosted area of the engine map (Atkinson cycle), and in the boosted area (Miller cycle).

After the summary of the main strategies and technologies that are nowadays being applied to gasoline engines to reduce the fuel consumption, it is important to remark the strategies that are being developed to work in synergy with the actual gasoline engines.

The variable compression ratio is a technology that has been developed for the past years and that each year seems to be closer to achieve mass production engines. This technology could reduce the amount of trade-offs



between high load and low/part load operating conditions mainly because of knocking problems. But it would increase the complexity of the engine calibration and the possible combinations with VVT or direct injection systems that could further reduce the fuel consumption of gasoline engines.

On the other hand, in the case of the lean burn strategy, this strategy has been in the road for over 10 years but it has not been fully exploited and there is still development and research being made in this area. The engine is operated with a lean mixture with the main objective of reducing the throttled area of the engine map and reduce the fuel consumption. This strategy is increasing its potential because of direct injection systems and the improvement of mixture preparation and reactivity on the surroundings of the spark plug. The main problem is the  $NO_x$  emissions, because when the engine operates in lean conditions the TWC cannot be used, in its place a two-way catalyst to convert  $HC$  and  $CO$ , and a  $NO_x$  trap or SCR with injected urea to convert  $NO_x$  emissions. This is the main drawback for this technology, but looking at the future, using an additional after-treatment system could not represent a major complication and the potential of this strategy could compensate the additional complexity of the after-treatment system.

And finally, the cooled EGR strategy implementation on turbocharged engines, which is one of the main focus of study in the research area for the last 8 years. This strategy can reduce the fuel consumption, knocking risks and exhaust gas temperature of turbocharged gasoline engines. There are different possible configurations to recirculate the exhaust gas into the intake of the engine. Each of them has advantages and disadvantages, as it was explained before in Table 2.1. A combination of a LP and HP EGR loop is the optimum configuration but this would increase the complexity of the control strategies of the engine, so the LP EGR seems to have more advantages and less disadvantages compared to the other configurations.

In this PhD-Thesis a deep study of the potential of a modern GTDI engine using a cooled EGR and lean burn strategy in synergy with a VVT and direct injection system to reduce the fuel consumption is performed. The influence of cooled EGR using a LP EGR loop is studied and explained in Chapter 4, by analyzing the combustion, the exhaust emissions production and the air management system impacts.

An optimization using the VVT and injection system was performed using 1D simulations and DoE, to reach the optimum configuration with the minimum tests performed. A comparison of the optimized operating points using EGR, with the original calibration using also EGR was performed, to analyze the potential and the impacts on the combustion and exhaust

emissions. Also, a brief analysis of different strategies, to increase the dilution misfire range to further increase the EGR rate and fuel consumption reduction, was performed to better understand the ignitability limits of the engine. This subjects are going to be covered in Chapter 5.

The lean burn strategy was also studied to understand its potential and the possible synergy with the cooled EGR strategy, also analyzing the combustion, exhaust emissions and air management system. The main target was to compare the lean burn with the cooled EGR strategy in order to better visualize the possibilities and potential of each strategy on the near future. This analysis and discussion is presented in Chapter 5.

This PhD-Thesis tries to improve the understanding of these strategies synergy with modern gasoline engines technologies, and their impacts on the engine performance and exhaust emissions. A methodology using 1D engine simulations was developed to face the increase of degrees of freedom when optimizing the engine parameters for the new added EGR strategy. Responses to questions about the future of gasoline engines path and how new strategies and technologies would further improve the thermal efficiency are going to be explained in the next chapters.

## Bibliography

- [1] *Energy Technology Perspectives 2012. Pathways to a Clean Energy System.* International Energy Agency IEA Publications, 2012.
- [2] Michel C. and Eckard H. "Critical evaluation of the European diesel car boom - global comparison, environmental effects and various national strategies". In *Environmental Sciences Europe*, 2013.
- [3] Weernink W.O. *Europeans, Japanese intensify hybrid, diesel debate*, volume 8. Europe: Automotive News, 2003.
- [4] Lancaster David R., Krieger Roger B., Sorenson Spencer C. and Hull William L. "Effects of Turbulence on Spark-Ignition Engine Combustion". In *SAE Technical Paper*, 1976.
- [5] Pulkrabek Willard W. *Engineering Fundamentals of the Internal Combustion Engine.* Upper Saddle River, New Jersey 07548, 1997.
- [6] Maly R. *Spark Ignition: Its Physics and Effect on the Internal Combustion Engine in Fuel Economy in Road Vehicles Powered by Spark-Ignition Engines.* Hilliard, J. C. and Springer, G. S. Plenum Press, New York, 1984.
- [7] Maly R. *Initiation and Propagation of Flame Fronts in Lean CH<sub>4</sub>-Air Mixtures by the Three Modes of Ignition Spark in Fuel Economy in Road Vehicles Powered by Spark-Ignition Engines.* Hilliard, J. C. and Springer, G. S. Plenum Press, New York, 1984.
- [8] Sher Eran and Keck James C. "Spark ignition of combustible gas mixtures". *Combustion and Flame*, Vol. 66 n<sup>o</sup> 1, pp. 17–25, 1986.

- [9] Kalghatgi Gautam T. "Spark Ignition, Early Flame Development and Cyclic Variation in I.C. Engines". In *SAE Technical Paper*, 1987. 870163.
- [10] Verhoeven Dean. "Spark Heat Transfer Measurements in Flowing Gases". In *SAE Technical Paper*, 1995. 952450.
- [11] Ko Y., Arpacı V. S. and Anderson R. W. "Spark ignition of propane-air mixtures near the minimum ignition energy: Part II. A model development". *Combustion and Flame*, Vol. 83 n° 1-2, pp. 88–105, 1991.
- [12] Eichenberger D. A. and Roberts W. L. "Effect of unsteady stretch on spark-ignited flame kernel survival". *Combustion and Flame*, Vol. 118 n° 3, pp. 469–478, 1999.
- [13] Xiong Y., Roberts W. L., Drake M. C. and Fansler T. D. "Investigation of pre-mixed flame-kernel/vortex interactions via high-speed imaging". *Combustion and Flame*, Vol. 126 n° 4, pp. 1827–1844, 2001.
- [14] Patterson Donald J. "Cylinder Pressure Variations, A Fundamental Combustion Problem". In *SAE Technical Paper*, volume 660129, 1966. 660129.
- [15] Peters N. "Laminar flamelet concepts in turbulent combustion". *Symposium (International) on Combustion*, Vol. 21 n° 1, pp. 1231–1250, 1988.
- [16] Peters N. and Williams F. A. "Premixed combustion in a vortex". *Symposium (International) on Combustion*, Vol. 22 n° 1, pp. 495–503, 1989.
- [17] Williams F. A. "An approach to turbulent flame theory". *Journal of Fluid Mechanics*, Vol. 40, pp. 401–421, 2 1970.
- [18] Beretta G. P., Rashidi M. and Keck J. C. "Turbulent flame propagation and combustion in spark ignition engines". *Combustion and Flame*, Vol. 52 n° 0, pp. 217–245, 1983.
- [19] Hill P. G. and Zhang D. "The effects of swirl and tumble on combustion in spark-ignition engines". *Progress in Energy and Combustion Science*, Vol. 20 n° 5, pp. 373–429, 1994.
- [20] Witze P. and Green R. "LIF and Flame-Emission Imaging of Liquid Fuel Films and Pool Fires in an SI Engine During a Simulated Cold Start". In *SAE Technical Paper*, 1997. 970866.
- [21] Goto Satoru and Fukuda Takahiro. "Study on NO<sub>x</sub> formation and reduction of lean-burn spark ignition gas engine". *JSAE Review*, Vol. 19 n° 4, pp. 351–354, 1998.
- [22] Wang B., Monasbach S., Schmutzhard S., Shuai S., Huang Y. and Kraft M. "Modelling soot formation from wall films in a gasoline direct injection engine using a detailed population balance model". In *Preprint Article. Department of Chemical Engineering and Biotechnology, University of Cambridge*, 2015.
- [23] Hermann, F. Zeuch T. and Klingmann J. "The Effect of Diluents on the Formation Rate of Nitrogen Oxide in a Premixed Laminar Flame". In *ASME 2004 Proceedings Combustion and Fuels*, Vienna, Austria, 2004.
- [24] Ouellette, P. Douville B. Hill P. G. and Ursu B. "NO<sub>x</sub> reduction in a directly injected natural gas engine". In *Proceedings of the ASME 1998 Internal Combustion Engine Division Fall Technical Conference*, September 2008.
- [25] Szczepanski D. *Factors influencing NO<sub>x</sub> emissions at Tarong and Stanwell power stations*. Tesis Doctoral, PhD-Thesis. The University of Queensland, 1998.
- [26] Michaels H. C. and Fulper B. K. "Nitrous oxide emission factors for mobile sources US EPA". In *AWMA emissions inventory conference*, New Orleans, USA, 1998.

- [27] Soltic P. and Hausberger S. “On-Road Emission Measurements and emission modeling results for a tractor-semi trailer in Trans-Alpine operation”. *13th International Scientific Symposium Transport and Air Pollution Boulder*, September 13-15, 2004.
- [28] O’Dell P. R. “Why carbon fuels will dominate”. In *The 21st Century’s Global Energy Economy Conference*. Brentwood, Multi-Science, 2004.
- [29] Ladommatos N., Abdelhalim S. and Zhao H. “Control of oxides of nitrogen from diesel engines using diluents while minimising the impact on particulate pollutants”. *Applied Thermal Engineering*, Vol. 18 n° 11, pp. 963–980, 1998.
- [30] Guillemot P. *Les émissions de polluants des moteurs à allumage commandé*. École du Pétrole et des Moteurs, 2008.
- [31] Alger T., Chauvet T. and Dimitrova Z. “Synergies between High EGR Operation and GDI Systems”. *SAE Int. J. Engines*, Vol. 1 n° 1, pp. 101–114, 2008. 2008-01-0134.
- [32] Aakko P. and Nylund N. “Particle Emissions at Moderate and Cold Temperatures Using Different Fuels”. In *SAE Technical Paper*, 2003. 2003-01-3285.
- [33] Mohr M., Forss A.N. and Lehmann U. “Particle Emissions from Diesel Passenger Cars Equipped with a Particle Trap in Comparison to Other Technologies”. *Environmental Science & Technology*, Vol. 40 n° 7, pp. 2375–2383, 2006. PMID: 16646477.
- [34] Braisher M., Stone R. and Price P. “Particle Number Emissions from a Range of European Vehicles”. In *SAE Technical Paper*, 2010. 2010-01-0786.
- [35] Mathis Urs, Mohr Martin and Forss Anna-Maria. “Comprehensive particle characterization of modern gasoline and diesel passenger cars at low ambient temperatures”. *Atmospheric Environment*, Vol. 39 n° 1, pp. 107–117, 2005.
- [36] Heywood J. B. *Internal combustion engine fundamentals*. Ed. McGraw-Hill Science/Engineering/Math, 1988.
- [37] Zhao F., Lai M. C. and Harrington D. L. “Automotive spark-ignited direct-injection gasoline engines”. *Progress in Energy and Combustion Science*, Vol. 25 n° 5, pp. 437–562, 1999.
- [38] Stevens E. and Steeper R. “Piston Wetting in an Optical DISI Engine: Fuel Films, Pool Fires, and Soot Generation”. In *SAE Technical Paper*, 2001. 2001-01-1203.
- [39] Steven A. “Attacking GDI engine particulate emissions”. In *Automotive Engineering Magazine*, 2014. 13624.
- [40] Glahn C., Kluin M., Konigstein A. and Cloos L.K. “Cooled External EGR - System Optimization of the Cooling and Charging System on a 3-Cylinder Gasoline DI T/C Engine”. In *24th Aachen Colloquium Automobile and Engine Technology*, pp. 189–204, 2015.
- [41] Lujan Jose Manuel, Climent Hector, Pla Benjamin, Rivas-Perea Manuel Eduardo, Francois Nicolas-Yoan, Borges-Alejo Jose and Soukeur Zoulikha. “Exhaust gas recirculation dispersion analysis using in-cylinder pressure measurements in automotive diesel engines”. *Applied Thermal Engineering*, Vol. 89, pp. 459–468, 2015.
- [42] He Y. “Development and Application of a Lean NOX Trap Model”. In *SAE Technical Paper*, 2006. 2006-01-0686.
- [43] Saito C., Nakatani T., Miyairi Y., Yuuki K., Makino M., Kurachi H., Heuss W., Kuki T., Furuta Y., Kattouah P. and Vogt C.D. “New Particulate Filter Concept to Reduce Particle Number Emissions”. In *SAE Technical Paper*, 2011. 2011-01-0814.

- [44] Chan T., Meloche E., Kubsh J., Rosenblatt D., Brezny R. and Rideout G. "Evaluation of a Gasoline Particulate Filter to Reduce Particle Emissions from a Gasoline Direct Injection Vehicle". *SAE Int. J. Fuels Lubr.*, Vol. 5 n° 3, pp. 1277–1290, 2012.
- [45] Hosaka T. and Hamazaki M. "Development of the Variable Valve Timing and Lift (VTEC) Engine for the Honda NSX". In *SAE Technical Paper*, 1991. 910008.
- [46] Watanabe I., Kawai T., Yonezawa K and Ogawa T. "The New Toyota 2.0-Liter Inline 4-Cylinder ESTEC D-4ST Engine - Turbocharged Direct Injection Gasoline Engine -". In *23rd Aachen Colloquium Automobile and Engine Technology*, 2014.
- [47] Luttermann C., Schunemann E. and Klauer N. "Enhanced VALVETRONIC Technology for Meeting SULEV Emission Requirements". In *SAE Technical Paper*, 2006. 2006-01-0849.
- [48] Kiga S., Mae Y., Akasaka Y. and Tomogane K. "Development of Innovative Variable Valve Event and Lift (VVVEL) System". In *SAE Technical Paper*, 2007. 2007-01-3548.
- [49] Kinoshita K., Ueda K., Ito F., Shinojima Y., Yanagizawa T., Sakaguchi T. and Yamazaki T. "Development of a Custom Integrated Circuit for Continuously Variable Valve Lift Mechanism System Control". In *SAE Technical Paper*, 2008. 2008-01-0913.
- [50] Stone R. *Introduction to Internal Combustion Engines*. Palgrave Macmillan, England, 4th edition, 2012.
- [51] Battistoni M., Foschini L., Postriotti L. and Cristiani M. "Development of an Electro-Hydraulic Camless VVA System". In *SAE Technical Paper*, 2007. 2007-24-0088.
- [52] Lou Z., Wen S, Qian J., Xu H., Zhu G. and Sun M. "Camless Variable Valve Actuator with Two Discrete Lifts". In *SAE Technical Paper*, 2015. 2015-01-0324.
- [53] Hara S., Suga S., Watanabe S. and Nakamura M. "Variable valve actuation systems for environmentally friendly engines". *Hitachi Review*, Vol. 58 n° 7, pp. 319–324, 2009.
- [54] Varnier O. *Trends and Limits of Two-Stage Boosting Systems for Automotive Diesel Engines*. Tesis Doctoral, Ph.D-Thesis. Universitat Politècnica de València, Departamento de Maquinas y Motores Termicos, 2012.
- [55] Turner, J. W. Popplewell A. Patel R. Johnson T. R. Darnton N. J. Richardson S. Bredda S. W. Tudor R. J. Bithell C. I. Jackson R. Remmert S. M. Cracknell R. F. Fernandes J. X. Lewis A. G. J. Akehurst S. Brace C. J. Copeland C. Martinez-Botas R. Romagnoli A. and Burluka A. A. "Ultra Boost for Economy: Extending the Limits of Extreme Engine Downsizing". *SAE Int. J. Engines*, Vol. 7 n° 1, pp. 387–417, 2014. 2014-01-1185.
- [56] Coltman D., Turner J. W. G., Curtis R., Blake D., Holland B., Pearson R. J., Arden A. and Nuglisch H. "Project Sabre: A Close-Spaced Direct Injection 3-Cylinder Engine with Synergistic Technologies to Achieve Low CO<sub>2</sub> Output". *SAE Int. J. Engines*, Vol. 1 n° 1, pp. 129–146, 2008. 2008-01-0138.
- [57] Herbst F., Staber-Schmidt C., Eilts P., Sextro T., Kammeyer J., Natkaniec C., Seume J., Porzig D. and Schwarze H. "The Potential of Variable Compressor Geometry for Highly Boosted Gasoline Engines". In *SAE Technical Paper*, 2011. 2011-01-0376.
- [58] Andersen, J. and Karlsson E. and Gawell A. "Variable Turbine Geometry on SI Engines". In *SAE Technical Paper*, 2006. 2006-01-0020.
- [59] George S., Morris G., Dixon J., Pearce D. and Heslop G. "Optimal Boost Control for an Electrical Supercharging Application". In *SAE Technical Paper*, 2004. 2004-01-0523.

- [60] Pallotti P., Torella E., New J., Criddle M. and Brown J. "Application of an Electric Boosting System to a Small, Four-Cylinder S.I. Engine". In *SAE Technical Paper*, 2003. 2003-32-0039.
- [61] Akihisa D. and Daisaku S. "Research on Improving Thermal Efficiency through Variable Super-High Expansion Ratio Cycle". In *SAE Technical Paper*, 2010. 2010-01-0174.
- [62] Knop V. and Essayem E. "Comparison of PFI and DI Operation in a Downsized Gasoline Engine". *SAE Int. J. Engines*, Vol. 6 n° 2, pp. 941–952, 2013.
- [63] Mori S. and Shimizu R. "Analysis of EGR Cyclic Variations in a Direct Injection Gasoline Engine by Using Raman Scattering Method". In *SAE Technical Paper*, 2002. 2002-01-1646.
- [64] Whitaker P., Kapus P., Ogris M. and Hollerer P. "Measures to Reduce Particulate Emissions from Gasoline DI engines". *SAE Int. J. Engines*, Vol. 4 n° 1, pp. 1498–1512, 2011.
- [65] Price P., Stone R., OudeNijeweme D. and Chen X. "Cold Start Particulate Emissions from a Second Generation DI Gasoline Engine". In *SAE Technical Paper*, 2007. 2007-01-1931.
- [66] Karjalainen Panu, Pirjola Liisa, Heikkilä Juha, Lahde Tero, Tzamkiozis Theodoros, Ntziachristos Leonidas, Keskinen Jorma and Ronkko Topi. "Exhaust particles of modern gasoline vehicles: A laboratory and an on-road study". *Atmospheric Environment*, Vol. 97, pp. 262–270, 2014.
- [67] Li Y., Zhao H., Stansfield P. and Freeland P. "Synergy between Boost and Valve Timings in a Highly Boosted Direct Injection Gasoline Engine Operating with Miller Cycle". In *SAE Technical Paper*, 2015. 2015-01-1262.
- [68] Miklanek L., Vitek O., Gotfryd O. and Klir V. "Study of Unconventional Cycles (Atkinson and Miller) with Mixture Heating as a Means for the Fuel Economy Improvement of a Throttled SI Engine at Part Load". *SAE Int. J. Engines*, Vol. 5 n° 4, pp. 1624–1636, 2012.
- [69] França O. "Impact of the Miller Cycle in the Efficiency of an FVVT (Fully Variable Valve Train) Engine During Part Load Operation". In *SAE Technical Paper*, 2009. 2009-36-0081.
- [70] Wang C., Daniel R. and Ma X. "Comparison of Gasoline (ULG), 2,5-Dimethylfuran (DMF) and Bio-Ethanol in a DISI Miller Cycle with Late Inlet Valve Closing Time". In *SAE Technical Paper*, 2012. 2012-01-1147.
- [71] De Bortoli Cassiani M., Bittencourt M., Galli L. and Villalva S. "Variable Compression Ratio Engines". In *SAE Technical Paper*, 2009. 2009-36-0245.
- [72] Roberts M. "Benefits and Challenges of Variable Compression Ratio (VCR)". In *SAE Technical Paper*, 2003. 2003-01-0398.
- [73] Kleeberg Henning, Tomazic Dean, Dohmen J $\ddot{A}$  $\frac{1}{4}$ rgen, Wittek Karsten and Balazs Andreas. "Increasing Efficiency in Gasoline Powertrains with a Two-Stage Variable Compression Ratio (VCR) System". In *SAE Technical Paper*, 2013. 2013-01-0288.
- [74] Schwaderlapp M., Habermann K. and Yapici K. "Variable Compression Ratio - A Design Solution for Fuel Economy Concepts". In *SAE Technical Paper*, 2002. 2002-01-1103.
- [75] John J. "Lean Burn Engine Concepts-Emissions and Economy". In *SAE Technical Paper*, 1975. 750930.

- [76] Gomez A. and Reinke P. "Lean burn: A Review of Incentives, Methods, and Tradeoffs". In *SAE Technical Paper*, 1988. 880291.
- [77] Hiroyuki Oda, Yasuyuki Morita, Toshimitsu Fujishima and Masashi Marubara. "Investigation of High-Compression Lean Burn Engine". In *SAE Technical Paper*, 1987. 871215.
- [78] Yu C., Kim T., Yi Y., Lee J., Seokhong N. and Kyuhoon C. "Development of KMC 2.4L Lean Burn Engine". In *SAE Technical Paper*, 1995. 950685.
- [79] Grandin B. and Angstrom H. E. "Replacing Fuel Enrichment in a Turbo Charged SI Engine: Lean Burn or Cooled EGR". In *SAE Technical Paper*, 1999. 1999-01-3505.
- [80] Saito H., Shirasuna T. and Nomura T. "Extension of Lean Burn Range by Intake Valve Offset". *SAE Int. J. Engines*, Vol. 6 n° 4, pp. 2072–2084, 2013. 2013-32-9032.
- [81] Lumsden G., Eddleston D. and Sykes R. "Comparing Lean Burn and EGR". In *SAE Technical Paper*, 1997. 970505.
- [82] Hacohen J., Ashcroft S. J. and Belmont M. R. "Lean Burn Versus EGR S. I. Engine". In *SAE Technical Paper*, 1995. 951902.
- [83] Grandin B., Angstrom H. E., Stalhammar P. and Olofsson E. "Knock Suppression in a Turbocharged SI Engine by Using Cooled EGR". In *SAE Technical Paper*, 1998. 982476.
- [84] Cairns A., Blaxill H. and Irlam G. "Exhaust Gas Recirculation for Improved Part and Full Load Fuel Economy in a Turbocharged Gasoline Engine". In *SAE Technical Paper*, 2006. 2006-01-0047.
- [85] Wei L., Ying W., Longbao Z. and Su L. "Study on improvement of fuel economy and reduction in emissions for stoichiometric gasoline engines". *Applied Thermal Engineering*, Vol. 27 n° 17-18, pp. 2919–2923, 2007.
- [86] Potteau S., Lutz P., Leroux S., Moroz S. and Tomas E. "Cooled EGR for a Turbo SI Engine to Reduce Knocking and Fuel Consumption". In *SAE Technical Paper*, 2007. 2007-01-3978.
- [87] Kaiser M., Krueger U., Harris R. and Cruff L. "Doing More with Less - The Fuel Economy Benefits of Cooled EGR on a Direct Injected Spark Ignited Boosted Engine". In *SAE Technical Paper*, 2010. 2010-01-0589.
- [88] Bermudez V., Lujan J. M., Climent H. and Campos D. "Assessment of pollutants emission and aftertreatment efficiency in a GTDi engine including cooled LP-EGR system under different steady-state operating conditions". *Applied Energy*, Vol. 158, pp. 459–473, 2015.
- [89] Alger Terrence, Gingrich Jess, Khalek Imad A. and Mangold Barrett. "The Role of EGR in PM Emissions from Gasoline Engines". *SAE Int. J. Fuels Lubr.*, Vol. 3 n° 1, pp. 85–98, 2010. 2010-01-0353.
- [90] Lujan Jose Manuel, Climent Hector, Novella Ricardo and Rivas-Perea Manuel Eduardo. "Influence of a low pressure EGR loop on a gasoline turbocharged direct injection engine". *Applied Thermal Engineering*, Vol. 89, pp. 432–443, 2015.
- [91] Kumano K. and Yamaoka S. "Analysis of Knocking Suppression Effect of Cooled EGR in Turbo-Charged Gasoline Engine". In *SAE Technical Paper*, 2014. 2014-01-1217.
- [92] Wheeler J., Polovina D., Ramanathan S., Roth K., Manning D. and Stein J. "Increasing EGR Tolerance using High Tumble in a Modern GTDI Engine for Improved Low-Speed Performance". In *SAE Technical Paper*, 2013. 2013-01-1123.

- [93] Gukelberger Raphael, Alger Terrence, Mangold Barrett, Boehler Jeff and Eiden Corey. “Effects of EGR Dilution and Fuels on Spark Plug Temperatures in Gasoline Engines”. *SAE Int. J. Engines*, Vol. 6 n° 1, pp. 447–455, 2013. 2013-01-1632.
- [94] Takaki D., Tsuchida H., Kobara T., Akagi M., Tsuyuki T. and Nagamine M. “Study of an EGR System for Downsizing Turbocharged Gasoline Engine to Improve Fuel Economy”. In *SAE Technical Paper*, 2014. 2014-01-1199.
- [95] Zhong L., Musial M., Reese R. and Black G. “EGR Systems Evaluation in Turbocharged Engines”. In *SAE Technical Paper*, 2013. 2013-01-0936.



# Chapter 3

## Experimental and theoretical tools

### Contents

---

<b>3.1</b>	<b>Introduction</b> .....	<b>79</b>
<b>3.2</b>	<b>Experimental Tools</b> .....	<b>80</b>
3.2.1	Engine characteristics .....	80
3.2.2	Experimental setup .....	85
3.2.2.1	Test bench cell characteristics .....	86
3.2.2.2	Engine dynamometer .....	87
3.2.2.3	Control and acquisition system .....	89
3.2.2.4	Exhaust emissions analysis .....	91
3.2.2.5	Engine testing procedure .....	94
3.2.3	Steady flow test bench .....	96
3.2.4	Turbocharger test bench .....	98
<b>3.3</b>	<b>Theoretical tools</b> .....	<b>100</b>
3.3.1	Combustion diagnosis .....	101
3.3.2	1D Engine modeling .....	104
3.3.3	Design of experiments .....	106
<b>3.4</b>	<b>Summary and conclusions</b> .....	<b>109</b>
	<b>Bibliography</b> .....	<b>110</b>

---

### 3.1 Introduction

For all research and development activities certain experimental and theoretical tools must be used in order to fulfill the main objectives of the

work. In this chapter a detailed presentation and explanation of these tools, that were used during the elaboration of this PhD-Thesis, is presented. It is important to deeply know the experimental and theoretical tools in order to understand the limits and how far the research work can be explored under these limitations.

The chapter is divided in two main sections. Section 3.2 is dedicated to the explanation of the characteristics of the experimental tools, which consist of: an engine, a test bench, a steady flow test bench and a turbocharger test bench. And Section 3.3 contains the explanation of the theoretical tools, which include: the combustions diagnosis model, the 1D engine simulation and the design of experiments.

## 3.2 Experimental Tools

In this section, a description of the different experimental tools used in this research work is presented. The engine characteristics, engine test bench, steady flow test bench and turbocharger test bench characteristics are detailed.

### 3.2.1 Engine characteristics

In this PhD-Thesis, a 2liter, 4 in line cylinder, turbocharged, direct injection, gasoline engine was used to perform all the engine tests. The engine includes a TWC as after-treatment system which complies with Euro V. This engine is typically installed in different mass production vehicles platforms and the main characteristics are presented in Table 3.1. The full load curve of engine torque and power can be seen in Figure 3.1.

The fuel injection system is capable of reaching 150 MPa of pressure. The injection pressure depends of the engine speed and load as can be seen in Figure 3.2. The injector is placed at  $45^\circ$  respect to the horizontal plane of the cylinder head. This placement uses the principle of “guided-wall injection”, which uses the piston to redirect the spray near to the spark plug area. The head and piston shape can be observed in Figure 3.3. And the injector characteristics are presented in Table 3.2.

The engine is also equipped with a cam phasing VVT system as it was mentioned in Chapter 2 Section 2.2.3.3. The phaser is operated by a valve using the engine oil to change the phasing of the camshaft. The phaser shape and details of the advancing and retarding flow chart control function can be observed in Figure 3.4.

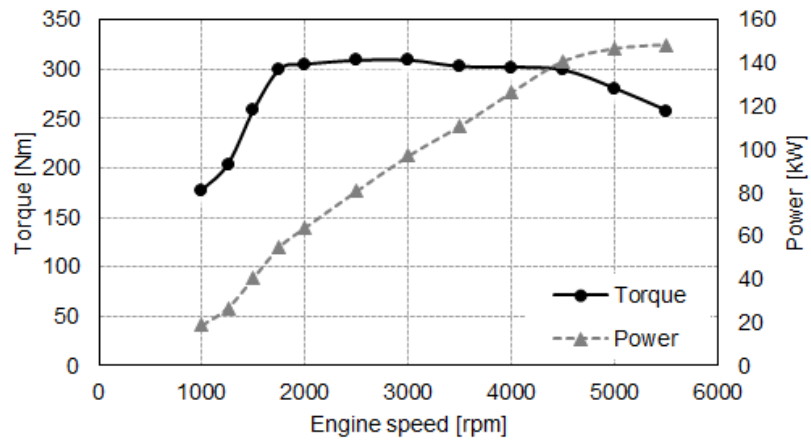


Figure 3.1. Engine torque and power curves at full load.

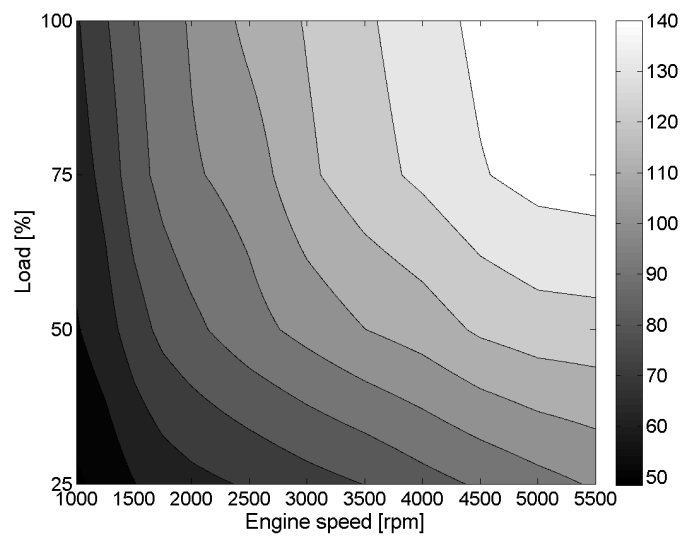
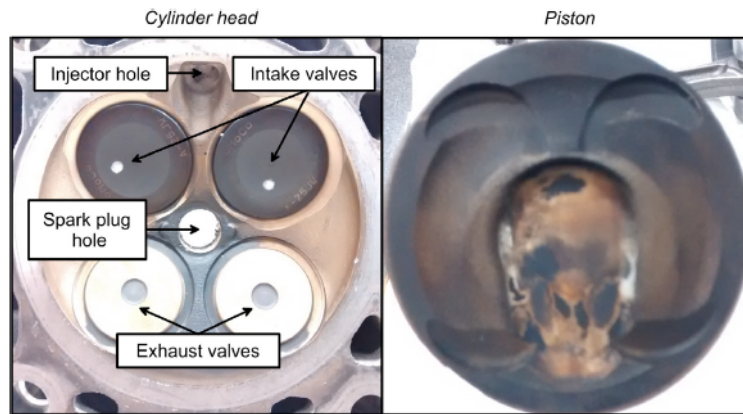
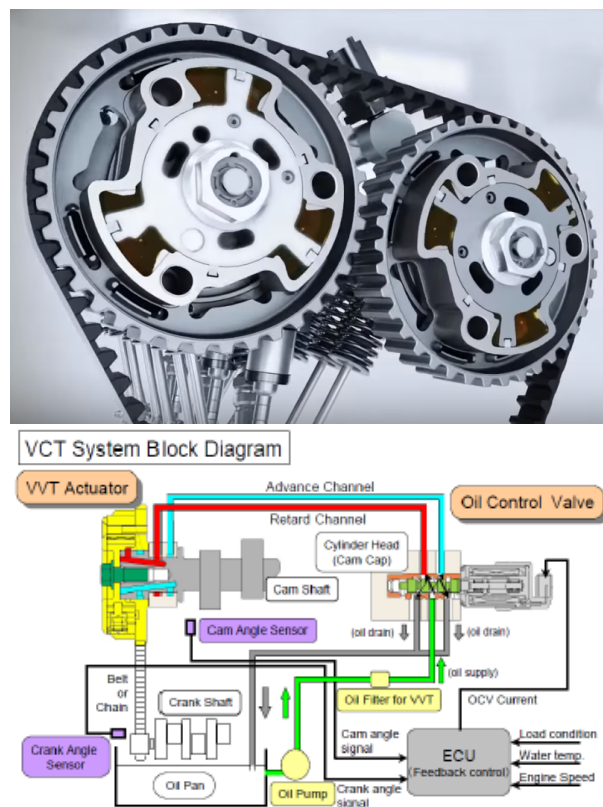


Figure 3.2. Injection pressure engine map in bar.



*Figure 3.3.* Cylinder head (left) and piston (right) of the investigated engine.



*Figure 3.4.* VVT system employed in the GTDI engine.

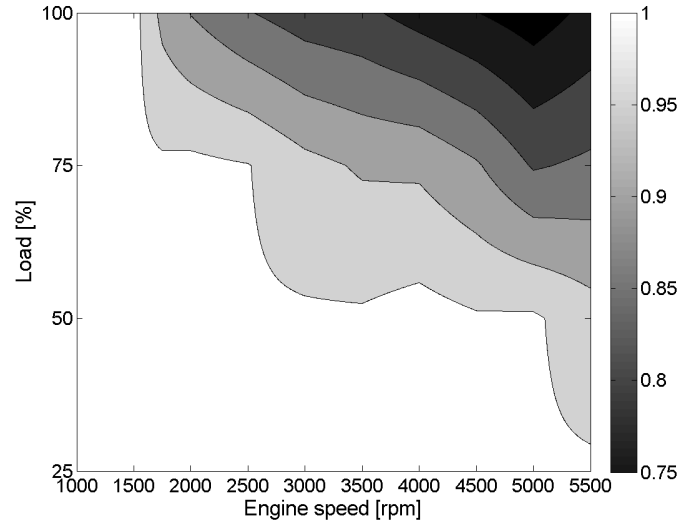
Characteristics	Units	Value
Type	[-]	4-stroke
Total displacement	[cm <sup>3</sup> ]	1999
Bore	[mm]	87.5
Stroke	[mm]	83.1
Number of cylinders	[-]	4
Valves per cylinder	[-]	4
Compression ratio	[-]	10.2:1
Fuel system	[-]	Direct injection
Max. Power/Eng. Speed	[kW/rpm]	143/5000
Max. Torque/Eng. Speed	[N m/rpm]	310/1750
Boost system	[-]	Turbocharger with fixed turbine with WG

**Table 3.1.** *Engine characteristics.*

Characteristics	Units	Value
Mass flow rate	[g/min at bar]	1026 at 100
Fuel input	[-]	Top feed injector
Fuel	[-]	Gasoline
Operating pressure	[bar]	150
Operating temperature range	[°C]	-31 to 130
Spray type	[-]	Multi-hole
Number of holes	[-]	7
Spray angle overall	[°]	110
Hole inner diameter	[mm]	0.165

**Table 3.2.** *Injector characteristics.*

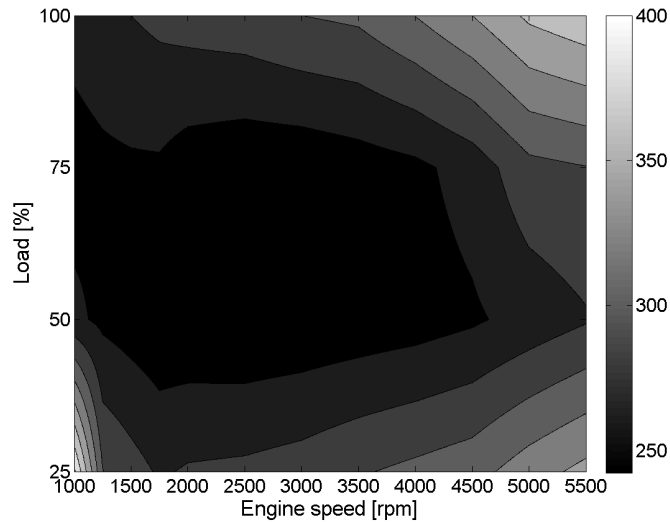
In order to assure the reliability of the exhaust components of the engine, mainly the turbine, the exhaust gas temperature is controlled using a fuel enrichment or over-fueling strategy, already mentioned and explained in Chapter 2. In Figure 3.5 an engine map is presented, showing the equivalence ratio in all the operating conditions and as it can be seen the fuel to air mixture gets richer with the increase in engine load and engine speed, reaching a maximum of 1.36 at 5000 rpm and 100% load.



*Figure 3.5. Equivalence ratio engine map.*

The maximum thermal efficiency of the engine is around 34% at 2000 rpm and 50% of load. The BSFC for different operating conditions can be seen in Figure 3.6, where a typical trend of a downsized engine can be observed. The lowest BSFC area is at low engine speed and part load, as it was stated in Chapter 2 and Figure 2.16. The full load at low engine speed is limited by pre-ignition and the high load and high engine speed is limited by knocking and, in the case of this engine, also by exhaust gas temperature. Discarding the area above part load, the efficiency engine map pattern presents the typical trend for an atmospheric gasoline engine: lower at low loads because of the throttling, which increases pumping losses, and also lower at high engine speed because of friction losses increase.

In summary, this engine arises as a good candidate to evaluate the impact of cooled EGR, taking into account that the engine is equipped with most of the technologies of modern downsized gasoline engines: VVT, direct injection and turbocharger. In this case the results could be directly applied to downsized gasoline engines in development or already in mass production phase.



**Figure 3.6.** Brake specific fuel consumption engine map in g/kWh.

### 3.2.2 Experimental setup

In order to be able to perform the engine tests, an experimental setup must be developed. This experimental setup is composed by a test bench cell, an engine dynamometer, exhaust emissions analyzer and an engine testing procedure that must be followed in order to assure accurate results to induce the less error possible to the measurements.

As it was mentioned in Chapter 2, this engine originally did not had installed an EGR loop. To be able to perform the research work, a custom low pressure and mixed pressure EGR loops were designed and installed into the engine.

In Figure 3.7 a simplified layout of the engine setup is presented. The placement of the sensors and exhaust gas analyzers can be appreciated in the engine setup layout, which are going to be detailed Section 3.2.2.1. The low pressure and mixed pressure EGR loops used the same EGR cooler and the same EGR valve regulator. The setup of the engine had to be changed in order to perform the test with mixed or low EGR loop, since only one of them could be used at a time.

A selector valve was used between the inlet and outlet of the TWC in order to measure the conversion efficiency of  $NO_x$ ,  $CO$  and  $HC$  exhaust emissions.

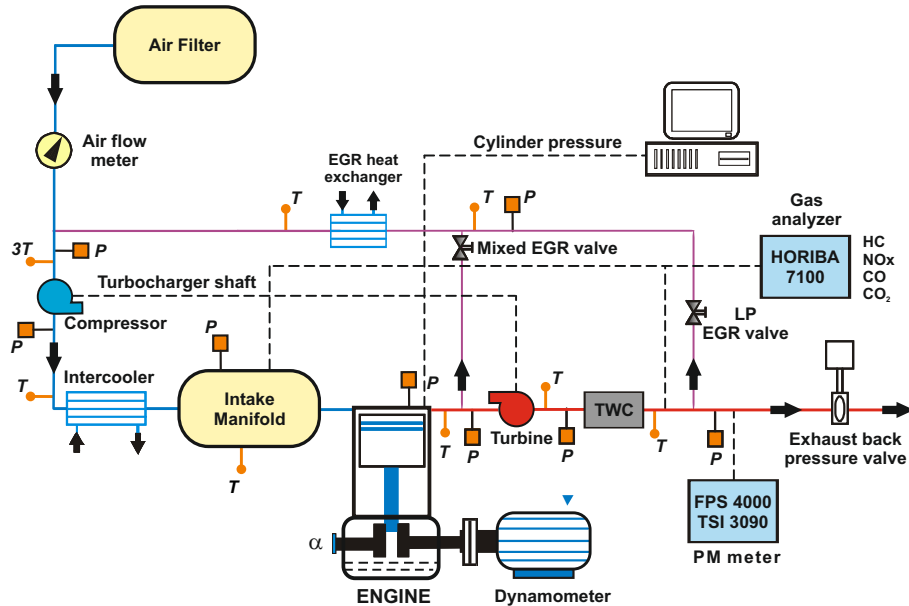


Figure 3.7. Engine tests experimental setup layout.

A more detailed explanation, of the procedure and setup, is presented in Section 3.2.2.4.

The fuel used for the engine tests was a 98 octane pump fuel gasoline. Detailed fuel characteristics are presented in Table 3.3. The fuel was always obtained from the same source, although a methodology was developed, which is explained in Section 3.2.2.5, to verify engine performance and combustion when a new batch of fuel arrived.

### 3.2.2.1 Test bench cell characteristics

The setup of the engine test bench cell was developed specially for this engine, since it is the first multi-cylinder SI turbocharged gasoline engine that has been installed at CMT-Motores Termicos. The test cell bench is composed basically by an engine dynamometer, cooling system, acquisition system, exhaust emissions analyzers, fuel supplier system and a ventilation system.



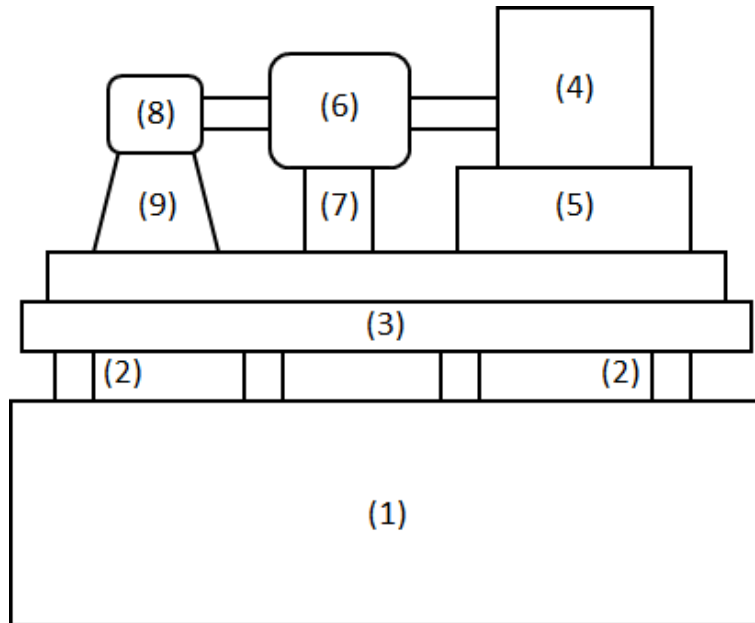
Characteristics	Units	Value
RON	[-]	98
Density at 15 °C	[kg/m <sup>3</sup> ]	735.7
Lower heating value	[MJ/kg]	44.09
Sulfur content	[ppm]	7.3
Oxygen	[wt%]	2
Aromatic	[Vol.%]	22.9
Benzene	[Vol.%]	0.68
Distillation T <sub>10Vol.%</sub>	[°C]	51.3
Distillation T <sub>50Vol.%</sub>	[°C]	85.8
Distillation T <sub>90Vol.%</sub>	[°C]	142.9

**Table 3.3.** *Fuel characteristics.***3.2.2.2 Engine dynamometer**

The base of the assembly (thermal engine + dynamometer) is supported by 14 springs, which permit the relative movement of the assembly against the ground. This installation is sprung to avoid shocks to the dynamometer, thermal engine and the surroundings, during transient operations of the engine.

The assembly can be divided into three main parts: the thermal engine, the engine brake and the electrical motor. Each one has its own base that goes into the commune sprung base as can be observed in Figure 3.8, where a basic layout of the assembly is presented. In the layout the different mentioned parts of the assembly can be seen and are enumerated as follows:

1. Ground of the assembly.
2. Springs.
3. Commune base.
4. Thermal engine and accessories.
5. Thermal engine base.
6. Engine brake.
7. Engine brake base.



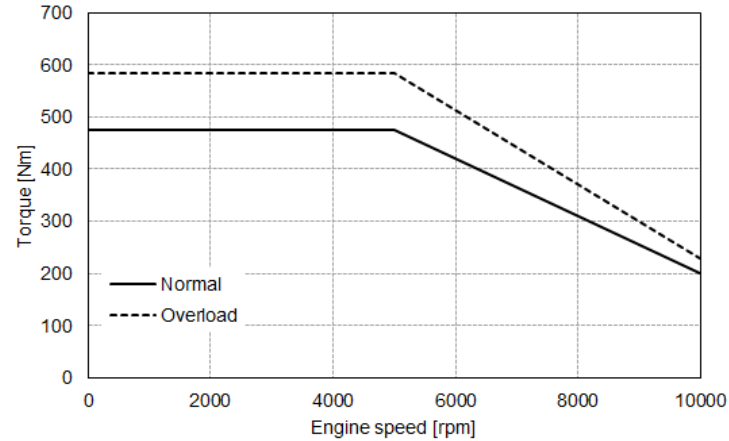
*Figure 3.8. Dynamometer assembly layout.*

8. Electrical motor.

9. Electrical motor base.

The engine dyno used is a Schenck Dynas3 – LI250, which was developed for testing a wide range of modern engines. Air cooling by blowers simplifies dynamometer installation and does not require tapping into other cooling systems inside the test cell. This dynamometer can perform transients and steady state tests. The low moments of inertia and high overload capacity together with speed gradients above 12.000 rpm/s guarantee a highly dynamic response. The capability of performing transient tests can be used to perform homologation cycles or transient response of the engine at different engine loads.

The absorbing torque of the dynamometer can be observed in Figure 3.9, where it is seen that the maximum torque that can be absorb by the engine dyno is higher than the maximum torque that can produce the engine in all engine speeds.



**Figure 3.9.** Torque absorption capacity of the engine dyno Schenck Dynas3 – LI250.

### 3.2.2.3 Control and acquisition system

The engine is controlled using a software interface developed by Horiba called “Stars” that communicates with the engine dynamometer hardware control and the ECU engine pedal. This software permits the implementation of homologation cycles and transient tests.

The control system also operates the PID’s, controlling the engine coolant temperature, the inter-cooler outlet air temperature, the fuel temperature and the EGR cooler outlet temperature if needed. The EGR valve and the exhaust back-pressure valve can be also operated manually through the software.

The sensors used in the acquisition systems of the engine test cell bench are composed by averaged and instantaneous pressure and temperature sensors, the crank-angle encoder and the engine sensors.

Instantaneous pressure sensors were used in the intake manifold, exhaust manifold and engine cylinder 1. A Kistler 4045A5 piezoresistive pressure sensor was placed in the intake and exhaust manifold with a Kistler Type 4603 amplifier, to be able to capture the absolute pressure and calibrate the 1D model developed for the analysis of this research work. The exhaust piezoresistive sensor cooling system was redesigned due to the inaccurate measurements effect of the high exhaust gas temperature of this engine. The details of the cooling system redesign are explained in Benajes et al. work [1], where a methodology was developed to address the problem and a solution was found.

A Kistler 6961A250 piezoelectric pressure sensor is used to measure the in-cylinder pressure since it has to withstand high pressure and temperature values. The measured in-cylinder pressure is then adjusted at the IVC with the intake pressure measured by the piezoresistive pressure sensor. This pressure sensor used a Kistler Type 5015 as amplifier.

In addition to these 3 mentioned instantaneous pressure sensors, another 5 average pressure sensors, PME transmitter P40, were placed in interesting places of the air and exhaust loops, and their placement can be seen in the engine setup layout presented before in Figure 3.7. To complete the setup 10 thermocouples were also placed in interesting spots of the air and exhaust lines. Their placements can be also seen in the engine setup layout presented before in Figure 3.7. The accuracy of the pressure and temperature sensors is presented in Table 3.4.

The crank-angle signal was measured using a Kistler crank-angle encoder type 2613A with its proper Kistler signal conditioner. The TDC was determined based on the Hohenberg proposal [2]; further details are found in Benajes et al. research work [3].

The fuel measurement system employed in this research work is an AVL 733S fuel balance. The fuel consumption is determined using an appropriate weighing vessel linked by a bending beam to a capacitive displacement sensor. Due to the fact that the weighing vessel has to be refilled for each measurement this is a discontinuous measurement principle. The mass of fuel consumed is therefore determined gravimetrically, which means that the density does not have to be determined in addition. The fuel consumption can thus be determined to an accuracy of 0.12%. The operation of this system is automatically performed by the “Stars” software, controlling the filling of the volume used to measure the fuel mass flow going into the engine. The accuracy and specifications of this fuel balance can be observed in Table 3.4. In the case of the air mass flow measurement, an ABB Sensyflow FMT700-P flow meter was used to measure the air mass flow that goes into the engine. This sensyflow has an accuracy of less than 1% of the measured value and has a response of less than 12 ms, which suits perfectly to perform transient tests.

After the presentation of all the measurement equipment, a summary of the accuracy obtained for different parameters of the engine is presented in Table 3.5.

The acquisition of the average measurements (average pressures, temperatures, torque, exhaust emissions, and others) is performed by the computer containing the “Stars” control software. The instantaneous measurements (instantaneous pressures) are recorded using a Yokogawa DL850V vehicle

Characteristics	Units	Value
Measuring range	[kg/h]	0 to 150
Vessel capacity	[g]	1800
Measurement uncertainty	[%]	0.12
Ambient temperature	[°C]	0 to 60
Fuel temperature	[°C]	-10 to 70
Fuel supply flow	[kg/h]	100
Fuels	[-]	Otto, Diesel with FlexFuel up to 100%

**Table 3.4.** *Fuel balance characteristics.*

Sensor	Variable	Accuracy [%]
Piezoelectric 6961A250	In-cylinder pressure	$\pm 0.7$
Piezoresistive 4045A2	Intake and exhaust pressure	$\pm 0.7$
Average pressure sensors	Pressure of all fluids	$\pm 0.9$
Thermocouples	Temperature of all fluids	$\pm 0.35$
Encoder 2613A	Engine speed	$\pm 0.006$
Torque meter	Engine torque	$\pm 0.1$
Fuel balance	Fuel mass flow	$\pm 0.12$
Air flowmeter	Air mass flow	$\pm 0.12$

**Table 3.5.** *Sensors accuracy.*

edition and then this data is transferred to the computer and saved by a software called “Yoko”, developed by CMT-Motores Termicos using the “LabVIEW” environment from National Instruments company. In addition, the ECU parameters and sensors recording is performed by other computer through a commercial software known as “Inca” from ETAS Group. The methodology and procedure used to perform the acquisition for each tested operating conditions is explained in detail in Section 3.2.2.5.

### 3.2.2.4 Exhaust emissions analysis

To measure the  $HC$ ,  $CO$  and  $NO_x$  emissions a Horiba MEXA-7100DEGR gaseous emissions bench was used. It is composed of six exhaust gas analyzers: total hydrocarbons (flame ionization detector), oxides of nitrogen

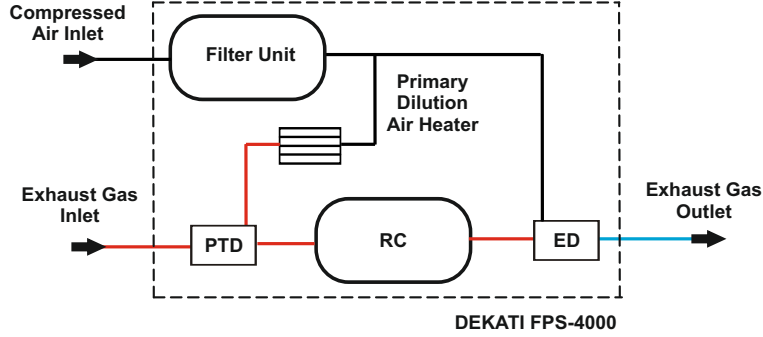


Figure 3.10. Dekati FPS-4000 dilution system layout.

(chemiluminescence detector), carbon monoxide (non-dispersive infrared detector), oxygen (magneto-pneumatic detection), exhaust carbon dioxide (non-dispersive infrared detector), and engine intake carbon dioxide (non-dispersive infrared detector) for calculating engine EGR rate. The engine intake carbon dioxide analyzer had a lower range and in this way, the exhaust dilution ratio was known quite accurately.

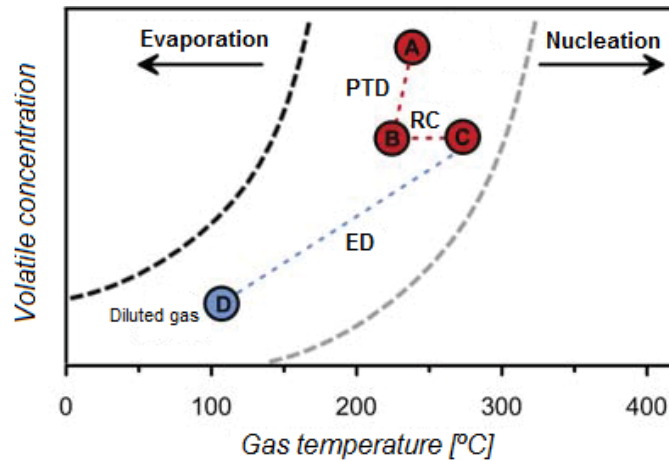
The EGR rate was obtained experimentally from the  $CO_2$  measurements in exhaust and intake manifold according to the expression used by Payri et al. [4]:

$$EGR_{rate} = \frac{[CO_2]_{Int} - [CO_2]_{Amb}}{[CO_2]_{Exh} - [CO_2]_{Amb}} \quad (3.1)$$

In order to measure the  $PM$  emissions a Dekati FPS-4000 partial exhaust dilution system was used to prepare the exhaust sample. Dilution of the exhaust gas is necessary before making sensitive particle size distribution or filtered  $PM$  chemical composition analyses to best preserve the exhaust chemical and physical properties as close as possible to what they were in the exhaust system.

The dilution system that was used has two conditioning stages: a primary dilution through a porous tube diluter (PTD) and a residence chamber (RC), and a secondary dilution through an ejector diluter (ED). In Figure 3.10 a schematic representation of the Dekati FPS-4000 dilution system is observed.

Just after leaving the exhaust, the gas sample passes through a short 0.25 inch diameter tube that connects the exhaust sample probe (which is perforated through the entire diameter of the exhaust pipe to ensure uniform exhaust sampling) to the diluter's primary dilution stage. The primary



*Figure 3.11. Different stages of exhaust gas sample through the dilution process.*

dilution stage consists of a perforated tube dilution, housed inside an electrical resistance probe heater. Once inside the primary dilution section, the exhaust sample flows through a perforated tube which traverses an open cavity within the diluter, which is filled with filtered and dehumidified dilution air. Dilution air preparation is performed by the air filtration and diffusion dryer unit. Then passes through the residency chamber to finish the primary stage. Once exiting the residency chamber the exhaust sample enters directly into the secondary ejector diluter section, as shown in the configuration of Figure 3.10.

Due to the big impact that the dilution conditions can have over the *PM* size distribution, producing new particles or eliminating already formed particles [5], the methodology proposed by Desantes et al. [6] in their research work was followed. Figure 3.11 shows the path that the exhaust gas follows through the dilution process following the methodology already mentioned.

The primary dilution air is introduced over 220 °C into the porous tube, which generates an iso-thermic dilution with the exhaust gas sample (A to B in Figure 3.11), allowing the reduction of volatile components concentration reducing the possibilities of generating new particles [7]. Afterwards, the exhaust gas enters into the residency chamber which is heated (B to C in Figure 3.11), allowing the stabilization of the diluted particles [8]. Lastly, in the ejector, the previously stabilized diluted gas is mixed with high quantities of air, reducing the temperature and therefore the concentration of the

particles (C to D in Figure 3.11). At this final point the sample is ready to be introduced in the measurement spectrometer.

To measure the particle size distributions a spectrometer TSI Engine Exhaust Particle Sizer 3090 was used. The great advantage of the TSI is its ability to measure 5.6 to 560 nm particle size distributions at a 10 Hz sampling rate, and requires no working fluid for condensation growth of the particle sizes for optical counting.

The TSI is able to simultaneously electro-statically charge all particles (electrostatic charge is proportional to particle surface area) and measure all particle size concentrations at the same time. The TSI measurement is performed in three steps, as it is represented in Figure 3.12: positively charge all particles by passing through a corona discharge, repel the particles contained in the downward sample flow from the central high voltage electrode toward the outer annular electro-meters based on particle electrostatic charge classification (smallest charged particles are driven to the first electro-meter, etc.), and finally calculate the particle concentration from the charge collected on each electro-meter. Therefore it follows that the particle size resolution will depend on the number of annular electro-meters placed in series, which in the case of the TSI is 22 electro-meter channels [9].

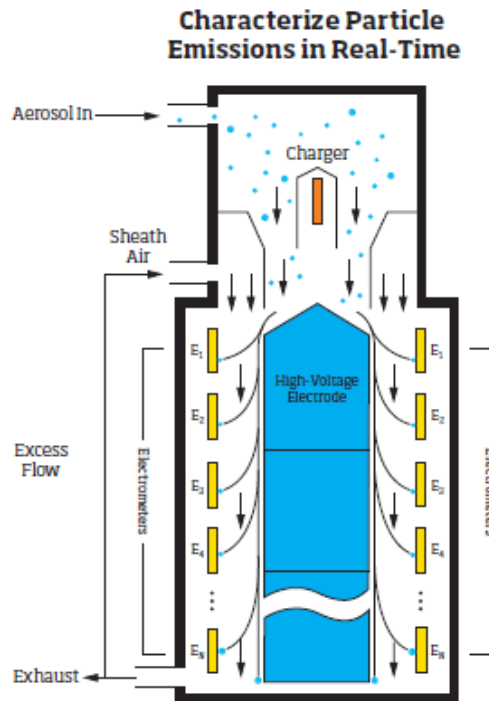
### **3.2.2.5 Engine testing procedure**

In order to be able to measure different days of the year and compare the results, an engine testing procedure must be followed. In this case, since it was the first time that in CMT-Motores Termicos a research work was been performed in a turbocharged SI gasoline policylinder engine, the testing procedure was developed from scratch.

The procedure of engine warm-up was followed in the same manner every testing day. The engine warm-up consisted in an operating condition at low engine speed (1500 rpm) and load until the engine reached 60 °C and then a part load at 2000 rpm was maintained until the cooling temperature stabilized around 90 °C. During this warm-up procedure the inter-cooler outlet temperature was also controlled by a PID and the stabilization was also achieved. The fuel temperature at the inlet of the high pressure pump of the engine was also stabilized during the warm-up .

The engine warm-up was followed by the measurement of the reference operating points, in this case, 2000 rpm and 50% load and 3000 rpm and 50%. This reference operating points are going to be measured in order to compare each testing day and verify that the engine and components are





**Figure 3.12.** Schematic of TSI 3090 measurement procedure. Source: TSI Incorporated [9].

operating without any issues. The principal parameters that were checked during this measurement were: the brake specific fuel consumption, torque, intake manifold pressure, exhaust manifold pressure, spark timing and exhaust emissions. After succeeding with the two initial steps, the engine is put in idle and a brief check of the engine test bench cell is performed in order to verify any leaks or malfunctions of the engine or engine components. Once the engine test cell inspection is performed, the engine test plan of the day can be started.

When an operating point is going to be measured, a smooth ramp of engine speed and pedal is input in “Stars” software in order to bring the engine conditions to the desired load and engine speed testing conditions. Then the values of EGR rate, spark advance, VVT or throttle angle are adjusted depending on the test. Once the engine is on the desire testing conditions, a stabilization period of time is required, looking at the cooling temperature, exhaust manifold temperature, injected fuel mass flow, intake temperature and, if it is the case, EGR rate and EGR outlet temperature. After this

period of time, the exhaust gas analyzer is activated and another stabilization period is required to stabilize the measurement of exhaust emissions.

After all the stabilization periods are reached, the data acquisition is performed. As it was explained before, the acquisition is composed by three different software that records the test data. When it is time to save the data, a simultaneous recording signal is deployed on the three acquisition software. The average signals are recorded for 60 s with a resolution of 0.1 s and the instantaneous signals are recorded for 100 engine cycles with a resolution of 0.25 CAD. It is important to remark that the fuel balance volume has to be enough at least to measure the fuel consumption through the 60 s recording time.

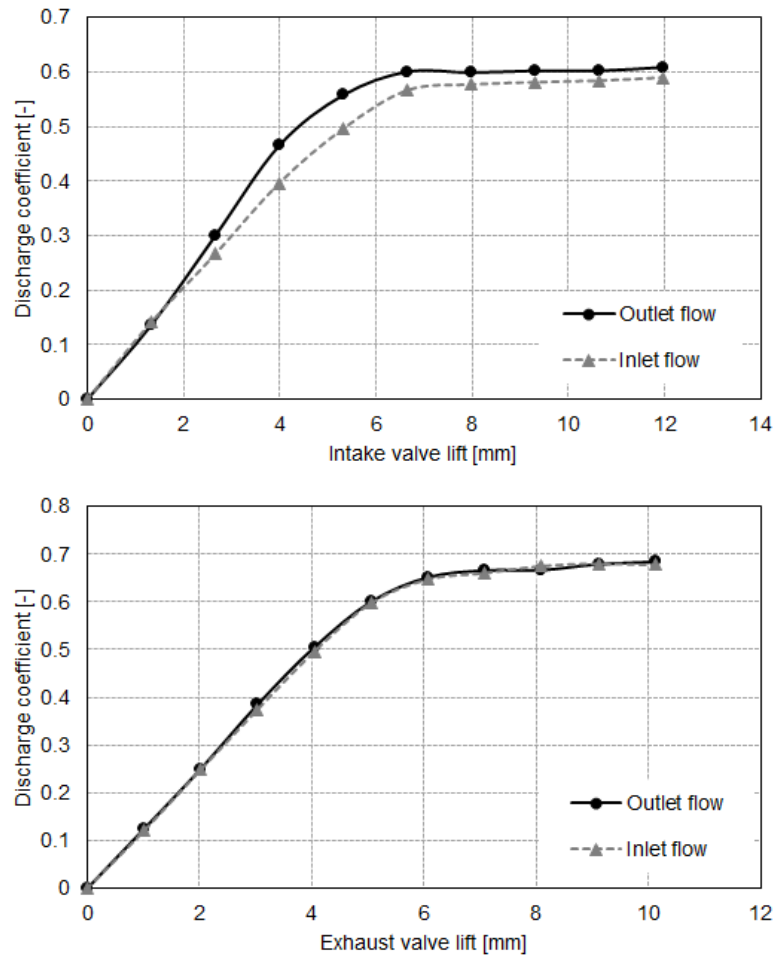
In the case of transient cycles the procedure is somehow different. To perform, for example, NEDC homologation cycles, the starting conditions of the engine must be well checked, because the cycle is performed on cold engine conditions. Obviously the tested cycle is followed nearly to ensure that the engine is operating in good condition. In the case of performing the cycle in hot condition, the warm-up procedure and stabilization period of time, explained before, must be followed before starting with the cycle.

It is important to remark that the exhaust emissions measurement for transient cycles are quite difficult, since each line of the exhaust gas analyzer has its own delay. A methodology developed at CMT-Motores Termicos is followed in order to determine the measurement delay of each exhaust emissions. The engine was operated in a steady condition at a certain engine speed and low load, when all the exhaust measurements were stabilized, a sudden increase in the pedal signal was performed at iso-engine speed. This sudden variation in pedal produces a variation in exhaust emissions and the time that passes between the pedal modification and the exhaust emission measurement change is identified as the delay time of measurement. This delay time, can vary from day to day and in order to be as accurate as possible this test can be performed after the cycle finishes. In order to trust the recorded data, the testing procedure described before must be followed. Following these steps leads to improve the accuracy and repeatability of the measurements. This is a must to perform a high standard research work.

### **3.2.3 Steady flow test bench**

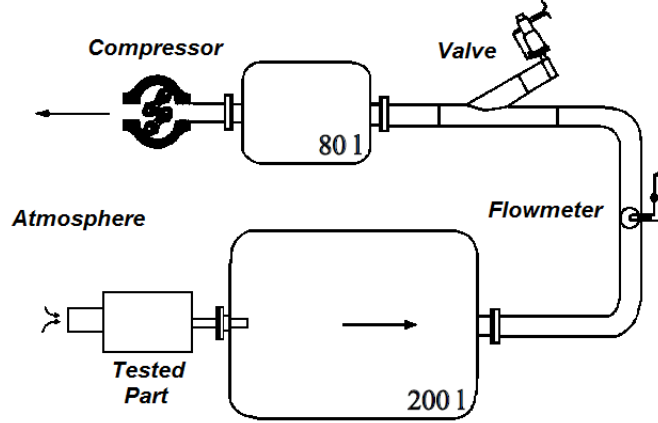
In order to be able to develop a 1D engine model and simulate with good accuracy the air and exhaust loop of the engine, different parts from the systems were tested in the steady flow test bench in order to measure the

discharge of coefficient associated to a reference diameter. The cylinder head was also measured for aspiration and expulsion to also determine the coefficient of discharge for intake and exhaust valves for different lift positions. The results are depicted in Figure 3.13.



**Figure 3.13.** Coefficient of discharge for the intake valve (top graph) and exhaust valve (bottom graph).

The steady flow test bench is basically composed by a compressor connected to a big volume, that mitigates the pressure fluctuation that can be induced by the compressor start and stop, and a piping system. A schematic layout of the installation is presented in Figure 3.14.



**Figure 3.14.** Schematic layout of the steady test bench. Source: Adapted from Climent [10].

The discharge coefficients were obtained using [11]:

$$Cd = \frac{\dot{m}_{part}}{\dot{m}_{isen}} \quad (3.2)$$

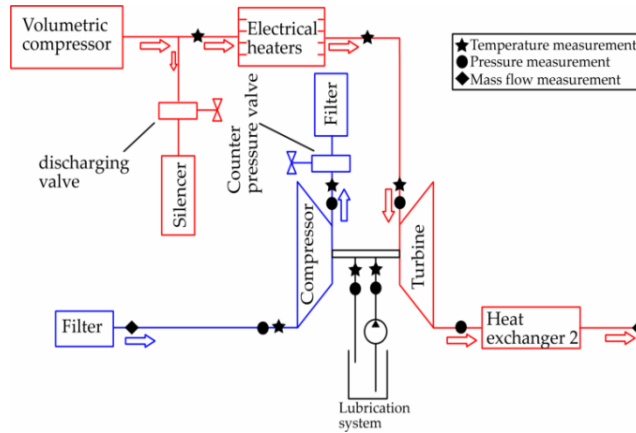
where  $\dot{m}_{part}$  is the measured mass flow going through the part and  $\dot{m}_{isen}$  is the isentropic mass flow that is calculated using:

$$\dot{m}_{isen} = A_{ref} \frac{P_{0,in}}{\sqrt{RT_{0,in}}} \sqrt{\frac{2\gamma}{\gamma-1}} \sqrt{\left(\frac{P_{0,out}}{P_{0,in}}\right)^{\left(\frac{2}{\gamma}\right)} - \left(\frac{P_{0,out}}{P_{0,in}}\right)^{\left(\frac{\gamma+1}{\gamma}\right)}} \quad (3.3)$$

where  $A_{ref}$  is the area referenced to a diameter,  $P_{0,out}$  is the measured outlet pressure,  $T_{0,out}$  is the measured outlet temperature,  $\gamma$  is the specific heat of the air and  $P_{0,in}$  is the measured inlet pressure.

### 3.2.4 Turbocharger test bench

The turbocharger test bench was used to measure the compressor and turbine maps. A schematic layout of the facility is presented in Figure 3.15. The main characteristics of this turbocharger testing facility are presented below [12, 13]:

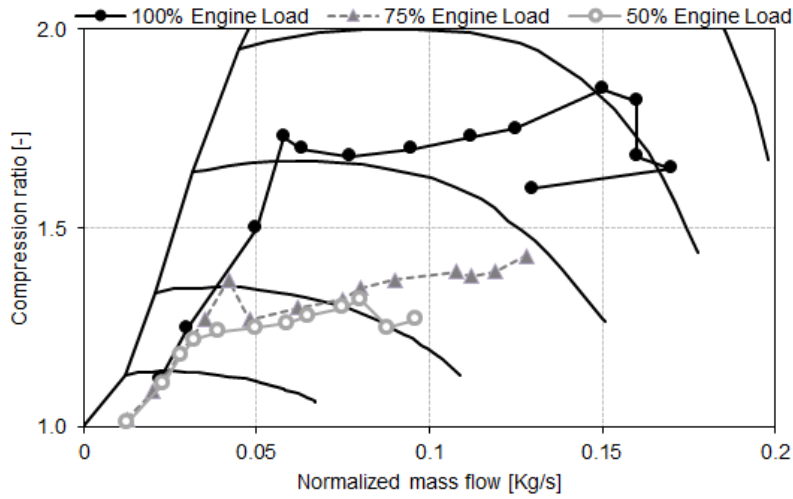


*Figure 3.15. Schematic layout of turbocharger test bench.*

- A screw compressor with a maximum mass flow capacity of 0.2 kg/s, at a maximum discharging pressure of 3 bar (gauge), provides the mass flow necessary to the turbine.
- A heater after the screw compressor to increase mass flow temperature to a maximum of 674 K.
- The amount of energy available to the turbine is controlled with the screw compressor speed and heating power.
- At compressor side, downstream the compressor, there is an electronically driven back-pressure valve which modifies compression ratio and mass flow.
- Temperature and pressure sensors are placed in inlet and outlet pipes of compressor and turbine; the installation of these sensors regarding to depth, angular and longitudinal positions was made according to SAE J1826 standards. Table 3.6, shows representative information about measurement range and accuracy of the sensors.
- An independent lubrication system delivers oil at flow rate and pressure adjustable to allow different sizes of turbochargers testing; this lubrication system includes a heater and a cooler that give the option to adjust the temperature at turbocharger inlet lube port.

Sensor type	Variable	Measuring range	Error
Piezoresistive	Pressure	0 ~ +5 bar 0 ~ -1 bar*	$\pm 0.025$ bar
Temperature	Thermocouple (K type)	-200 ~ +1200 ( $^{\circ}\text{C}$ )	$\pm 2.2$ $^{\circ}\text{C}$
Flow	Hot wire	0 ~ 720 kg/h	$\pm 0.72$ kg/h

**Table 3.6.** Sensor characteristics in turbocharger test bench facility (\*Only for compressor inlet).



**Figure 3.16.** Turbocharger compressor map with the engine operating points for 100%, 75% and 50% of engine load.

The measured compressor map of the turbocharger used in the engine is presented in Figure 3.16, where it can be seen the engine operating points for 100%, 75% and 50% of engine load in all the engine speed range. This map was used to build the 1D engine model compressor side of the turbocharger.

### 3.3 Theoretical tools

Once the measurement equipment and testing procedure were defined, the last important piece of the puzzle are the theoretical tools used to post-process and analyze the measurements. It does not mean anything to have the best equipment and testing methodology if the capability of analysis of the data is

limited. To be able to perform a high standard research work and achieve the main objective, good theoretical tools are needed.

In this case, to be able to extract the maximum information from the measurements a combustion diagnosis, an 1D engine model and a design of experiments were used as tools to analyze the engine combustion, air management and exhaust emissions. In the case of this research work also an optimization methodology and tool was developed to fulfill some of the targets of this PhD-Thesis.

### 3.3.1 Combustion diagnosis

The information about the thermodynamic variables during the engine cycle is very valuable for the diagnostics of the combustion process. In this research work, the diagnostic tool uses the experimental pressure signal as input data and, after averaging, filtering, and referring to absolute pressure at IVC and crank angle values, it solves the heat release law (time evolution of heat release fraction), and the in-cylinder instantaneous gas temperature average by combination of both the first principle of thermodynamics and the state equation. These are typically zero-dimensional and single-zone models, hence, do not take into account the air entrainment, vaporization of fuel droplet and spatial variation of mixture composition and temperature. However, the analysis of global combustion parameters such as the start of combustion or CA50 is still valid since they are directly related to the instantaneous evolution of the energy released by the combustion process, independently from the local conditions where this energy is being released. This tool was originally developed to analyze Diesel combustion. Since this is a gasoline engine a two-zone model was developed particularly to analyze the combustion process in gasoline SI engines.

The rate of heat release (RoHR) analysis and derived combustion-related parameters, that are presented in this research work, are calculated using CALMEC, an in-house internal combustion engine combustion diagnosis software used by La puerta et al. in their research works and PhD-Thesis [14–16]. This model requires different measured instantaneous signals, such as the in-cylinder pressure and a non combustion testing in order to calculate the thermodynamic and mechanical phasing delay of the in-cylinder pressure signal; as well as other engine working conditions (mass flows, temperatures).

Then, this model applies the first law of thermodynamics along the closed engine cycle, between intake valve closing and exhaust valve opening. It uses the state equation of ideal gas to calculate the mean gas temperature

in the chamber. Along with the previous two basic equations, several sub-models are employed to estimate the blow-by flow, the instantaneous volume considering deformations in the combustion chamber, and the heat transfer and the corresponding wall temperatures. An influence of measurement errors and estimated parameters, using the described combustion diagnosis model, was performed by Payri et al. in their research work [17], where a detailed explanation of the equations used in the combustion model can be seen. A most recent research work was also performed by Benajes et al. [18] using this model. In addition, a global energy balance in a Diesel engine was performed, using this model, by Payri et al. in their research work [19] in which also the equations used in the combustion diagnosis model to perform this global energy balance are explained.

The main hypothesis behind this model are briefly described as follows:

- The pressure in the combustion chamber is assumed to be uniform. This hypothesis is valid because the flow speed and flame propagation speed is much lower than the speed of sound.
- The fluid in the chamber is considered a mixture of air, fuel and stoichiometric burned products. Although it is assumed the uniformity of composition and temperature of the mixture, it is important to emphasize that the model considers three species (air, fuel and burned gases) at the time of evaluating the thermodynamic properties of the gas enclosed in the cylinder. In addition, the consideration of combustion products burning at stoichiometric conditions is valid, since the fuel is primarily burned in a reaction surface of the flame front with stoichiometric air/fuel ratio.
- Perfect gas behavior is assumed for the gas mixture. Mölenkamp showed the validity of this assumption in the pressure and temperature ranges of diesel engines [20]. However, this hypothesis may be argued when applied to gaseous fuel. Lapuerta compared the results of a similar combustion model but using different state equations for the gaseous fuel, and the study showed that the differences in mean temperature and energy release are relatively small [16], yet they could be relevant if the results are used to predict emissions formation.
- Correlations based on the temperature are used to calculate sensible internal energy of the gas mixture.
- The internal energy is calculated considering the mean gas temperature. This is the hardest hypothesis since burned products are much hotter



than mean temperature at the combustion beginning, even though later they become closer.

- The heat transmitted to the walls is calculated utilizing a modified heat transfer coefficient obtained with Woschni's expression [21–23]. An additional heat transfer nodal model is used to calculate the different wall temperatures (piston, liner, cylinder head) [24, 25].

Assuming the previous hypotheses, the model resolves the first-law of thermodynamics, presented in equation 3.4, at time-steps defined by the angular resolution of the cylinder pressure signal (0.25CAD).

$$\Delta HRL = m_{cyl} \cdot \Delta u_{cyl} + \Delta Q_w + P \cdot \Delta V - (h_{fuel, inj} - u_{f, g}) \cdot \Delta m_{fuel, evap} + R_{cyl} \cdot T_{cyl} \cdot \Delta m_{bb} \quad (3.4)$$

where  $\Delta HRL$  is the energy released by the fuel assuming constant calorific power along the combustion process,  $m_{cyl} \cdot \Delta u_{cyl}$  the variation in internal sensible energy experienced by the gas enclosed in the control volume,  $\Delta Q_w$  the heat transfer between the gas enclosed in the control volume and the combustion chamber walls that surrounds it,  $p \cdot \Delta V$  the work done by the gas enclosed in the control volume over the piston surface during the calculation step; the instantaneous volume is the sum of the combustion chamber volume, the volume displaced by the piston (depending on crank angle) and the mechanical deformations (estimated by a sub-model) produced by the gas pressure and the inertial efforts,  $(h_{fuel, inj} - u_{fuel, g}) \cdot \Delta m_{fuel, evap}$  the flow work of the injected fuel, evaporation and heating up to the gas temperature. The fuel enthalpy refers to the injection conditions whereas fuel internal energy refers to the evaporated fuel at in-cylinder conditions,  $R_{cyl} \cdot T_{cyl} \cdot \Delta m_{bb}$  the energy lost by the control volume due to blow-by losses through the piston rings. For the determination of the blow-by mass loss  $m_{bb}$ , an isentropic discharge through a nozzle connecting the cylinder with the carter was supposed, in combination with a coefficient that is adjusted by comparison with experimental measurement of blow-by.

From the calculated heat release law (HRL) and the derivative of the energy released (RoHR), the following global combustion related parameters are derived:

- SoC: Angle where the combustion starts to release energy.
- CA50: Center of gravity of combustion, corresponding to the angle where the 50% of the energy has been released.

- CA10, CA75, CA90: Angles where the 10%, 75% and 90% of the energy has been released.
- EOC: In this investigation the end of combustion has been defined as the angle where 90% of the energy has been released (CA90).
- Combustion duration: Angular difference between CA90 and CA10

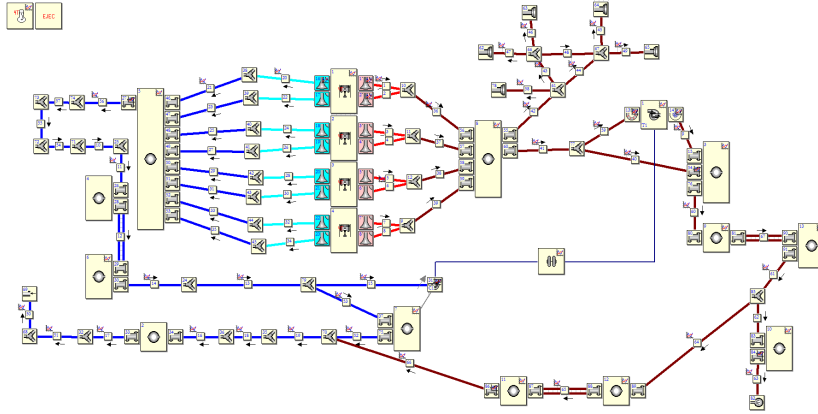
The CA50 and combustion duration are going to be use as parameters to analyze the effects of cooled EGR on the SI turbocharged direct injection gasoline engine.

### 3.3.2 1D Engine modeling

Wave propagation phenomena during gas exchange processes inside internal combustion engines are assumed to be one dimensional. In the case under consideration, the *OpenWAM<sup>TM</sup>* software, which solves the unsteady, non-linear and one-dimensional flow equations using a finite difference scheme, was used to model the engine. This software has already been used to simulate steady and transient phenomena with suitable accuracy in previous works [26–29].

Although simpler engine modeling approaches exist, such as mean value engine models or filling and emptying models, the use of a 1D model is compulsory in this study. The reason is that, pressure pulses in intake and exhaust systems must be considered to assess the effect of the VVT. In this scenario, an engine is basically composed of three kinds of elements: ducts, volumes and junctions. Volumes (such as cylinders, plenum, silencer components and atmosphere) are calculated using a zero dimensional approach, by solving mass and energy conservation equations [30].

In-cylinder heat release rate during combustion process, via Wiebe function, is an input to the engine simulation since information coming from the combustion diagnosis model is provided. Effective area of connections (such as exhaust and intake valves, intake throttle, EGR valve, WG position, exhaust back-pressure valve) between ducts and volumes is solved by means of a discharge coefficient, which has been previously obtained in characterization tests in a steady flow bench. Compressor and turbine maps measured in the characterization turbocharger test bench [31] are also inputs to the 1D model. The engine model interface is presented in Figure 3.17, where it can be observed how the intake and exhaust lines, and EGR loop are represented in *OpenWAM<sup>TM</sup>*.



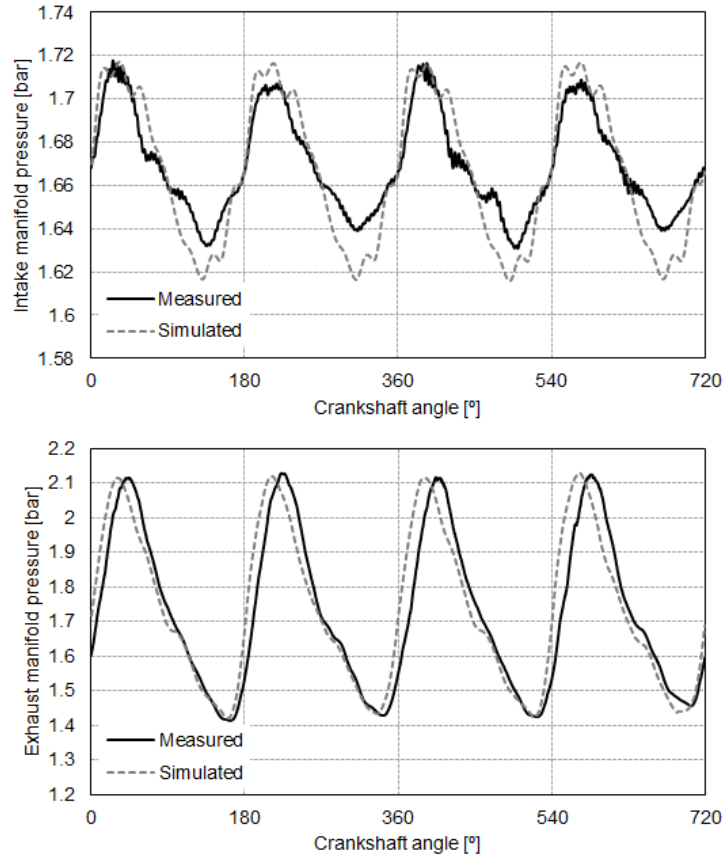
**Figure 3.17.** 1D engine model representation on the interface of the OpenWAM<sup>TM</sup> software.

To validate the model, engine test bench and simulation results were compared in order to verify that the model was able to predict the real engine steady state operating conditions.

An exhaustive explanation of the 1D model validation, operating without EGR, can be seen in the Serrano et al. [30] research work. Predicted instantaneous pressure in the intake and exhaust manifold presents good agreement as observed in Figure 3.18 at full load and 2500 rpm. Similar results were obtained at all the other engine operating conditions.

After showing instantaneous results, comparisons between measured and calculated cycle-averaged parameters are given in Figure 3.19, where volumetric efficiency is plotted. It is observed that errors stayed below 5%. That accuracy was considered enough for the work requirements and it can be considered that the model predicts with high accuracy engine steady operating conditions from 1500 to 5500 rpm at full load.

In this framework a 1D model validation, operating with EGR, was also performed. The validation was performed at the highest possible EGR rate for 5 different operating conditions: 2000 rpm at low load, 2000 rpm and 3000 rpm at part load and 2000 rpm and 3000 rpm at full load. Since the main objective of the study is the optimization of the VVT configuration for the two tested part load operating conditions, 2000 rpm and 3000 rpm, a comparison between the simulated and measured in-cylinder pressure for both operating conditions can be seen in Figure 3.20.

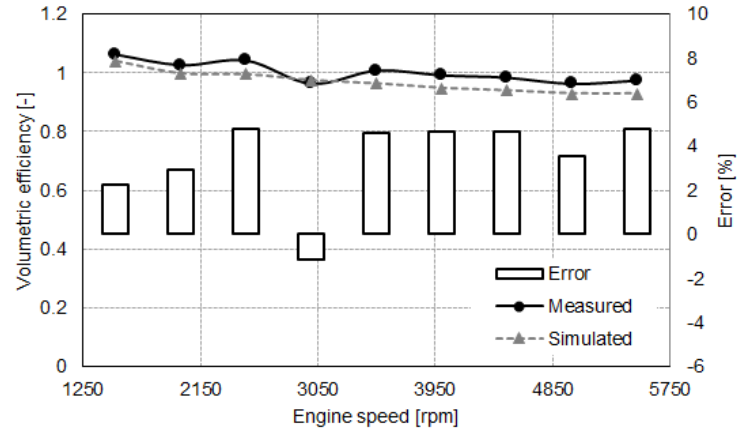


**Figure 3.18.** Intake (top) and exhaust (bottom) manifold instantaneous pressure comparison between measured (solid line) and calculated (dashed line) results at full load and 2500 rpm.

A good correlation between the instantaneous and cycle-average measured and simulated parameters was observed. Therefore, it can be assumed that the 1D model calculates with accuracy the fluid dynamics inside engine systems with unsteady and high temperature flow conditions.

### 3.3.3 Design of experiments

The DoE (or experimental design) is a mathematical design used to obtain the effect of some variables on the performance or output of a certain phenomenon with a reduce amount of tests compared to the classical



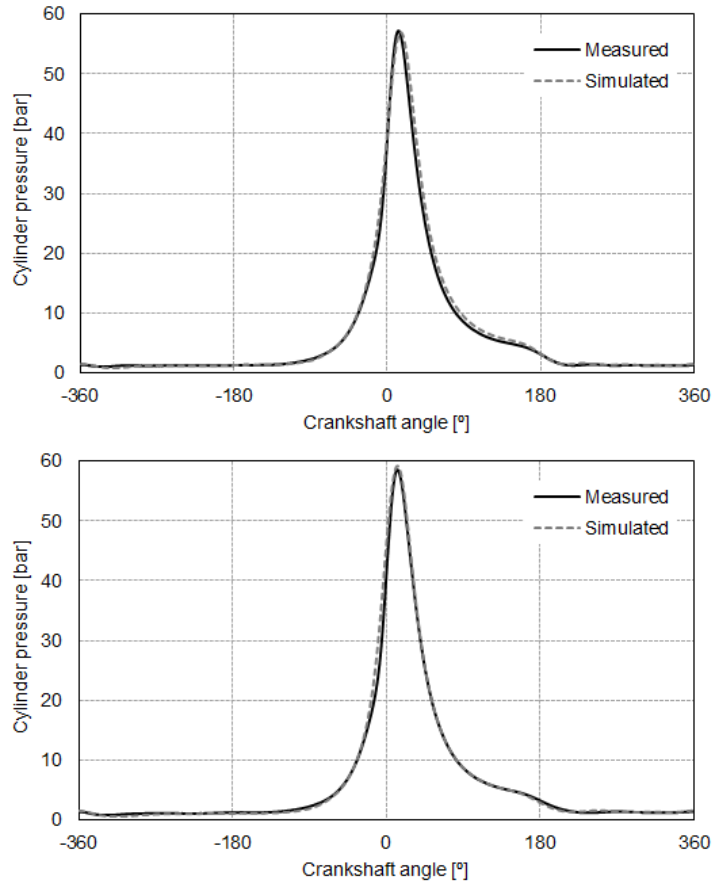
**Figure 3.19.** Volumetric efficiency comparison at full load engine conditions.

parametric study approach. The DoE's are being gaining attention lately with the more complex diesel and gasoline engine parameters calibration. Using a DoE approach not only reduces the amount of testing but it can be also used afterwards to optimize a certain output, for example, minimize fuel consumption.

Choosing the right mathematical DoE approach for the plan of experiments is the most important part of the process, because it will impact directly on the accuracy of the model and therefore the quantity of tests that are needed to be performed in order to warranty a good accuracy. Sometimes additional data have to be acquired due to lack of tests to represent accurately the output. It is also important to comment, that the number of inputs of the model will also have a big influence in the accuracy and number of tests required to build the model .

Nowadays there are tools available to support the creation of DoE's and model based calibration (MBC). One of the most important is called Ascmo, and it is being used by several big automotive companies. This software provides support to build DoE models for steady and transient state. Another software that also has some DoE and MBC support is Matlab. It is not as developed as Ascmo, but it suited the needs of this PhD-Thesis perfectly in terms of tools available and accessibility.

In this PhD-Thesis the Matlab tool called Model Based Calibration (MBC) model fitting was used in order to obtain the effect of different parameters on



**Figure 3.20.** Comparison between measured and simulated cylinder pressure for 2000 rpm - 10 bar BMEP (top) and 3000 rpm - 10 bar BMEP (bottom) .

the engine performance, combustion and exhaust emissions of the engine, with a low quantity of tests. This surface of response, created with the MBC model fitting Matlab tool, were used later to optimize the parameters configuration to minimize the engine fuel consumption. The type of DoE used in this research work was a D-Optimal Design.

Traditional DoE's (Full Factorial Designs, Fractional Factorial Designs, and Response Surface Designs) are appropriate for calibrating linear models in experimental settings where factors are relatively unconstrained in the region of interest. In some cases, however, models are necessarily nonlinear, in other cases, certain treatments (combinations of factor levels) may be expensive

or infeasible to measure. D-optimal designs are model-specific designs that address these limitations of traditional designs.

A D-optimal design is generated by an iterative search algorithm and seeks to minimize the covariance of the parameter estimates for a specified model. This is equivalent to maximizing the determinant  $D = |XTX|$ , where  $X$  is the design matrix of model terms (the columns) evaluated at specific treatments in the design space (the rows). Unlike traditional designs, D-optimal designs do not require orthogonal design matrices, and as a result, parameter estimates may be correlated. Parameter estimates may also be locally, but not globally, D-optimal [32].

This D-optimal design was used to create the MBC that would represent the outputs response for different values of the inputs. This MBC was created to optimize the fuel consumption and analyze the exhaust emissions for different combinations of VVT parameters (intake and exhausts) and EGR rates at 50% of engine load for 2000 rpm and 3000 rpm. Later a new MBC model was created to analyze the effects of different lambda values and EGR rates and their effect on fuel consumption and exhaust emissions, also at the same two operating conditions already mentioned before.

After using a DoE approach, the number of tests were fairly reduced and a faster and more efficient methodology was later developed using MBC's and 1D simulations. This will be presented in Chapter 4 Section 4.3.1.

### 3.4 Summary and conclusions

As mentioned before, in order to achieve good and credible results in a research work, the limitations on the experimental and theoretical tools must be known before starting with the experiments, or at least to know which tools or methodologies must be developed during the process in order to achieve the main objectives.

The experimental tools available are usually dependent of the resources of the research center where the research work is taken place. In this case the worst limitation was the ECU variables modification and the limits imposed by the hardware that was used to perform the research work. In the other hand, all the equipments of measurement were the optimum configuration to achieve good and accurate measurements.

In the case of the theoretical tools, they usually can be improved and developed in order to achieve the analysis and post-process necessary for each application. For this gasoline engine research work, different theoretical tools

were developed in order to be able to fully post-process and analyze all the different instantaneous and average output parameters of the engine. The combustion diagnosis tool was modified in order to post-process gasoline engine results, the 1D wave action software was also modified to be able to simulate a direct injection gasoline engine and the design of experiments methodology was developed from scratch.

## Bibliography

- [1] Benajes Jesus, Bermudez Vicente, Climent Hector and Rivas-Perea Manuel Eduardo. “Instantaneous pressure measurement in pulsating high temperature internal flow in ducts”. *Applied Thermal Engineering*, Vol. 61 n° 2, pp. 48–54, 2013.
- [2] Hohenberg G. “Definition und Eigenschaften des thermodynamischen Verlustwinkels von Kolbenmaschinen”. *Autmobile Index 4*, pp. 15–21, 1976.
- [3] Benajes Jesus, Olmeda Pablo, Martin Jaime and Carreno Ricardo. “A new methodology for uncertainties characterization in combustion diagnosis and thermodynamic modelling”. *Applied Thermal Engineering*, Vol. 71 n° 1, pp. 389–399, 2014.
- [4] Payri F., Lujan J., Climent H. and Pla B. “Effects of the Intake Charge Distribution in HSDI Engines”. In *SAE Technical Paper*, 2010. 2010-01-1119.
- [5] Abdul-Khalek I., Kittelson D. and Brear F. “The Influence of Dilution Conditions on Diesel Exhaust Particle Size Distribution Measurements”. In *SAE Technical Paper*, 1999. 1999-01-1142.
- [6] Desantes J.M., Bermúdez V., Molina S. and Linares W. “Methodology for measuring exhaust aerosol size distributions using an engine test under transient operating conditions”. *Measurement Science and Technology*, Vol. 22 n° 11, pp. 115101, 2011.
- [7] Mathis U., Mohr M. and Zenobi R. “Effect of organic compounds on nanoparticle formation in diluted diesel exhaust”. *Atmospheric Chemistry and Physics Discussions*, 2004.
- [8] Montajir R., Kawai T., Goto Y. and Odaka M. “Thermal Conditioning of Exhaust Gas: Potential for Stabilizing Diesel Nano-Particles”. In *SAE Technical Paper*, 2005. 2005-01-0187.
- [9] *TSI 2006 Model 3090: engine exhaust particle sizer spectrometer. Operation and service manual (Shoreview, MN: TSI)*. 2006.
- [10] Climent H. *Contribucion al modelado unidimensional de motores de dos tiempos de pequena cilindrada*. Tesis Doctoral, Ph.D-Thesis. Universitat Politecnica de Valencia, Departamento de Maquinas y Motores Termicos, 2002.
- [11] Daugherty R.L. and Franzini J.B. *Fluid Mechanics*. McGraw-Hill, New York, 1965.
- [12] Lujan J., Bermudez V., Serrano J. and Cervello C. “Test bench for turbocharger groups characterization”. In *SAE Technical Paper*, 2002. 2002-01-0163.
- [13] Galindo J., Serrano J. R., Guardiola C. and Cervello C. “Surge limit definition in a specific test bench for the characterization of automotive turbochargers”. *Experimental Thermal and Fluid Science*, Vol. 30 n° 5, pp. 449–462, 2006.



- [14] Lapuerta M. *Un modelo de combustion fenomenologico para un motor Diesel de inyeccion directa rapido*. Tesis Doctoral, PhD-Thesis. Universitat Politecnica de Valencia, Departamento de Maquinas y Motores Termicos, 1988.
- [15] Armas O. *Diagnostico experimental del proceso de combustion en motores Diesel de inyeccion directa*. Tesis Doctoral, PhD-Thesis. Universitat Politecnica de Valencia, Departamento de Maquinas y Motores Termicos, 1998.
- [16] Lapuerta M., Armas O. and Hernández J. J. “Diagnosis of DI Diesel combustion from in-cylinder pressure signal by estimation of mean thermodynamic properties of the gas”. *Applied Thermal Engineering*, Vol. 19 n° 5, pp. 513–529, 1999.
- [17] Payri F., Molina S., Martin J. and Armas O. “Influence of measurement errors and estimated parameters on combustion diagnosis”. *Applied Thermal Engineering*, Vol. 26 n° 23, pp. 226–236, 2006.
- [18] Benajes J. V., Lopez J. J., Novella R. and Garcia A. “Advanced Methodology for improving testing efficiency in a single-cylinder research diesel engine”. *Experimental Techniques*, Vol. 32 n° 6, pp. 41–47, 2008.
- [19] Payri Francisco, Olmeda Pablo, Martin Jaime and Carreno Ricardo. “A New Tool to Perform Global Energy Balances in DI Diesel Engines”. *SAE Int. J. Engines*, Vol. 7 n° 1, pp. 43–59, 2014. 2014-01-0665.
- [20] Molenkamp H. “Zur Genauigkeit der Brenngesetzrechnung eines Dieselmotors mit Nichtunterteiltem Brennraum”. *MTZ Motortechnische Zeitschrift*, Vol. 37 n° 7-8, pp. 285–291, 1976.
- [21] Woschni G. “A Universally Applicable Equation for the Instantaneous Heat Transfer Coefficient in the Internal Combustion Engine”. In *SAE Technical Paper*, 1967. 670931.
- [22] Woschni G. “Die Berechnung der Wandverluste und der thermischen Belastung der Bauteile von Dieselmotoren”. *MTZ Motortechnische Zeitschrift*, Vol. 31 n° 12, pp. 491–499, 1970.
- [23] Payri F., Margot X., Gil A. and Martin J. “Computational Study of Heat Transfer to the Walls of a DI Diesel Engine”. In *SAE Technical Paper*, 2005. 2005-01-0210.
- [24] Torregrosa A., Olmeda P., Degraeuwe B. and Reyes M. “A concise wall temperature model for DI Diesel engines”. *Applied Thermal Engineering*, Vol. 26 n° 11-12, pp. 1320–1327, 2006.
- [25] Degraeuwe B. *Contribution to the thermal management of DI Diesel engines*. Tesis Doctoral, PhD thesis. Universitat Politecnica de Valencia, Departamento de Maquinas y Motores Termicos, 2007.
- [26] Payri F., Benajes J., Galindo J. and Serrano J. R. “Modelling of turbocharged diesel engines in transient operation. Part 2: Wave action models for calculating the transient operation in a high speed direct injection engine”. *Proceedings of the Institution of Mechanical Engineers, Part D: Journal of Automobile Engineering*, Vol. 216 n° 6, pp. 479–493, 2002. 10.1243/09544070260137507.
- [27] Payri F., Reyes E. and Galindo J. “Analysis and Modeling of the Fluid-Dynamic Effects in Branched Exhaust Junctions of ICE”. *Journal of Engineering for Gas Turbines and Power*, Vol. 123 n° 1, pp. 197–203, 2000. 10.1115/1.1339988.
- [28] Torregrosa A. J., Galindo J., Guardiola C. and Varnier O. “Combined experimental and modeling methodology for intake line evaluation in turbocharged diesel engines”. *International Journal of Automotive Technology*, Vol. 12 n° 3, pp. 359–367, 2011.

- [29] Galindo J., Lujan J. M., Serrano J. R., Dolz V. and Guilain S. “Design of an exhaust manifold to improve transient performance of a high-speed turbocharged diesel engine”. *Experimental Thermal and Fluid Science*, Vol. 28 n° 8, pp. 863–875, 2004.
- [30] Serrano Jose, Climent Hector, Dolz Vicente and Rivas Manuel Eduardo. “Analysis of Variable Geometry Turbine and Variable Valve Timing Combined Potential in a GTDI Engine Using 1D Simulation”. In *SIA Congress*, 2011.
- [31] Kaiser M., Krueger U., Harris R. and Cruff L. “Doing More with Less - The Fuel Economy Benefits of Cooled EGR on a Direct Injected Spark Ignited Boosted Engine”. In *SAE Technical Paper*, 2010. 2010-01-0589.
- [32] *D-Optimal Designs, Mathworks help guide*, 2016.

# Chapter 4

## Influence of EGR on a GTDI engine

### Contents

---

<b>4.1</b>	<b>Introduction</b> .....	<b>113</b>
<b>4.2</b>	<b>Methodology</b> .....	<b>118</b>
<b>4.3</b>	<b>Steady state results and analysis</b> .....	<b>123</b>
4.3.1	Part load tests .....	124
4.3.1.1	Raw effect of cooled EGR on engine performance and exhaust emissions .....	124
4.3.1.2	Spark advance optimization .....	125
4.3.2	Full load tests .....	137
4.3.2.1	Combustion and engine performance ....	139
4.3.2.2	Air management .....	146
4.3.2.3	Exhaust raw emissions .....	148
4.3.3	Low load test .....	152
4.3.3.1	Engine performance and exhaust emissions	153
<b>4.4</b>	<b>Transient operation results and analysis</b> .....	<b>157</b>
<b>4.5</b>	<b>Summary and conclusions</b> .....	<b>165</b>
	<b>Bibliography</b> .....	<b>169</b>

---

### 4.1 Introduction

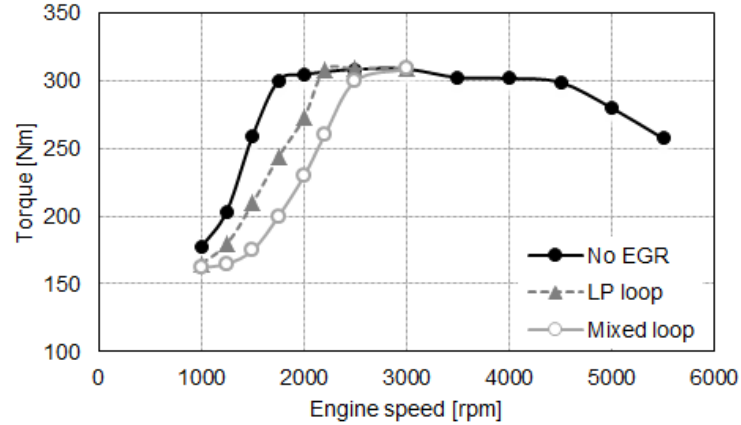
The increasingly stringent pollutant emission regulations are leading the engine research to a low fuel consumption and low exhaust emissions era. SI

gasoline engines are gaining attention since CI diesel engines are struggling with the upcoming pollutant emission regulations. In the last decade, great research and development efforts are being carried out to design more efficient SI engines in terms of fuel consumption and production costs, while exhaust emissions are already under control by means of the well-known three-way catalyst technology, as it was mentioned in Chapter 2.

An attractive strategy to reduce fuel consumption on SI engines consists of downsized engines with direct injection systems, where the displacement decreases and a turbocharging system compensates this loss of engine size, so the new engine configuration delivers the same torque and power as the reference engine. This discussion is shown in more detail in these references [1–3] and in the literature review presented in Chapter 2.

The downsizing technology implies some difficulties, such as knock or exhaust temperature, because of high engine load that engines have to withstand. These difficulties, also already mentioned in detail in Chapter 2, can be mitigated by introducing cooled EGR into the engine. This strategy (cooled EGR) will be also used to reduce fuel consumption, as described by Víték et al. and Wei et al. in their research work [4, 5]. The EGR reduces the knocking tendency, the pumping losses, the exhaust gas temperature and the heat losses through the cylinder walls. It has been reported how introducing in some cases just 5% to 10% of cooled EGR at high loads avoids the need of operating the engine in rich fuel-to-air ratio conditions (over-fuelling or enrichment strategy) to control the exhaust gas temperature as observed by Bandel et al. in their research work [6].

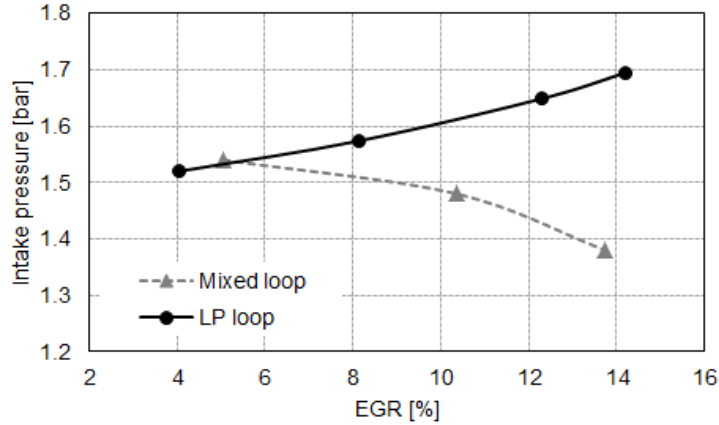
Some studies confirmed the EGR influence as a good method to reduce fuel consumption. Grandin et al. [7] evaluated the knock suppression in a turbocharged SI engine by using cooled EGR. They found considerable knock suppression at maximum power output comparable with what was achieved with fuel enrichment. Cairns et al. [8] studied the reduction in fuel consumption at partial and high load using cooled EGR and found a reduction in fuel consumption at partial load of 3% and at high load around 17%. Potteau et al. [9] focused their research on the potential of cooled EGR to reduce knocking and fuel consumption evaluating a high pressure (HP) and a low pressure (LP) EGR configuration. They found a considerable improvement in fuel consumption at partial and high load, noticing a significant advantage of the LP EGR system in comparison to the HP EGR system. Kumano et al. [10] also followed the same line of research on knocking suppression combining simulation and testing activities, quantifying in a 0.3% of fuel consumption reduction per 1% of EGR added.



**Figure 4.1.** Engine torque for the original engine configuration, with a LP EGR loop and with a mixed EGR loop.

These previous investigations encourage further research efforts to gain knowledge on the real potential of cooled EGR for being standardized in future GTDI engines, and particularly, in its LP EGR loop configuration where the effects of the EGR can be maximized compared to the mixed and HP EGR loop configuration, as found by Takaki et al. [11]. Cairns et al. [12] evaluated different cooled EGR loop configurations and their advantages and disadvantages, and Zhong et al. [13] also discussed about different cooled EGR systems in a turbocharged SI engine. They found that the LP EGR system was the best configuration to ensure EGR operation in the entire engine operating range in order to minimize fuel consumption and exhaust gas emissions.

In this research work the main objective was to achieve the maximum engine map range conditions where the cooled EGR could be used. For this reason a simple evaluation at low engine speed and high load, between a mixed EGR loop and a LP EGR loop, was performed in order to verify the limitations of each system. In Figure 4.1 the torque curve of the engine with no EGR, with a LP EGR loop and with a mixed EGR loop is presented. It can be observed that using a LP EGR loop reduces the low end torque of the engine shifting the maximum torque from 1750 rpm to 2200 rpm. In the case of using a mixed EGR loop the low end torque is even lower than with a LP configuration, shifting the maximum torque from 1750 rpm to 2500 rpm. This results are similar to the results found by Takaki et al. [11], also mentioned in more detailed in Chapter 2.



**Figure 4.2.** Intake pressure influence for different EGR rates using a mixed and LP EGR loop.

In Figure 4.2 the evolution of the intake pressure for different EGR rates using a mixed and LP EGR loop can be observed at 2000 rpm and full load. In the LP loop the intake pressure increases when the EGR rate is increased in order to maintain a constant air mass flow and therefore torque. But in the case of a mixed EGR loop, the intake pressure starts to decrease after achieving 5% of EGR, which means that the turbine cannot provide enough power to the compressor, in order to at least maintain the compression ratio, because the EGR is extracted before the turbine reducing the amount of exhaust gas that passes through the turbine.

Figure 4.2 demonstrates that the mixed EGR loop is already limited at 5% EGR and 2000 rpm while the LP EGR loop could still achieve 14% EGR rate at the same conditions. This implies a loss of torque as it was also observed in Figure 4.1, proving that a LP loop is the most suitable EGR system for this research work.

In this chapter, the research work focuses on a detailed evaluation and discussion of the impact of a LP EGR loop installed in a GTDI engine, analyzing the advantages and disadvantages of this EGR loop architecture in steady and transient operating conditions. Some research works studying the transient behavior of EGR can be found on the bibliography. As it was discussed by Takaki et al [11] in their research work, LP EGR loops have a big disadvantage compared to HP EGR loops because of the longer path that EGR must travel before getting to the engine, as it was also commented in the

literature review on Chapter 2. This higher delay or longer time that EGR takes to get into the engine, needs more complex control systems in order to take this delay into account under different transient conditions to adjust the ignition advance, VVT settings and other important engine parameters.

There are some authors as Sarlashkar et al. [14], which are developing new control strategies in order to improve cycle efficiency, knock resistance and lower  $NO_x/PM$  emissions, without sacrificing performance and drivability. This control strategy developed by Sarlashkar et al. is to control a specific EGR configuration called, dedicated EGR or D-EGR. This D-EGR is a loop of EGR feeding only one of the cylinder of the engine as it is described in the research work of Alger et al. [15].

In other cases, as observed in the research work of Liu et al. [16], a model was develop to estimate the amount of EGR for different conditions (transient and steady operating conditions), this model was validated on the test bench and therefore could be used in the future for control strategies. One of the most important things, as it is mentioned in Liu et al research work, is the good modeling of the airpath volumes and geometry in order to well estimate the delay time associated to EGR during transient conditions. This model was developed for a LP EGR loop.

It seems that the control of EGR amount and delay during transients plays a big role as it is mentioned in the small literature available nowadays. In this PhD-Thesis, a study of engine exhaust raw emissions for a given vehicle during NEDC cycles is going to be performed for two different EGR valve openings. This would lead to an understanding of the potential of cooled EGR for exhaust emissions reduction during a NEDC cycle and the impact on the fuel consumption.

The experimental facility consists of a SI GTDI 2.0l 4-stroke 4-cylinder engine, as mentioned in Chapter 3, equipped with a custom LP EGR loop designed to provide the flexibility needed for carrying out the reported research activities. Theoretical tools, such as an advanced combustion diagnostic model, were combined in synergy with dynamometer test cell experiments to improve the understanding of the different trends observed. The discussion of results includes the analysis of the cylinder gas thermodynamic evolution, exhaust pollutant emissions, engine efficiency, and finally the turbocharger requirements and performance.

This chapter is going to be divided in four main sections. First, the methodology, where the operating conditions and test procedure are presented. Second, the steady operation results and analysis, where the tests results of the cooled EGR benefits on steady operating conditions are going to be presented

for low, part and full load operating conditions for two different engine speeds. Third, transient operation results and analysis, where the tests results of the cooled EGR influence on transient operating engine conditions are going to be presented for NEDC cycles using a Ford Mondeo as base vehicle of the study. And fourth, conclusions and summary, where a brief summary and final conclusions of the results are presented.

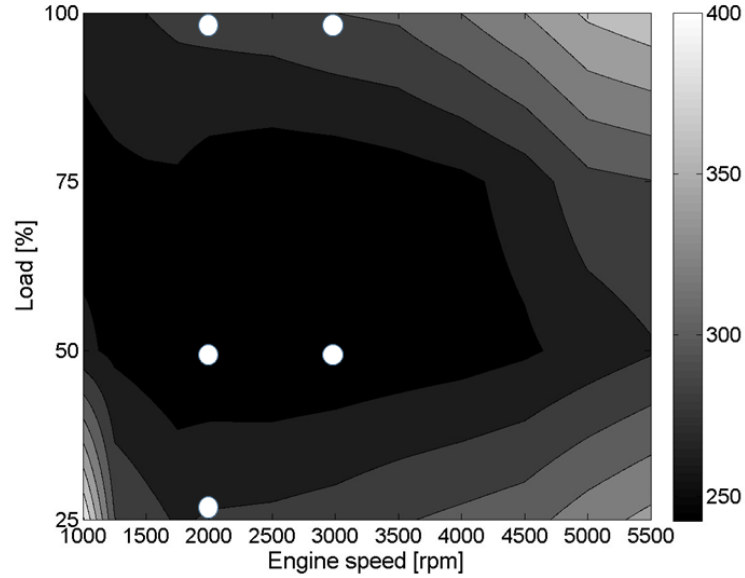
## 4.2 Methodology

In this chapter, the influence of EGR on the performance, combustion, air management and exhaust emissions are going to be analyzed. Therefore, in order to be able to collect the maximum amount of information a parametric type of test was designed for 5 operating points (OP). Three OP were chosen at 2000 rpm and the other two at 3000 rpm. In this way, the effect of engine speed on the maximum dilution limit can be analyzed and also the combustion duration compared to the cycle duration. At 2000 rpm, low, part and full load conditions were chosen, being 25%, 50% and 100% of engine load respectively, and in the case of 3000 rpm OP, part and full conditions were chosen, being 50% and 100% respectively.

A low load condition was chosen in order to analyze if cooled EGR has an improvement on the engine efficiency compared to the original situation, where VVT is used to perform IGR. In the case of part load conditions, a light knocking limitation was observed at 2000 rpm for the original OP, giving a good base conditions to analyze the knock suppression effect of EGR. However, at 3000 rpm and part load, the influence of cooled EGR is analyzed starting from a reference condition without knocking limitations. Finally, to provide a global view of the EGR impact analysis, at full load both OP have knocking limitations in their original conditions and also have an enrichment strategy, with lighter enrichment at 2000 than at 3000 rpm. This would serve to investigate the knock suppression and exhaust gas temperature reduction effect of cooled EGR. To fully understand the location on the engine map of the 5 selected OP, an engine BSFC map with the selected OP in white dots is presented in Figure 4.3. Also the operating conditions are presented in Table 4.1.

After choosing the OP that are going to be tested with cooled EGR, a test plan was developed in order to fully analyze the effects of cooled EGR using a LP configuration in a GTDI engine. The initial analysis is going to be performed by only adding EGR to the engine and maintaining constant the air mass flow, intake manifold temperature, spark timing and fuel mass





**Figure 4.3.** BSFC engine map in g/kWh with the tested operating points using EGR.

Operating point	Engine speed [rpm]	Load [%]	Air mass flow [kg/h]
OP 1 (Low Load)	2000	25	60
OP 2 (Part Load)	2000	50	110
OP 3 (Full Load)	2000	100	190
OP 4 (Part Load)	3000	50	170
OP 5 (Full Load)	3000	100	280

**Table 4.1.** Selected operating conditions.

flow, in order to observe the effect of cooled EGR on the combustion and exhaust emissions without optimizing the combustion phasing. Later, the spark timing was optimized to phase the combustion to its maximum torque phasing in order to achieve the minimum fuel consumption without having knocking. The tests at low and part load engine conditions were performed until the maximum dilution limit of the engine was achieved. In the case of full load OP, limitations in the software and the hardware could not permit to introduce EGR until the maximum dilution limit of the engine and therefore the EGR rate was limited to 14% at 2000 rpm and 10% at 3000 rpm.

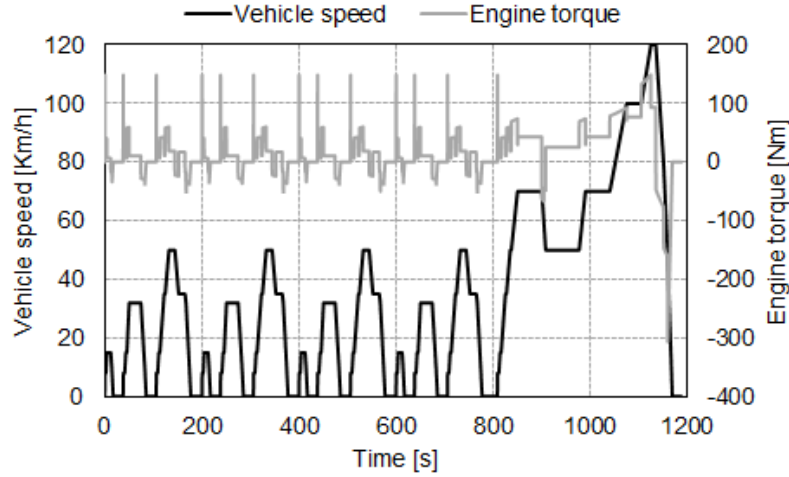
Parameter	Unit	Value
Weight	[kg]	1587
Cd*A	[m <sup>2</sup> ]	0.676
Rolling resistance	[N]	460
Tyre diameter	[m]	0.632
Gear ratio 1st	[-]	15.02
Gear ratio 2nd	[-]	8.46
Gear ratio 3rd	[-]	5.53
Gear ratio 4th	[-]	4.05
Gear ratio 5th	[-]	3.19
Gear ratio 6th	[-]	2.60

**Table 4.2.** Ford Mondeo vehicle data.

The measurement procedure explained in Chapter 3 is followed in order to guarantee the repetitive and accuracy of these tests. In this case the engine test cell was used in its best version, measuring all engine test cell parameters, ECU engine outputs and exhaust emissions ( $CO$ ,  $HC$ ,  $NO_x$  and  $PM$ ).

The transient study was performed using NEDC cycles as reference. The vehicle used to perform this NEDC cycles is a Ford Mondeo and the basic vehicle data needed to perform NEDC cycle tests is shown in Table 4.2. Using this basic vehicle data, a coastdown of the vehicle is calculated and later introduced in the control software of the dynamometer. The control software will follow a trace of torque, which is calculated based on the vehicle speed trace of the cycle, coastdown, gear ratios, final drive and tyre diameter of the vehicle and can be seen in Figure 4.4. The normative provides the gear at each part of the NEDC cycle.

Four different setups were tested to perform the NEDC cycle, each of them repeated five times in order to have consistent results and discard non-consistent tests. The first setup used was the original engine conditions, where no cooled EGR was introduced into the engine in order to have a base to compare. The second setup consisted in the EGR valve open to 25% for all the cycle and therefore the EGR rate was between 0% and 6% as it can be seen in Figure 4.5, depending on engine conditions and pressure difference between the exhaust and the compressor inlet. The third setup was similar to the second setup but with the EGR valve opening at 40%, achieving EGR rates between 0% and 10% as it can be seen in Figure 4.6, also depending on

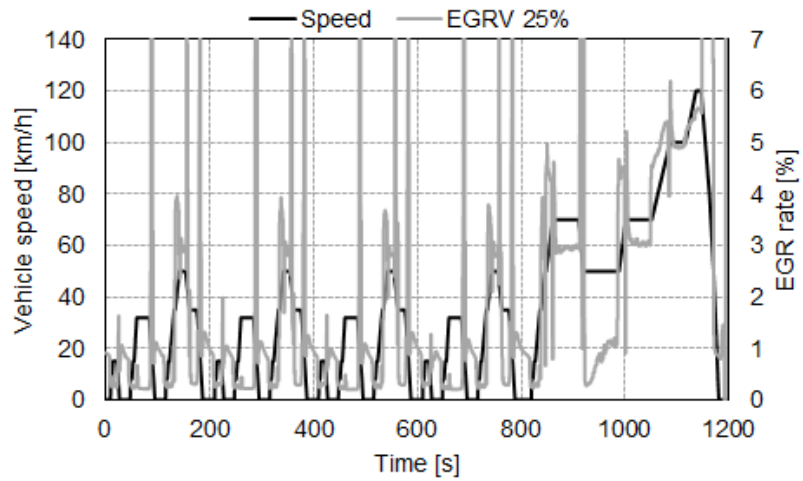


**Figure 4.4.** NEDC cycle speed trace and calculated torque trace to follow in the engine test bench.

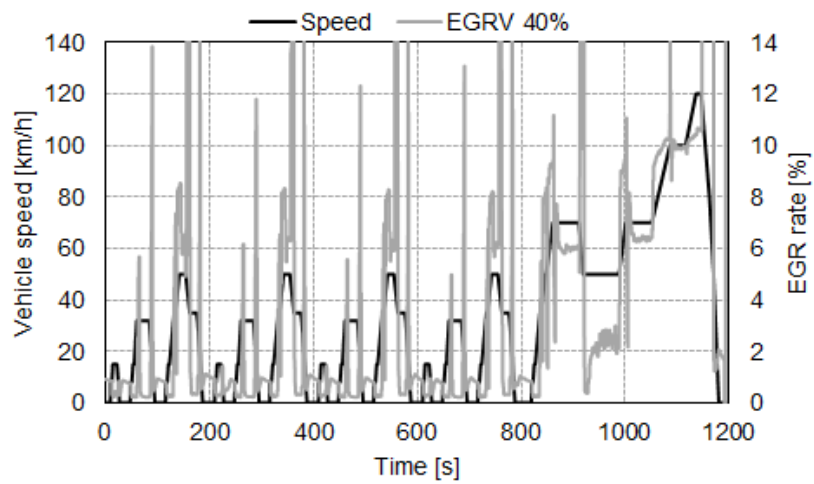
engine conditions and pressure difference between the exhaust system and the compressor inlet. And the fourth and last setup consisted in opening the EGR valve to 25% only during the extra-urban part of the cycle, as it can be seen in Figure 4.7, where only EGR rate it is observed in the extra-urban part of the cycle. Similar values of EGR rate as in the second setup are observed, since it is the same opening of the EGR valve. These results are going to be used to analyze the influence of EGR in the air loop behavior, engine performance and exhaust emissions. The NEDC cycles were measured in hot conditions and all tests were performed starting at the same engine coolant temperature conditions and warm-up time.

As it was observed in Figure 4.5, Figure 4.6 and Figure 4.7, in the three cases there is a presence of EGR rate peaks during the deceleration zones of the engine in the cycle. During the decelerations there is a fuel-cut off strategy and therefore no  $CO_2$  is present on the exhaust. But the  $CO_2$  that was traveling to the intake has to be consumed by the engine, so as it can be seen in Equation 4.1 used by Payri et al. [17] to calculate EGR rate, when the denominator of the equation tends to zero the EGR rate tends to infinite.

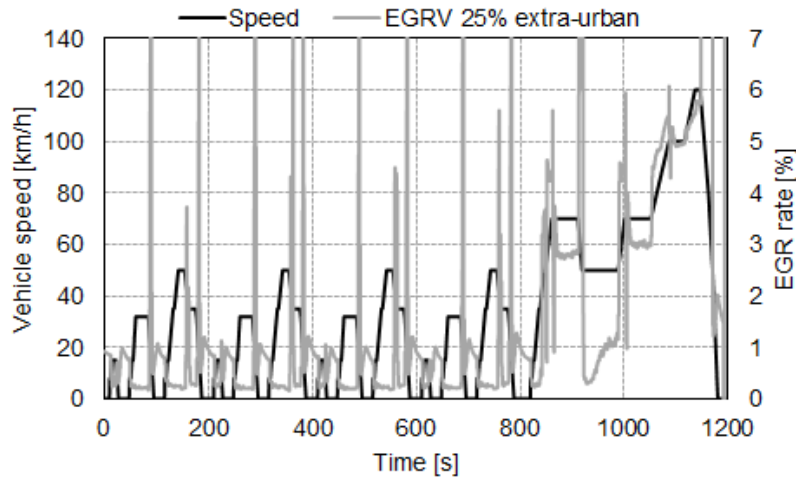
$$EGR_{rate} = \frac{[CO_2]_{Intake} - [CO_2]_{Ambient}}{[CO_2]_{Exhaust} - [CO_2]_{Ambient}} \quad (4.1)$$



**Figure 4.5.** NEDC cycle speed trace and EGR rate when a 25% of opening is used on the EGR valve.



**Figure 4.6.** NEDC cycle speed trace and EGR rate when a 40% of opening is used on the EGR valve.



**Figure 4.7.** NEDC cycle speed trace and EGR rate when a 25% of opening is used on the EGR valve during the extra-urban part of the cycle.

A basic methodology had to be developed in order to measure the delay time of each part of the exhaust analyzer in order to afterwards synchronize the exhaust emissions signal so it can match with the actual behavior of the engine in each part of the NEDC cycle. A test of tip-in was performed each day from 0% to 50% of engine load at iso-engine speed of 2000 rpm, before performing the NEDC cycle tests in order to be able to calculate these exhaust gas analyzer delays. The tip-in was performed until 50% of engine load to exclude turbocharger lag of the equation and simplify the post-processing.

### 4.3 Steady state results and analysis

In this section the results and analysis of the five tested steady engine operating points are going to be presented. As it was explained in the methodology section, an analysis of combustion, performance, air management and exhaust emissions of each OP is performed. The section is going to be divided in three subsections, depending on the engine load condition: low, part and full load.

### 4.3.1 Part load tests

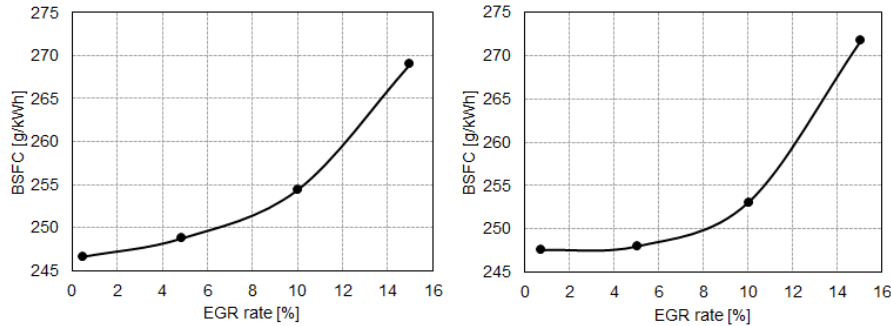
The study was performed at 2000 rpm and 3000 rpm, and 10 bar of BMEP. This section is going to be divided in two sub-sections. The first one explains and analyzes the effect of cooled EGR on the engine performance and exhaust emissions. The second sub-section shows the potential of cooled EGR by optimizing the spark advance to obtain the optimum phasing in order to minimize the engine fuel consumption and observe its influence on the combustion, for different EGR rate conditions.

#### 4.3.1.1 Raw effect of cooled EGR on engine performance and exhaust emissions

In this section, the effect of cooled EGR on the engine performance and exhaust emissions is analyzed at part load engine conditions. The tests were performed at iso-air mass flow, iso-intake temperature, iso-fuel mass flow and iso-spark advance, and cooled EGR was introduced into the engine from 0% to 15% of rate.

It is well known how EGR creates a dilution effect and decreases the oxygen concentration and the mixture reactivity, as mentioned in Chapter 2. This decrease in mixture reactivity increases the combustion duration. Therefore, when cooled EGR is introduced into the engine and the spark timing is maintained constant while increasing the EGR rate, it can be observed in Figure 4.8, how the BSFC of the engine increases because of the combustion retard. This effect is detected at both engine speeds. It can also be observed, how the dilution effect on the engine fuel consumption is bigger at 3000 rpm because of the higher engine speed and for the same amount of dilution the combustion degradation leads to higher increase in combustion duration than at 2000 rpm and therefore worst fuel consumption because of the more retarded combustion.

The effect of higher combustion durations with constant spark timing also affects other engine outputs, such as the exhaust manifold temperature or turbine inlet temperature, where an increase is observed when operating with higher EGR rates as it can be seen in Figure 4.9. The effect is worst in the case of 3000 rpm since the higher engine speed with the same combustion degradation leads to higher combustion duration in crank-angle degrees and, therefore, higher temperature at EVO. On the other hand, cooled EGR reduced the pumping losses of the engine, as it can be seen in Figure 4.9, where the intake manifold pressure is presented for different EGR rates, observing



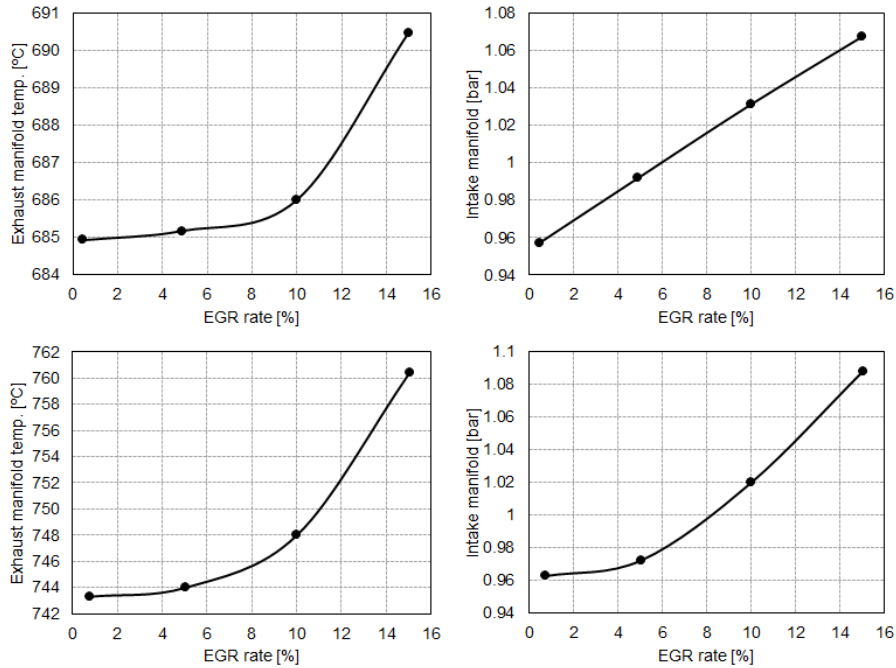
**Figure 4.8.** Engine BSFC at 2000 rpm and 50% load (left graph) and at 3000 rpm and 50% (right graph) for different EGR rates.

that it increases with the increase of EGR rate, reducing the engine pumping work at both engine speeds.

Regarding exhaust emissions, the reduction in mixture reactivity and the increase in combustion duration because of the introduction of cooled EGR also reduces the combustion temperature [18]. The reduction in combustion temperature and oxygen concentration reduces the  $NO_x$  formation, as it can be seen in Figure 4.10, where the  $NO_x$  emissions decrease as the EGR rate increases. It can also be observed that  $CO$  emissions also decreased while the EGR rate increased because of the reduction of  $CO_2$  dissociation reaction producing less  $CO$ . On the other hand it can be seen how  $HC$  emissions increase when the EGR rate increases, due to the lower combustion temperature and oxygen concentration that reduces the  $HC$  oxidation process and increases the probability of the quenching of the flame, increasing the amount of final  $HC$  emissions at EVO. It can be seen how the effect and trend is the same for 2000 rpm and 3000 rpm.

#### 4.3.1.2 Spark advance optimization

After analyzing the effect of cooled EGR in the engine performance and exhaust emissions, it can be seen how the original spark timing, VVT parameters and fuel injection timing values have to be re-optimized to operate with cooled EGR. Taking this into account, this section will explain briefly the methodology developed to optimize the spark timing and will also serve to understand the potential of cooled EGR with an optimized combustion phasing that could maximize torque and therefore minimize BSFC.

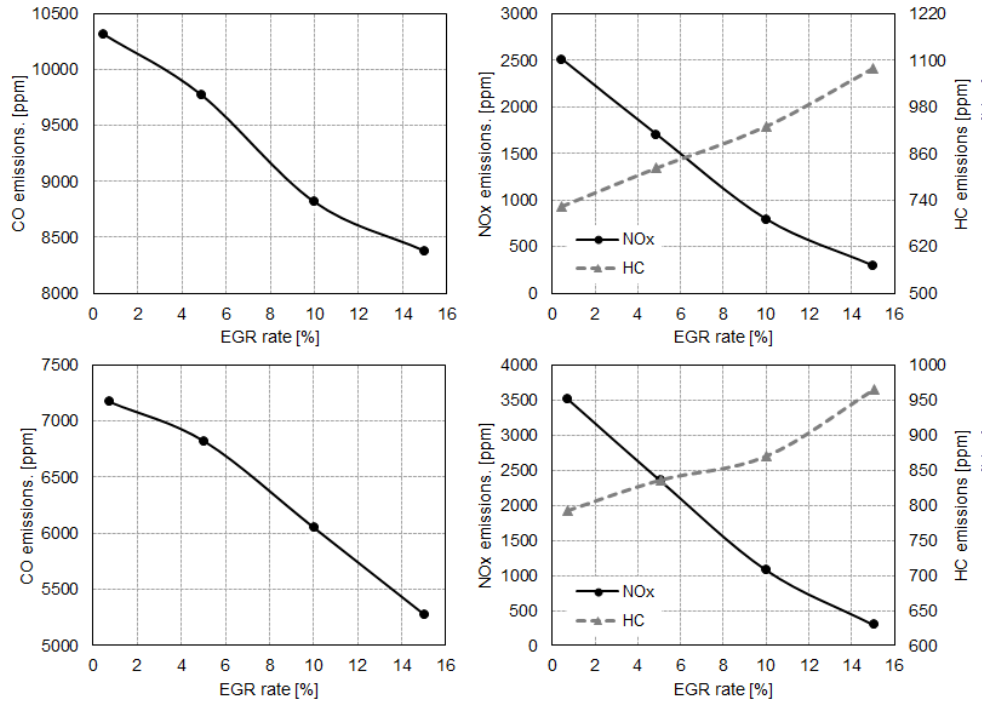


**Figure 4.9.** Exhaust manifold temperature (upper left graph) and intake manifold pressure (upper right graph) at 2000 rpm and 50% load and exhaust manifold temperature (bottom left graph) and intake manifold pressure (bottom right graph) at 3000 rpm and 50% for different EGR rates.

To start the optimization process the spark timing needs to be optimized to phase the combustion retard produced by the dilution effect of EGR, already explained before. The spark timing is optimized for each tested EGR rate and for two engine speeds, 2000 rpm and 3000 rpm. This spark timing optimization process consists in advancing the spark crank-angle degree until the maximum torque is achieved. For these tests the air mass flow, fuel mass flow and intake temperature conditions for different EGR rates were maintained constant during the EGR sweep.

The combustion, performance, air management and exhaust emissions of the engine are going to be analyzed for this optimized spark advance setup to further understand the potential of introducing cooled EGR in a GTDI engine with an optimum combustion phasing that minimizes engine BSFC.



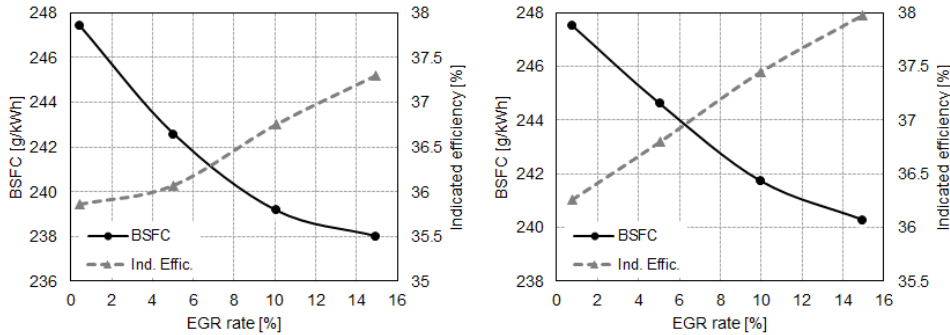


**Figure 4.10.** CO (upper left graph), NO<sub>x</sub> and HC emissions (upper right graph) at 2000 rpm and 50% load and CO (bottom left graph), NO<sub>x</sub> and HC emissions (bottom right graph) at 3000 rpm and 50% load for different EGR rates.

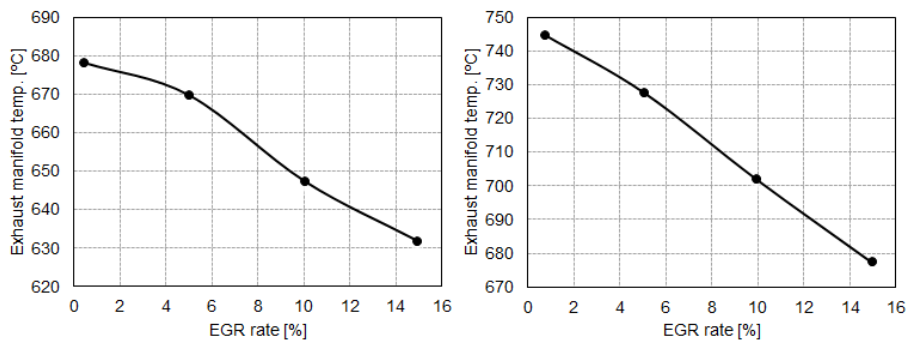
#### 4.3.1.2.1 Combustion and engine performance

A spark advance optimization is performed for each EGR rate step, as it was mentioned before, from 0% to 15% every 5%. After the optimization of the spark timing for each EGR rate step, the introduction of 15% of cooled EGR reduced the engine BSFC in 3.8% and increased the indicated efficiency in 1.6% absolute value at 2000 rpm. Also reduced the fuel consumption in 3% and increased the indicated efficiency also in 1.6% absolute value at 3000 rpm as it can be seen in Figure 4.11 where the indicated efficiency and the BSFC are plotted for different EGR rates. A similar result was found by Potteau et al. in their research work [9], where a 3% of fuel consumption reduction was observed at part load conditions.

The evolution of the exhaust manifold temperature for different EGR rates can be seen in Figure 4.12. The exhaust gas temperature was also reduced from 678°C to 630°C at 2000 rpm and from 745°C to 690°C at 3000 rpm, using



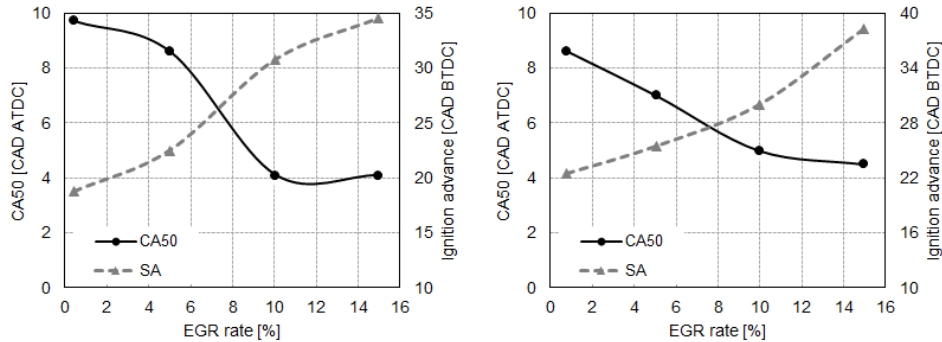
**Figure 4.11.** Engine BSFC and indicated efficiency at 2000 rpm and 50% load (left graph) and at 3000 rpm and 50% (right graph) for different EGR rates.



**Figure 4.12.** Exhaust manifold temperature at 2000 rpm and 50% load (left graph) and at 3000 rpm and 50% (right graph) for different EGR rates.

15% EGR rate in both engine speed conditions. This reduction in the exhaust gas temperature is due to the reduction in the combustion temperature and the new optimized combustion phasing. These EGR effects on the combustion are going to be explained in more detail later in this section.

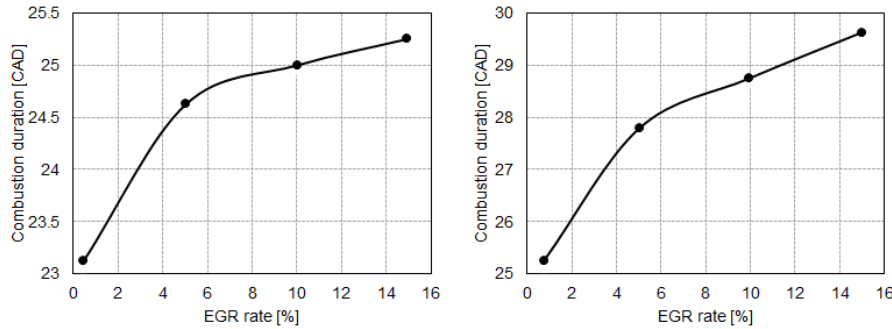
Analyzing the 5% EGR rate operating conditions at 2000 rpm, the ignition advance was still limited by knocking. An advance on the CA50 can be observed in Figure 4.13 (left graph), where the ignition advance was increased in 4.5 CAD, improving the combustion phase compared to the reference operating conditions in 2 CAD. The CA50 is also advanced for the 10% and 15% EGR rate conditions, compared to the original and 5% EGR conditions. It was also seen how increasing the EGR rate, advanced the combustion phasing to an optimum CA50. This is due to the reduction in heat transfer and



**Figure 4.13.** CA50 and spark advance at 2000 rpm and 50% load (left graph) and at 3000 rpm and 50% (right graph) for different EGR rates.

therefore the optimum combustion phasing is placed closer to TDC. This effect is widely explained in the research work of Carvalho et al. [19] where it is said that an adiabatic combustion has its optimum phasing at TDC. In the case of 3000 rpm, the original conditions were not limited by knocking and therefore it can be seen in Figure 4.13 (right graph), that CA50 was around 8 CAD ATDC at the original operating conditions. It can be observed the same effect of EGR in the optimum combustion phasing when the EGR rate increases, as at 2000 rpm. It is important to remark that when engine speed increases, the ignition advance should increase to achieve the same combustion phasing because the combustion duration in CAD will increase, for the same combustion speed, due the increase of engine speed. Therefore to phase the combustion an earlier start of de combustion is needed, as it can be observed in Figure 4.13. Comparing the spark advance values between 2000 rpm and 3000 rpm, it can be observed that more ignition advance is needed for 3000 rpm than for 2000 rpm.

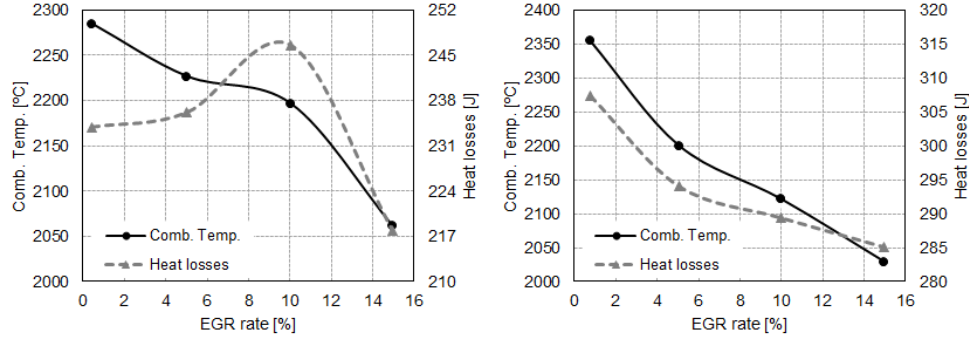
The combustion duration increased when EGR was introduced into the engine for both engine speeds, as it was mentioned before, due to the dilution effect of the EGR that reduced the oxygen concentration in the mixture decreasing its reactivity, also found by Grandin et al. in their research work [7]. It can be observed in Figure 4.14 how combustion duration increases for both engine speeds, but as expected, it increases more at 3000 rpm than at 2000 rpm because of the engine speed effect explained before. The combustion duration increases more than 2 CAD at 2000 rpm and more than 4 CAD at 3000 rpm for the same 15% EGR rate conditions.



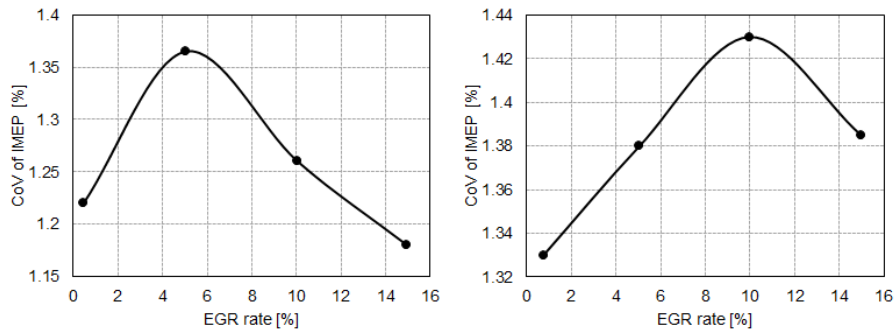
**Figure 4.14.** Combustion duration at 2000 rpm and 50% load (left graph) and at 3000 rpm and 50% (right graph) for different EGR rates.

Regarding the combustion temperature, it can be observed in Figure 4.15 how adding cooled EGR reduces the combustion temperature at 2000 rpm and 3000 rpm. This reduction in combustion temperature is a consequence of the EGR dilution effect already mentioned before, which reduces combustion reactivity, increasing the combustion duration as observed in Figure 4.14. This reduction in the combustion temperature also reduces the heat losses during the cycle, for both engine speeds, when the EGR rate is at 15%, as it can be observed also in Figure 4.15. In the case of 3000 rpm it can be observed how heat losses decreased as the EGR rate increased but in the case of 2000 rpm it can be seen how with 5% and 10% of EGR rate, the heat losses increased despite the reduction in combustion temperature. This is due to the re-phasing of the combustion near the TDC, as it was presented in Figure 4.13 in the CA50 evolution for different EGR rate. Having the CA50 near TDC increases the turbulence due to the smaller in-cylinder volume where the combustion process occurs and therefore increases the heat losses. The new optimum CA50 at 10% EGR rate was also possible because knocking was not more a limitation at this EGR rate conditions, at 2000 rpm.

It can also be observed how the combustion temperature, in the case of 2000 rpm, changes its trend after 10% of EGR rate because, as it was stated before, the re-phasing of the combustion also increases the combustion temperature, and the total reduction of the combustion temperature, observed in Figure 4.15 left graph, is a combination of the temperature increase because of the combustion re-phasing and the temperature decrease because of EGR dilution effect. It can be seen how after 10% of EGR rate the trend changes drastically because the combustion phasing remains at the same CAD position



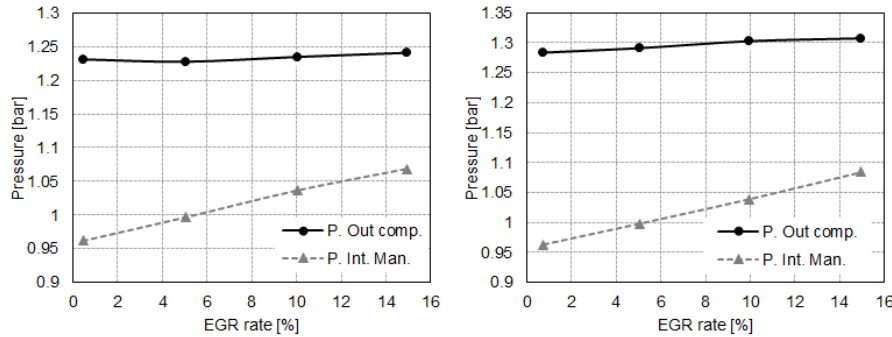
**Figure 4.15.** Combustion temperature and heat losses at 2000 rpm and 50% load (left graph) and at 3000 rpm and 50% (right graph) for different EGR rates.



**Figure 4.16.** Coefficient of variation of the IMEP at 2000 rpm and 50% load (left graph) and at 3000 rpm and 50% (right graph) for different EGR rates.

and only the effect of dilution effect produced by the EGR is observed, decreasing also the heat losses.

After the entire combustion analysis it is important to finally observe the coefficient of variation (CoV) of the IMEP in order to analyze if cooled EGR affects the stability of cycle to cycle combustion in the range that the tests were performed. In Figure 4.16 the CoV of the IMEP is presented for both engine speeds and different EGR rate conditions. It is observed that the CoV stayed almost at the same level as the original conditions without EGR but the trend that can be observed at 2000 rpm or 3000 rpm cannot be analyzed in any way because of the small difference between the different tests.



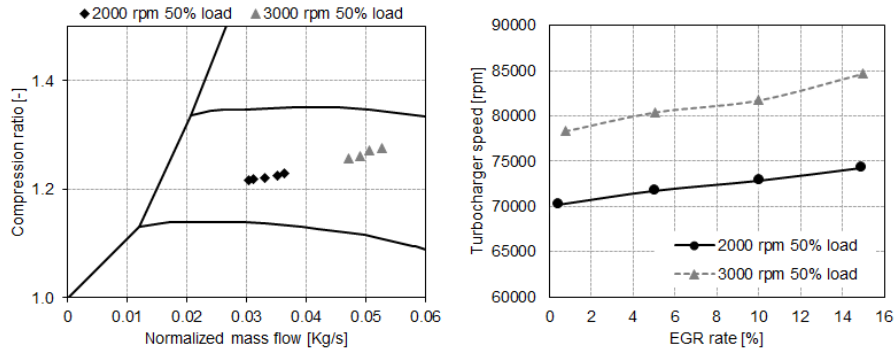
**Figure 4.17.** Intake manifold pressure at 2000 rpm and 50% load (left graph) and at 3000 rpm and 50% (right graph) for different EGR rates .

In this partial load conditions the effect of knocking suppression, at 2000 rpm, and dilution effect due to the introduction of cooled EGR, at both engine speeds, was observed. The CA50 was able to be phased at the optimum crank angle at 2000 rpm, because of the knocking mitigation. The heat losses were reduced and the exhaust gas temperature was also reduced without compromising the CoV of the IMEP at high EGR rates at both engine speeds. The best configuration at this load at 2000 rpm is the 15% EGR rate operating conditions which reduced the fuel consumption in 4.8%, the exhaust gas temperature in 48°C and keeps a low IMEP CoV under 1.2%. In the case of 3000 rpm the best configuration is also at 15% EGR rate operating conditions which reduces the fuel consumption in 3%, the exhaust gas temperature in 55°C and keeps a low IMEP CoV under 1.4%.

#### 4.3.1.2.2 Air management

In order to analyze the air management area, it must be taken into account that the tests were performed at iso-air mass flow and iso-intake temperature, as stated before. In Figure 4.17 the intake pressure for both engine speeds is plotted as a function of the EGR rate. The intake pressure increases as the EGR rate increase due to the increase in mass in the same intake volume and the unchanged volumetric efficiency of the engine at each engine speed for different EGR rate conditions.

The compressor outlet pressure rested the same value during the increase of the EGR rate for both engine speed conditions, as can be observed in Figure 4.17, while the intake pressure increased. The compressor outlet

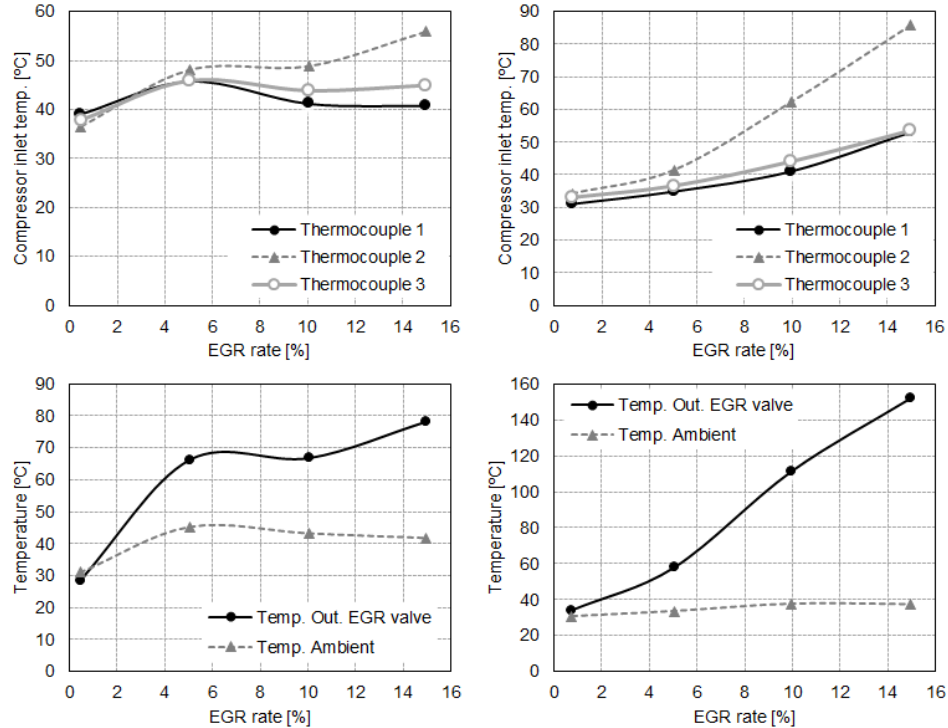


**Figure 4.18.** Compressor map operating points (left graph) and turbocharger speed (right graph) at 2000 rpm and 50% load and at 3000 rpm and 50% for different EGR rates.

pressure was higher than the observed pressure in the intake manifold because the throttle valve was controlling the load (air mass flow) of the engine at these operating conditions. This could be also controlled by opening the waste-gate and controlling the outlet compressor pressure and so the intake manifold pressure with the throttle valve fully open. However, if the steady operating condition is followed by a full load transient demand the turbocharger response will have more lag than having the waste-gate fully closed and controlling the intake pressure with the throttle valve as in this case.

The compressor mass flow increased while the outlet compressor pressure rested at the same value, moving the compressor operating point to the right of the compressor map, as left graph of Figure 4.18 shows, and therefore increasing turbocharger speed. The turbocharger speed increased as the EGR rate increased, this can be observed in the right graph of Figure 4.18.

At the compressor inlet, three thermocouples were placed  $120^\circ$  separated in radial position, downstream the connection of the EGR pipe. The main goal was to identify a potential non homogeneous distribution of the EGR with the fresh air at the compressor inlet and therefore one of the thermocouples was placed aligned to the EGR outlet. In Figure 4.19 an evolution of the compressor inlet temperature while increasing the EGR rate for both engine speed conditions is plotted in the two top graphs, where the thermocouple number two is the one that is aligned with the EGR outlet. The difference on the inlet temperature between the three thermocouples at low EGR rates are negligible but at 15% EGR rate the difference is higher between the thermocouple number two and the others, which certifies that EGR and air



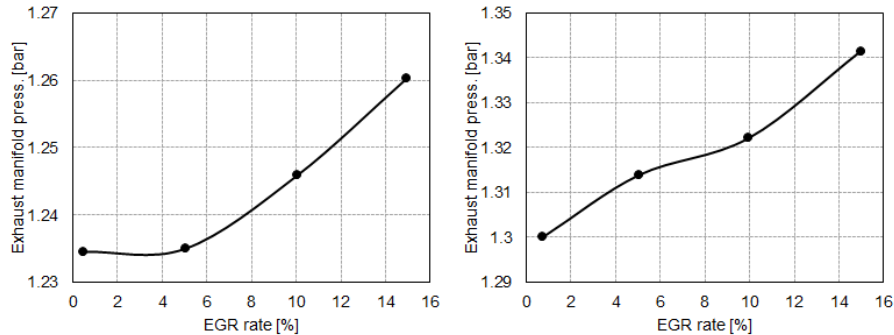
**Figure 4.19.** Compressor inlet temperature (top graphs), temperature ambient and EGR valve outlet temperature (bottom graphs) at 2000 rpm and 50% load (left graph) and at 3000 rpm and 50% (right graph) for different EGR rates.

are not well mixed before entering the compressor. This could lead to a future compressor reliability problem as EGR rate and compressor compression ratio, increase, so it is recommended that the EGR outlet is designed to improve the EGR/air mixing before the compressor inlet.

The tests at 2000 rpm were performed at different EGR outlet temperature compared to 3000 rpm but very similar ambient temperature, as it can be seen in bottom left graph of Figure 4.19, where the temperature at the EGR outlet is higher for the tests performed at 3000 rpm and therefore the difference in the measurements of the thermocouples placed at the compressor inlet is higher than in the case of 2000 rpm despite the difference of air and EGR mass flow.

Regarding the exhaust manifold pressure, an increase of 25 mbar at 2000 rpm and 40 mbar at 3000 rpm is observed at the maximum tested EGR rate, as illustrated in Figure 4.20. This increase is because with the addition of





**Figure 4.20.** Exhaust manifold pressure at 2000 rpm and 50% load (left graph) and at 3000 rpm and 50% (right graph) for different EGR rates.

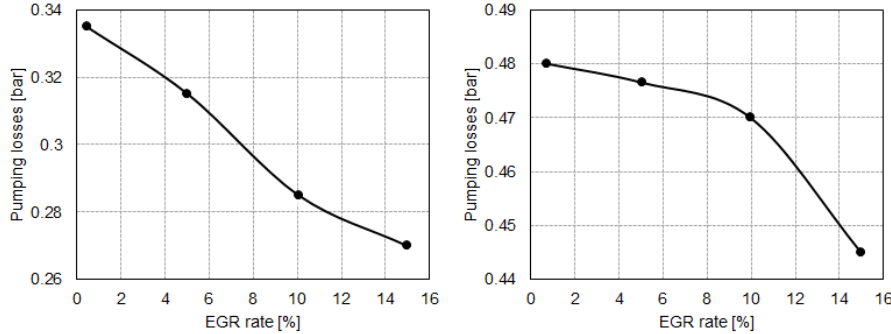
EGR, the total mass that is passing through the engine is higher than in the original conditions and since the waste-gate is fully closed at this partial load engine conditions, the pressure before the turbine increases.

Concerning the pumping losses, these were reduced in 19.5% at 2000 rpm and 7.3% at 3000 rpm compared to the reference operating conditions; the evolution can be seen in Figure 4.21. The reduction at 2000 rpm is due to the 100 mbar increase on the intake pressure, caused by the increase in the intake mass because of the EGR addition, despite the 25 mbar of exhaust pressure increase. On the other hand at 3000 rpm the intake pressure increase was also around 100 mbar but the reduction in pumping losses were lower than at 2000 rpm due to the higher exhaust manifold pressure increase of 40 mbar.

The pumping losses also helped to reduce the fuel consumption in conjunction with the new combustion phasing and heat losses reduction explained before on the combustion and performance section. The 15% EGR rate operating conditions did not present a difficulty to the compressor at this engine load. The only disadvantage found was the water condensation after the inter-cooler that could obviously harm the engine if it is not treated correctly.

#### 4.3.1.2.3 Exhaust emissions

In addition to the positive effects of cooled EGR on the engine performance, it also had a beneficial effect on pollutant exhaust emissions. The behavior of the exhaust pollutant emissions for different EGR rates can be observed in Figure 4.22 for 2000 rpm and in Figure 4.23 for 3000 rpm. As expected the



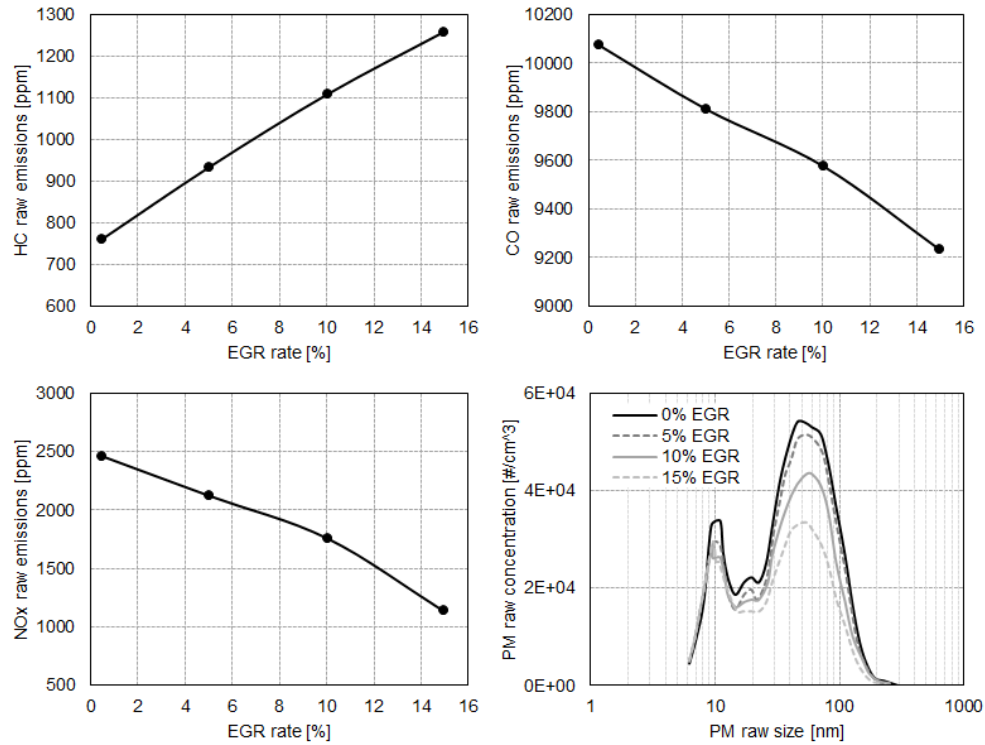
**Figure 4.21.** Pumping losses at 2000 rpm and 50% load (left graph) and at 3000 rpm and 50% (right graph) for different EGR rates.

EGR presence reduced the  $NO_x$  emissions in almost 54% at 2000 rpm and 72% at 3000 rpm. This reduction in  $NO_x$  emissions is due to the reduction of the combustion temperature and in-cylinder oxygen concentration, reducing the formation of  $NO_x$ , as explained in Chapter 2.

The  $HC$  emissions increased in 65% at 2000 rpm and 57% at 3000 rpm, because of the lower in-cylinder temperature and the longer combustion duration. Despite the reduction in the in-cylinder temperature, the combustion new phase compensates this phenomenon having also lower CoV of the IMEP compared to the reference point as it was presented before in Figure 4.16.

The  $CO$  emissions were reduced in almost 9% at 2000 rpm and 23% at 3000 rpm using 15% of EGR rate. This reduction in  $CO$  emissions is due to a reduction in the level of dissociation of  $CO_2$  because the combustion temperature decreases due to the EGR dilution effect.

The particulate matter ( $PM$ ) emissions were also reduced because of the reduction on the combustion temperature, reducing the  $PM$  formation rate. Similar results were also presented by Alger et al. using a port fuel injection gasoline engine in their research work [20]. The evolution can be seen in Figure 4.22 for 2000 rpm and in Figure 4.23 for 3000 rpm on the bottom right graph, where a decrease in concentration is observed as the EGR rate is increased for both engine speeds. In 2000 rpm operating conditions, between 10% EGR and 15% EGR the smallest size  $PM$  concentration almost rested at the same value, whether a reduction in the largest size  $PM$  concentration is observed.

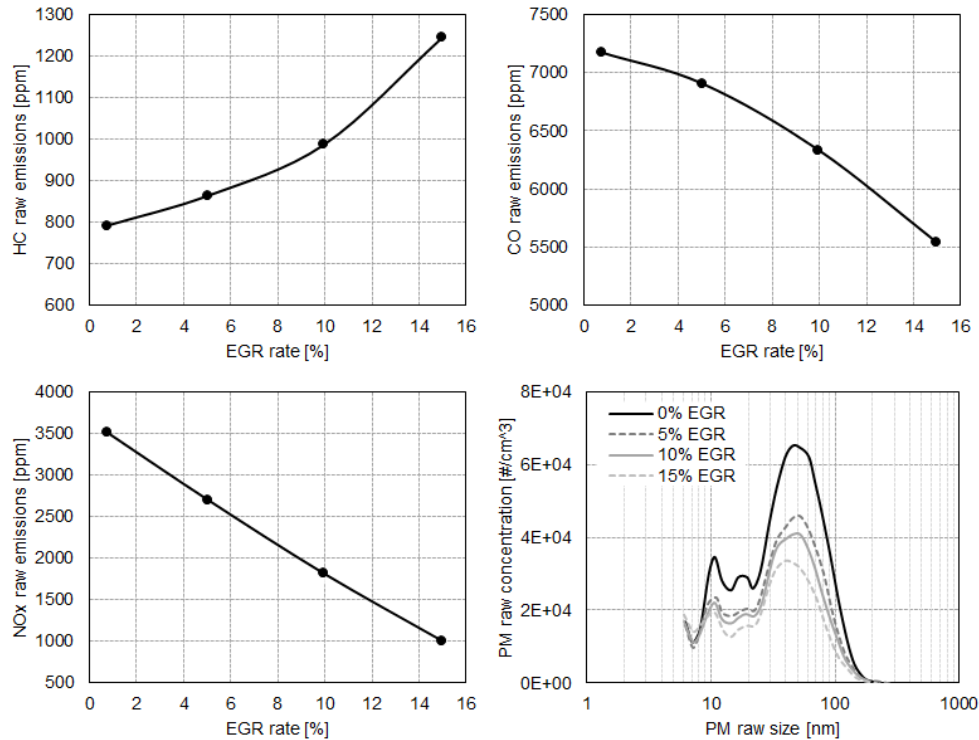


**Figure 4.22.** Exhaust raw emissions at 2000 rpm and 50% load for different EGR rates. *HC* emissions (top left graph), *CO* emissions (top right graph), *NO<sub>x</sub>* emissions (bottom left graph) and *PM* emissions (bottom right graph).

In summary, the *NO<sub>x</sub>*, *CO* and *PM* emissions were reduced, using 15% of cooled EGR rate, compared to the reference point at both tested engine speed conditions. The increase in *HC* emissions do not represent a major problem since the three way catalyst (TWC) has over 98% of *HC* efficiency conversion, as it was explained in Bermúdez et al. research work [21], reducing the difference between the original engine conditions without EGR and the optimum spark advance conditions using cooled EGR, to 10 ppm at 2000 rpm and 9 ppm at 3000 rpm after the catalyst.

#### 4.3.2 Full load tests

Following the same testing methodology already explained in the part load section, an EGR rate sweep was performed at 2000 rpm and 17 bar and at



**Figure 4.23.** Exhaust raw emissions at 3000 rpm and 50% load for different EGR rates. HC emissions (top left graph), CO emissions (top right graph), NO<sub>x</sub> emissions (bottom left graph) and PM emissions (bottom right graph).

3000 rpm and 18 bar of BMEP. The EGR rate sweep was performed from 0% to 14% for 2000 rpm and from 0% to 10% at 3000 rpm. The tests were performed at iso-air mass flow, iso-fuel mass flow and iso-intake temperature, and the spark timing was optimized at minimum best timing (MBT) value or trace knock limit value for the each test, in order to minimize the engine BSFC for all EGR rate tested conditions.

At this engine load, no further optimization of VVT settings and injection timing is going to be performed because the original configuration of VVT was already optimized to reduce IGR for full load operation and the addition of cooled EGR does not change these optimum settings as it could be the case at part load engine conditions. Regarding the injection timing no optimization was considered since both evaluated operating conditions at full load are limited by knocking and therefore increasing the mixture reactivity

or decreasing the volumetric efficiency, in the case of 2000 rpm will limit the amount of EGR rate that can be introduced because the iso-air mass flow conditions cannot be maintained due to the original turbocharger. This will be explained in more detail in the air management section.

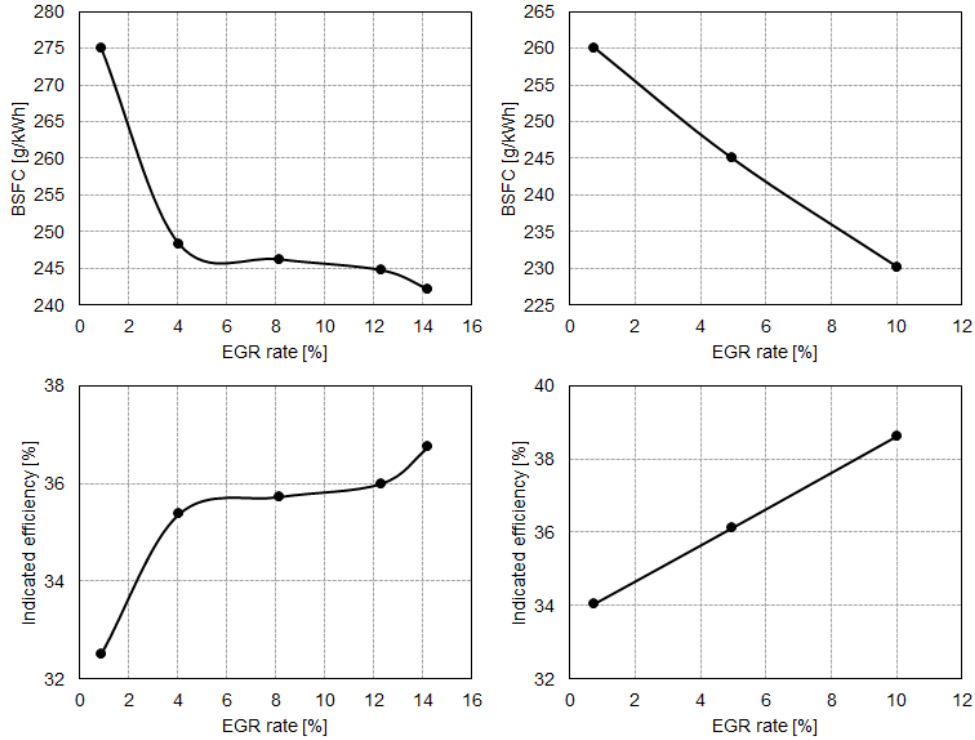
The combustion, performance, air management and exhaust emissions of the engine are analyzed for both engine speed conditions, to further explain the effects and advantages of cooled EGR at full load operating conditions. The section is divided into three sub-sections: combustion and engine performance, air management and exhaust emissions to analyze both engine speeds conditions.

#### 4.3.2.1 Combustion and engine performance

This engine uses an enrichment strategy to control the turbine inlet temperature. In the case of high load engine conditions, the enrichment is needed from 2000 rpm until maximum engine speed 6500 rpm as it was presented in Figure 3.5 in Chapter 3. Introducing cooled EGR allows the engine to operate in stoichiometric conditions, at a certain EGR rate, this will massively improve BSFC. This was observed by Bandel et al. [6], showing that with a small amount of cooled EGR rate the enrichment strategy can be eliminated at full load. According to the top left graph of Figure 4.24, introducing 14% of cooled EGR at 2000 rpm leads to a fuel consumption reduction of 12%, also increasing in more than 4.5% the indicated efficiency absolute value compared to the original operating conditions. In the case of 3000 rpm it can be observed in the top right graph of Figure 4.24 that the reduction in BSFC is 11.5% introducing 10% of cooled EGR and an increase of 4.5% on the indicated efficiency absolute value. Similar results were found by Potteau et al. in their research work [9], where a 17% of fuel consumption reduction was observed at full load conditions.

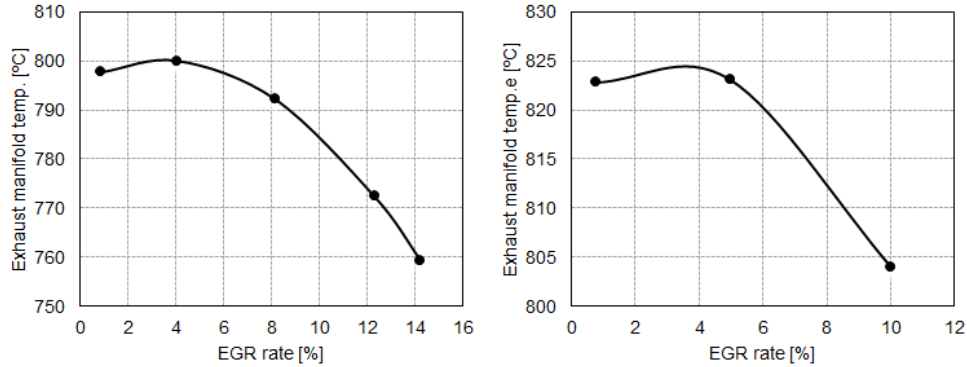
The observed reduction on engine BSFC is higher than at part load engine conditions, due to the knocking limitation and enrichment strategy at high load operating conditions, hence the room for improvement is bigger than at partial load. It must be taken into account that the original operating condition at part load almost had an indicated efficiency of 35.8% at 2000 rpm and 36.2% at 3000 rpm, in the case of high load is around 32.5% at 2000 rpm and 34% at 3000 rpm. These results are within the results found by Alger et al. [18], Cairns et al. [8] and Zhong et al. [13] in their research work.

Results included in the top left graph of Figure 4.24 confirm how a sharp fuel consumption reduction was achieved by only introducing 4% of EGR rate



**Figure 4.24.** BSFC (top left graph) and indicated efficiency (bottom left graph) for EGR rates at 2000 rpm and 100% of engine load and BSFC (top right graph) and indicated efficiency (bottom right graph) for EGR rates at 3000 rpm and 100% of engine load.

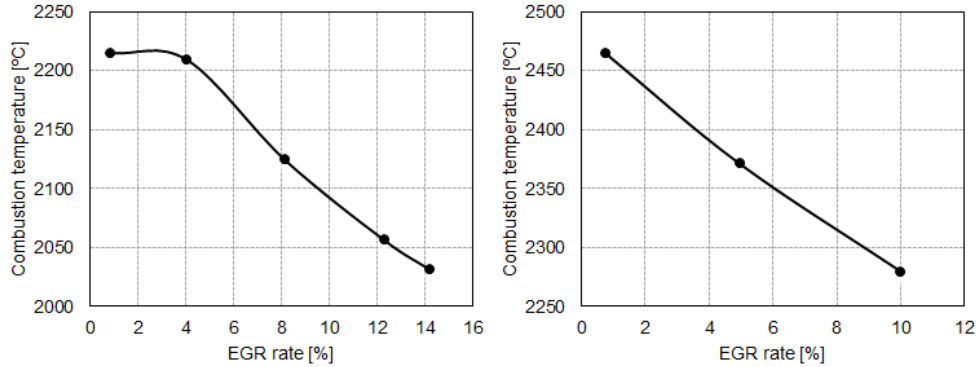
at 2000 rpm due to the over-fuelling elimination, maintaining the exhaust gas temperature at almost the same value as the reference operating conditions, as can be observed in the left graph of Figure 4.25. For higher EGR rates, the exhaust manifold temperature decreases due to the dilution effect of cooled EGR that lowers the combustion temperature. This will be explained in more detail later. Concerning the case of 3000 rpm it was observed that the exhaust manifold temperature could also be maintained compared to the original conditions at 5% of EGR rate, as it can be observed in the right graph of Figure 4.25, but the mixture was still enriched in order to control the exhaust manifold temperature. Although at 10% of EGR rate it can be observed that the exhaust manifold temperature is reduced compared to the original conditions and the mixture is at stoichiometric conditions. Further analysis is going to be presented later in this section.



**Figure 4.25.** Exhaust manifold temperature for EGR rates at 2000 rpm and 100% of engine load (left graph) and at 3000 rpm and 100% of engine load (right graph).

The combustion temperature at 2000 rpm remains at almost the same value as that of the original conditions for a 4% of EGR rate, as depicted in the left graph of Figure 4.26, and for higher EGR rates the combustion temperature decreases despite the improvement in the combustion phasing towards to MBT positions (advanced CA50), as it can be observed in the top left graph of Figure 4.27. This is mainly due to the dilution effect (less oxygen concentration) caused by cooled EGR that reduces the mixture reactivity and therefore the combustion rate. Despite the improvement in the combustion phasing the combustion temperature decreases. The reduction in mixture reactivity and combustion rate also increase the combustion duration as it can be observed in the bottom left graph of Figure 4.27. A reduction in heat losses is observed in the left graph of Figure 4.29.

The initial conditions for the combustion at 2000 rpm and 4% EGR rate case, differs from the original operating conditions in oxygen concentration, temperature and pressure. In the case of original conditions, the reactivity is decreased by the reduction of the cylinder temperature due to the vaporization of the extra injected fuel. This compensates the increase of reactivity because of the richer mixture and the increase in volumetric efficiency, improving the combustion phasing and reducing the combustion temperature. These effects can be seen in a study performed by Gurupatham et al. on rich flame propagation in SI engines [22]. At 4% EGR rate conditions, operating in stoichiometric conditions leads to a decrease in the vaporized fuel quantity compared to the original conditions, which results in higher cylinder temperature at the onset of the combustion process and increases



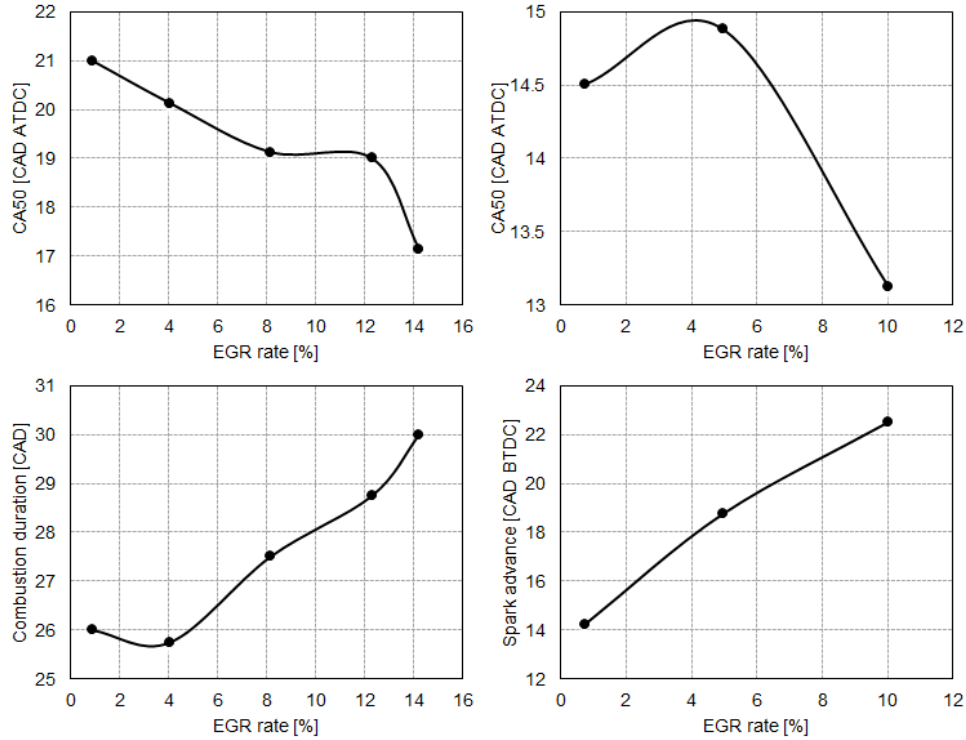
**Figure 4.26.** Combustion temperature for EGR rates at 2000 rpm and 100% of engine load (left graph) and at 3000 rpm and 100% of engine load (right graph).

the reactivity of the mixture, but the EGR dilution effect compensates and finally leaves the combustion duration and knocking resistance similar to those of the reference point. Thus, this is the main reason for the observed similar exhaust gas temperature, combustion duration and combustion phasing.

Analyzing the 8% and 12% EGR rate conditions at 2000 rpm, the same effects as those described for the 4% EGR case were observed and thus, the combustion duration tends to increase while increasing the EGR rate. The CoV of the IMEP also increases according to the left graph of Figure 4.28, since the mixtures have less reactivity because of the EGR dilution effect, the cycle-to-cycle ignition consistency is negatively affected. The CA50 is advanced, as it is observed in the top left graph of Figure 4.27, because of the increase in knocking resistance. The combustion temperature decreases, blocking the heat losses through the cylinder walls, as confirmed by the left graph of Figure 4.29. The exhaust gas temperature also drops while increasing the EGR rate because of the earlier combustion and the reduction of the combustion temperature as can be seen in left graph of Figure 4.26.

Furthermore the 14% EGR rate operating conditions at 2000 rpm shows the same behaviour but with a higher improvement in the CA50, over 2 CAD, due to the higher knocking resistance at this EGR rate. The combustion duration increases and so the CoV compared to the other points, as shown in the left graph of Figure 4.28. The heat losses are higher compared to the 12% EGR operating conditions. The small decrease in the combustion temperature and new combustion phasing could explain the increase in heat losses compared to the 12% EGR operating conditions, as it can be observed

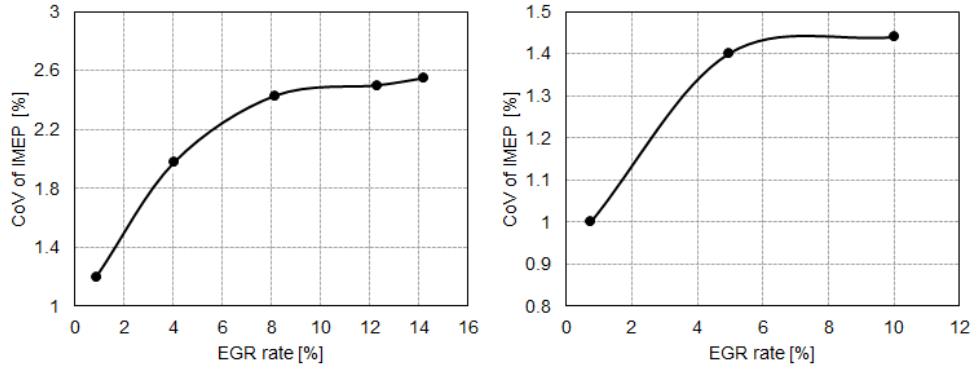




**Figure 4.27.** CA50 (top left graph) and combustion duration (bottom left graph) for EGR rates at 2000 rpm and 100% of engine load and CA50 (top right graph) and combustion duration (bottom right graph) for EGR rates at 3000 rpm and 100% of engine load.

in the left graph of Figure 4.29. Looking at the left graph of Figure 4.25, the exhaust temperature also decreases compared to the 12% EGR operating point.

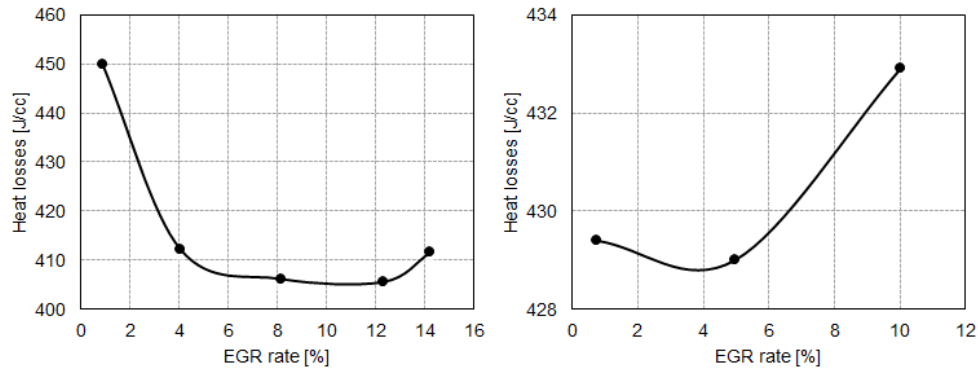
In the case of 3000 rpm it can be observed in the right graph of Figure 4.25 that at 5% EGR rate the exhaust manifold temperature is almost the same value as that of the original conditions without EGR. A similar behaviour was already presented before for 2000 rpm at 4% of EGR rate conditions. Although in this case the enrichment strategy is not completely eliminated, but it was reduced from 0.89 to 0.91 lambda, therefore the combustion temperature at 5% EGR rate is lower compared to original conditions combustion temperature as it can be observed in the right graph of Figure 4.26 and furthermore, also the heat losses are reduced as it can be observed in the right graph of Figure 4.29.



**Figure 4.28.** CoV of the IMEP for different EGR rates at 2000 rpm and 100% of engine load (left graph) and at 3000 rpm and 100% of engine load (right graph).

The combustion duration is increased compared to that of original conditions, as observed in the bottom right graph of Figure 4.27, due to the reduction in the mixture reactivity caused by the cooled EGR reduction of oxygen concentration and the enrichment effect already explained before for 2000 rpm and 4% of EGR rate conditions, taking into account that the CA50 is almost the same as that of the original conditions, as it can be observed in the top right graph of Figure 4.27. This will also explain the lower combustion temperature already mentioned before. The CA50 could not be improved because of knock limitations. Regarding the CoV of the IMEP, it is observed in the right graph of Figure 4.28 that it increases, as it was expected and already observed in 2000 rpm tests, because of the lower mixture reactivity caused by the enrichment strategy and the cooled EGR.

For the 10% of EGR rate engine condition at 3000 rpm, it can be seen in the right graph of Figure 4.25 that the exhaust manifold temperature is decreased with the engine operating at stoichiometric conditions. The combustion temperature is further reduced compared to the other conditions (0% and 5% of EGR rate) as it can be seen in the right graph of Figure 4.26, despite the improvement in combustion phasing (advance CA50) and lower combustion duration compared to the other conditions (0% and 5% of EGR rate) as it can be observed in the right graphs of Figure 4.27. This is achieved by the increment of mixture reactivity due to the elimination of the enrichment strategy, as mentioned before, and the improvement of the combustion phasing increasing the turbulence, similar to the effect already observed in part load engine conditions at 2000 rpm. As it was seen at 2000



**Figure 4.29.** Heat losses for different EGR rates at 2000 rpm and 100% of engine load (left graph) and at 3000 rpm and 100% of engine load (right graph).

rpm, the heat losses increased due to this advanced combustion phasing and therefore higher turbulence during the combustion, as observed in the right graph of Figure 4.29. And finally in the case of the CoV of the IMEP, it can be observed in the right graph of Figure 4.28 how it is at the same value as that of 5% EGR rate conditions, which is expected after the improvement of the combustion phasing and the mixture reactivity.

At this high load conditions the effect of knocking suppression and dilution effect due to the introduction of cooled EGR was also observed as in part load tests. The CA50 was able to be advanced but was still limited by knocking at the maximum possible EGR rate for both engine speed conditions. The heat losses were reduced compared to the reference operating conditions at 2000 rpm and increased in the case of 3000 rpm. The over-fueling strategy was eliminated by only using 4% of EGR rate without compromising the exhaust gas temperature at 2000 rpm and 10% of EGR rate was necessary at 3000 rpm. With higher EGR rates, in the case of 2000 rpm, the exhaust gas temperature and fuel consumption was further reduced without compromising the CoV of the IMEP. The best results in terms of engine performance were provided by the 14% of EGR rate at 2000 rpm, which reduces the fuel consumption by 12%, the exhaust gas temperature in more than 50°C and maintained an acceptable IMEP CoV of 2.5%, and 10% of EGR rate for 3000 rpm that reduced the fuel consumption by 11.5%, the exhaust gas temperature in more than 15°C and maintained an acceptable IMEP CoV of 1.44%.

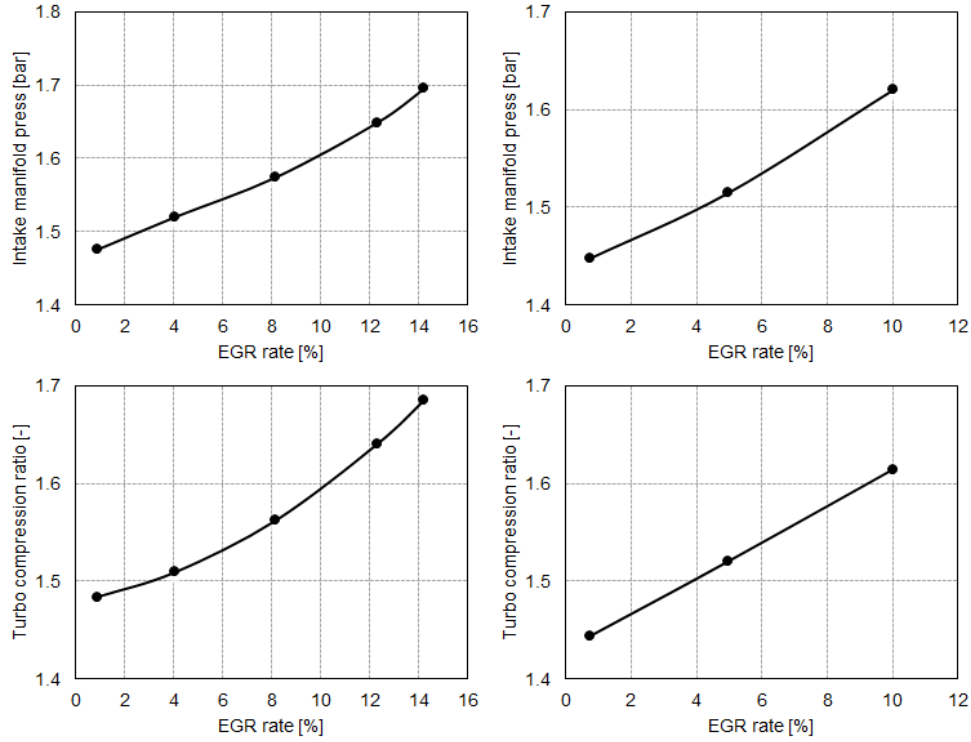
#### 4.3.2.2 Air management

The full load original operating condition at 2000 rpm for this engine is set at 19.5 bar. Due to the turbocharger limitations the tests were performed at 17 bar limiting the EGR rate to 14%. At this engine load, the throttle valve is fully open and the only possibility to maintain iso-air mass flow while increasing the EGR rate is to increase the intake pressure by increasing the compression ratio of the compressor. This is achieved by closing the wastegate valve on the turbine. In the case of 3000 rpm the tests were performed at full load 19.5 bar, because the turbocharger was not a limitation factor at this engine speed but the tests were performed only until 10% of EGR rate due to original logic limitations of the ECU.

The intake pressure increases with the EGR rate for both engine speeds as it can be seen on the top graphs of Figure 4.30. To achieve this intake pressure, the compression ratio of the compressor must be increased for both engine speeds conditions as seen in the bottom graphs of Figure 4.30. While increasing the compression ratio, the turbocharger speed also increases as shown in the right graph of Figure 4.31 for both engine speeds, 18% at 2000 rpm and 15% at 3000 rpm compared to the reference operating conditions. Compared to the partial load operating conditions, where the compression ratio of the compressor was not affected because of the throttle valve regulation, at full load a radical increase in the compression ratio is needed in order to maintain iso-air mass flow conditions while increasing the EGR rate.

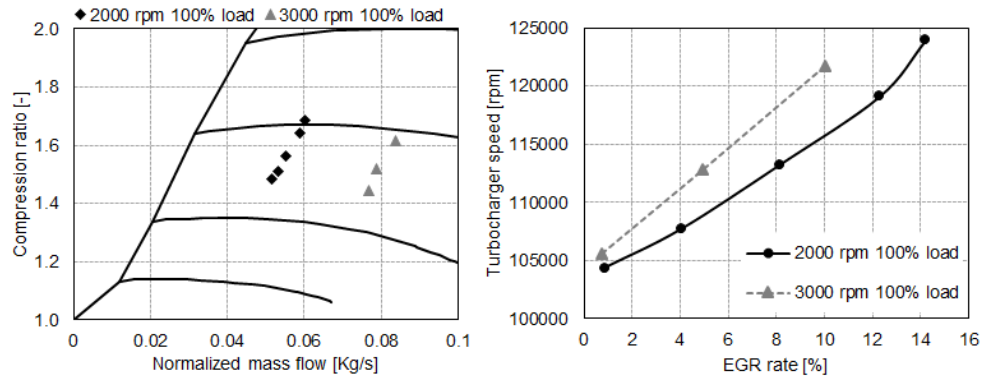
The compressor operating conditions shifts in diagonal on the compressor map for both engine speed conditions, shown in the left graph of Figure 4.31. This explains the large increase on the turbocharger speed compared to the partial load operating conditions, where the compression ratio was the same during the EGR rate increase. On the other hand when analyzing the three thermocouples placed at the compressor inlet, it can be observed in Figure 4.32 that increasing the EGR rate increases the difference between the thermocouple 2 (aligned with the EGR outlet) and the others, in the case of both engine speed conditions. Similar results were seen at the partial load tests.

Furthermore the pumping losses increase, for both engine speeds, with the EGR rate and the evolution is included in the top graphs of Figure 4.33. The increase is more than 16% compared to the reference operating conditions. The increase is due to the higher compression ratio of the compressor, needing more power from the turbine and then increasing its expansion ratio and finally the exhaust manifold pressure, as can be seen in the bottom graphs of Figure 4.33.

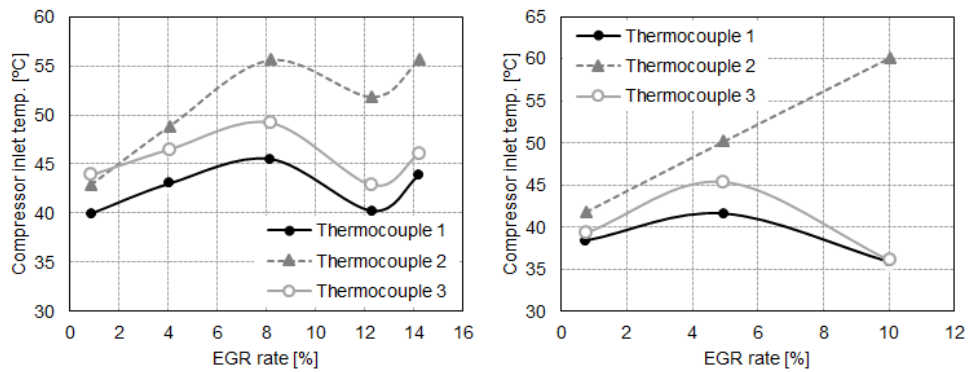


**Figure 4.30.** Intake manifold pressure (top left graph) and turbocharger compression ratio (bottom left graph) for different EGR rates at 2000 rpm and 100% of engine load and intake manifold pressure (top right graph) and turbocharger compression ratio (bottom right graph) for different EGR rates at 3000 rpm and 100% of engine load.

Therefore, the pumping losses do not contribute to decrease the fuel consumption at this engine load conditions, so it is mainly caused by the new combustion phasing, over-fueling elimination and heat losses reduction only at 2000 rpm. The 14% EGR rate presented a limitation to the turbocharger in the case of 2000 rpm, because it was not possible to achieve the 19.5 bar at this engine speed with the original turbocharger. The other disadvantage found was the water condensation after the inter-cooler for both engine speed conditions, as it was also observed on the partial load tests.



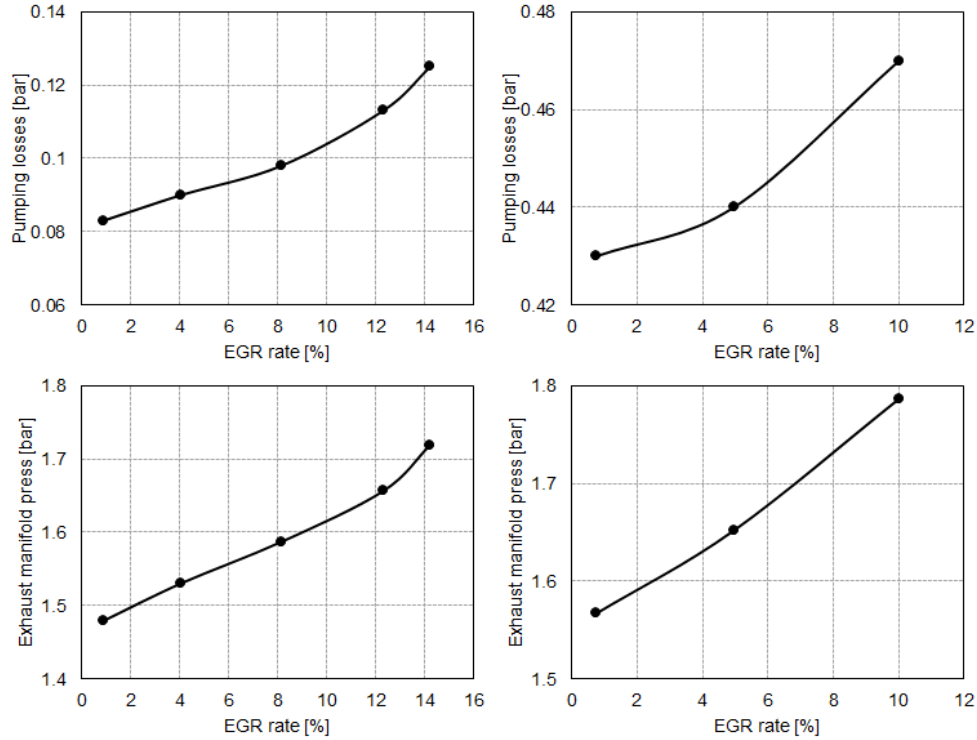
**Figure 4.31.** Compressor map (left graph) and turbocharger speed (right graph) for different EGR rates at 2000 rpm and 100% of engine load and 3000 rpm and 100% of engine load.



**Figure 4.32.** Temperature at compressor inlet in three different positions placed in the same virtual diameter, each of them separated by  $120^\circ$ , for different EGR rates at 2000 rpm and 100% of engine load (left graph) and at 3000 rpm and 100% of engine load (right graph).

#### 4.3.2.3 Exhaust raw emissions

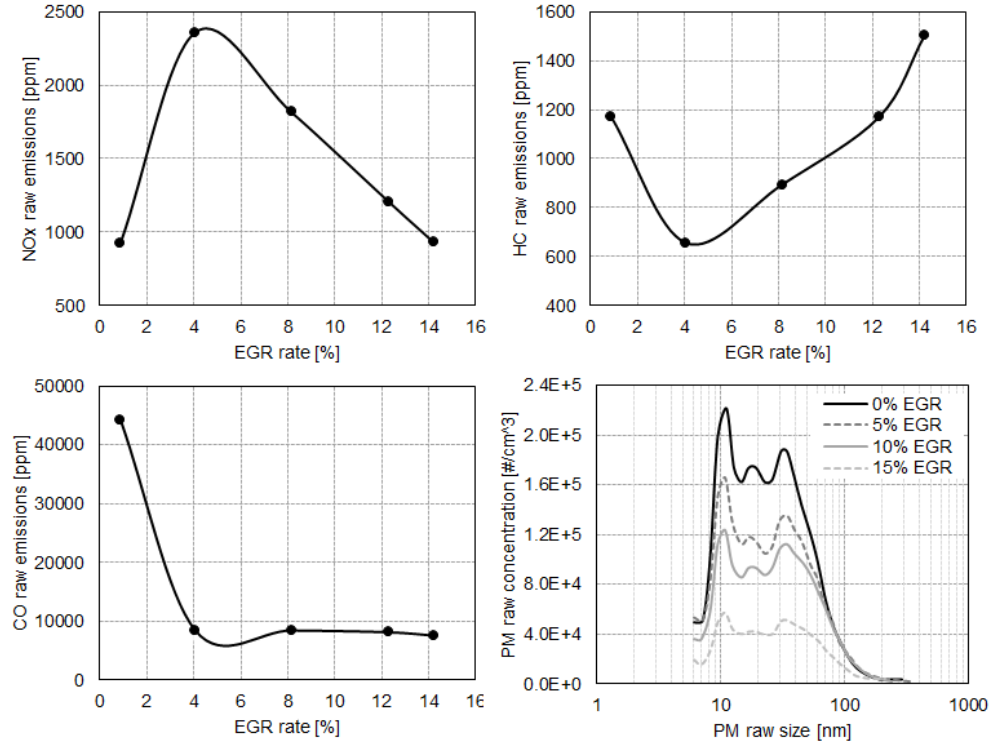
Before analyzing the exhaust pollutant emissions, it must be considered that the reference operating condition, for both engine speeds, operates with rich mixture.  $NO_x$  emissions increases in the top left graph of Figure 4.34 between the reference point and the 4% EGR operating conditions, because it operates in stoichiometric conditions while the reference condition operates



**Figure 4.33.** Pumping losses (top left graph) and exhaust manifold pressure (bottom left graph) for different EGR rates at 2000 rpm and 100% of engine load and pumping losses (top right graph) and exhaust manifold pressure (bottom right graph) for different EGR rates at 3000 rpm and 100% of engine load.

with a rich mixture, so the EGR case generates more suitable environment for  $NO_x$  production despite the similar combustion temperature due to the higher oxygen concentration. After this EGR level,  $NO_x$  emissions decrease while increasing the EGR rate until reaching the same concentration as the reference operating conditions with 14% of EGR.

A similar trend can be observed for 3000 rpm in the top left graph of Figure 4.35 compared to the trend at 2000 rpm between 0% and 4% EGR rate, but in this case the  $NO_x$  emissions increased until the highest EGR rate at this load conditions (10% EGR rate) because it was at the highest EGR rate where the engine could be operated at stoichiometric conditions without exceeding the turbine inlet temperature limit and so the decrease of

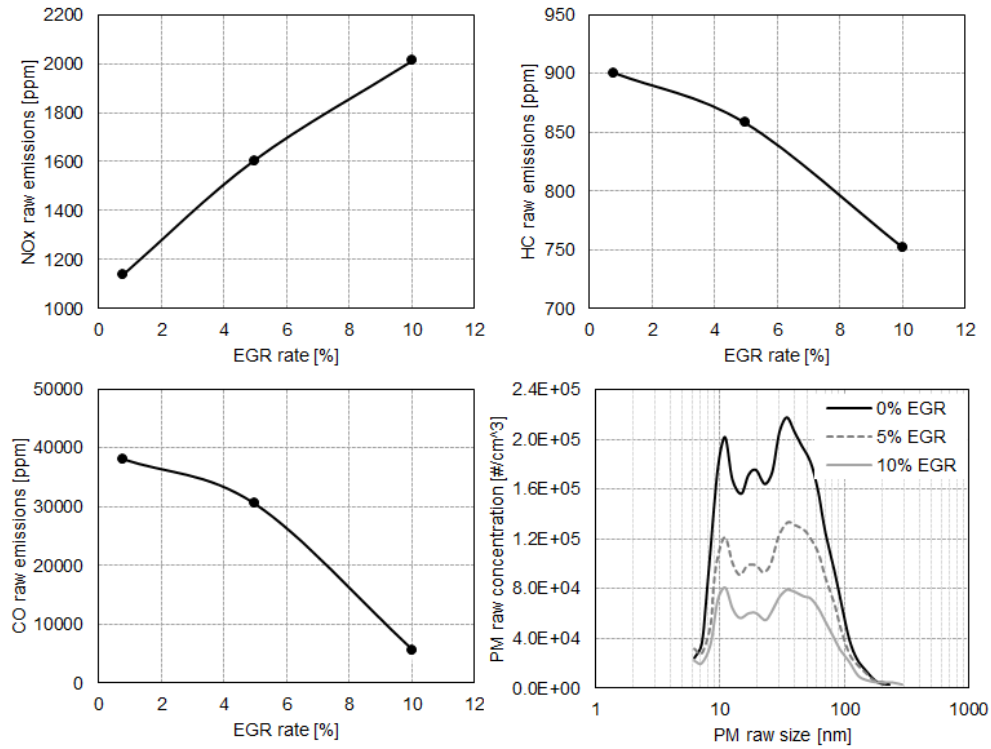


**Figure 4.34.** Exhaust raw emissions with optimized SA at 2000 rpm and 100% load.  $NO_x$  emissions (top left graph),  $HC$  emissions (top right graph),  $CO$  emissions (bottom left graph) and  $PM$  emissions (bottom right graph).

$NO_x$  emissions observed at 2000 rpm between 4% and 14% EGR rate cannot be seen at 3000 rpm because of the limit of 10% EGR rate at this conditions.

As expected  $HC$  emissions present an opposite behaviour compared to  $NO_x$  at 2000 rpm, as confirmed by top right graph of Figure 4.34, where  $HC$  decrease between the reference operating conditions and 4% EGR, and then increase with the EGR. Switching from a rich mixture on the reference conditions to a stoichiometric mixture at the 4% EGR operating conditions reduces the  $HC$  emissions. A richer mixture over the stoichiometry always produces more  $HC$  emissions because of the lack of oxygen to burn the extra fuel. Later, from 4% EGR in advance, an increase in  $HC$  emissions is observed while increasing the EGR rate because of the decrease in combustion temperature and the longer combustion duration, similar effect to part load conditions. In the case of 3000 rpm the same opposite trend of  $HC$  emissions





**Figure 4.35.** Exhaust raw emissions with optimized SA at 3000 rpm and 100% load.  $NO_x$  emissions (top left graph), HC emissions (top right graph), CO emissions (bottom left graph) and PM emissions (bottom right graph).

compared to  $NO_x$  emissions is observed in the top right graph of Figure 4.35, but as it was mentioned before, the stoichiometric conditions at this engine conditions were achieved at the maximum EGR rate and therefore only a decrease of HC emissions was observed at 3000 rpm which is the same as the range from 0% to 4% observed at 2000 rpm.

Regarding the CO emissions, for both engine speed an important decrease can be seen in the bottom left graph of Figure 4.34 for 2000 rpm and the bottom left graph of Figure 4.35 for 3000 rpm. The main reason is passing from a rich mixture to a stoichiometric mixture. Then, the reduction observed at 2000 rpm between 4% and 14% EGR rate is due to the reduction in the  $CO_2$  dissociation because of the lower combustion temperature, reducing CO emissions.

Also the main reason for the  $PM$  decrease observed in the bottom right graph of Figure 4.34 for 2000 rpm and of Figure 4.35 for 3000 rpm, between the reference conditions and the 4% EGR rate at 2000 rpm and 10% EGR rate at 3000 rpm, is the elimination of the rich mixture or enrichment strategy. Then at 2000 rpm, the decrease observed between 4% and 8% EGR cases is due to the decrease in the combustion temperature, reducing the  $PM$  formation rate. Similar results were also presented by Alger et al. using a port fuel injection gasoline engine in their research work [20].

Introducing cooled EGR in this engine load helps to operate in stoichiometric conditions, allowing the catalyst to work in the efficient range where a 98 – 99% of conversion efficiency is achieved, as mentioned before, improving the reference operating conditions catalyst efficiency, which is really low in the reference engine conditions because of the enrichment strategy.

As a summary,  $CO$  and  $PM$  emissions decrease using 14% EGR rate at 2000 rpm and 10% EGR rate at 3000 rpm, compared to the reference operating conditions.  $NO_x$  emissions were kept at the same value as the reference point at 2000 rpm and in the case of 3000 rpm  $NO_x$  emissions were increased in 77% compared to the original conditions. The increase in  $HC$  emissions at 2000 rpm and  $NO_x$  emissions at 3000 rpm, do not represent a major problem since the TWC can operate in the maximum conversion efficiency range because of the stoichiometric mixture, improving all the after catalyst emissions in high percentages. In addition, in the case of 3000 rpm the  $HC$  emissions were reduced in 17% compared to the original conditions.

### 4.3.3 Low load test

Only one operating point was chosen at low load, since at this load there is no knock limitations and the combustion is phased in its optimum crank angle position, plus there is no exhaust temperature problems (no enrichment strategy) and even more important, the VVT system can perform IGR in order to reduce fuel consumption. So in this case the engine is not going to take advantage of the main benefits of cooled EGR and the mixture dilution increase (IGR+EGR) could reduce too much the combustion efficiency and therefore lose the small benefits of reducing the heat transfer and pumping losses. Although the tests were performed to understand the potential of using cooled EGR at low load engine conditions.

The tests was performed at 2000 rpm and 5 bar of BMEP following the same methodology as before: maintaining constant the air mass flow, intake manifold temperature, fuel mass flow and increasing the EGR rate until

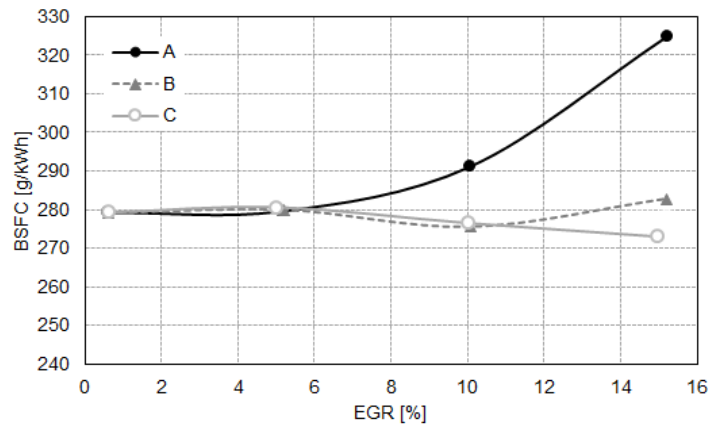
reaching the maximum dilution limit of the engine. The first set of tests (A) were performed increasing the EGR rate but maintaining the spark advance fixed, to observe the effect of the dilution on the performance and emissions of the engine. After this first set of tests, a second set of tests (B) were performed to modify the spark advance for each EGR rate condition in order to achieve the optimum combustion phasing. Finally, a third set of tests (C) were carried out, performing the same tests B but changing the VVT parameters to reduce the amount of IGR, for each EGR rate condition, in order to maximize the cooled EGR effect and analyze its full potential at this engine condition.

#### 4.3.3.1 Engine performance and exhaust emissions

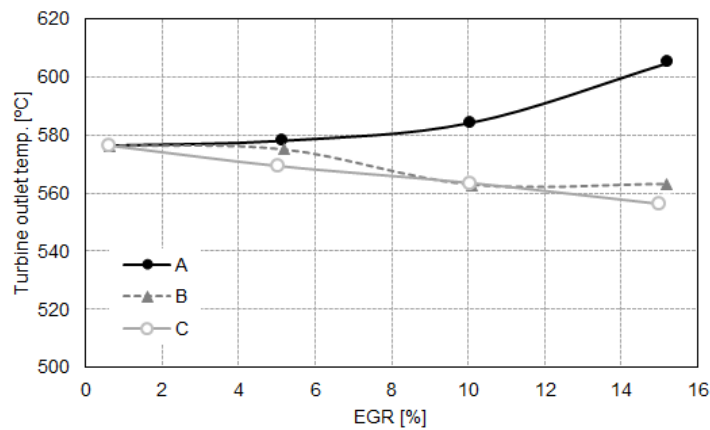
In this operating conditions the maximum amount of EGR rate achieved was around 15% before starting to have misfires. Knowing that the principal attractive advantage of introducing cooled EGR into the engine is the reduction of fuel consumption, in Figure 4.36 it can be observed the BSFC of tests A, B and C, for different EGR rates. It can be seen how cooled EGR reduces the combustion reactivity and therefore the combustion rate, by observing the increase in fuel consumption for tests A, where the spark advance was set constant. In the case of tests A it can be seen how increasing the EGR rate also increases the exhaust temperature which is caused by the longer combustion duration, as observed in Figure 4.37 where the exhaust temperature is presented for tests A, B and C, for different EGR rates.

Regarding tests B, it can be observed that cooled EGR indeed reduce the fuel consumption but until a certain EGR rate, around 10% of EGR, because at 15% of EGR the fuel consumption started to increase slightly compared to 10% of EGR rate operating conditions. In this case, the exhaust temperature is reduced because the CA50 is maintained constant and because of the cooled EGR the combustion temperature is lower and therefore the exhaust gas temperature at the EVO is lower. This can be supported by analyzing the  $NO_x$  emissions, that can be observed in Figure 4.38, where  $NO_x$  emissions are represented for tests A, B and C, for different EGR rates. In the case of tests B it can be seen that when EGR rate increases,  $NO_x$  emissions decreases, which implies that the combustion temperature is decreasing since the oxygen concentration is not so different from the original operating conditions. It was mentioned in Section 2.2.2.2 of Chapter 2 how  $NO_x$  emissions are controlled basically by the combustion temperature and the oxygen concentration [23].

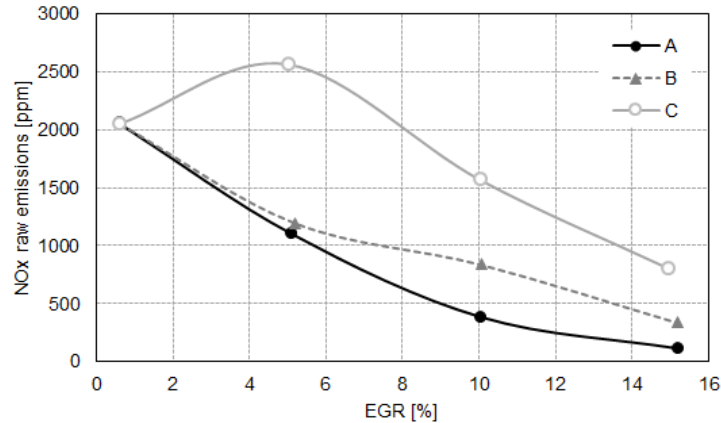
Analyzing tests C, in Figure 4.36 it can be observed how the fuel consumption is reduced by increasing the EGR rate until the limit of dilution



**Figure 4.36.** Tests A, B and C: BSFC at 2000 rpm and 25% load for different EGR rates.



**Figure 4.37.** Tests A, B and C: exhaust manifold temperature at 2000 rpm and 25% load for different EGR rates.

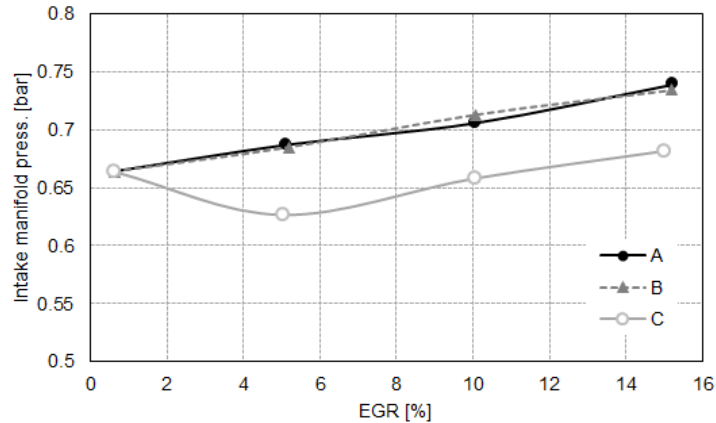


**Figure 4.38.** Tests A, B and C:  $NO_x$  emissions at 2000 rpm and 25% load for different EGR rates.

(15% of EGR). In this case the fuel consumption continued to decrease after 10% of EGR, this was due to the fact that the amount of IGR was decreased because of the different VVT settings compared to tests B. The IGR reduction can be supported by observing at Figure 4.38 where it can be seen that during tests C the  $NO_x$  emissions were higher than during tests B, which implies a reduction of residual gases inside the cylinder. This can be also supported by analyzing the intake manifold pressure for different EGR rates, represented in Figure 4.39, where it can be seen that despite the added 5% of EGR, the intake manifold pressure needed to achieve the same air mass flow as the original operating conditions is lower. This supports the hypothesis of IGR reduction due to the new VVT settings, compared to the original intake manifold pressure conditions.

The reduction of fuel consumption compared to tests B at 15% of EGR is due to the lower amount of high temperature residual gases in the cylinder (IGR) and the same amount of cooled EGR, which at the end gives a lower total dilution of the mixture and a higher ratio of cooled EGR compared to IGR, which also decreases further the combustion temperature and therefore heat transfer for the same amount of dilution, improving the thermal efficiency of the engine and reducing the fuel consumption by 2% compared to the original operating point.

Regarding  $HC$  and  $CO$  emissions, represented in Figure 4.40, for different EGR rates and setups, it can be seen how introducing cooled EGR increases

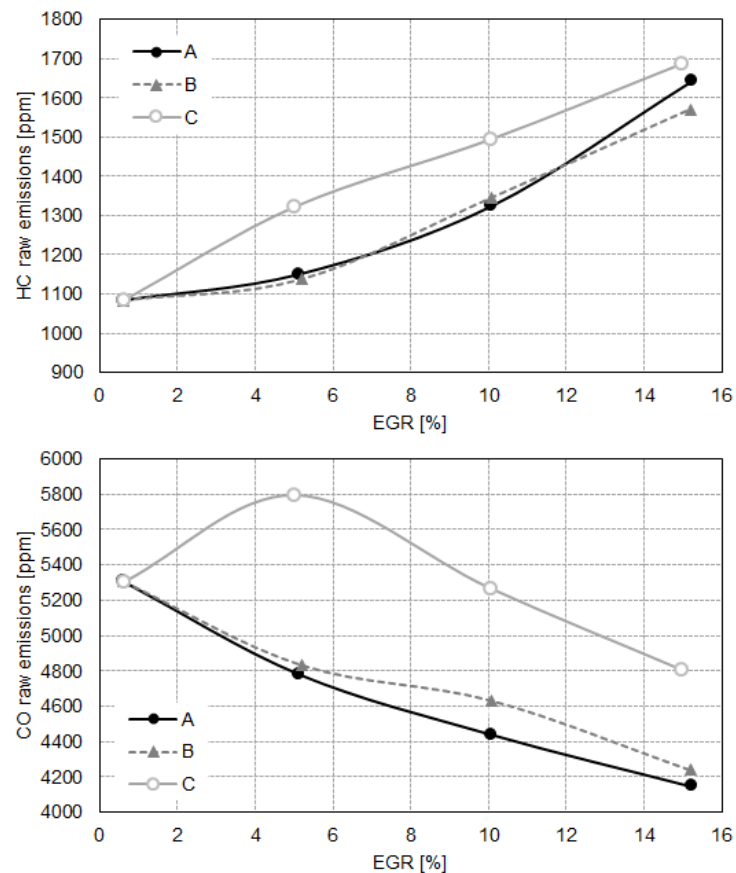


**Figure 4.39.** Tests A, B and C: intake manifold pressure at 2000 rpm and 25% load for different EGR rates.

*HC* emissions in tests A, B and C, due to a decrease of combustion temperature and oxygen concentration when increasing the EGR rate and therefore the *HC* oxidation efficiency decreases. It can be seen how also for tests C *HC* emissions are higher than for tests A and B, this is due to the lower amount of IGR and therefore the lower temperature at the start of the combustion, which increases *HC* emissions despite the higher oxygen concentration.

Regarding *CO* emissions, it can be seen how adding cooled EGR reduces *CO* emissions for all the tests except for tests C, between 0% and 5% of EGR rate, where the *CO* emissions are increased compared to the original operating point. This is also due to the lower amount of IGR which reduces the total amount of dilution and therefore increases *CO* emissions due to the higher oxygen concentration, despite that the decrease effect of introducing cooled EGR can be also observed after 5% of EGR rate. It is important to remark that *CO* emissions are reduced due to the reduction in oxygen concentration and combustion temperature, reducing the *CO*<sub>2</sub> dissociation, as it can be seen in the reactions presented in Section 2.2.2.3 of Chapter 2.

It was seen how cooled EGR can reduce fuel consumption even in low load operating conditions. It is also important to notice the increase in *HC* emissions and the decrease in exhaust manifold temperature which impacts directly in the conversion efficiency of the TWC as Bermúdez et al. [21] showed in their research work. Taking this into account it must be



**Figure 4.40.** Tests A, B and C: HC (top graph) and CO (bottom graph) emissions at 2000 rpm and 25% load for different EGR rates.

said that cooled EGR does not have the balance between temperature and dilution that IGR has. In addition, the control strategies difficulties that can arise during transient conditions compared to VVT systems control strategy and accuracy. Therefore, cooled EGR seems that is not suited for low load engine conditions.

#### 4.4 Transient operation results and analysis

In this section the results of the NEDC cycles using four different setups are going to be presented and analyzed. Starting with a basic comparison between

Setup	Unit	Urban	Extra-urban	Mixed
No EGR	[l/100]	10.64	7.66	8.77
EGRV 20%	[l/100]	10.78	7.58	8.78
EGRV 40%	[l/100]	10.61	7.66	8.76
EGRV 20% extra-urban	[l/100]	10.62	7.6	8.79

*Table 4.3. Ford Explorer data.*

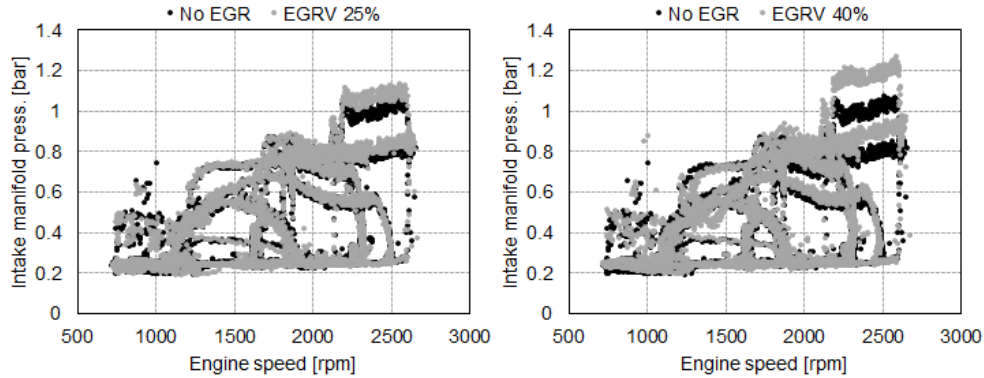
the different setups, that will be made using engine speed based graphs. The analysis of engine performance and influence of cooler EGR on the air loop is going to be performed using the second and third setup compared to the original setup, since the fourth setup is the same EGR rate as the second setup but only in the extra-urban part of the cycle. Afterwards, for the exhaust emissions comparison and analysis, all setups are used since the accumulated exhaust emissions at the end of the cycle are going to be different for each one.

Taking into account that the spark advance was not optimized for different EGR rate conditions and the original spark advance was maintained for all the different setups, no fuel consumption benefit of introducing cooled EGR was expected. In Table 4.3, it can be observed the fuel consumption for the different setups, it can be observed that the setup did not influence the fuel consumption of the vehicle during the NEDC cycle.

In order to achieve the desired torque during the NEDC cycle the engine adjusted intake air mass flow, intake pressure, spark advance and VVT settings, based on the original engine calibration. When introducing cooled EGR, in order to maintain the desired torque at all the engine conditions the intake manifold pressure had to be increased to compensate the addition of the EGR mass flow, as it can be seen in Figure 4.41, where the intake manifold pressure is presented in an engine speed based graph, comparing the 25% and 40% EGR valve opening setup to the original setup without EGR. The increase in the intake pressure is because the quantity of mass is increased on the same volume for the same amount of air mass because of the addition of the EGR mass, this is in the same trend-line as the results already explain in steady state conditions in Chapter 4 and Chapter 5.

When total intake mass flow is increased, the turbocharger operating conditions change, the compression ratio will also increase in some engine operating conditions in order to maintain at least the same air intake mass



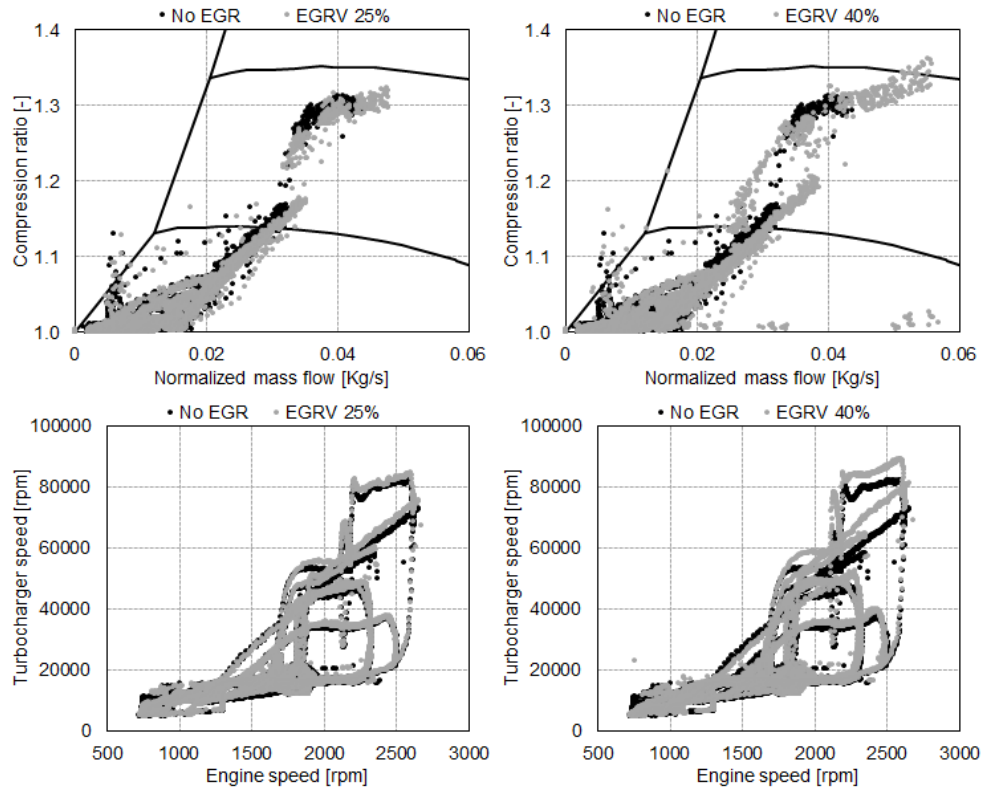


**Figure 4.41.** NEDC cycle engine speed based graphs presenting the intake pressure for 25% EGR valve opening setup compared to the original setup in the left graph and the 40% EGR valve opening setup compared to the original setup in the right graph.

flow as the original conditions without EGR. In Figure 4.42 the NEDC instantaneous results are plotted in a compressor map, top graphs, and the turbocharger speed is presented in an engine speed based graph in the bottom graphs, for both comparisons between 25% and 40% of EGR valve opening setup with the original setup (no EGR).

It can be observed, how the compressor operating conditions move to the right of the compressor map in the case of the higher compression ratio conditions, as it was also observed in the steady operating conditions already analyzed. It is also important to remark that at low load conditions the difference between the original setup and the 25% and 40% of EGR valve opening setup is smaller also due to the lower EGR mass flow at these engine conditions.

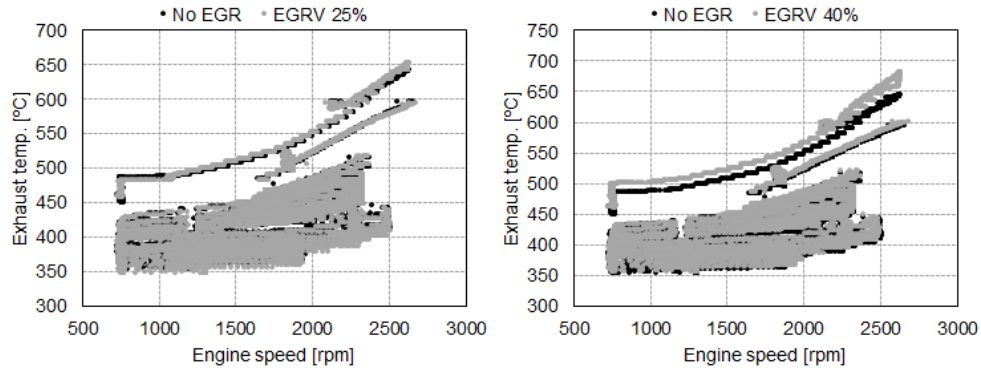
A direct consequence of increasing the compression ratio and total mass flow through the compressor is the increment of the turbocharger speed, as it can be observed in the bottom graphs of Figure 4.42. This can be also correlated with the movement of the operating conditions in the compressor map, as it was analyzed before, compared to the original. It can be also observed that for higher EGR rate conditions the difference is bigger compared to the original conditions, comparing the right graphs to the left graphs. The compressor operating conditions at higher compression ratios and higher mass flows are further to the right of the map for the 40% of EGR valve opening setup than for the other two setups because of the higher EGR rates when this



**Figure 4.42.** NEDC cycle engine speed based graphs presenting the compressor map (bottom graphs) and turbocharger speed (top graphs) for 25% EGR valve opening setup compared to the original setup (left graphs) and the 40% EGR valve opening setup compared to the original setup (right graphs).

setup is used, therefore more mass flow and more compression ratio is needed in order to maintain at least the same air mass flow as the original conditions.

Regarding the exhaust temperature, a comparison between the 25% and 40% of EGR valve opening setup with the original setup was performed in order to analyze the effect of cooled EGR in this engine parameter. In Figure 4.43 the turbine outlet temperature is plotted in an engine speed based graph, on the left comparing the 25% of EGR valve opening setup with the original setup and on the right graph the 40% of EGR valve opening setup with the original setup. The temperature is barely the same for low load conditions, but it can be seen that for higher load conditions a difference can be observed: the higher the EGR rate the higher the exhaust temperature. This

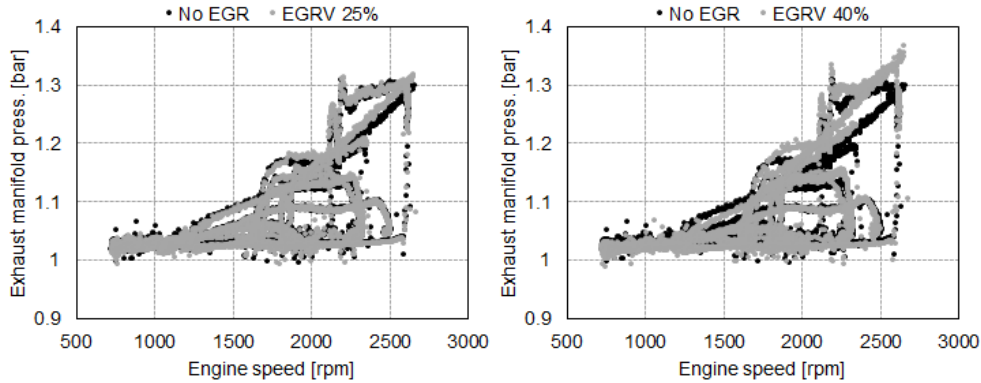


**Figure 4.43.** NEDC cycle engine speed based graphs presenting the turbine outlet temperature for 25% EGR valve opening setup compared to the original setup in the left graph and the 40% EGR valve opening setup compared to the original setup in the right graph.

is because the spark advance was not in its optimized value for the different EGR rate conditions and therefore the combustion is retarded and the exhaust temperature is higher than the original conditions when EGR rate increases. This was also observed in the steady tests before, where the effects of cooled EGR were explained without optimizing the spark advance in order to re-phase the combustion.

The exhaust temperature comparison was performed after the turbine outlet, because before the turbine due to engine pulsation and low mass flow the measurements are less accurate and since the compression ratio of the turbocharger barely changes during the NEDC, as it can be observed in the top graphs of Figure 4.42, a comparison using the turbine outlet temperature seemed better in this case due to its higher measurement accuracy.

The increase in exhaust temperature and in mass flow going through the engine increases the expansion ratio in the turbine and therefore increases the exhaust manifold pressure. In Figure 4.44, the exhaust manifold pressure (or the exhaust pressure before the turbine) is presented for both comparisons between 25% and 40% of EGR valve opening setup with the original setup. It can be seen that the difference between 25% of EGR valve opening setup and the original setup is smaller than the difference observed between the 40% of EGR valve opening setup and the original setup. This is due to the higher EGR rates obtained for the 40% of EGR valve opening setup in all engine conditions compared to the 25% of EGR valve opening setup, which is translated in more

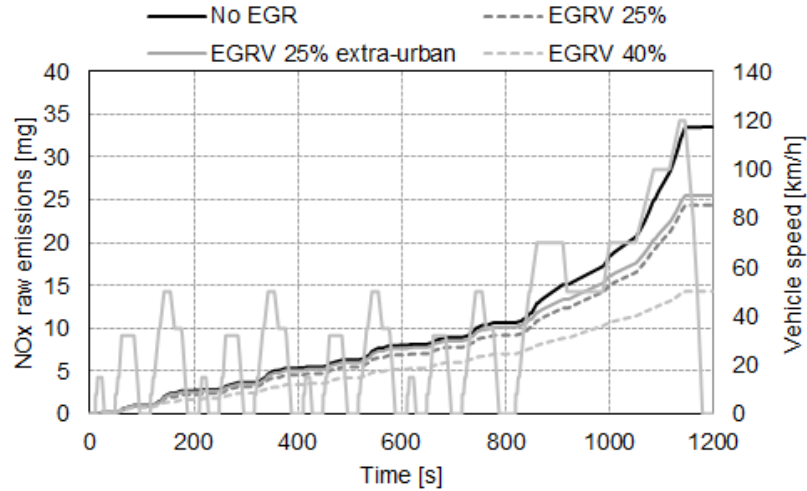


**Figure 4.44.** NEDC cycle engine speed based graphs presenting the exhaust manifold pressure for 25% EGR valve opening setup compared to the original setup in the left graph and the 40% EGR valve opening setup compared to the original setup in the right graph.

mass flow, as it was observed in the right graph of Figure 4.43, and also higher exhaust manifold temperature.

Regarding the exhaust emissions, introducing cooled EGR reduced  $NO_x$  raw emissions, as it was expected taking into account the analysis performed in Chapter 4 and Chapter 5. This can be seen in Figure 4.45, where cumulative  $NO_x$  raw emissions are presented during the NEDC cycle for the four configurations. It can be seen that the highest reduction was observed for the EGRV 40%, as it was expected, because of the higher EGR rate presented in this configuration in all engine conditions. And following that same analysis philosophy, the smaller reduction of  $NO_x$  emissions was observed for the EGRV 25% only used in extra-urban part of the cycle, but the difference was smaller compared to the EGRV 25% setup because the EGR rate during the urban part of the cycle with this configuration is somehow small compared to the EGRV 40% setup as it was presented before in Figure 4.5, Figure 4.6.

The  $HC$  emissions increased when the EGR rate was higher because of the combustion degradation and lower combustion temperature caused by the lower reactive diluted mixture, this was already deeply explained in previous sections when analyzing steady operation. In Figure 4.46 cumulative  $HC$  raw emissions are presented during the NEDC cycle for the four configurations. It can be observed that the highest  $HC$  emissions obtained were using the EGRV 40% setup, as it was expected because of its higher EGR rate compared to

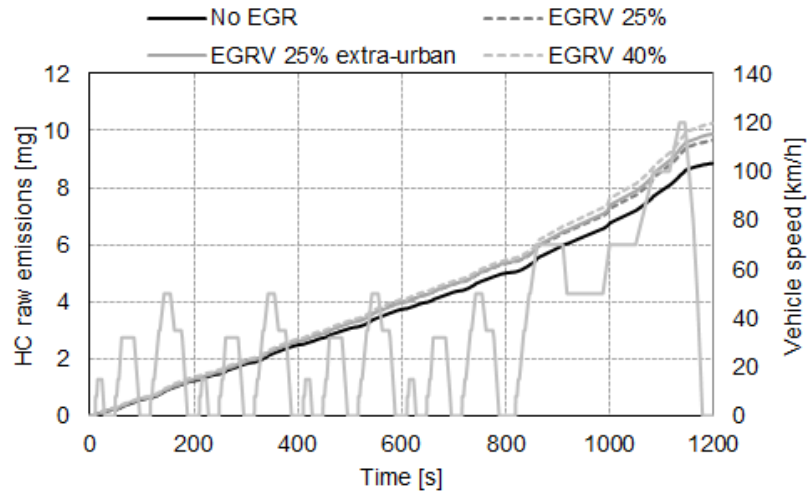


**Figure 4.45.** NEDC cycle  $NO_x$  raw emissions for 25%, 40% and 25% extra-urban EGR valve opening setup compared to the original setup.

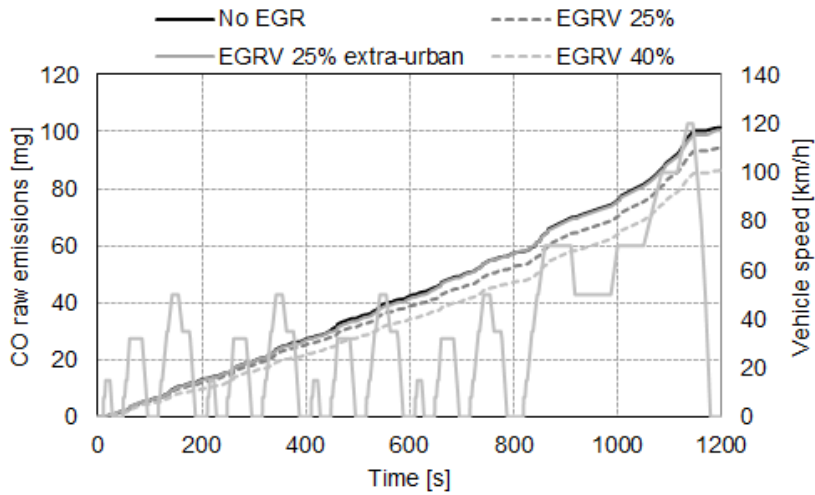
the other configurations. This was followed by the EGRV 20% and then by the EGRV 20% extra-urban, and obviously the lowest  $HC$  emissions were obtained with the original setup.

On the other hand  $CO$  raw emissions were reduced for all EGR setups. As already discussed,  $CO$  emissions are reduced when cooled EGR is introduced into the engine due to the reduction on the combustion temperature and therefore on the  $CO_2$  dissociation reaction forming less  $CO$  emissions. In Figure 4.47 cumulative  $CO$  raw emissions are presented during the NEDC cycle for the four configurations. It was observed that using the EGRV 40% setup, produced the highest reduction in  $CO$  emissions because of its higher EGR rates compared to the other cycles therefore less combustion temperature causing less  $CO_2$  dissociation. This result was followed by the  $CO$  emissions reduction of EGRV 20% setup and then by EGRV 20% extra-urban setup, being this last one almost similar to  $CO$  emissions observed at original conditions.

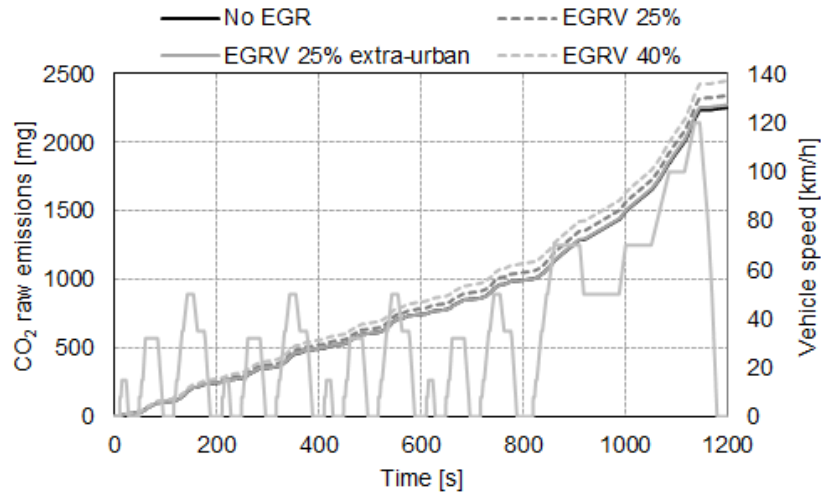
This reduction in  $CO$  emissions caused by the reduction of dissociation of  $CO_2$  emissions increased  $CO_2$  emissions for the setups using cooled EGR as it can be observed in Figure 4.48. The trend in this graph is the opposite as the  $CO$  emissions graph. For the EGRV 40% setup, that has the highest EGR rate during the NEDC cycle,  $CO_2$  raw emissions are also the highest, followed by the EGRV 20% setup, then by the EGRV 20% extra-urban and finally by



**Figure 4.46.** NEHC cycle HC raw emissions for 25%, 40% and 25% extra-urban EGR valve opening setup compared to the original setup.



**Figure 4.47.** NECO cycle CO raw emissions for 25%, 40% and 25% extra-urban EGR valve opening setup compared to the original setup.



**Figure 4.48.** NEDC cycle  $CO_2$  raw emissions for 25%, 40% and 25% extra-urban EGR valve opening setup compared to the original setup.

the original setup which showed the lower accumulated  $CO_2$  emissions, this increase could be also due to a small increase in fuel consumption not able to being detected by the fuel balance.

It was observed how adding cooled EGR without optimizing the spark advance did not influence the fuel consumption of the vehicle during a NEDC cycle and using the EGRV 40% setup helped reduce in 48% the  $NO_x$  raw emissions and in 14.4% the  $CO$  raw emissions. On the other hand increased in 16% the  $HC$  raw emissions and in 8% the  $CO_2$  raw emissions.

## 4.5 Summary and conclusions

The use of EGR has proved to decrease the engine BSFC and exhaust gas temperature, and to increase the knocking resistance of the mixture. The potential for simultaneously reducing  $NO_x$ ,  $CO$  and  $PM$  emissions has been also confirmed.

The effect of cooled EGR on the combustion, engine performance and exhaust emissions was observed by performing an EGR rate sweep at 2000 rpm and 10 bar of BMEP and 3000 rpm and 10 of BMEP without optimizing the combustion phasing. It was observed that cooled EGR increased the engine BSFC by 9.8% at 2000 rpm and by 9% at 3000 rpm. The increased in BSFC is

mainly due to the combustion retard caused by the mixture reactivity decrease. Cooled EGR has a dilution effect in the mixture and reduces the oxygen concentration, reducing the overall mixture reactivity, which causes a slower flame propagation and therefore a longer combustion. This is the main cause of the exhaust temperature increase of 15°C at 2000 rpm and 17°C at 3000 rpm both at 15% of EGR rate. Regarding the exhaust emissions a decrease in  $NO_x$  emissions of 88.2% and  $CO$  emissions of 19.5% at 2000 rpm was observed, mainly due to the combustion temperature decrease as it was explained later in the chapter, product of the dilution effect of cooled EGR. The same reason was the cause of  $HC$  emissions increase of 49% at 2000 rpm. The trend was similar at 3000 rpm, observing a decrease on  $NO_x$  emissions and  $CO$  emissions of 90% and 26.4% respectively, and an increase on  $HC$  emissions of 18%.

After a basic analysis of the cooled EGR impact on the combustion, engine performance and exhaust emissions, an optimization of the combustion phasing was performed for each EGR rate in order to fully observe the advantages and disadvantages with an optimized combustion phasing to minimize fuel consumption. This analysis was performed in 5 steady state operating points, 2000 rpm low, part and full engine load conditions, and 3000 rpm part and full engine load conditions. Part engine load conditions were the first part of the analysis, 2000 rpm and 10 bar of BMEP and 3000 rpm and 10 bar of BMEP, showing an improvement on BSFC of 3.8% at 2000 rpm and 3% at 3000 rpm using 15% of cooled EGR rate. This reduction in BSFC comes basically from the reduction of pumping and heat losses, the increase of the specific heat ratio of the mixture, and in the case of 2000 rpm due to the improvement in the combustion phasing by reducing the risk of knocking at this engine conditions. The reduction in pumping losses was obtained because of the increase of intake manifold pressure in order to maintain a constant air mass flow during the EGR rate sweep, and at the same time a smaller increase on the exhaust manifold pressure, contributing to the reduction of pumping losses. A pumping losses reduction of 19.5% at 2000 rpm and 8% at 3000 rpm was observed. In addition, heat losses were reduced due to the combustion temperature reduction observed during the increase of EGR rate, a reduction of 230°C at 2000 rpm and 320°C at 3000 rpm was observed at 15% of EGR rate. This reduction of combustion temperature and new optimized combustion phasing reduced the exhaust temperature by 46°C at 2000 rpm and by 76°C at 3000 rpm.

An improvement on the combustion and engine performance was shown after the optimization of the combustion phasing for both part load engine speed conditions using the maximum EGR rate tested, 15%. The impact on the exhaust emissions was also presented, showing a decrease of  $NO_x$  and



*CO* emissions of 54% and 8.5% at 2000 rpm and 71.4% and 22.7% at 3000 rpm. An increase of *HC* emissions was observed at 2000 rpm of 65% and at 3000 rpm of 55%. Regarding *PM* emissions, a reduction of number was observed when increasing the EGR rate. At 2000 rpm, the *PM* with a diameter between 7 and 22 nm were reduced from an average value of  $2.5E+4$  to  $2E+4$ . In the case of the *PM* with a diameter between 22 and 100 nm were reduced from an average values of  $4E+4$  to  $2E+4$ . The trend at 3000 rpm was similar, with a reduction of small *PM* from  $3E+4$  to  $1.5E+4$  and for bigger *PM* from  $4.5E+4$  to  $2.5E+4$ . The exhaust emissions had a similar trend as it was observed in the previous study performed without optimizing the combustion phasing but with a smaller reduction of  $NO_x$  and *CO* emissions, and a bigger increase in *HC* emissions, for the same engine conditions and same EGR rate.

During the analysis at full engine load conditions, similar results were obtained as those already shown in the part load engine conditions analysis, but on the other hand the advantages at full load are even higher when cooled EGR is introduced. An engine BSFC improvement of 12% at 2000 rpm with 14% of EGR rate and 11.5% at 3000 rpm with 10% of EGR rate was observed after optimizing the combustion phasing at trace knock for both engine speed conditions. At full engine load conditions it is almost standard for every GTDI engine to have knocking limitation to phase the combustion phasing in its optimum position and an enrichment strategy in order to control the exhaust temperature at the turbine inlet in order to warranty the reliability of the components. Cooled EGR allowed the combustion phase to be advanced because of the reduction of the mixture reactivity also reducing the combustion temperature, as explained in part load conditions, decreasing the combustion exhaust temperature and making possible the elimination of the enrichment strategy. At 2000 rpm the enrichment strategy could be eliminated by just adding 4% of EGR rate while in the case of 3000 rpm the EGR rate has to be increased up to 10%. The main contributors for the engine BSFC reduction at high load are the elimination of enrichment strategy, the advance of the combustion phasing, the reduction of heat losses and the increase of specific heat ratio of the mixture.

At full load engine conditions the impact on exhaust emissions when cooled EGR is added is different because of the enrichment strategy elimination. The reduction of *CO* emissions is massive compared to partial load: a reduction of 83% at 2000 rpm and 85% at 3000 rpm was observed. The  $NO_x$  emissions were not reduced as in part load conditions but in the case of 2000 rpm the  $NO_x$  emissions were maintained at the same value as the original condition without EGR but at 3000 rpm  $NO_x$  emissions were increased in 77%. This is mainly due to the elimination of the enrichment strategy which had a

lower oxygen concentration than the conditions with 10% of EGR rate. The *HC* emissions were increased in 22% at 2000 rpm and reduced in 16.5% at 3000 rpm. In the case of *PM* emissions, a reduction was also observed at these engine conditions using cooled EGR, following the same trend as in partial load conditions but with a higher reduction because of the enrichment strategy elimination. At 2000 rpm, the *PM* with, were reduced from an average value of  $12\text{E}+4$  to  $3\text{E}+4$ . The trend at 3000 rpm was similar, with a reduction of *PM* from  $11\text{E}+4$  to  $4\text{E}+4$ . The main advantage at this engine conditions is that the TWC can be used to convert the exhaust emissions because the mixture is at stoichiometric conditions reducing all the tailpipe emissions drastically.

When cooled EGR was introduced at low engine load conditions, it was observed that the benefits were smaller than at part and full engine conditions. The engine BSFC improvement was 2.2% at 2000 rpm and 5 bar of BMEP using 15% of EGR rate and with an optimized VVT settings because with original setting only an improvement of 1% was observed. At this conditions the engine can use IGR in order to decrease engine exhaust emissions and fuel consumption and therefore the addition of cooled EGR did not change too much the conditions. However, when VVT setting were optimized to reduce the amount of IGR a further improvement using the same amount of cooled EGR rate was observed. With cooled EGR replacing IGR a lower combustion temperature could be obtained, reducing the heat losses. Although IGR was mostly replaced by cooled EGR  $\text{NO}_x$  and  $\text{CO}$  emissions were reduced by 61% and 9.5% respectively. *HC* emissions were increased by 55.5%, the main reason of this increase is the combustion temperature reduction. At low loads the benefit was within the measurement error accuracy and therefore it was concluded that no further study was going to be performed later during the development of this research work. It seems that optimizing the amount of IGR, a good trade-off can be obtained between BSFC and exhaust emissions, and it would be easier to implement compared to a LP EGR loop which in terms of controls is more complicated while offering similar results. This research work offers a broader view at low engine load conditions that it is missing in the literature.

With all engine load conditions already analyzed, it is clear to mention that cooled EGR offers a big improvement in engine BSFC value from part load to full load engine conditions (10 to 18 – 20 bar BMEP). Regarding exhaust emissions, no significant change it is observed at part load because the TWC will reduce the difference at the tailpipe to almost 0 in the *HC* emissions increase. But at full load, the possibility of using the TWC to convert the exhaust emissions, because of the enrichment strategy elimination, is an

important advantage and therefore also a significant reduction of all exhaust emissions at the tailpipe.

The main disadvantages observed during the study were: the increase of the compressor inlet temperature that for higher compression ratios could represent a limitation due to reliability issues, the water condensation at the inter-cooler placed after the compressor, that had to be removed periodically to prevent the engine to suck it in and the turbocharger limitation at 2000 rpm, because it was not possible to achieve the original engine torque due to limitation on the boost pressure that could be produced at that engine speed so maybe two-stage turbocharging systems or variable geometry turbines are needed to achieve low end torque. In this case the control of cooled EGR was not necessary because all the tests were performed at steady state conditions but it could represent a problem during transient engine operation.

It was observed how all advantages and disadvantages of cooled EGR were similar between the steady and transient conditions. The spark advance was not optimized for different EGR rates in transient conditions and therefore the improvement observed in fuel consumption in steady operation could not be achieved. However, regarding the exhaust emissions, similar results were observed, reducing  $NO_x$  in 48% and  $CO$  emissions in 14.4%, and increasing  $HC$  emissions in 15%. It was also observed that the reduction of  $CO$  emissions because of the reduction of  $CO_2$  dissociation due to the combustion temperature reduction when cooled EGR was introduced and possible small increase in fuel consumption, not being able to detect by the fuel balance, caused an increase in 8.6% of  $CO_2$  emissions.

## Bibliography

- [1] Lumsden G., Eddleston D. and Sykes R. "Comparing Lean Burn and EGR". In *SAE Technical Paper*, 1997. 970505.
- [2] Shahed S. M. and Bauer Karl-Heinz. "Parametric Studies of the Impact of Turbocharging on Gasoline Engine Downsizing". In *SAE Technical Paper*. SAE International, 2009. 2009-01-1472.
- [3] Fraser Neil, Blaxill Hugh, Lumsden Grant and Bassett Mike. "Challenges for Increased Efficiency through Gasoline Engine Downsizing". *SAE Int. J. Engines*, Vol. 2 n° 1, pp. 991–1008, 2009. 2009-01-1053.
- [4] Vitek O., Macek J., Polasek M., Schmerbeck S. and Kammerdiener T. "Comparison of Different EGR Solutions". In *SAE Technical Paper*, 2008. 2008-01-0206.
- [5] Wei Haiqiao, Zhu Tianyu, Shu Gequn, Tan Linlin and Wang Yuesen. "Gasoline engine exhaust gas recirculation - A review". *Applied Energy*, Vol. 99 n° 0, pp. 534–544, 2012.

- [6] Bandel W., Fraidl G. K., Kapus P. E., Sikinger H. and Cowland C. N. “The Turbocharged GDI Engine: Boosted Synergies for High Fuel Economy Plus Ultra-low Emission”. In *SAE Technical Paper*, 2006. 2006-01-1266.
- [7] Grandin B., Angstrom H. E., Stalhammar P. and Olofsson E. “Knock Suppression in a Turbocharged SI Engine by Using Cooled EGR”. In *SAE Technical Paper*, 1998. 982476.
- [8] Cairns A., Blaxill H. and Irlam G. “Exhaust Gas Recirculation for Improved Part and Full Load Fuel Economy in a Turbocharged Gasoline Engine”. In *SAE Technical Paper*, 2006. 2006-01-0047.
- [9] Potteau S., Lutz P., Leroux S., Moroz S. and Tomas E. “Cooled EGR for a Turbo SI Engine to Reduce Knocking and Fuel Consumption”. In *SAE Technical Paper*, 2007. 2007-01-3978.
- [10] Kumano K. and Yamaoka S. “Analysis of Knocking Suppression Effect of Cooled EGR in Turbo-Charged Gasoline Engine”. In *SAE Technical Paper*, 2014. 2014-01-1217.
- [11] Takaki D., Tsuchida H., Kobara T., Akagi M., Tsuyuki T. and Nagamine M. “Study of an EGR System for Downsizing Turbocharged Gasoline Engine to Improve Fuel Economy”. In *SAE Technical Paper*, 2014. 2014-01-1199.
- [12] Cairns Alasdair, Fraser Neil and Blaxill Hugh. “Pre Versus Post Compressor Supply of Cooled EGR for Full Load Fuel Economy in Turbocharged Gasoline Engines”. In *SAE Technical Paper*, 2008. 2008-01-0425.
- [13] Zhong L., Musial M., Reese R. and Black G. “EGR Systems Evaluation in Turbocharged Engines”. In *SAE Technical Paper*, 2013. 2013-01-0936.
- [14] Sarlashkar J., Rengarajan S. and Roecker R. “Transient Control of a Dedicated EGR Engine”. In *SAE Technical Paper*, 2016. 2016-01-0616.
- [15] Alger Terry and Mangold Barrett. “Dedicated EGR: A New Concept in High Efficiency Engines”. *SAE Int. J. Engines*, Vol. 2 n° 1, pp. 620–631, 2009. 2009-01-0694.
- [16] Liu F., Pfeiffer J., Caudle R., Marshall P. and Olin P. “Low Pressure Cooled EGR Transient Estimation and Measurement for an Turbocharged SI Engine”. In *SAE Technical Paper*, 2016. 2016-01-0618.
- [17] Payri F., Lujan J., Climent H. and Pla B. “Effects of the Intake Charge Distribution in HSDI Engines”. In *SAE Technical Paper*, 2010. 2010-01-1119.
- [18] Alger T., Chauvet T. and Dimitrova Z. “Synergies between High EGR Operation and GDI Systems”. *SAE Int. J. Engines*, Vol. 1 n° 1, pp. 101–114, 2008. 2008-01-0134.
- [19] Carvalho Leonardo, Melo Tadeu and Neto Rubelmar. “Investigation on the Fuel and Engine Parameters that Affect the Half Mass Fraction Burned, CA50, Optimum Crank Angle”. In *SAE Technical Paper*, 2012. 2012-36-0498.
- [20] Alger Terrence, Gingrich Jess, Khalek Imad A. and Mangold Barrett. “The Role of EGR in PM Emissions from Gasoline Engines”. *SAE Int. J. Fuels Lubr.*, Vol. 3 n° 1, pp. 85–98, 2010. 2010-01-0353.
- [21] Bermudez V., Lujan J. M., Climent H. and Campos D. “Assessment of pollutants emission and aftertreatment efficiency in a GTDi engine including cooled LP-EGR system under different steady-state operating conditions”. *Applied Energy*, Vol. 158, pp. 459–473, 2015.
- [22] Gurupatham Anand and Teraji Atsushi. “A Study of Rich Flame Propagation in Gasoline SI Engine Based on 3D Numerical Simulations”. In *SAE Technical Paper*. The Automotive Research Association of India, 2011. 2011-28-0125.

- [23] Hermann, F. Zeuch T. and Klingmann J. “The Effect of Diluents on the Formation Rate of Nitrogen Oxide in a Premixed Laminar Flame”. In *ASME 2004 Proceedings Combustion and Fuels*, Vienna, Austria, 2004.



# Chapter 5

## Engine calibration optimization to operate with cooled EGR and additional fuel saving strategies

### Contents

---

<b>5.1</b>	<b>Introduction</b> .....	<b>174</b>
<b>5.2</b>	<b>Optimization process and fuel saving strategies</b> ..	<b>177</b>
5.2.1	Methodology .....	177
5.2.2	Results and analysis .....	181
5.2.2.1	VVT parameters optimization .....	181
5.2.2.2	Injection timing optimization .....	195
5.2.2.3	Additional strategies to reduce fuel consumption .....	202
<b>5.3</b>	<b>Lean burn strategy and synergy with cooled EGR</b>	<b>214</b>
5.3.1	Methodology .....	215
5.3.2	Results and analysis .....	217
5.3.2.1	Lean burn strategy on a GTDI engine ...	217
5.3.2.2	Lean burn and cooled EGR synergy influence on a GTDI engine .....	229
<b>5.4</b>	<b>Summary and conclusions</b> .....	<b>238</b>
	<b>Bibliography</b> .....	<b>242</b>

---

## 5.1 Introduction

In the previous chapter, the influence of cooled EGR on the engine performance, combustion, air management and exhaust emissions was analyzed with two approaches: (a) without modifying the spark advance and (b) optimizing the spark timing to minimize engine fuel consumption. These analysis and results showed the potential of reducing the engine fuel consumption when cooled EGR is introduced in a GTDI engine. Also the potential to reduce  $NO_x$ ,  $CO$  and  $PM$  emissions with a drawback of increasing  $HC$  emissions which can be afterwards reduced by the TWC. All these benefits were already observed by some authors as Alger et al. [1] [2], Cairns et al. [3] and Lujan et al. [4].

To fully understand and analyze the maximum potential of cooled EGR to minimize engine fuel consumption, a further optimization process of some of the important engine parameters that can play an important role on the engine performance and thermal efficiency, needs to be performed. In this chapter an optimization process of the VVT settings and injection timing to operate with cooled EGR is going to be performed.

The VVT settings optimization process presents a DoE approach mixed with a 1D methodology developed to optimize these parameters using simulation and testing. Engine 1D models have proved on recent years to be an useful tool in order to obtain accurate results and optimize control strategies, design ranges for VVT, engine components, such as turbochargers, compressor by-pass valve and many more. Vitek et al [5] showed a turbocharger optimization process based on 1D simulations, declaring that the proposed method provides the fastest way to the best solution even for the case of a VGT turbine. There is also the work performed by Bozza et al. [6] where they show an optimization process of VVT phasing and lift to minimize the fuel consumption of an atmospheric gasoline engine and also in another research work the air/fuel ratio control development process for a VVT gasoline engine using 1D simulations [7]. Also 1D engine simulations can serve to analyze and optimize a engine component as it is shown by Lujan et al. [8] in their research work, where they analyzed the operation of a compressor by-pass valve and optimize the geometry to avoid compressor surge on transient conditions, such as rapid decelerations.

Regarding the DoE approach that was used in the optimization process of the VVT settings, it has been proved over the last years the potential on the optimization process of engine calibrations to minimize fuel consumption and fulfill exhaust emission homologation limits. In the present study a simple



approach to minimize fuel consumption is followed, since exhaust emissions do not present a trade-off in this case. Jiang et al. [9] present in their research work a model-based calibration (MBC) approach for a gasoline engine to optimize VVT, air/fuel ratio and spark advance, and the results demonstrate that the model-based approach is a well suited method for engine calibration, and the integrated system provides an effective solution for implementing MBC. This MBC approach is based in a DoE approach similar to the process that it is followed in this chapter.

After optimizing the VVT setting a simpler parametric approach is followed to optimize injection timing or, at least, understand its influence on the engine performance, combustion and exhaust emissions. Some research works have been already published with different approaches. A good example is the work presented by Vijayashree et al. [10], where they optimize the fuel injection timing in a gasoline single cylinder research engine using artificial neural networks for different engine speeds from 800 rpm to 5000 rpm taking into account exhaust emissions and engine performance trade-off, concluding that this approach presents a big potential and saves time and cost. The only difference of all these research works already observed in the literature, is that they do not include the optimization of these engine parameters when cooled EGR is introduced into the engine, and mainly for this reason it is an important topic of this PhD-Thesis.

Once the optimization process is somehow completed, a final vision of possible strategies that can be used to further improve the engine behaviour to operate with cooled EGR are briefly explained. These strategies include engine results that were obtained using multiple injections, increasing the coolant temperature of the engine and inducing a swirl effect in the combustion chamber by modifying the cylinder head. Some research work has been done in these areas but without using cooled EGR.

A big part of this chapter is going to be dedicated to analyze the lean burn strategy used to reduce the engine fuel consumption, that has been in development for almost 20 years. The potential of this technology is already known, but it is in the exhaust emissions area where this strategy has the most possible solutions and therefore difficulties, mainly because the TWC cannot be used due to the lean mixture. The lean burn strategy follows the same principle as cooled EGR: it basically improves engine fuel consumption by dilution and therefore reducing pumping losses, heat losses and increasing the specific heat ratio of the mixture as it was analyzed by Bandel et al. and Yang et al. [11] [12] in their research work. The big difference between lean burn and cooled EGR is that operating with lean mixture conditions increases the

knocking risk at some point and therefore the dilution has to be greater (using a leaner mixture). This is clearly observed at 2000 rpm part load conditions, which will be explained in this chapter later.

As final part of the chapter, the lean burn strategy is used to reduce the engine fuel consumption in synergy with cooled EGR in order to control the pollutant exhaust emissions. Previous investigations had compared both technologies. Hacoheh et al. [13] in 1995 compared the lean burn and EGR strategies using a SI gasoline engine, from a performance and pollutant exhaust emissions point of view, using image analysis techniques to study the combustion process. Lumsden et al. [14] in 1997 also compared lean burn and EGR strategies using an engine capable of achieving 24 : 1 lean mixtures, and found that the lean burn strategy offered more fuel reduction capability but penalized pollutant exhaust emissions. On the other hand Grandin et al. [15] in 1999 compared lean burn and cooled EGR to replace fuel enrichment at high load, lowering tail pipe emissions but in the lean burn case with a  $NO_x$  penalty. In 2001 Ward et al. [16], studied an ignition system to improve the SI gasoline engine tolerance to lean mixture and high cooled EGR rates. The ignition system could deliver 150 mJ when typical ignition systems at that time would deliver between 30 mJ and 50 mJ. The research and development of new ignition systems and effects on the spark plugs due to high diluted mixtures continues to be a subject on the research area nowadays [17]. All these mentioned studies in the late 90's and early 2000's were performed on SI port fuel injection (PFI) gasoline engines.

In 2013, Tang et al. [18] compared the combustion characteristics and performance of cooled EGR and lean burn strategy in a SI PFI gasoline engine. Tang, defined a dilution factor that is going to be employed in this research work to analyze the performance, combustion and pollutant exhaust emissions using a lean burn strategy with cooled EGR. These previous investigations encourage further research efforts to gain knowledge on the real potential of lean burn and cooled EGR strategies to be standardized in future SI GTDI engines. In this framework, the research work focuses on a detailed evaluation and discussion of the impact of using cooled EGR in a SI GTDI engine operating with a lean burn strategy.

This chapter is going to be divided into three main sections: the optimization process and the study of the fuel consumption saving strategies, the study of lean burn and its possible synergy with cooled EGR and finally summary and conclusions.

## 5.2 Optimization process and fuel saving strategies

In this section, two main sub-sections are presented: the methodology and the analysis of the results. In the results and analysis subsection three main parts are presented. First, the VVT settings optimization and comparison with results obtained in last Chapter 4. Second, the injection timing optimization and effect on engine performance and exhaust emissions with a comparison to the best conditions achieved until the moment. And finally, a brief explanation of other strategies that could be used to further improve the engine conditions to operate with cooled EGR.

### 5.2.1 Methodology

After analyzing the effect of cooled EGR in the engine performance and exhaust emissions in Chapter 4, it was observed how the original spark advance has to be re-optimized to operate with cooled EGR. Taking this into account, this section will explain briefly the methodology developed to optimize the VVT and injection timing. This will also serve to understand the full potential of cooled EGR in modern SI gasoline engines by adapting the original engine calibration to these new operating conditions. The calibration optimization was carried out at part load engine conditions, as already mentioned in Chapter 4. This can be easily justified mainly because at this engine conditions VVT settings are optimized to reduce engine fuel consumption using IGR, therefore not optimized to operate with cooled EGR, and also because at this engine conditions the average normal driving area it is usually found. The two OP optimized in this chapter are 2000 rpm and 3000 rpm, both at 10 bar of BMEP, as can be seen in Table 5.1.

To start the optimization process the spark advance needs to be optimized to phase the combustion retard produced by the dilution effect of the cooled EGR already explained in the Chapter 4. The spark advance is going to be optimized for each tested conditions at 2000 rpm and 3000 rpm. This spark advance optimization process consists in advancing the spark advance until the maximum torque is achieved. For these tests the iso-air mass flow, iso-fuel mass flow and iso-intake temperature conditions for different EGR rates, VVT configurations and injection timing were maintained.

For the VVT settings optimization process, a methodology was developed using 1D simulations and a DoE approach to design the test plan. As it was mentioned before, the optimization process was also performed for both engine speeds, 2000 rpm and 3000 rpm. The test plan was generated by using a D-

Operating point	Engine speed [rpm]	Load [%]	Air mass flow [kg/h]
OP 1 (Part Load)	2000	50	110
OP 2 (Part Load)	3000	50	170

**Table 5.1.** Selected operating conditions.

Operating point	EGR rate [%]	IVO [CAD ATDC]	EVC [CAD ATDC]
OP 1	2	-30.0	8.0
OP 2	2	11.0	8.0
OP 3	18	-30.0	8.0
OP 4	2	-30.0	49.0
OP 5	11	-5.4	8.0
OP 6	8	11.0	49.0
OP 7	18	11.0	22.4
OP 8	2	-5.4	32.6
OP 9	18	-15.7	49.0
OP 10	12	-30	32.6

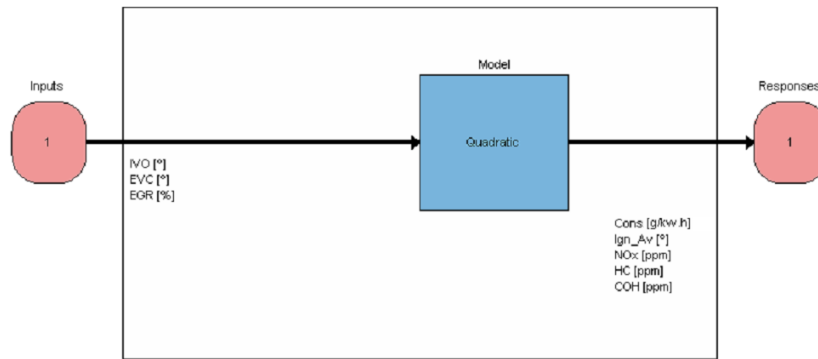
**Table 5.2.** DoE test plan for 2000 rpm and 10 bar BMEP engine conditions.

optimal approach in the MBC Matlab tool, as it was already mentioned in Section 3.3.3 of Chapter 3. This test plan has three inputs: IVO, EVC and EGR rate. Then it has several outputs that can be modeled by the MBC but the most important are fuel consumption and exhaust emissions. The test plan generated for 2000 rpm and 3000 rpm can be seen in Table 5.2 and Table 5.3. A quadratic model was created with a second level order for each input and with all possible interactions between them as mathematical approach for the DoE equation. The inputs and outputs can be seen in Figure 5.1. For each test observed in Table 5.1, the optimum spark advance has to be found so this does not influence the output of each test, as mentioned before.

After the test plan is performed, all the inputs and outputs are used to create the model base design (MBD). Afterwards the mathematical equation found to model each output can be used to optimize any output at a time or some outputs at the same time. In the present case only the fuel consumption was optimized. After finding the optimum input values to

Operating point	EGR rate [%]	IVO [CAD ATDC]	EVC [CAD ATDC]
OP 1	2	-30	49
OP 2	2	-29	8
OP 3	2	11	49
OP 4	10	-30	25
OP 5	7	11	8
OP 6	11	-6	49
OP 7	2	-6	25
OP 8	17	-29	49
OP 9	17	-17	8
OP 10	17	11	36

**Table 5.3.** DoE test plan for 3000 rpm and 10 bar BMEP engine conditions.



**Figure 5.1.** DoE inputs, quadratic model and outputs.

minimize fuel consumption it was therefore tested at the test bench to confirm the predictions.

In parallel to this methodology, a 1D based simulation methodology was also developed in order to reduce the amount of tests that had to be performed and optimize the VVT parameters to minimize engine fuel consumption. The 1D engine model was built and validated for non-EGR and EGR operating conditions as it was explained in Section 3.3.2 of Chapter 3. The methodology consists in observing the maximum EGR rate that can give a benefit in fuel consumption with an optimized spark advance but with original VVT values. Afterwards, these engine conditions are simulated in the 1D engine model and

parametric studies on the intake valve opening (IVO) and the exhaust valve closing (EVC) positions were performed to determine the optimum settings for the VVT. The main engine outputs that were analyzed to determine the optimum VVT setup were: the internal exhaust gas recirculation (IGR), pumping losses, heat losses and indicated efficiency.

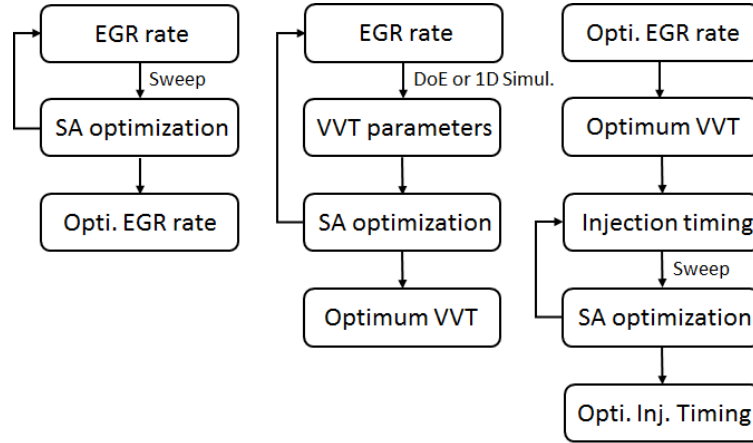
If the IGR is minimized, more volume is available to introduce cooled EGR and maximize the fuel consumption reduction. The pumping losses and heat losses have to be reduced also in order to improve the thermal efficiency of the engine and therefore reduce the fuel consumption. All these effects are going to be observed in the indicated engine efficiency which is also taken into account to choose the optimum intake and exhaust VVT positions to minimize engine fuel consumption.

After the selection of the optimum VVT parameters using 1D simulations, they are compared to the values obtained using the MBC created from the DoE test plan and finally an analysis is performed to understand the potential of simulation and DoE's.

Once the spark advance and VVT parameters are optimized, a simple parametric study of injection timing (also called injection timing sweep) was performed at the optimum EGR rate, VVT parameters and spark advance conditions that further reduced the engine fuel consumption for both engine speed conditions. The spark advance was re-optimized for each new injection timing value. The injection timing step for the sweep was 10 CAD with a range of 0 to 60 CAD of advance from the original injection timing value. A simple flow-chart of the optimization methodology process is presented in Figure 5.2 where it can be observed all the different steps and the required procedure to achieve the optimization.

With the optimum configuration of VVT settings and EGR rate, a study of three strategies to further reduce the engine fuel consumption was performed. This study was performed for 2000 rpm and 10 bar of BMEP, because one OP was considered to be enough to analyze and observe the feasibility of these strategies. These strategies are: multiple injections, higher coolant temperature operation and induced swirl motion in the combustion chamber. In this case, a brief analysis of the effect of each of these strategies on the combustion, engine performance and exhaust emissions is going to be presented.

The next section is divided into different sub-sections; one for each optimization process and study: VVT settings optimization, injection timing optimization and strategies to reduce engine fuel consumption.



*Figure 5.2. Optimization process flow-chart.*

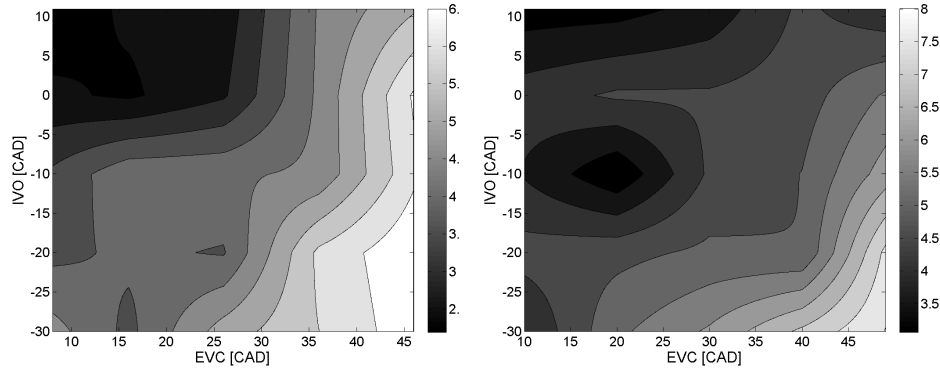
## 5.2.2 Results and analysis

This section explains the optimization developed methodology using DoE approach and 1D simulations to optimize the VVT parameters for different EGR rates conditions and analyzes the injection timing optimization for the optimized operating conditions of EGR rate and VVT parameters. In addition three strategies to increase the EGR rate operational range or further reduce the fuel consumption are going to be tested and analyzed using the optimum VVT settings setup at the optimum EGR rate conditions.

### 5.2.2.1 VVT parameters optimization

In this section, several 1D simulations were performed in two partial load operating conditions, at 2000 rpm and 3000 rpm, in order to optimize the VVT configuration to maximize the fuel consumption reduction in synergy with cooled EGR.

The IGR is used in SI gasoline engines at low and part load conditions to reduce pollutant exhaust emissions, reduce fuel consumption and warm up faster the engine and catalyst after a cold start. Introducing cooled EGR does not help to warm the engine faster, but when it is at hot operating temperature, it reduces  $NO_x$ ,  $CO$  and  $PM$  emissions, heat losses and pumping losses, as it was analyzed in last Chapter 4. If IGR is minimized, more volume is available to introduce cooled EGR and maximize the fuel consumption reduction. In Figure 5.3 it can be observed that using early EVC, 10 – 20



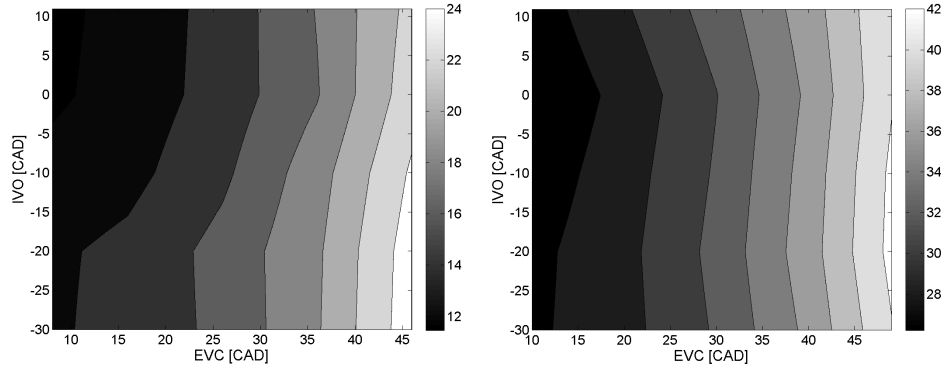
**Figure 5.3.** IGR in % at 2000 rpm and 50% load (left graph) and at 3000 rpm and 50% (right graph) for different IVO and EVC values at the maximum EGR rate conditions.

CAD ATDC, and late IVO, 0 – 10 CAD ATDC, reducing the overlap as much as possible, low IGR can be achieved for 2000 rpm. These results differ from the research work presented by Bourhis et al. [19] where it was found that increasing the overlap, decreased the IGR. For 3000 rpm similar EVC ranges were seen between 10 – 20 CAD ATDC, on the IVC another optimum range was found between –5 and –15 CAD ATDC plus the late IVC range between 3 and 10 CAD ATDC, that is reduced compared to the IVC 2000 rpm optimum range. The lower IGR percentage that could be achieved with the original VVT mechanical limitations is around 2.5% at 2000 rpm and around 3.5% at 3000 rpm.

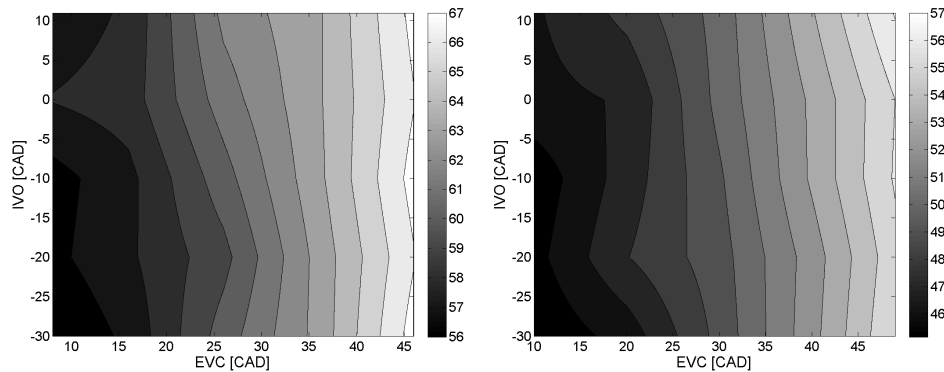
In Figure 5.4 a representation of the pumping losses for different VVT configurations can be seen. At 2000 rpm it is observed that an optimum area was found using early EVC, between 10 and 20 CAD ATDC and having a fairly early IVO, between –5 and 10 CAD ATDC. On the other hand at 3000 rpm the EVC range is a little more limited between 10 and 15 CAD ATDC and the IVO has a wider range, between –15 and 10 CAD ATDC, than at 2000 rpm. The optimized VVT configuration to minimize pumping losses matches the optimized VVT configuration to minimize IGR.

Furthermore, heat losses are a consequence of mixture reactivity and therefore combustion temperature and duration, and cycle mean temperature. In Figure 5.5 heat losses for different VVT configurations are presented for two part load operating conditions at 2000 rpm and 3000 rpm. It can be seen that at 2000 rpm the early EVC continues to be the optimum range, between 10





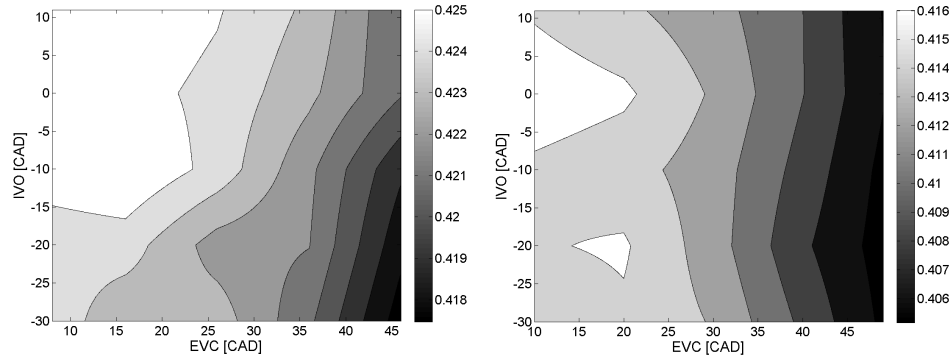
**Figure 5.4.** Pumping losses in  $J$  at 2000 rpm and 50% load (left graph) and at 3000 rpm and 50% (right graph) for different IVO and EVC values at the maximum EGR rate conditions.



**Figure 5.5.** Heat losses in  $J$  at 2000 rpm and 50% load (left graph) and at 3000 rpm and 50% (right graph) for different IVO and EVC values at the maximum EGR rate conditions.

and 15 CAD ATDC. On the other hand, an early IVO was seen as the optimum range between  $-30$  and  $-15$  CAD ATDC. The same behavior was observed at 3000 rpm, where an early EVC, between 10 and 15 CAD ATDC, and IVO, between  $-30$  and  $-15$  CAD ATDC, were the optimum VVT configuration.

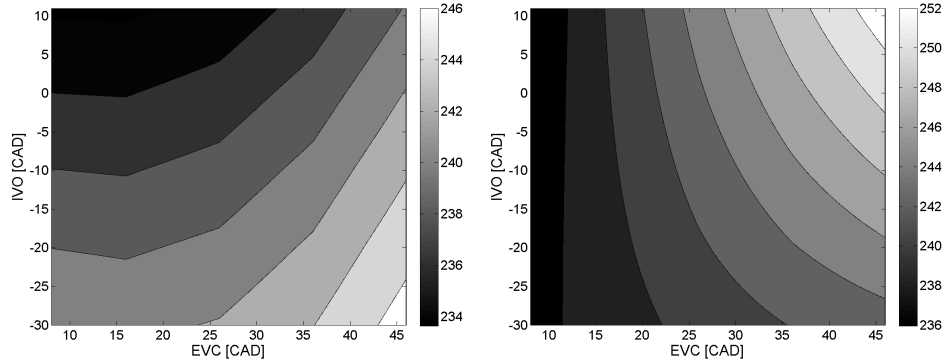
To finally select the optimum VVT configuration to minimize the fuel consumption, the indicated efficiency was analyzed. In Figure 5.6, the indicated efficiency is plotted for different VVT configurations in the two simulated operating conditions, 2000 rpm and 3000 rpm at part load. At



**Figure 5.6.** Indicated efficiency in % at 2000 rpm and 50% load (left graph) and at 3000 rpm and 50% (right graph) for different IVO and EVC values at the maximum EGR rate conditions .

2000 rpm the maximum indicated efficiency is obtained with an early EVC range, between 10 – 20 CAD ATDC, and a later IVO, between –15 and 10 CAD ATDC. On the other hand, at 3000 rpm, a more restricted optimum area can be seen, where also an early EVC range was seen as the optimum, between 10 and 20 CAD ATDC, but the IVO optimum range was reduced between –5 and 5 CAD ATDC. The indicated efficiency takes into account, the pumping losses and heat losses, giving the perfect trade-off analysis to finally select the optimum VVT configurations for both operating conditions. In addition, this VVT configuration matches the optimum VVT range found to minimize the IGR.

A DoE was developed to optimize the VVT configuration in order to minimize the fuel consumption for the two operating engine conditions on the dyno test bench. For each operating engine conditions a minimum best timing (MBT) was achieved by advancing the timing to phase the combustion on the optimum angle and in some cases knock limited. The DoE model used was a D-optimal, as mentioned in Chapter 3, finding an optimized VVT configuration to minimize the fuel consumption for both engine speed conditions with a precision of less than 0.5% of error between prediction and measurement. In Figure 5.7 the fuel consumption, generated with the DoE model, for different VVT configurations at the maximum EGR rate can be observed. At 2000 rpm the optimum VVT configuration range matches the optimum range obtained via 1D simulations. The optimum VVT configuration for 2000 rpm was 0 CAD ATDC for the EVC and 10 CAD ATDC for the IVO, which reduces the overlap to 0 as it was also seen in the 1D simulations.



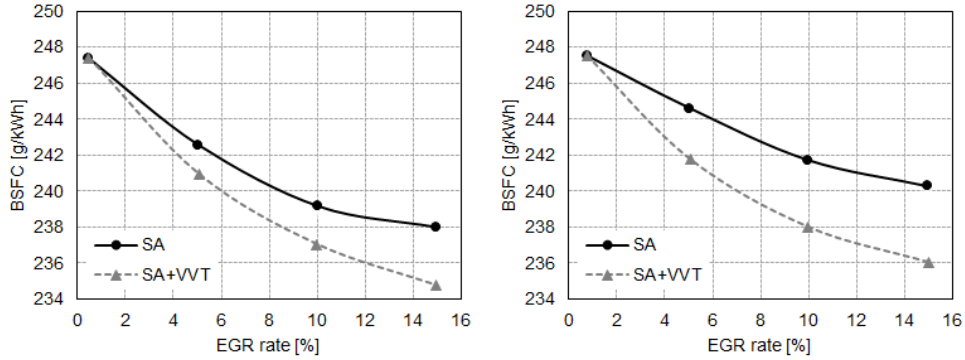
**Figure 5.7.** BSFC in  $g/kWh$  at 2000 rpm and 50% load (left graph) and at 3000 rpm and 50% (right graph) for different IVO and EVC values at the maximum EGR rate conditions.

The same tendency was observed at 3000 rpm operating conditions, where the optimum DoE VVT configuration matches the optimum VVT configuration range obtained via 1D simulations. The optimum configuration for 3000 rpm was 8 CAD ATDC for the EVC and a range between  $-10$  and 10 CAD ATDC for the IVO, as can be observed in Figure 5.7.

Once VVT settings were optimized to minimize fuel consumption, an EGR rate sweep was performed, from 0% to 15% every 5%, to analyze the impact on engine performance, exhaust emissions and compare with original VVT setting results. These tests, as it was mentioned before, were performed at iso-air mass flow, iso-fuel mass flow and iso-intake temperature.

After the optimization of spark advance for each EGR rate step and with the optimized VVT settings, the introduction of EGR up to 15% reduced the fuel consumption in 5.2% at 2000 rpm, and in 4.7% at 3000 rpm as it can be seen in Figure 5.8, where the BSFC is plotted for different EGR rates and different optimized settings for both engine speeds. At 2000 rpm by optimizing the VVT settings the fuel consumption was reduced in 1.4% compared to the optimum operating point at 15% EGR rate with optimized SA and at 3000 rpm the improvement was around 1.8% compared to the optimum operating point at 15% EGR rate with optimized SA as can be seen in Figure 5.8.

One of the important achievements of the new optimized VVT settings is the lower percentage of IGR compared to the original conditions. This is observed in Figure 5.9 where the combustion duration is plotted for different EGR rates for the initial study with only optimized SA and for the new tests

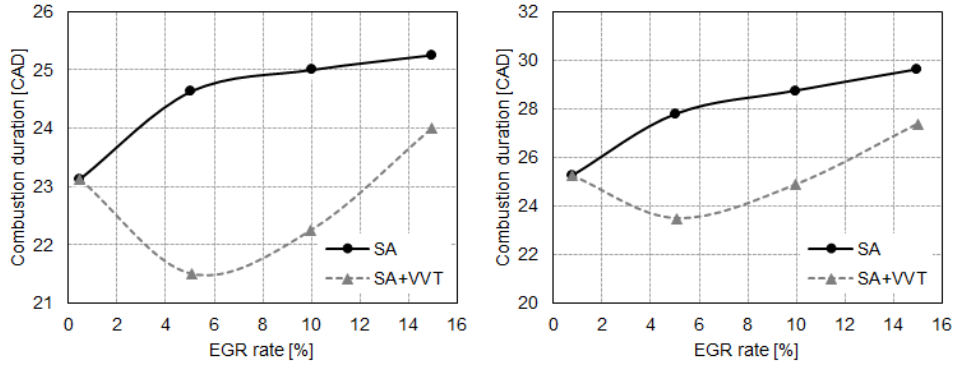


**Figure 5.8.** Engine BSFC with SA and VVT settings optimized at 2000 rpm and 50% of load (left graph) and at 3000 rpm and 50% (right graph) for different EGR rates.

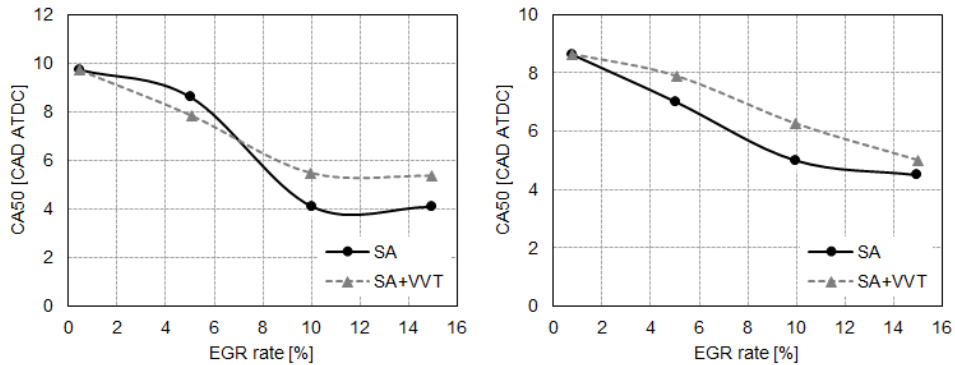
with optimized VVT settings with the re-optimized SA in both engine speed conditions. The combustion duration is reduced at 5% of EGR rate compared to the original conditions due to the lower amount of residual gases in the cylinder for the same amount of cooled EGR rate. With less residual gases than the original conditions the combustion is faster because more oxygen concentration is available and the mixture has more reactivity. Afterwards as the EGR rate increases the combustion duration increases due to the reduction in oxygen concentration and, therefore, in the mixture reactivity. The effect is visible for both engine speeds.

In order to be able to conclude that less residual gases are the main cause of the lower combustion duration mentioned before, a comparison of CA50 is performed in Figure 5.10, where the CA50 is plotted for both optimized settings setup and both engine speeds. It can be observed that CA50 in both optimized setups is almost at the same value within an error of  $\pm 1$  CAD. In most of the cases, it is even more retarded in the optimized VVT and SA setup. This confirms that combustion phasing is not affecting the propagation of the turbulent flame and therefore the combustion duration difference is due to the lower residual gases in the optimized VVT and SA setup.

Regarding the combustion temperature, similar plots are presented in Figure 5.11, where the combustion temperature is plotted for both optimized settings setup and both engine speed with different EGR rate. The combustion temperature at 2000 rpm is lower for the optimized VVT and SA compared to the optimize SA tests for the same EGR rate due to the reduction of IGR and more retarded IVC, which directly impacts the initial combustion temperature.



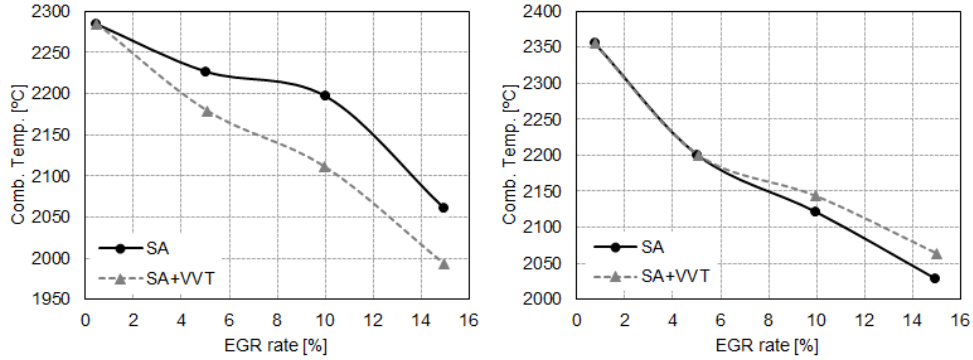
**Figure 5.9.** Combustion duration with optimized SA and optimized VVT settings and SA at 2000 rpm and 50% load (left graph) and at 3000 rpm and 50% (right graph) for different EGR rates.



**Figure 5.10.** CA50 with optimized SA and optimized VVT settings and SA at 2000 rpm and 50% load (left graph) and at 3000 rpm and 50% (right graph) for different EGR rates.

The reduction of in-cylinder temperature at the start of the combustion should lead to a slower combustion, but in this case because of the increase in oxygen concentration, also due to the reduction on residual gases in the cylinder, the combustion is faster at 5% and 10% of EGR rate compared to original conditions, as it was seen in left graph of Figure 5.9 presented before.

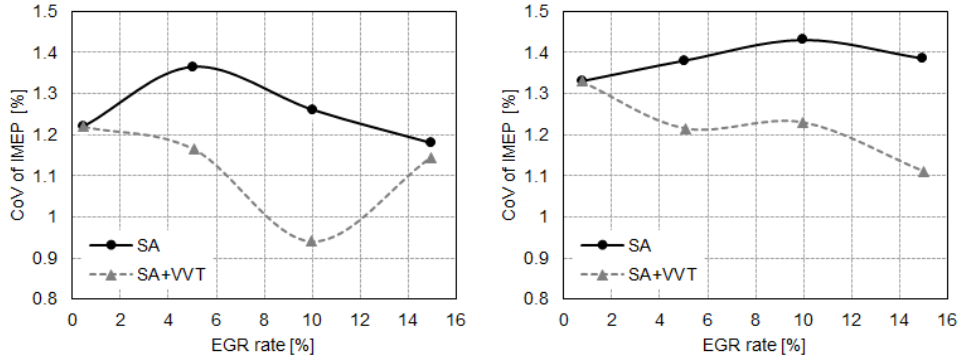
In the case of 3000 rpm, it can be seen in the right graph of Figure 5.11 that the combustion temperature rested almost at the same value at 5% of EGR rate for both settings setup. From that point the combustion temperature



**Figure 5.11.** Combustion temperature with optimized SA and optimized VVT setting and SA at 2000 rpm and 50% load (left graph) and at 3000 rpm and 50% (right graph) for different EGR rates.

with the optimized VVT and SA was higher than with the optimized SA despite the reduction of IGR. It can be seen in right graph of Figure 5.9 that the combustion duration and trend is the same as at 2000 rpm, but in this case the IGR contribution to the combustion temperature at the optimized SA setup conditions was lower than at 2000 rpm explaining the combustion trend difference for the optimized VVT and SA setup between 2000 rpm and 3000 rpm.

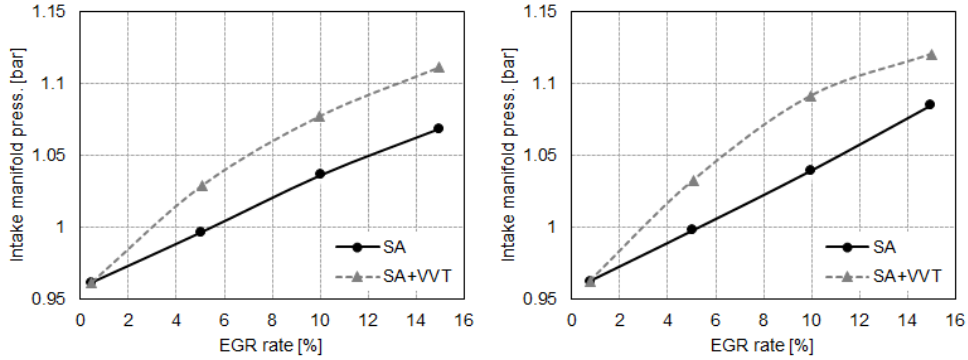
Concerning the CoV of the IMEP on the optimized VVT and SA, it can be observed in Figure 5.12 plotted with optimized SA setup and both engine speed for different EGR rates. At 2000 rpm (left graph) it can be seen that the CoV of the IMEP is reduced for 5% and 10% of EGR rate comparing the optimized VVT and SA setup with the optimized SA setup, which is reasonable due to the lower dilution effect at the same cooled EGR rate because of the lower IGR. But at 15% of EGR rate it can be seen how the CoV of the IMEP is practically the same for both optimized settings setup despite the lower mixture dilution in the optimized VVT and SA setup. This is explained by the much lower combustion temperature and therefore the initial temperature of the combustion that directly affects the ignitability of the mixture increasing the cycle to cycle variation. This effects is not observed at 3000 rpm, as it can be seen in right graph of Figure 5.12, since the combustion temperature values for 10% and 15% of EGR rate are higher with the optimized VVT and SA setup compared to the optimize SA setup. In fact at 3000 rpm the CoV of the IMEP was lower with optimized VVT and SA setup compared to optimized SA setup for the entire EGR rate range.



**Figure 5.12.** CoV of the IMEP with optimized SA and optimized VVT setting and SA at 2000 rpm and 50% load (left graph) and at 3000 rpm and 50% (right graph) for different EGR rates.

In order to analyze the air management of the engine, it must be taken into account that these tests were performed at iso-air mass flow and iso-intake temperature as mentioned before. The analysis will be focused on the intake manifold pressure, exhaust manifold pressure and pumping losses with the optimized VVT and SA setup for different EGR rates and its comparison with optimized SA setup tests.

The effect of new VVT settings on the intake manifold pressure for both engine speeds and different EGR rates can be seen in Figure 5.13. It is observed how the new intake cam phasing affects the intake manifold pressure, for both engine speeds, due to the effect that has on the volumetric efficiency of the engine. The new IVC is retarded compared to original IVC, this will be translated in a backflow to the intake manifold after the intake stroke is completed because the intake valve will continue to be open after the piston starts the compression phase. This IVC retard will divide the compression stroke in two parts, which is the so called Miller cycle, explained in Chapter 2. In Figure 5.14, it can be observed the modeling results of intake and exhaust mass flows comparison between the original VVT settings and optimized VVT settings for both engine speeds. The backflow existence will decrease the volumetric efficiency of the engine and, in order to maintain the iso-air mass flow required to perform the tests, the intake pressure must be increased to compensate the lost volumetric efficiency. The difference of intake pressure at 15% of EGR rate between the optimized VVT and SA setup compared to the optimized SA setup at 2000 rpm is around 45 mbar and around 36 mbar at 3000 rpm as it can be observed in Figure 5.13.

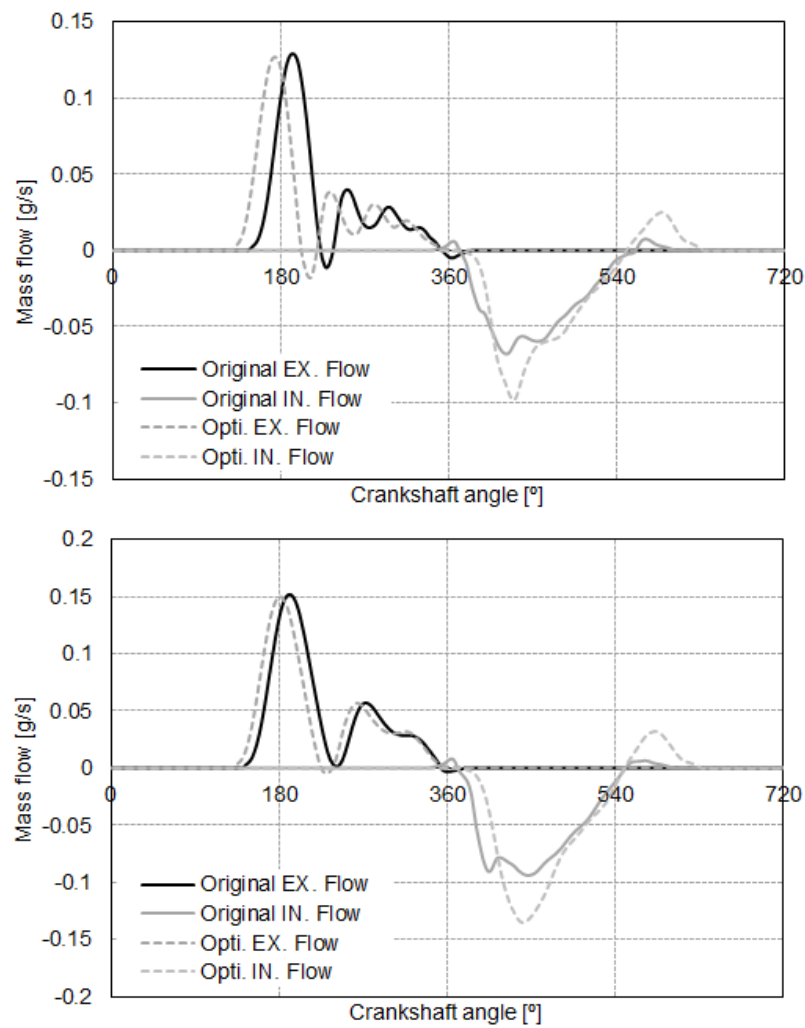


**Figure 5.13.** Intake manifold pressure with optimized SA and optimized VVT setting and SA at 2000 rpm and 50% load (left graph) and at 3000 rpm and 50% (right graph) for different EGR rates.

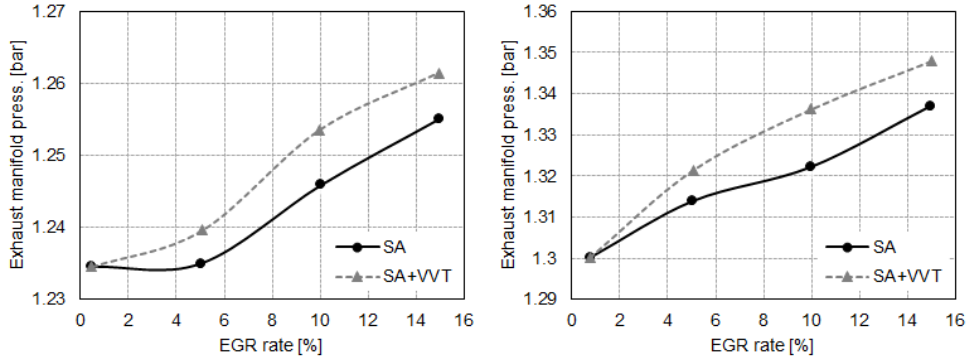
Regarding the exhaust manifold pressure, the optimized VVT and SA setup increases more the exhaust pressure during the sweep of EGR rate than the optimized SA setup for both engine speed as can be seen in Figure 5.15. This increase in exhaust manifold pressure with the optimized VVT and SA setup at 2000 rpm is due to the increase in exhaust manifold temperature because of the earlier EVO compared to the original exhaust VVT setting, as can be observed in Figure 5.14, where the exhaust mass flow on the optimized VVT and SA setup starts to exit the cylinder before the exhaust mass flow of the original VVT configuration. With an earlier EVO, the time for expansion of the exhaust gas in the cylinder is reduced and therefore the exhaust gas temperature at EVO is higher, increasing exhaust manifold temperature and therefore pressure because the exhaust manifold volume is maintained constant. To support this hypothesis the exhaust manifold temperature with the optimized VVT and SA setup and the optimized SA setup for both engine speed at different EGR rates is presented in Figure 5.16. It can be seen, that for the optimized VVT and SA setup the exhaust manifold temperature is higher, as mentioned before, due to the earlier EVO in both engine speeds. In the case of 3000 rpm the difference of optimized EVO with the original setup is smaller than at 2000 rpm, but the combustion temperature is higher than with the optimized SA setup, as it was observed in Figure 5.11, contributing to the higher temperature at EVO and therefore at the exhaust manifold.

At 2000 rpm the increase in intake manifold pressure at 15% of EGR is almost 50 mbar and the increase in exhaust manifold pressure is around 6mbar, this is translated in a big reduction of pumping losses for this new optimized

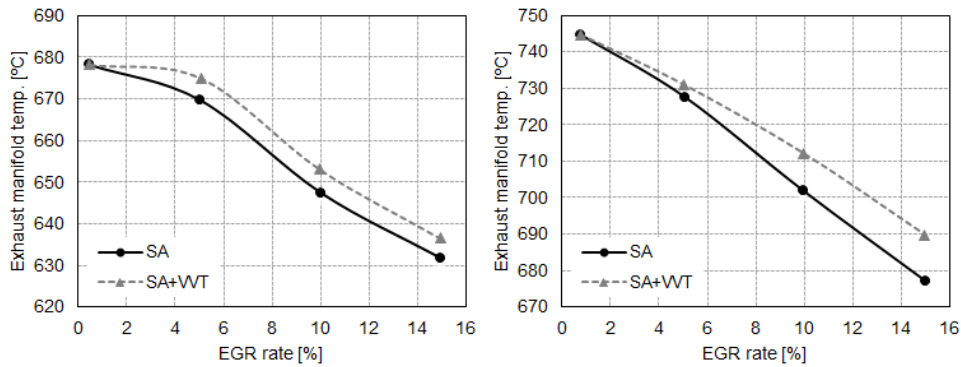




**Figure 5.14.** Intake and exhaust instantaneous mass flows with original VVT setting and optimized VVT setting at 2000 rpm and 50% load (top graph) and at 3000 rpm and 50% (bottom graph) for 15% of EGR rate.



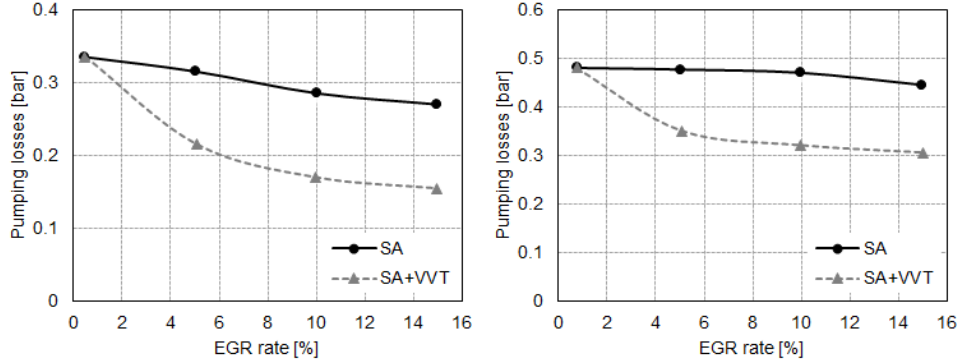
**Figure 5.15.** Exhaust manifold pressure with optimized SA and optimized VVT setting and SA at 2000 rpm and 50% load (left graph) and at 3000 rpm and 50% (right graph) for different EGR rates.



**Figure 5.16.** Exhaust manifold temperature with optimized SA and optimized VVT setting and SA at 2000 rpm and 50% load (left graph) and at 3000 rpm and 50% (right graph) for different EGR rates.

VVT and SA setup for all tested EGR rates, as it can be observed in the left graph of Figure 5.17, where the pumping losses are plotted for the different settings setup and different EGR rates. The reduction of pumping losses at 15% of EGR rate is 43% compared to the same EGR rate for the optimized SA setup and 54% compared to the original conditions.

In the case of 3000 rpm the increase in intake manifold pressure at 15% of EGR rate is around 36 mbar and the increase in exhaust manifold pressure is around 10mbar, this is translated in a big reduction of pumping losses for

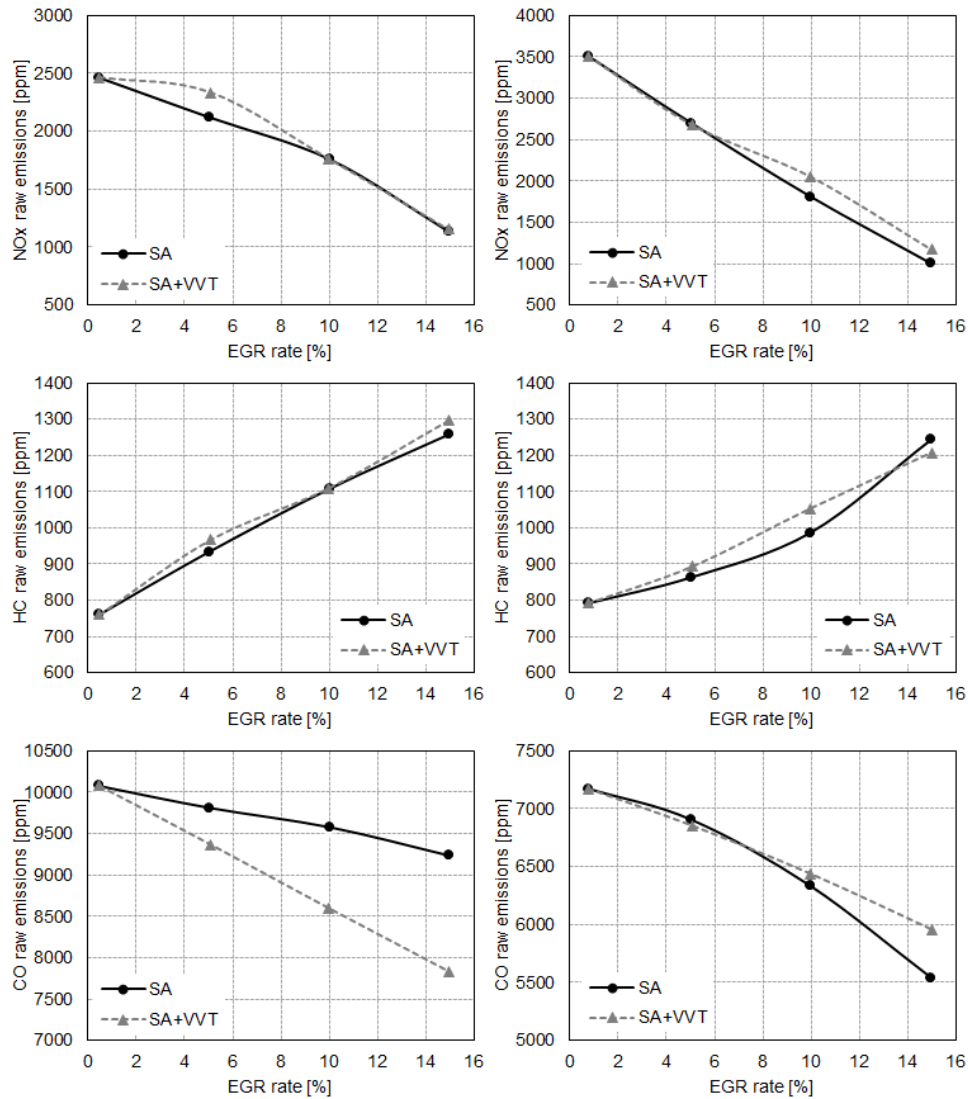


**Figure 5.17.** Pumping losses with optimized SA and optimized VVT setting and SA at 2000 rpm and 50% load (left graph) and at 3000 rpm and 50% (right graph) for different EGR rates.

this new optimized VVT and SA setup for all tested EGR rates, as it can be observed in the right graph of Figure 5.17, where the pumping losses are plotted for the different setups and different EGR rates for 3000 rpm and 10 bar of BMEP. The reduction of pumping losses at 15% of EGR rate is 32% compared to the same EGR rate for the optimized SA setup and 37% compared to the original conditions. As it was expected, the reduction in pumping losses is lower than at 2000 rpm, due to the higher increase in exhaust manifold pressure and the lower increase in the intake pressure compared to 2000 rpm.

In addition to the positive effects of cooled EGR on the engine performance, it also had a beneficial effect on pollutant exhaust emissions as stated before. The comparison of exhaust pollutant raw emissions with both settings setup and different EGR rates for both engine speeds can be observed in Figure 5.18. In this case only the comparison of  $NO_x$ ,  $HC$  and  $CO$  is made, because  $PM$  emissions were not measured for the new optimized VVT and SA setup.

Analyzing  $NO_x$  emissions it can be observed at 2000 rpm that the trend is similar between both setups with the only difference at 5% of EGR rate, where it can be seen that  $NO_x$  emissions are higher for the optimized VVT and SA setup compared to optimized SA setup. This is due to the increase in oxygen concentration because of the reduction of IGR. Despite the lower combustion temperature observed at this combustion temperature the oxygen concentration leads to the creation of  $NO_x$  emissions. In the case of higher EGR rates the effect of temperature reduction and oxygen concentration increment is compensated and the same amount of  $NO_x$  emissions are



**Figure 5.18.** Exhaust emissions with optimized SA and optimized VVT setting and SA at 2000 rpm and 50% load (left graphs) and at 3000 rpm and 50% (right graphs) for different EGR rates. NO<sub>x</sub> emissions (top graphs), HC emissions (middle graphs) and CO emissions (bottom graphs).

produced for both setups. The total reduction at 15% EGR rate is 54% compared to original conditions. In the case of 3000 rpm, it can be also observed the same trend for both setting setups. However, at 10% and 15% of EGR rate the optimized VVT and SA setup produces more  $NO_x$  emissions than the optimized SA setup due to the higher combustion temperature, already observed before in Figure 5.11. Despite this increase,  $NO_x$  emissions were reduced in 67% compared to original conditions.

Regarding  $HC$  emissions, it can be seen in the middle graphs of Figure 5.18 that for both engine speeds and settings setup the trend is the same, increasing the  $HC$  emission when EGR rate increases due to lower oxygen concentration and lower combustion temperature as stated before in Section 4.3.1.2. The total increase is 65% at 2000 rpm and 54% at 3000 rpm. In the case of  $CO$  emissions, it can be observed a big reduction at 2000 rpm of 15% for the optimized VVT and SA setup compared to the optimized SA setup, this is mainly due to the lower combustion temperature decreasing the thermal dissociation of  $CO_2$ . The opposite is observed at 3000 rpm where an increase is observed for 10% and 15% of EGR rate with the optimized VVT and SA setup compared to the optimized SA setup, due to the higher combustion temperature which promotes the dissociation of  $CO_2$  producing more  $CO$  emissions. Despite this increase,  $CO$  emissions were reduced in 27% compared to original conditions.

A methodology using 1D simulations to optimize the VVT settings was developed and validated using a DoE test plan on engine dyno bench, achieving good results. It was presented how the optimization of VVT settings can improve the fuel consumption of the engine without increasing exhaust emissions for the same EGR rate conditions. A complete analysis was performed for engine performance, combustion, air management and exhaust emissions. It was observed that the fuel consumption was reduced mainly by the reduction on pumping losses and CoV of the IMEP for both engine speeds, and in the case of 2000 rpm a reduction of heat losses was also achieved due to the lower combustion temperature. The introduction of EGR up to 15% reduced the fuel consumption in 5.2% at 2000 rpm, and in 4.7% at 3000 rpm, as it was observed in Figure 5.8, compared to the original conditions.

### 5.2.2.2 Injection timing optimization

As it was mentioned in Chapter 4, in the introduction and methodology sections of this Chapter 5, a start of injection (SOI) or injection timing optimization was also performed for 2000 rpm and 10 bar of BMEP. The

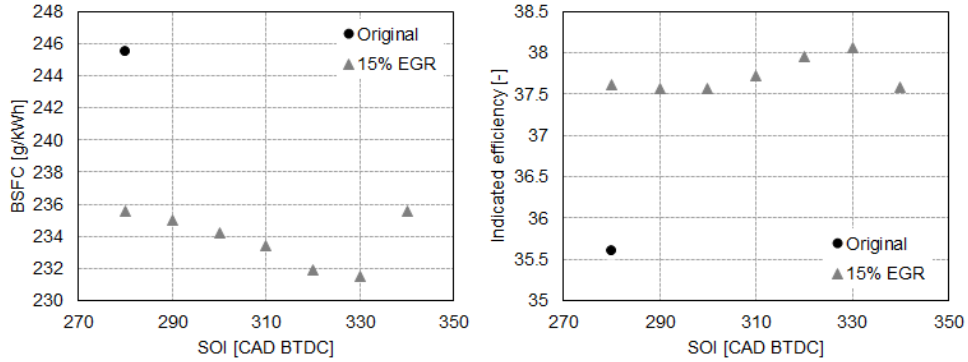
methodology used to performed the optimization of SOI is a standard parametric test using different SOI at 15% of EGR rate with the optimized VVT and SA setup found for this EGR rate. For each SOI, an optimum SA had to be found since mixing and evaporation rate conditions change and therefore combustion phasing changes. The SOI starting point was at the original value, 280 CAD BTDC, and a sweep was performed until 340 CAD BTDC with a step of 10 CAD. The tests were performed at iso-air mass flow, iso-intake air temperature, iso-engine temperature and iso-fuel mass flow as stated for other tests before.

First a brief explanation of parametric tests to optimized SOI is going to be presented, analyzing the main engine parameters to understand the influence of the SOI on the combustion, air management and emissions. Second, a comparison of this new optimized setup including the new SOI against the optimized SA setup and the optimized VVT and SA setup is going to be presented to understand the impact of this final step of the optimization on the main engine parameters.

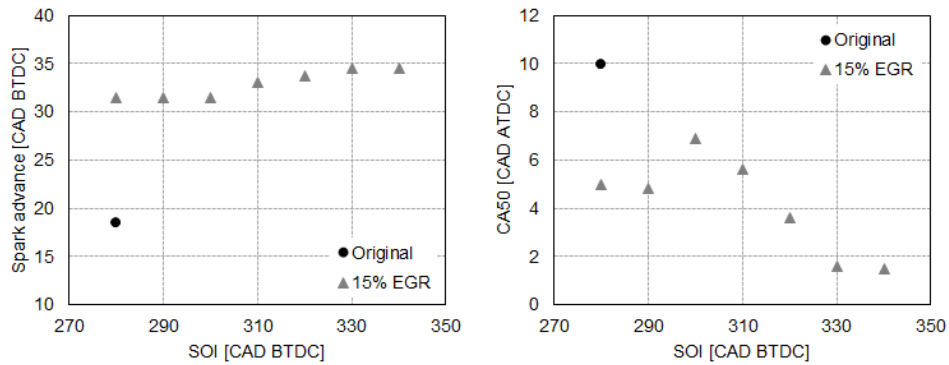
The SOI sweep was performed until the BSFC reached a minimum value. This was obtained at 330 CAD BTDC as it can be seen in the left graph of Figure 5.19 where the BSFC is plotted for different SOI values and in the right graph of Figure 5.19 the indicated efficiency for different SOI values. It can be seen how retarding the SOI decreased the BSFC until 330 CAD BTDC and suddenly increased at 340 CAD BTDC. It is also observed how indicated efficiency increases when SOI is retarded but does not follow the same opposite trend as BSFC in the range between 290 and 310 CAD BTDC. The BSFC was decreased in 6.8% compared to the original conditions and an increased of 3% absolute value of indicated efficiency was also observed for the optimum SOI at 330 CAD BTDC.

The SOI variation influences the mixture process, the evaporation rate, the interaction of the jet with the piston and the engine volumetric efficiency. Because of these reasons the combustion results are better understood with CFD simulation but in this case it was not possible to perform. However, the results that are presented here could explain all the reasons with a deeper analysis.

It was already seen in the right graph of Figure 5.19 that there is a strange range between 290 and 310 CAD BTDC where the indicated efficiency did not followed the opposite trend of BSFC graph. It can be seen in Figure 5.20, where the SA (left graph) and CA50 (right graph) is plotted for different SOI values, how CA50 for 300 and 310 CAD BTDC does not follow the trend of other SOI values. It can also be seen that SA was not retarded or did not



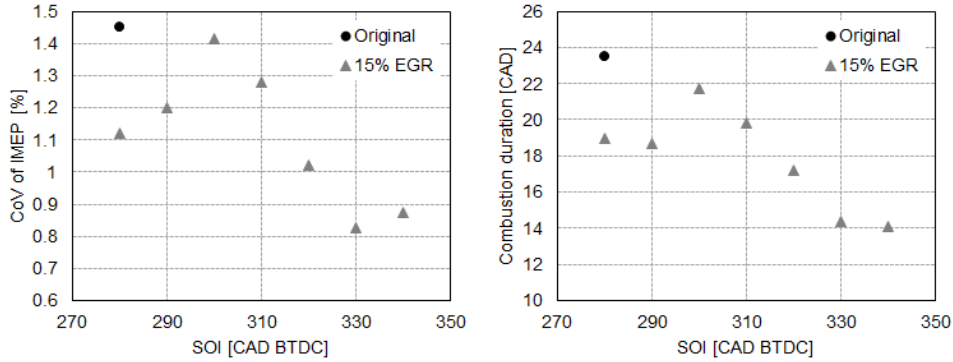
**Figure 5.19.** BSFC (left graph) and indicated efficiency (right graph) for different start of injection values at 2000 rpm and 50% of engine load.



**Figure 5.20.** Spark advance (left graph) and CA50 (right graph) for different start of injection values at 2000 rpm and 50% of engine load.

change drastically in order to cause that big difference on CA50. Although the CA50 optimum crank angle seems to be more advanced for more retarded SOI values until 330 CAD BTDC where it seems to find a plateau.

The big difference on CA50 observed before is related to mixing conditions and instability of mixture conditions around the spark plug when the spark is released. The combustion instability can be observed in Figure 5.21 where the CoV of the IMEP is represented for different SOI values in the left graph. It can be seen how the CoV of the IMEP increases between 290 and 310 CAD BTDC of SOI, the same range mentioned before. This CoV instability is translated in more cycles with poor combustion processes. Therefore,



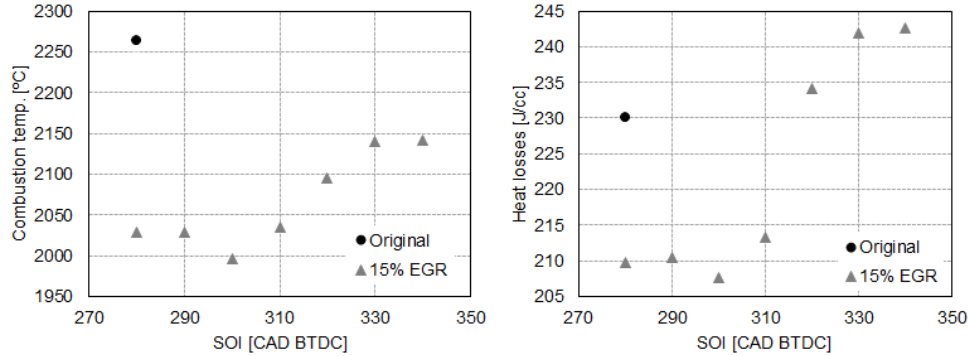
**Figure 5.21.** CoV of the IMEP (left graph) and combustion duration (right graph) for different start of injection values at 2000 rpm and 50% of engine load.

no improvement in the indicated efficiency as it can be observed in right graph of Figure 5.19 and also a retarded CA50 as observed in right graph of Figure 5.19. This would also be translated in a higher combustion duration as it can be observed in the right graph of Figure 5.21, although the combustion duration is decreased as SOI is advanced until 330 CAD BTDC. Regarding the small changes in combustion duration and combustion phasing, the exhaust temperature is maintained constant at around 630, as it can be observed in the right graph of Figure 5.24, where the exhaust manifold temperature is plotted for different SOI values.

Regarding the combustion temperature, it is observed in the left graph of Figure 5.22, where the combustion temperature is plotted for different SOI values, how the combustion temperature follows an opposite trend compared to the CA50 results. It can be seen that for more advance CA50 the combustion temperature increases and for less advance CA50 the opposite. This is mainly an effect of combustion temperature and also combustion stability as it was explained before. As it must be expected, the heat losses follows the same trend as the combustion temperature, as it can be seen in the right graph of Figure 5.22. The heat losses are drastically increased when the CA50 is near the TDC, as in the case of the range from 320 to 340 CAD BTDC SOI values, due to the increase in the turbulence because of the small volume, increasing the heat losses against the piston, head and cylinder walls.

Concerning the effect of SOI on the engine volumetric efficiency, it can be seen in left graph of Figure 5.23 where the intake manifold pressure is plotted for different SOI values. The intake manifold increases when the SOI



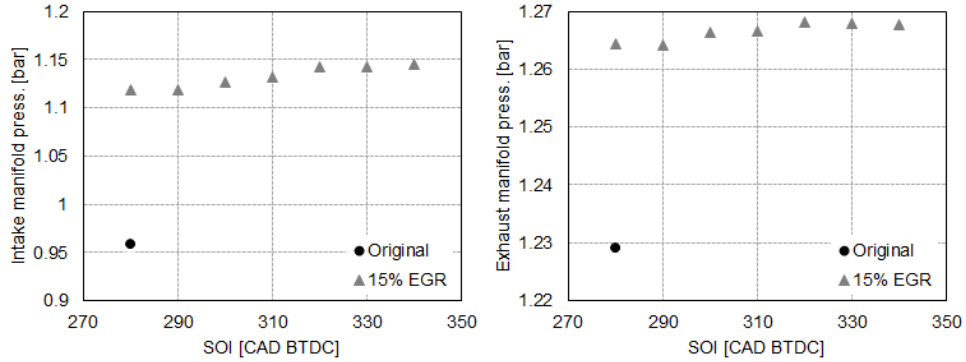


**Figure 5.22.** Combustion temperature (left graph) and heat losses (right graph) for different start of injection values at 2000 rpm and 50% of engine load.

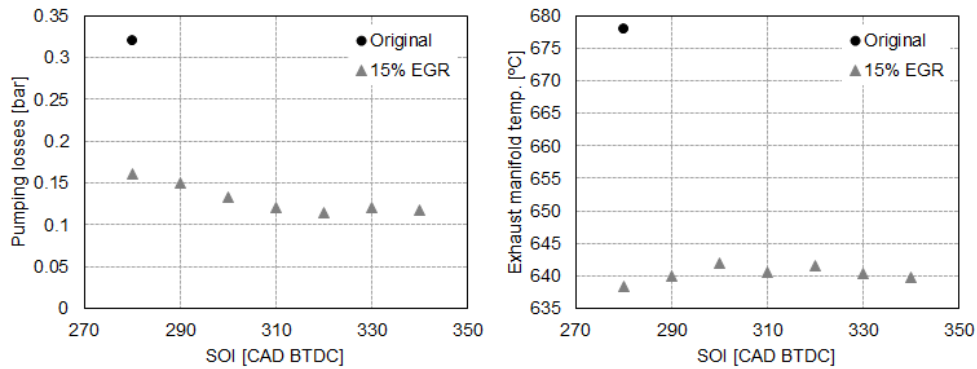
is advanced in order to maintain the iso-air mass flow conditions for each test. The intake manifold pressure is increased in 23 mbar in order to compensate the loss of engine volumetric efficiency. The loss of engine volumetric efficiency when SOI is advanced is due to the effect of injecting the fuel mass when the amount of air mass flow going into the cylinder has not enough speed. Since it is not at its peak and is still accelerating, this will block the amount of air that can get in that period of time and the evaporation effect of reducing the in-cylinder temperature does not fully compensate this loss in air mass flow momentum and therefore the engine volumetric efficiency decreases, as it was observed by Wyszynski et al. in their research work [20]. Regarding the exhaust manifold pressure it can be seen how the pressure it is almost the same for all the tests with a variation of 3 mbar.

The increase in the intake manifold pressure and the constant exhaust manifold pressure is translated in pumping losses reduction. It can be seen in the left graph of Figure 5.24 where the pumping losses are plotted for different SOI values. The pumping losses are reduced compared to the original SOI value, 280 CAD BTDC, due to the already mentioned increased intake manifold pressure. It can be seen also how it reaches a plateau between 320 and 340 CAD BTDC SOI. The reduction of pumping losses is 25% compared to the original SOI condition from 0.16bar to 0.12bar

Regarding the exhaust emissions, in Figure 5.25  $NO_x$ ,  $CO$  and  $HC$  raw emissions are plotted for different SOI values. In addition, the combustion efficiency is plotted for different SOI values and is calculated using  $HC$  and  $CO$  emissions in order to complete the analysis. In the case of  $NO_x$  emissions,



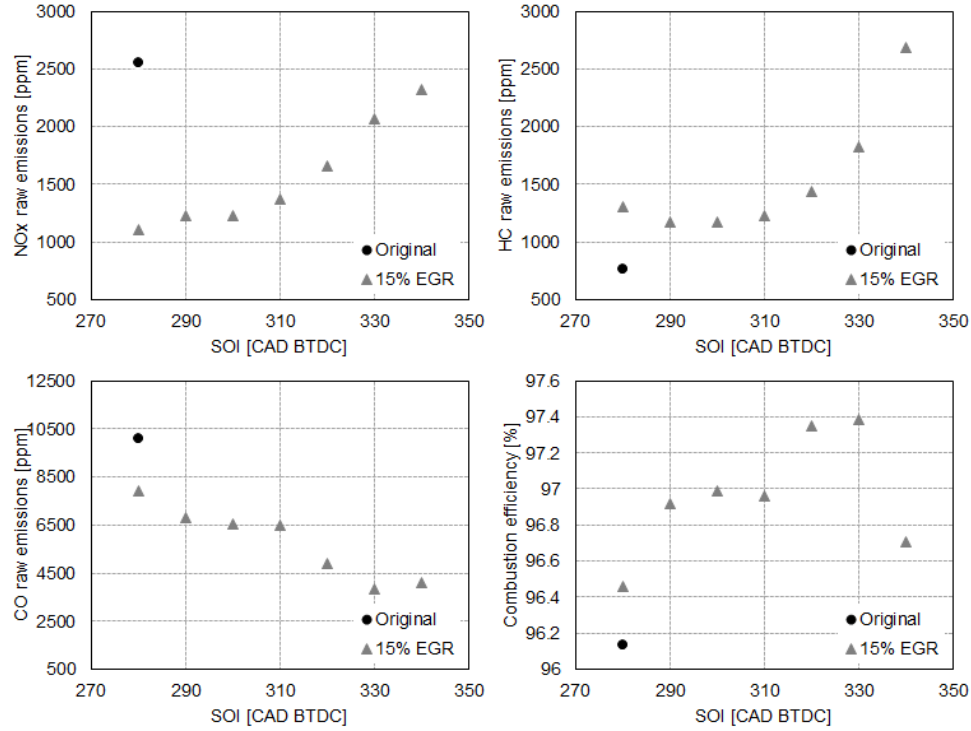
**Figure 5.23.** Intake manifold pressure (left graph) and exhaust manifold pressure (right graph) for different start of injection values at 2000 rpm and 50% of engine load.



**Figure 5.24.** Pumping losses (left graph) and exhaust manifold temperature (right graph) for different start of injection values at 2000 rpm and 50% of engine load.

it can be seen in the top left graph of Figure 5.25 how  $NO_x$  emissions increased by advancing the SOI due to the increase of combustion temperature, already presented before, increasing the production of  $NO_x$  emissions governed by the thermal reaction. This can be achieved due to the increase of reactivity of the mixture, richer mixture, around the spark plug at the start of the combustion, resulting in a higher combustion rate and therefore higher combustion temperature.

$HC$  emissions were also increased when the SOI is retarded, this is mainly due to higher interaction between the fuel jet and piston, increasing the



**Figure 5.25.** Exhaust raw emissions and combustion efficiency for different start of injection values at 2000 rpm and 50% of engine load.  $NO_x$  (top left graph),  $HC$  (top right graph),  $CO$  (bottom left graph) raw emissions and combustion efficiency (bottom right graph).

amount piston wetting and therefore increasing  $HC$  emissions despite the increase in combustion temperature. If  $PM$  emissions would have been measured it could also be seen an increase of  $PM$  emissions due to the same piston wetting effect. This was already mentioned during the literature review in Section 2.2.2.4 of Chapter 2 in the research work performed by Stevens et al. [21], where they studied the formation of  $PM$ , observing the fuel film and pool fires in a optical DISI engine for different injection timings and how this parameter could affect the  $PM$  formation. Furthermore the  $CO$  emissions were reduced as the SOI was advanced, this basically depends on the amount of  $CO_2$  produced. In this case less  $CO_2$  is produced for the same amount of fuel because more  $HC$  is produced and therefore less  $CO$  can be produced from the dissociation of  $CO_2$ .

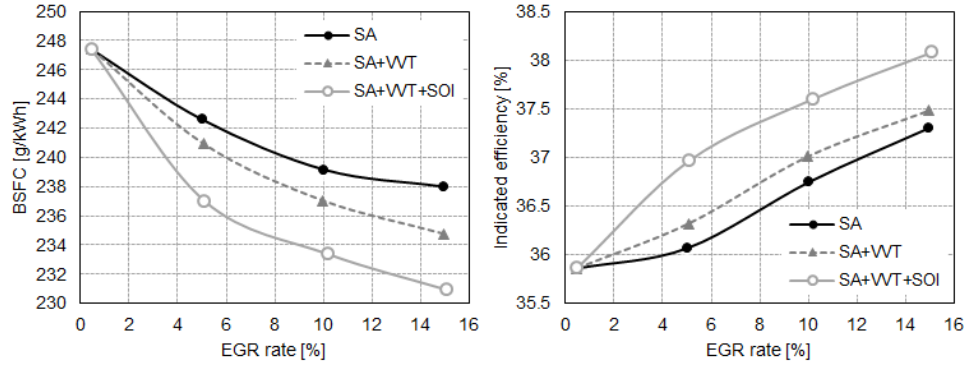
It can be seen in the bottom right graph of Figure 5.25 that the combustion efficiency increases as the SOI is advanced achieving a maximum value at 330 CAD BTDC, that actually matches the optimum SOI value for minimum BSFC as already observed in the left graph of Figure 5.19.

It was observed how an improvement of engine thermal efficiency can be achieved by advancing the SOI. An improvement of 1.7% compared to the original SOI value at the optimized VVT and SA conditions with the same amount of EGR rate. The improvement is mainly due to the pumping losses reduction, the increase in combustion efficiency and the big reduction of the CoV of the IMEP. Regarding exhaust emissions,  $NO_x$  emissions were increased but still remain under the original condition value,  $HC$  emissions increased in 40% compared to the same conditions using original SOI and in 138% compared to the original conditions. This increase in  $HC$  emissions supposed an increase of 16 ppm at the tailpipe supposing a TWC efficiency of 98.5% of conversion.  $CO$  emissions were further reduced compared to the same conditions using the original SOI. The reduction is around 51% and compared to the original conditions a reduction of 72% is achieved.

After analyzing the effect of SOI and the optimum SOI value that minimizes fuel consumption, a sweep of EGR rate is performed with this optimized SOI and it is compared with the optimized SA setup and the optimized VVT and SA setup in order to observe the evolution and the decrease of fuel consumption for each step of the optimization process. In Figure 5.26 the BSFC is plotted in the left graph and the indicated efficiency is plotted in the right graph for different EGR rates using three different settings setup: optimized SA, optimized VVT and SA, and optimized VVT, SA and SOI. The best improvement in BSFC is 6.8% compared to the original conditions and an increased of 3% absolute value of indicated efficiency was observed compared to the original one.

### 5.2.2.3 Additional strategies to reduce fuel consumption

It was observed how optimizing other engine parameters and technologies to operate in synergy with cooled EGR engine fuel consumption could be further reduced. In this last sub-section a simple analysis approach is followed in order to briefly give an idea of other possible strategies to further improve the operation of a GTDI engine with cooled EGR. The results that will be presented here are only for 2000 rpm and 10 bar BMEP operating conditions. A brief analysis of engine performance and exhaust emissions are detailed using the following strategies in synergy with cooled EGR: multiple injection



**Figure 5.26.** BSFC (left graph) and indicated efficiency (right graph) for different EGR rates at 2000 rpm and 50% of engine load with different setting setups.

strategies, higher engine coolant temperature conditions and induced swirl motion.

The testing conditions were at the maximum rate of EGR that could be obtain at 2000 rpm and 10 bar BMEP before misfire (17.5% EGR rate) in order to understand if the synergy with some of these tested new strategies could improve the fuel consumption at this stage of mixture dilution. This could also lead into a dilution range extension at this operating condition. The optimum VVT settings were used in order to perform these tests.

During the tests the air mass flow, fuel mass flow, intake temperature and EGR rate were maintained constant for all the different injection strategies setups. Although the spark advance was optimize for every different setup in order to minimize the engine fuel consumption under those conditions.

### 5.2.2.3.1 Multi-injections

The term multi-injections in this section is referred to two injections: one main injection and a second small injection closer to TDC compression in order to increase the mixture reactivity around the spark plug and improve cycle-to-cycle variation and combustion efficiency. In Table 5.4, the injection timing and fuel quantity percentage of the total fuel injected conditions of the first and second injection are presented.

The results in this section are going to be presented in tables, since it is complicated to represent the effect on each setup in a single graph because

Parameter	Unit	OP1	OP2	OP3	OP4	OP5	OP6	OP7
EGR rate	[%]	0	17.5	17.5	17.5	17.5	17.5	17.5
Main timing	[CAD BTDC]	280	280	280	280	280	280	280
Main fuel	[%]	100	100	93.5	89.5	93.5	81.8	81.8
Second timing	[CAD BTDC]	N/A	N/A	90	90	160	160	190
Second fuel	[%]	0	0	6.5	10.5	6.5	18.2	18.2

**Table 5.4.** *Engine operating conditions.*

Test	BSFC [g/kWh]	Heat losses [J/cc]	Pumping losses [bar]
OP1	246.1	242.2	0.32
OP2	234.7	208.1	0.11
OP3	238.5	206.6	0.11
OP4	237.9	207.8	0.11
OP5	237.3	211.3	0.11
OP6	244.0	197.8	0.12
OP7	243.6	197.7	0.12

**Table 5.5.** *Engine performance results.*

of the different injection timing and different quantity of fuel injected of the second injection.

In Table 5.5, the main results of engine performance for each test condition are presented. It can be seen that having a second injection did not further improve the BSFC. It actually did not reach the same value as the optimum operating point using cooled EGR with the original injection strategy. The best setup found using a second injection, as it can be seen in Table 5.5, was using a small percentage of the total fuel injected, 6.5% of the total injected fuel mass flow, and with two different injection timing, 90 CAD and 160 CAD BTDC. But, as it was mentioned before, this setup was still around 1% worst than the optimum VVT conditions using cooled EGR with the original injection strategy.

In Table 5.6, some important combustion parameters are presented for all the different injection strategies setups. It can be observed that optimum CA50 for most of the setups are closer to TDC. This could be due to the instability of CCV combustion in most of the setups, because of the second

Test	CA50 [CAD ATDC]	Comb. Dur. [CAD]	Comb. T. [°C]	CoV IMEP [%]
OP1	8.5	22.0	2323.4	1.3
OP2	4.5	24.5	2002.9	1.18
OP3	2.5	22.9	2031.6	1.54
OP4	2.3	22.6	2040.3	1.38
OP5	3.5	22.6	2023.5	1.24
OP6	4.7	24.0	1981.6	1.29
OP7	6.1	25.6	1955.5	1.65

**Table 5.6.** Engine combustion results.

injection that is going to change the mixture equivalence ratio around the spark-plug compared to original conditions and, therefore, the engine could have been not designed or optimized to perform stratification in the mixture causing some cycle-to-cycle instability. It is obvious that without having computational fluid dynamics with injection and combustion simulations in these conditions, the explanation already given is just a hypothesis.

It can be seen that for the combustion temperature and therefore heat losses, the difference with the optimum condition using cooled EGR (OP2) is negligible. It is also observed, that pumping losses for all injection strategy setups are more or less on the same region as the original optimum condition using cooled EGR. The only difference, as it was mentioned before, compared to the original optimum conditions using cooled EGR, is the combustion stability and therefore it can be seen that the CoV of the IMEP of optimum conditions is lower compared to all the different injection strategies setups.

Regarding the exhaust emissions, it can be seen that  $NO_x$  emissions were almost the same value for all cooled EGR tests, as it is presented in Table 5.7 where  $NO_x$ ,  $HC$  and  $CO$  raw exhaust emissions are presented for all the tests performed. In the case of  $HC$  emissions it can be seen that for some tests are lower than the optimum conditions operating with cooled EGR but with higher  $CO$  emissions. These differences in  $HC$  and  $CO$  emissions comes from the stratification of the mixture, producing less  $HC$  that will produce more  $CO_2$  and therefore dissociate forming more  $CO$  emissions at the same combustion temperature.

It was observed that multi-injection strategy involves more complex phenomena such as fuel to air mixing modification, injection wall wetting and cylinder head turbulence among others. This makes it difficult to analyze and

Test	$NO_x$ [ppm]	$HC$ [ppm]	$CO$ [ppm]
OP1	2684.8	834.4	8533.8
OP2	810.2	1488.8	6704.2
OP3	642.2	1308.1	8969.7
OP4	676.6	1213.9	9163.7
OP5	729.3	1510.0	8381.1
OP6	413.4	1779.1	7298.1
OP7	621.7	1564.6	6972.0

**Table 5.7.** Engine exhaust raw emissions results.

optimize this kind of strategy and it could need too much effort in order to obtain some good results. But it has to be taken into account that the engine must be designed from the beginning to operate with multiple injections in order to be able to extract all the potential of this strategy.

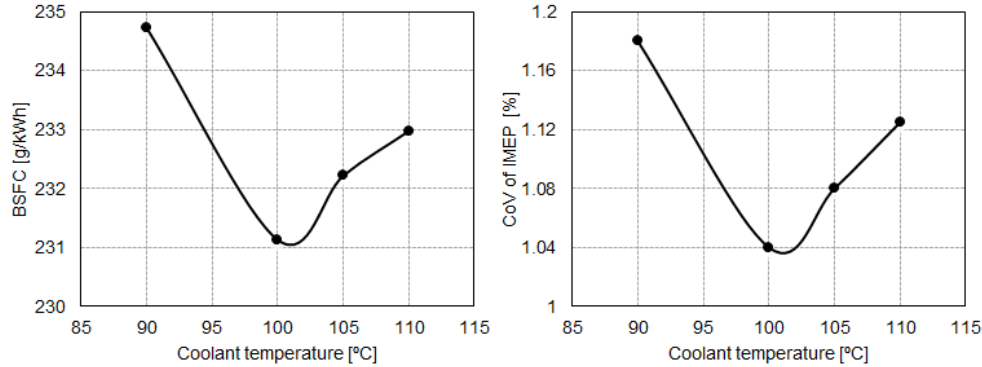
#### 5.2.2.3.2 Engine coolant temperature

This strategy basically consists in increasing the operating coolant temperature of the engine. This would generally impact the engine fuel consumption, as it was explained in the literature review Chapter 2. There are some GTDI engines on the market with a two-stage coolant circuit that can operate at higher temperature at low and part load engine conditions.

The tests were performed at 2000 rpm and 10 bar of BMEP with 17.5% of EGR rate, maintaining constant air-mass flow, fuel-mass flow, intake temperature and spark advance during the engine coolant temperature sweep. The engine coolant temperature was varied from 100°C to 110°C with a step of 5°C and compared to the original engine coolant temperature conditions, 90°C.

The engine BSFC of the engine was reduced by increasing the engine coolant temperature, as it is presented in the left graph of Figure 5.27. A reduction of 1.3% is achieved at 100°C of coolant temperature compared to the optimum operating conditions using the optimum VVT settings and 17.5% of EGR rate. It is also observed that for higher engine coolant temperature tests, 105°C and 110°C, the BSFC increases compared to 100°C engine coolant temperature conditions but it is still lower than with the original engine coolant temperature conditions.



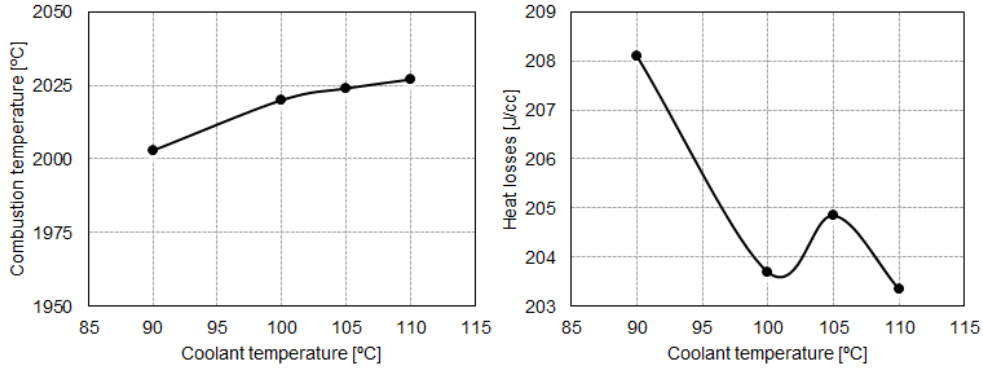


**Figure 5.27.** BSFC (left graph) and CoV of the IMEP (right graph) for different engine coolant temperature at 2000 rpm and 50% of engine load.

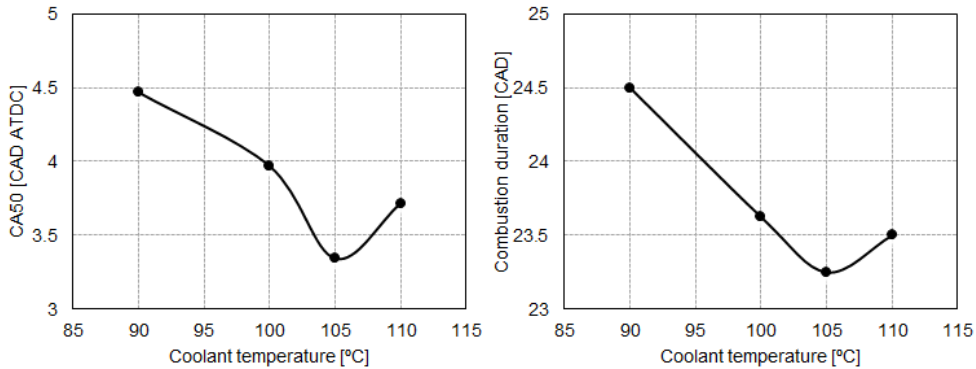
In the right graph of Figure 5.27, the CoV of IMEP is presented for different engine coolant temperatures. It can be observed that the curve and trend of this graph is similar to the curve and trend of the BSFC graph observed on the left graph of Figure 5.27. This could be the main cause of fuel consumption evolution in these tests. Further analysis it is going to be performed after showing some other engine parameters results.

Regarding the combustion, it can be seen in the left graph of Figure 5.28, where the combustion temperature is presented for the different engine coolant temperature tests, that the combustion temperature increased when the engine coolant temperature increased. And as it can be observed in the right graph of Figure 5.28 the heat losses were almost constant for all the tests compared to the original coolant temperature conditions. When the engine coolant temperature increases it generates a higher in-cylinder temperature at the beginning on the compression stroke and therefore the combustion temperature increases. This increase in combustion temperature also should increase the heat exchange but because the cylinder walls, piston and cylinder head is also hotter, no change on the heat losses were observed but only a change on the combustion temperature. Also it has to be taken into account that the increase in combustion temperature in absolute values is rather small.

When the coolant temperature increases also the mean cycle temperature increases and therefore the temperature at the start of the combustion is also higher, increasing the mixture reactivity and therefore advancing the combustion phasing and reducing the combustion duration for the same spark advance, as it can be observed in Figure 5.29. The CA50 is presented in the

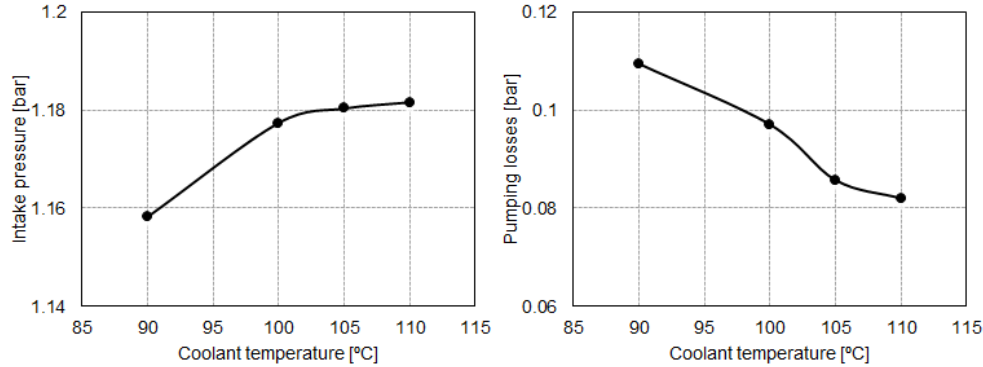


**Figure 5.28.** Combustion temperature (left graph) and heat losses (right graph) for different engine coolant temperature at 2000 rpm and 50% of engine load.



**Figure 5.29.** CA50 (left graph) and combustion duration (right graph) for different engine coolant temperature at 2000 rpm and 50% of engine load.

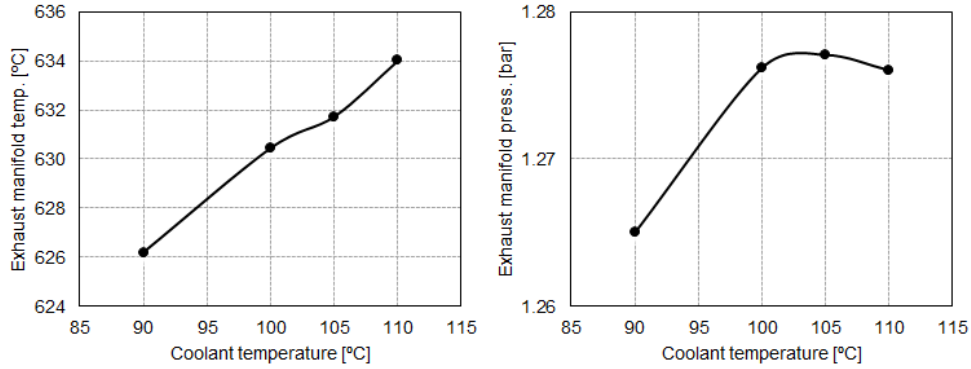
left graph of Figure 5.29 for different engine coolant temperatures. It can be observed that, indeed, the combustion phasing is advanced for all the tests compared to the original coolant temperature conditions and in consequence the combustion duration it is reduced, as it was explained before, due to the increase of the mixture reactivity in addition to the new advance combustion phasing, as it can be observed in the right graph of Figure 5.29. It has to be taken into account, as for the combustion temperature increase, that the absolute value of decrease in CA50 and combustion duration is rather small and within the limits of measurements accuracy.



**Figure 5.30.** Intake manifold pressure (left graph) and pumping losses (right graph) for different engine coolant temperature at 2000 rpm and 50% of engine load.

Analyzing the air management of the engine for higher coolant temperature conditions, it can be observed that the intake manifold pressure had to increase in order to maintain the air mass flow constant for higher engine coolant temperature conditions, as it can be observed in the left graph of Figure 5.30. This is due to the higher in-cylinder temperature during the intake stroke and therefore a lower density, which leads to increase the intake manifold pressure in order to maintain the same amount of air mass going into the cylinder. The intake manifold pressure increase reduced the pumping losses compared to the original coolant temperature operating conditions, as it can be observed in the right graph of Figure 5.30, where the pumping losses are presented for different engine coolant temperature conditions.

As it was presented, the pumping losses were reduced for higher coolant temperature operating conditions compared with the original conditions and this is all benefit from the intake manifold pressure increase since the exhaust manifold pressure was maintained around the same value as the original coolant temperature conditions as it can be observed in the right figure of Figure 5.31. It can be observed in the left graph of Figure 5.31 where the exhaust manifold temperature is plotted for all the different engine coolant temperature conditions tested, that the temperature increases with the increase of the coolant temperature, despite the shorter combustion duration. This is caused by the increase of combustion temperature that will end with a higher temperature of the exhaust gases during the expansion stroke. This exhaust gases will also have less heat transfer with the cylinder and head walls, because the engine is operating with a higher coolant temperature and when

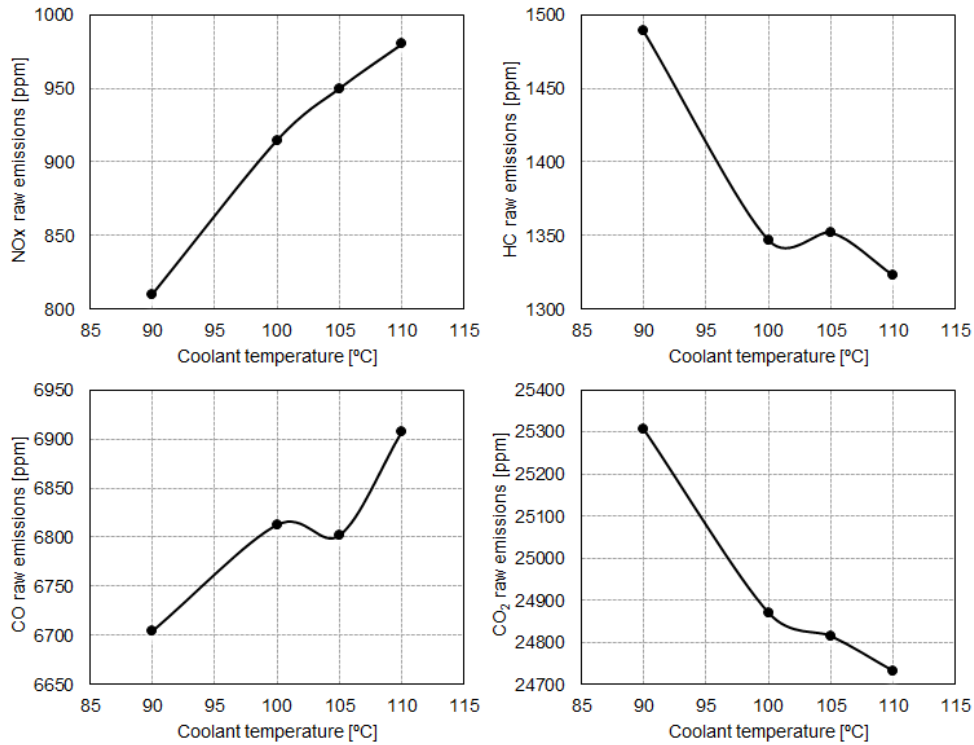


**Figure 5.31.** Exhaust manifold temperature (left graph) and exhaust manifold pressure (right graph) for different engine coolant temperature at 2000 rpm and 50% of engine load.

the exhaust valves opens the exhaust gas is at higher temperature than with the original operating conditions.

Regarding the exhaust emissions a variation of  $NO_x$  emissions was expected with the combustion temperature increase for higher coolant temperature conditions. As it is shown in the left top graph of Figure 5.32,  $NO_x$  emissions increased with the increase of the engine coolant temperature, this is basically due to the increase of the combustion temperature as it was explained in Chapter 2. The increase on the mean temperature of the cycle also increased the mixture reactivity. As it was mentioned before, this increases the combustion efficiency and, therefore, less  $HC$  emissions are produced as it can be seen in the top right graph of Figure 5.32. The reduction of  $HC$  emissions means that more fuel is completely burned and therefore more  $CO_2$  is formed. However, with the higher temperatures some of the  $CO_2$  is dissociated, as it was already explained in Chapter 2 the dissociation reaction purely depends on temperature conditions, producing more  $CO$  emissions as it can be observed in the bottom left graph of Figure 5.32. This, will also be in relation with the reduction of  $CO_2$  presented in the bottom right graph of Figure 5.32.

It was observed how increasing the engine coolant temperature operating conditions could reduce the BSFC in the same range as optimizing the injection timing. In this case a reduction of 1.3% was observed compared to the original engine coolant operating conditions, mainly due to the improvement of combustion stability and reduction in pumping losses. Regarding the exhaust emissions no relevant impact was observed although  $NO_x$  and  $CO$  emissions

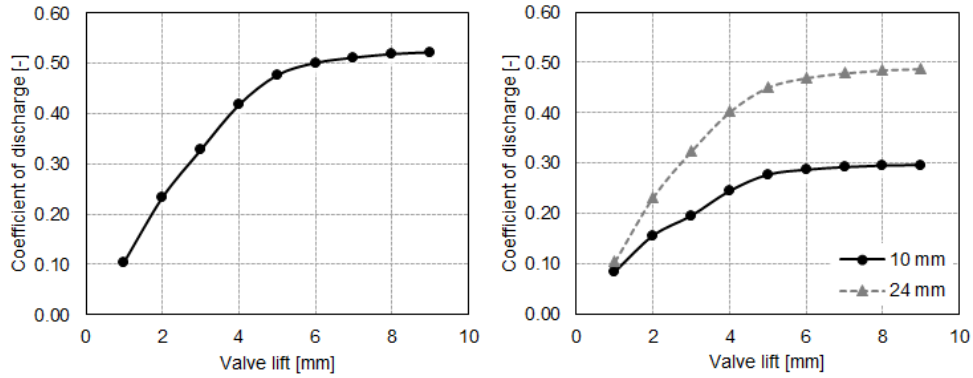


**Figure 5.32.**  $NO_x$  raw emissions (top left graph), HC emissions (top right graph), CO emissions (bottom left graph) and  $CO_2$  emissions (bottom right graph) for different engine coolant temperature at 2000 rpm and 50% of engine load.

were increased. However, taking into account that the absolute value of this increase is fairly low it can be considered that this strategy did not impacted in an important manner the exhaust emissions of the engine.

### 5.2.2.3.3 Induced swirl motion

The main objective of this strategy is to increase the in-cylinder turbulence to increase the reactivity of the mixture during the combustion and obtain a faster combustion that could enlarge the dilution limits of this engine at this specific engine conditions. This test was also performed at 2000 rpm and 10 bar of BMEP with 17.5% of EGR rate, maximum rate of EGR before obtaining misfire, which is a similar approach as presented in the multi-injection strategy section.

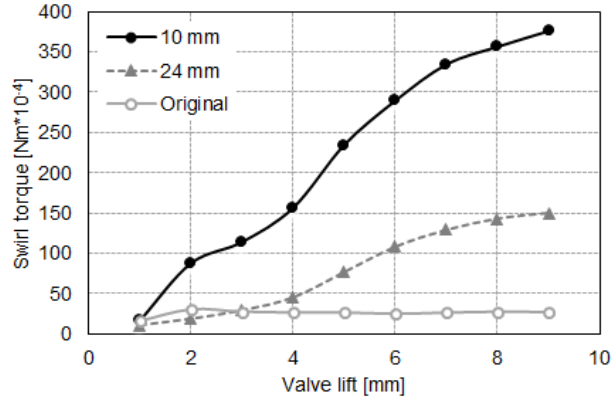


**Figure 5.33.** Coefficient of discharge of the original cylinder head (left graph) and with a 10 mm and 24 mm of diameter restriction in one of the intake ports for different valve lift values.

The main objective was to induce a swirl motion in the cylinder during the intake stroke. This, in combination with the original tumble motion that produced the original cylinder head, could produce a higher turbulence during the combustion. The swirl motion was obtained by restricting one of the intake ports in each cylinder, and two diameters, 10 mm and 24 mm, of restriction were tested at the steady flow bench in order to quantify the difference in swirl coefficient compared to the original cylinder head setup. These tests were performed with both intake valve open and exhaust valves closed. The coefficient of discharged was also measured in order to measure the impact of restricting one of the intake ports in order to achieve the swirl motion.

As it was expected, the restriction imposed in one of the intake ports to generate the swirl motion reduced the coefficient of discharge of the intake valves. This can be observed in Figure 5.33, where in the left graph the original coefficient of discharge of both intake valves open is presented for different valve lift values and in the right graph the discharge coefficient using a 10 mm and 24 mm diameter restriction in one of the intake ports for different valve lift values. When the restriction diameter is reduced the coefficient discharge is also reduced.

The 10 mm restriction diameter was the cylinder head configuration used to perform the tests on the engine test bench. This configuration produced the highest swirl motion, as it can be seen in Figure 5.34, where the torque generated by the air motion is represented for different cylinder head configurations and valve lift positions.



**Figure 5.34.** Torque measured in the flow bench for three different cylinder head setups and for different valve lift positions.

Test	BSFC [g/kWh]	Heat losses [J/cc]	Pumping losses [bar]
Original	234.7	208.1	0.11
10 mm	242.2	232.4	0.19

**Table 5.8.** Engine performance results.

The engine tests were performed maintaining constant air-mass flow, fuel-mass flow, intake temperature and spark advance for both tested cylinder head setups. The results obtained in the engine test bench using the highest cylinder head swirl motion configuration were not positive. As it can be seen in Table 5.8 where main engine performance parameters results are presented. BSFC was increased in 3.2% compared to the original cylinder head setup due to the increased on the heat losses, because of the increase of the turbulence during the combustion and the increasing of the pumping losses because of the decrease of the cylinder head permeability due to the intake port diameter restriction of 10 mm.

It can be seen that although the turbulence was increased during the combustion and heat losses were increased because of that, the combustion phasing was retarded by more than 2.5 CAD, as it can be observed in Table 5.9, where engine combustion results are presented. This can be due to the non-advantageous swirl motion for mixing, modifying the richness conditions at the spark plug during the ignition of the mixture and therefore reducing the

Test	CA50 [CAD ATDC]	Comb. Dur. [CAD]	Comb. T. [°C]
Original	4.5	24.5	2002.9
10 mm	7.0	24.9	1891.0

**Table 5.9.** Engine combustion results.

Test	$NO_x$ [ppm]	$HC$ [ppm]	$CO$ [ppm]
Original	810.2	1488.8	6704.2
10 mm	750.3	1530.4	6430.4

**Table 5.10.** Engine exhaust raw emissions.

combustion speed increasing the combustion duration and retarding CA50 as it can be observed in Table 5.8. Due to combustion phasing retard, the combustion temperature is lower compared to the original swirl motion conditions. On the other hand the CoV of the IMEP was almost at the same value for both tests.

Regarding the exhaust emissions it can be seen that there is not a big impact, as it can be observed in Table 5.10.  $NO_x$  emissions were decreased in a small percentage due to the lower combustion temperature compared to the original swirl motion conditions.  $HC$  emissions were increased also in a small percentage, also due to the lower combustion temperature. And  $CO$  emissions were decreased also due to the lower combustion temperature that slows the  $CO_2$  dissociation reaction and therefore less  $CO$  is produced.

### 5.3 Lean burn strategy and synergy with cooled EGR

In this section the lean burn strategy is studied and analyzed to operate together with cooled EGR. The influence on the engine combustion, performance, air management and exhaust emissions of this strategy and synergy with cooled EGR is presented.

In this section, two main sub-sections are presented: the methodology and the analysis of the results. In the results and analysis subsection two main parts are presented. First, the potential of a lean burn strategy on a GTDI



Operating point	Engine speed [rpm]	Load [%]	Air mass flow [kg/h]
OP 1 (Part Load)	2000	50	110
OP 2 (Part Load)	3000	50	170

**Table 5.11.** Selected operating conditions.

engine. And second, the synergy of lean burn and cooled EGR influence on a GTDI engine.

### 5.3.1 Methodology

In order to be able to collect the maximum amount of information, a parametric type of test was designed for two OP in order to analyze the lean burn potential. One OP was chosen at 2000 rpm and the other at 3000 rpm. In this way the effect of engine speed on the maximum dilution limit can be analyzed and also the combustion speed compared to the piston mean speed. At both engine speed conditions the OP were chosen on the engine part load conditions. These OP conditions can be observed in Table 5.11. The OP chosen for this section are at the same operating conditions as the part load OP chosen in Chapter 4.

Regarding the synergy analysis of lean burn and cooled EGR, a DoE test plan approach was chosen in order to be able to analyze the effects on engine performance, air management and exhaust emissions and also be able to optimize the lambda and EGR rate conditions in order to minimize the fuel consumption.

After choosing the OP that will be tested with a lean burn strategy, a test plan was developed in order to fully analyze the effects of the lean burn in a GTDI engine. The initial analysis will be performed gradually increasing the lambda value, then maintaining constant the fuel mass flow, intake manifold temperature, and adjusting the spark advance to minimize the engine fuel consumption. This would provide information to analyze the combustion, engine performance, air management and exhaust emissions when a lean burn strategy its employed.

Afterwards, a DoE test plan is created in order to analyze the effect of lean burn in synergy with cooled EGR. In this test plan also the fuel mass flow and air intake manifold temperature were kept constant, and the spark advance was optimized to minimize the fuel consumption in all the measured

Operating point	EGR rate [%]	Lambda [-]
OP 1	2.3	1.10
OP 2	17.0	1.13
OP 3	10.6	1.00
OP 4	2.0	1.02
OP 5	17.8	1.03
OP 6	9.8	1.08
OP 7	17.2	1.15

**Table 5.12.** DoE test plan for 2000 rpm and 10 bar BMEP engine conditions.

Operating point	EGR rate [%]	Lambda [-]
OP 1	2.0	1.03
OP 2	2.0	1.10
OP 3	6.8	1.05
OP 4	10.8	1.09
OP 5	11.1	1.00
OP 6	13.9	1.06
OP 7	10.6	1.00

**Table 5.13.** DoE test plan for 3000 rpm and 10 bar BMEP engine conditions.

OP. The DoE test plan preparation was the same as the methodology already described in previous sections to optimize the VVT settings for minimum engine fuel consumption. In this case a quadratic model was also chosen and with a second level order in all inputs with all possible interactions between inputs. The DoE test plan can be observed in Table 5.12 for 2000 rpm and in Table 5.13 for 3000 rpm.

The measurement procedure explained in Chapter 3 is followed in order to guarantee the repetitive and accuracy of these tests, measuring all engine test cell parameters, ECU engine outputs and exhaust emissions ( $CO$ ,  $HC$  and  $NO_x$ ). Once the tests were performed, an analysis and discussion of the influence of lean burn over the performance, combustion, air management and exhaust emissions is detailed in the following paragraphs. Later an analysis of the synergy of lean burn and cooled EGR is presented, and an optimization process of fuel consumption and its effects on exhaust emissions is presented

in order to study the potential of synergy of these two important engine fuel consumption reduction strategies.

### 5.3.2 Results and analysis

In this section the results and analysis of the two tested steady engine operating conditions are going to be presented. As it was explained in the methodology section, an analysis of combustion, engine performance, air management and exhaust emissions of each OP was performed. The section is divided in two subsections. In the first, the analysis of the lean burn potential is presented and in the second, a synergy analysis and optimization process to minimize fuel consumption of a lean burn and cooled EGR is described.

#### 5.3.2.1 Lean burn strategy on a GTDI engine

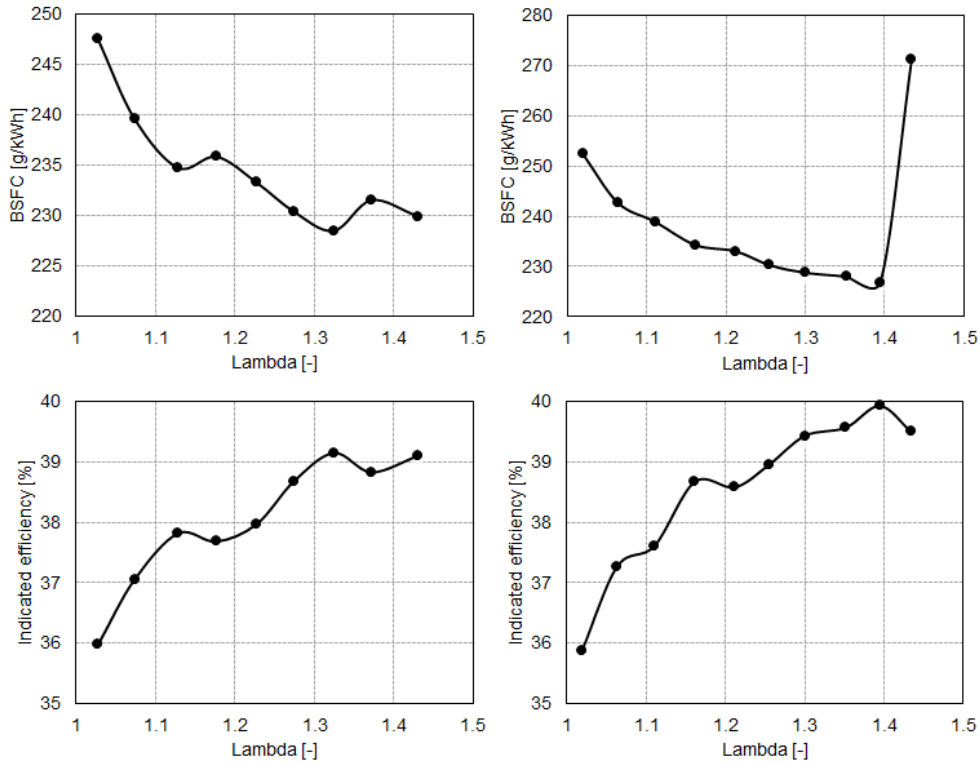
As it was mentioned before, in this section a parametric testing approach was followed in order to analyze the influence of lean mixtures on the engine performance. The tests were performed at iso-fuel mass flow and iso-intake temperature with a step of 0.05 lambda value from 1 to almost 1.45. This sub-section is divided in two parts: the first, where a combustion and engine performance analysis is performed, and the second, where the impact on the exhaust raw emissions is analyzed.

##### 5.3.2.1.1 *Combustion and engine performance*

Increasing the lambda value or increasing the amount of air maintaining constant the injected fuel mass flow at 2000 rpm reduced the BSFC by 7.5% with a lambda of 1.32. In the case of 3000 rpm the reduction was around 10% with a lambda of 1.39, as it can be observed on the top graphs of Figure 5.35, where the BSFC is presented for different lambda values. It can be observed that the BSFC trend at 3000 rpm (top right graph of Figure 5.35) is not the same compared to 2000 rpm BSFC trend (top left graph of Figure 5.35), where it can be seen that the trend is not smooth and in some cases for a leaner mixture the BSFC is not reduced, as it can happen between lambda 1.13 and 1.18. This is related to the combustion phasing, because at this point the ignition advance had to be limited by knocking conditions as it will be later analyzed.

On the bottom graphs of Figure 5.35, where the indicated efficiency is represented for different lambda values, it can be seen how the trend is opposite

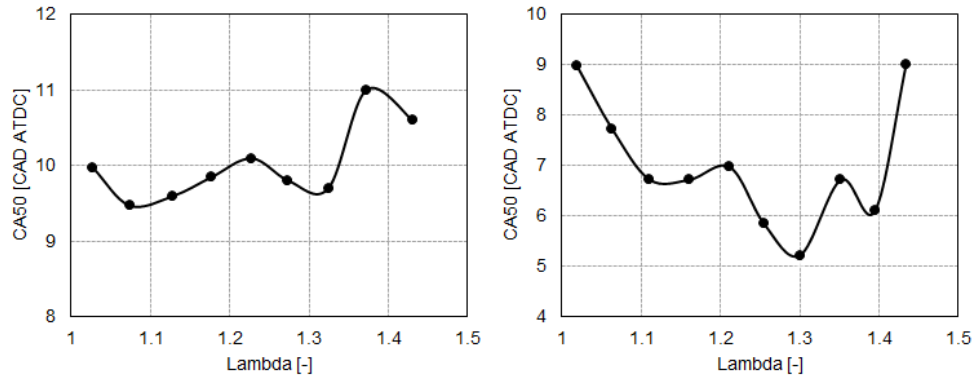
to the BSFC trend, as it was expected, because with more indicated efficiency less BSFC is achieved. The increase of the absolute indicated efficiency value is around 3% at 2000 rpm and around 4% at 3000 rpm.



**Figure 5.35.** Engine BSFC (top graphs) and indicated efficiency (bottom graphs) at 2000 rpm and 50% load (left graphs) and at 3000 rpm and 50% (right graphs) for lambda values.

The combustion phasing at 2000 rpm, CA50 placement, was between 9 and 11 CAD ATDC for all lambda values, as it can be observed in the left graph of Figure 5.36. Some of the operating conditions, between lambda 1.05 and 1.25, were limited by knocking and, therefore, the CA50 had to be maintained constant. In the case of lambda conditions between 1.35 and 1.45, it can be observed that CA50 is retarded compared to the other operating points at different lambda values. This is due to the high CoV of the IMEP observed at this conditions near to the limit of inflammability of the engine and therefore there are some cycles where the combustion is quite poor. The CoV of the

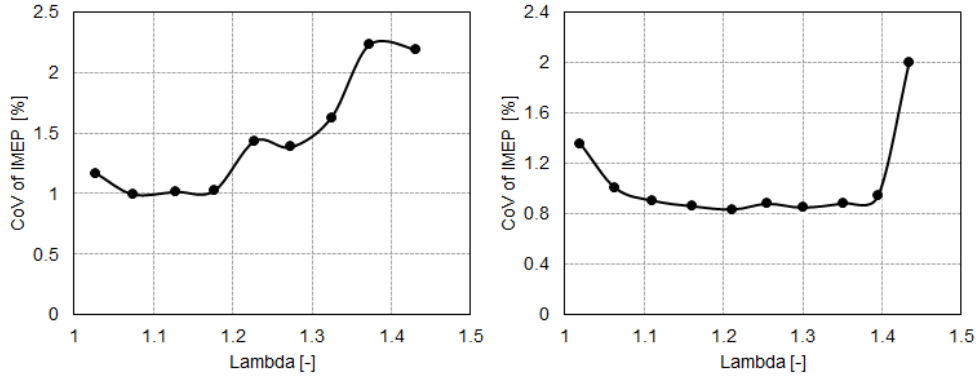
IMEP for 2000 rpm is presented in the left graph of Figure 5.37, where it is presented for different lambda values.



**Figure 5.36.** CA50 at 2000 rpm and 50% load (left graph) and at 3000 rpm and 50% (right graph) for different lambda values.

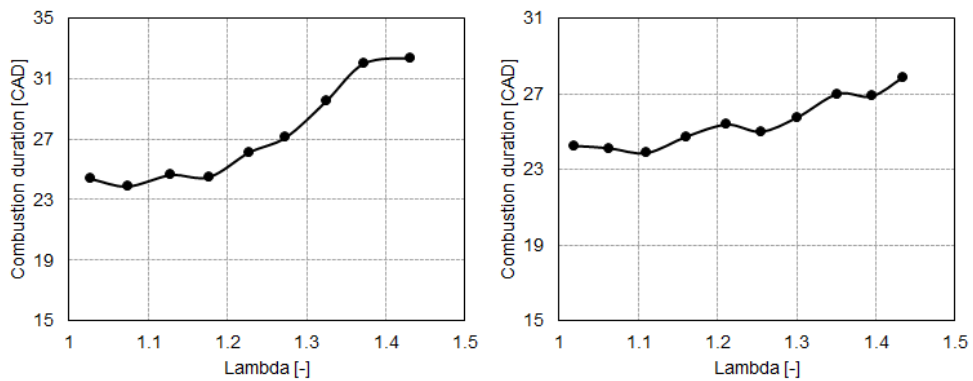
In the case of 3000 rpm the combustion phasing was improved for higher lambda values, as it can be seen in the right graph of Figure 5.36, where CA50 is represented for different lambda values. The optimum combustion phasing at 3000 rpm is more advanced, compared to 2000 rpm engine conditions, due to the higher engine speed and because there was no knocking limitation at these conditions that could limit the combustion phasing. Although, a drastic change in combustion phasing trend at lambda 1.45 is observed, because of the higher CoV of the IMEP presented in the right graph of Figure 5.37. This higher CoV of the IMEP and retarded combustion phasing is due to the problem of ignitability between cycles, as it was mentioned before. At this lambda conditions the engine is near the limit of inflammability and therefore there are some cycles with poor combustion due to this problem. It can also be observed that at these conditions, the BSFC is higher due to the same phenomena. At some point the indicated efficiency does not show this hard drop in efficiency because for the 100 cycles recorded the worst misfires were not recorded and therefore the calculated indicated efficiency for those 100 cycles is not as bad as the average BSFC for 60 seconds.

Regarding the combustion duration, it is seen how the dilution using air is not so different compared to EGR dilution. Both dilution strategies reduce the mixture reactivity and, therefore, for similar combustion phasing, as observed before in Figure 5.36 for 2000 rpm and 3000 rpm, the combustion duration increases when the lambda value increases. This can be observed in Figure 5.38



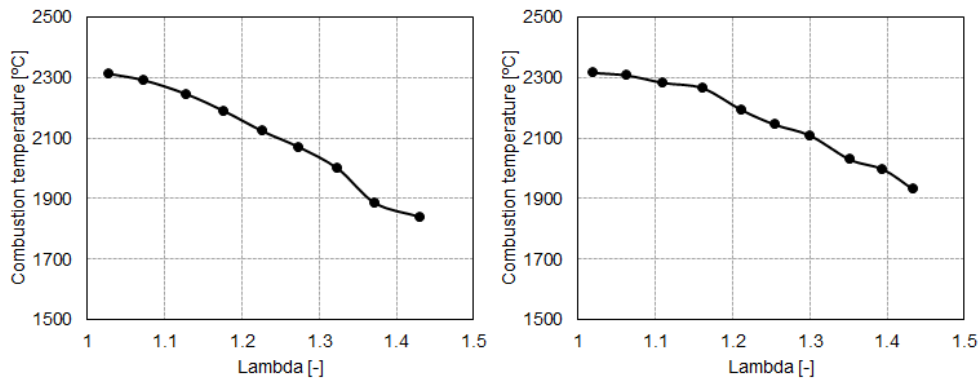
**Figure 5.37.** CoV of the IMEP at 2000 rpm and 50% load (left graph) and at 3000 rpm and 50% (right graph) for different lambda values.

for both engine speeds. It is observed that the combustion duration increases around 8 CAD at 2000 rpm and 3.3 CAD at 3000 rpm. The combustion duration increment at 2000 rpm is higher than at 3000 rpm because the combustion phasing was not improved due to knocking problems. On the other hand, at 3000 rpm, it was observed how the combustion phasing was improved when the lambda value was increased and therefore this compensated the loss of mixture reactivity by taking advantage of the higher turbulence that is present at TDC during the combustion.



**Figure 5.38.** Combustion duration at 2000 rpm and 50% load (left graph) and at 3000 rpm and 50% (right graph) for different lambda values.

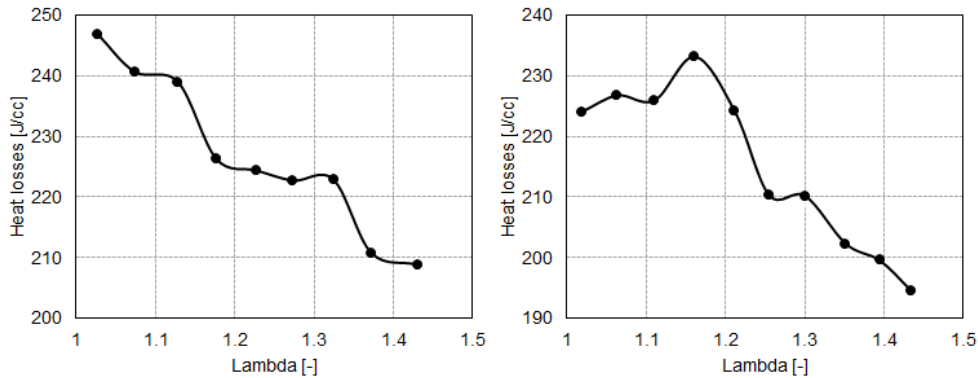
The evolution of the combustion temperature for both engine speeds is presented in Figure 5.39 for different lambda values conditions. As it was expected, it can be observed that the combustion temperature decreases when the lambda value is increased. This is due to the already mentioned dilution effect, caused by adding excess of air to the combustion reducing the reactivity of the mixtures. In the case of 2000 rpm, left graph of Figure 5.39, the combustion temperature was reduced in 473°C and in the case of 3000 rpm conditions, right graph of Figure 5.39, the combustion temperature was reduced in 397°C. At 3000 rpm the combustion temperature was maintained higher at the highest lambda value compared to 2000 rpm conditions since the combustion phasing at 3000 rpm was improved compared to 2000 rpm conditions, as it was presented before in Figure 5.36. The nearest the CA50 is to TDC, the higher the turbulence is and therefore also the combustion is faster producing higher combustion temperature.



**Figure 5.39.** Combustion temperature at 2000 rpm and 50% load (left graph) and at 3000 rpm and 50% (right graph) for different lambda values.

After analyzing the combustion temperature trend for higher values of lambda, it is expected to observe a reduction of heat losses at both engine speed conditions. The heat losses for both engine conditions are presented in Figure 5.40 for different lambda values. It can be observed that heat losses are a combination of combustion phasing (CA50) and combustion temperature. When the combustion is advanced near TDC, the heat losses increase due to the higher turbulence at TDC, which increases the convection coefficient to the walls of cylinder, piston and head. It can be seen at 3000 that between the stoichiometric conditions and lambda 1.15, the heat losses did not decrease but otherwise increase, mainly due to the improvement of the combustion phasing by more than 2 CAD at 1.15 lambda conditions, as it was presented

in Figure 5.36. Following the same type of analysis, it can be seen that the heat losses are a combination of combustion temperature and combustion phasing and it was observed how small changes in combustion phasing have more impact on heat losses than the combustion temperature.



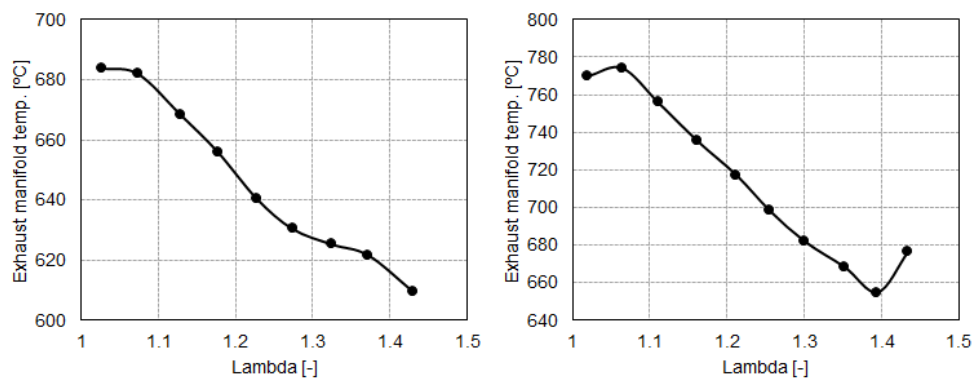
**Figure 5.40.** Heat losses at 2000 rpm and 50% load (left graph) and at 3000 rpm and 50% (right graph) for different lambda values.

The trend of combustion temperature, combustion phasing and combustion duration will impact directly the temperature at the exhaust manifold. As it can be observed in Figure 5.41, the exhaust manifold temperature is presented for both engine speed conditions to analyze the effect of the lambda on exhaust manifold temperature. It can be seen that the exhaust temperature decreases for both engine speed conditions when lambda value is increased, as it was expected due to the lower combustion temperature observed, despite the longer combustion duration at higher lambda conditions. At 3000 rpm, right graph of Figure 5.41, it can be seen that at the highest tested lambda value (1.43), the exhaust manifold temperature suddenly increases. This is due to the misfires, already presented before in the CoV of the IMEP graph in Figure 5.37, and the poor combustion obtained in some of the cycles, which have longer combustion duration and all the combustion is produced late on the expansion cycle increasing the exhaust manifold temperature.

A total reduction of 116(°C) was observed at 3000 rpm and a reduction of 74(°C) was observed at 2000 rpm, in the optimum lambda conditions. The exhaust temperature reduction at 3000 rpm was higher than at 2000 rpm despite the higher combustion temperature observed at 3000 rpm in Figure 5.39. Combustion phasing and combustion duration plays a important role on the final temperature on the exhaust gas. For this main reason at 3000



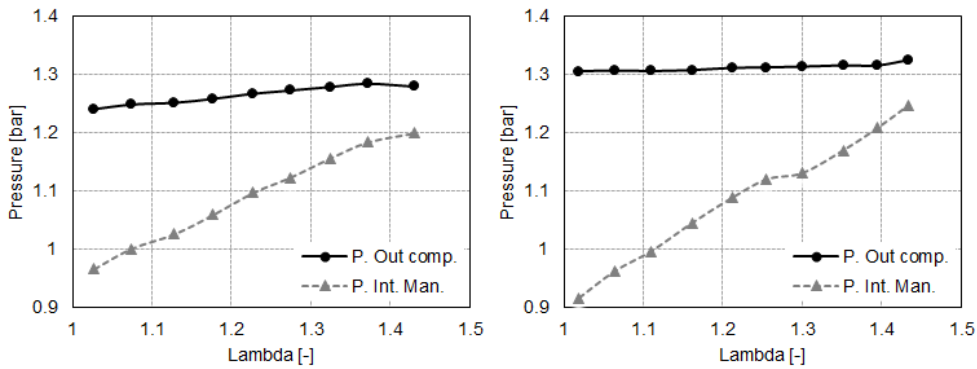
rpm, as it was presented before, the combustion is phased earlier compared to 2000 rpm conditions. In addition the combustion at 3000 rpm is faster than at 2000, rpm as it was already presented in Figure 5.38. The combustion at 2000 rpm finishes between 8 and 9 CAD after the combustion at 3000 rpm for a fixed lambda value of 1.4. Also the EVO at 2000 rpm is 4 CAD before the EVO at 3000 rpm, which also reduces the expansion time and could also magnify the difference between both engine speed conditions.



**Figure 5.41.** Exhaust manifold temperature at 2000 rpm and 50% load (left graph) and at 3000 rpm and 50% (right graph) for different lambda values.

In order to maintain constant the fuel mass flow injected and increase the lambda value, the air mass flow had to be increased. At this part load engine conditions, as it was observed in Chapter 4, the intake manifold pressure and air mass flow are still controlled by the throttle valve angle. As it can be observed in Figure 5.42, where the compressor outlet pressure and the intake manifold pressure are presented for different lambda values, the pressure at the compressor outlet is approximately maintained constant when the lambda is increased and the intake pressure increases in the case of both engine speed conditions. This basically proves that the throttle valve was controlling the intake pressure and air mass flow at this engine conditions. It can be seen that at 2000 rpm, left graph of Figure 5.42, that the intake pressure had to be increased in 0.23 bar compared to the original conditions until the maximum lambda conditions and in the case at 3000 rpm, right graph of Figure 5.42, the intake pressure increased by 0.33 bar. Despite the increase on the intake pressure, the throttle valve still controls the intake pressure and air mass flow passing through the engine because, as it was observed in Figure 5.42, the

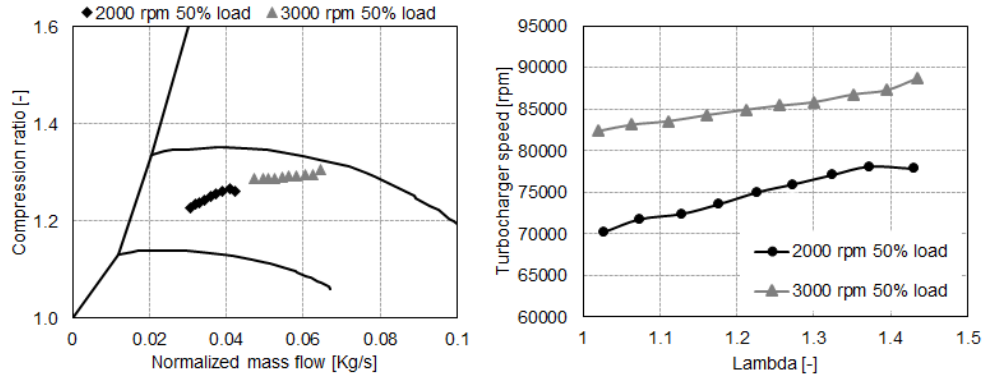
intake manifold pressure is still below the compressor outlet pressure for both engine speed conditions.



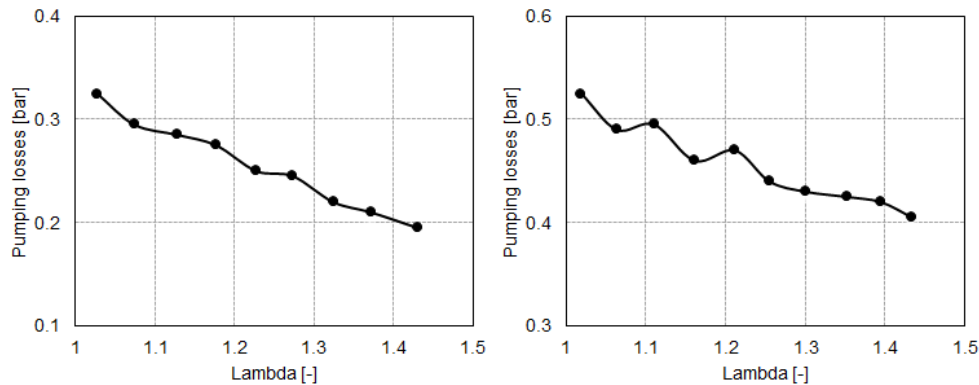
**Figure 5.42.** Compressor outlet pressure and intake manifold pressure at 2000 rpm and 50% load (left graph) and at 3000 rpm and 50% (right graph) for different lambda values.

This increase of air mass flow also impacts the compressor operating conditions and therefore turbocharger speed. The compressor compression ratio is maintained at the same value when the air mass flow is increased. It can be observed in the left graph of Figure 5.43 the compressor maps for both engine conditions and the evolution of the operating point in the compressor map when the lambda value is increased. As it was expected the operating point tends to move to the right of the map, since the air mass flow is increased and the compression ratio is maintained. Regarding the turbocharger speed it can be seen in right graph of Figure 5.43, where the turbocharger speed is presented for different lambda values, that the turbocharger speed increases when the lambda value increases. This can also be seen in the compressor maps looking at the evolution of the operating point and the turbocharger iso-speed lines, that the turbocharger speed should increase for both engine speed conditions during the increase of the lambda value.

The increase on the intake pressure also had an impact on the engine cycle. When the intake pressure is increased and the exhaust pressure is maintained the pumping losses during the cycle are reduced, as it can be observed in Figure 5.44, where pumping losses are presented for both engine speed conditions for different lambda values. The pumping losses were reduced in 40% at 2000 rpm and in 23% at 3000 rpm with a respective absolute value of 0.13 bar and 0.12 bar.



**Figure 5.43.** Evolution of compressor operating point in the compressor map (left graph) and turbocharger speed (right graph) at 2000 rpm and 50% load and at 3000 rpm and 50% for different lambda values.



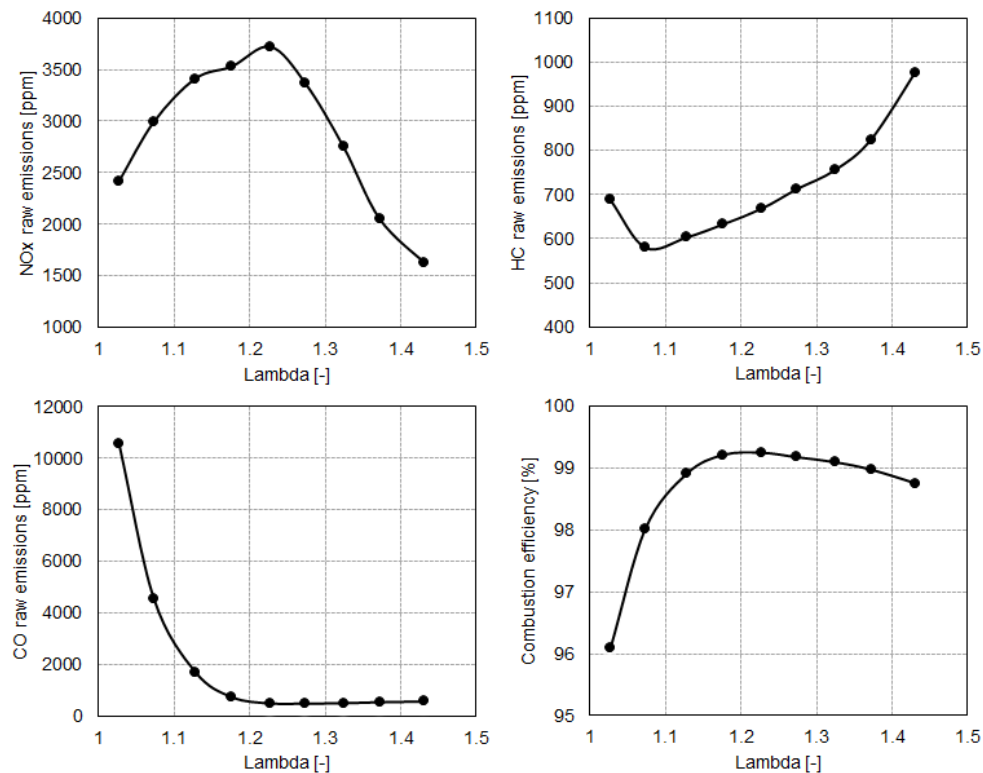
**Figure 5.44.** Pumping losses at 2000 rpm and 50% load (left graph) and at 3000 rpm and 50% (right graph) for different lambda values.

It was observed with this lean burn strategy how the engine performance can be improved without compromising the exhaust manifold temperature or turbocharger operating conditions. It was observed that the optimum lambda value for 2000 rpm and 10 bar of BMEP conditions was 1.32 which reduced in 7.2% the BSFC and in 74°C the exhaust manifold temperature. In the case of 3000 rpm and 10 bar of BMEP conditions, the optimum lambda value was around 1.39, achieving a reduction in BSFC of 10% and a reduction of 116°C on the exhaust manifold temperature. In the next section the trade-off

with exhaust raw emissions is analyzed in order to give a full overview of the advantages and disadvantages of using a lean burn strategy in a GTDI engine.

### 5.3.2.1.2 Exhaust raw emissions

The  $NO_x$ ,  $HC$  and  $CO$  exhaust raw emissions were measured in order to analyze the impact of lean mixtures on the engine exhaust emissions. In Figure 5.45 and Figure 5.46 the exhaust raw emissions and combustion efficiency for different lambda values are presented respectively at 2000 rpm and 3000 rpm. It is observed that each exhaust emission has a similar behavior at both engine speeds.



**Figure 5.45.** Exhaust raw emissions and combustion efficiency (bottom right graph) at 2000 rpm and 50% load for different lambda values.  $NO_x$  (top left graph),  $HC$  (top right graph),  $CO$  (bottom left graph) and combustion efficiency (bottom right graph).

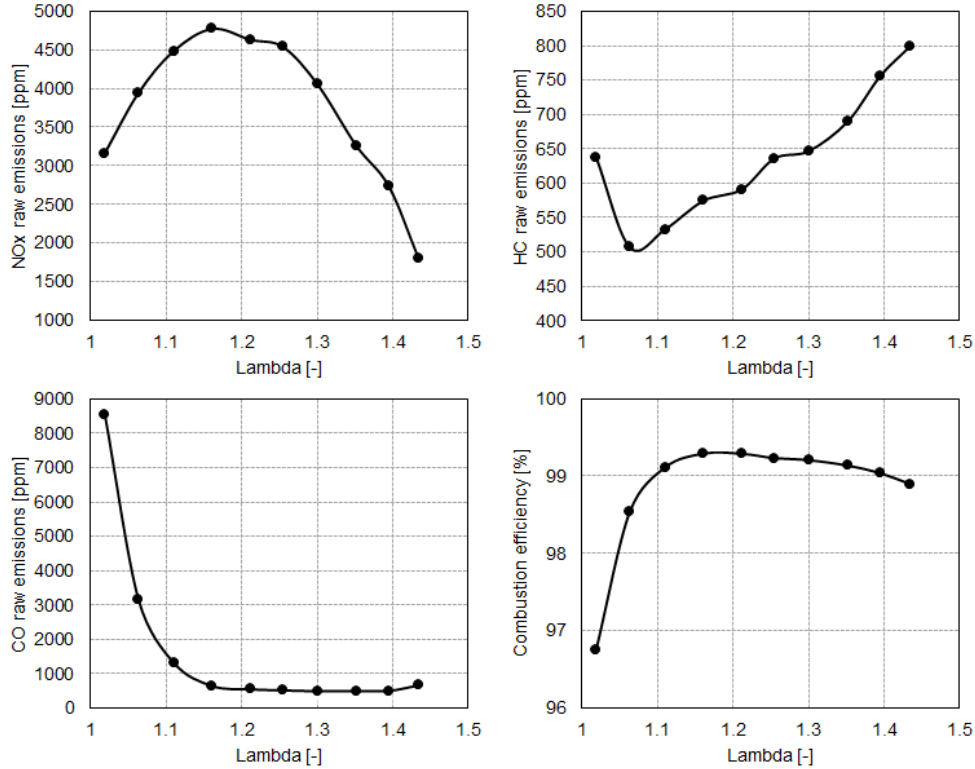
In the case of  $NO_x$  emissions, it is observed that the concentration increases with the lambda value up to a maximum found at 1.22 at 2000 rpm and 1.16 at 3000. After the initial increasing trend, a decreasing evolution is present from the maximum concentration until the highest lambda value for both engine speed conditions, as plotted in the top left graph of Figure 5.45 and Figure 5.46.

The  $NO_x$  emissions have an increment trend at the initial part of the lambda increase because of the oxygen concentration increase, which helps form more  $NO_x$ . Then, a decrement trend is observed for higher lambda values despite the further increase in oxygen concentration, at this stage the combustion temperature has been reduced the amount necessary to counteract the higher oxygen concentration by slowing the  $NO_x$  emissions thermal formation reaction. Similar results of this behavior of  $NO_x$  emissions for lean mixtures can be observed in literature in the work performed by Yu et al. [22] they managed to expand the lean burn misfire limit until 1.6 lambda, achieving a reduction of 60.6% in  $NO_x$  emissions.

Regarding the  $HC$  emissions, a similar analysis as the one described for  $NO_x$  emissions needs to be performed in order to explain the change in trend observed in top right graphs of Figure 5.45 and Figure 5.46. When the lambda is increased, the oxygen concentration also increases, decreasing the  $HC$  emissions, as it is observed at 2000 rpm from lambda 1 to 1.07 and from 1 to 1.06 at 3000 rpm. After this initial decrease, because of the excess of oxygen available that usually oxidizes the  $HC$  emissions, a change of the trend is produced and a slowly increase of  $HC$  emissions is observed until the highest lambda value. This trend was observed for both engine speed. This change in trend is also a consequence of the combustion temperature reduction, already shown before in Section 5.3.2.1.1, because it makes the combustion more prone to quench, thus producing more  $HC$  emissions.

On the other hand,  $CO$  emissions have a decrement trend as lambda value increases, as observed in the bottom left graph of Figure 5.45 and Figure 5.46. A drastic reduction in  $CO$  emissions appears at both engine speed conditions, mainly due to the excess of oxygen which oxidizes the  $CO$  emissions after the combustion, hence forming more  $CO_2$ . In this case also the reduction of  $CO_2$  dissociation helps to form less  $CO$  emissions because of the combustion temperature reduction. A similar effect is observed in Chapter 4 when EGR is added and the combustion temperature is reduced and so the  $CO$  emissions.

The combustion efficiency improves as the oxygen concentration increases, until it reaches a maximum at around lambda 1.22 for both engine conditions, as depicted in the bottom right graph of Figure 5.45 and Figure 5.46. The



**Figure 5.46.** Exhaust raw emissions and combustion efficiency (bottom right graph) at 2000 rpm and 50% load for different lambda values.  $NO_x$  (top left graph), HC (top right graph), CO (bottom left graph) and combustion efficiency (bottom right graph).

combustion efficiency improved 3% of absolute value at 2000 rpm and 2.5% at 3000 rpm. After reaching the maximum value, the combustion efficiency slowly starts to decrease until the maximum lambda value for both engine speed conditions. This is mainly due to the slower combustion and lower combustion temperature which tends to quench more easily, damaging the burn of the fuel.

A 14% increment of  $NO_x$  emissions, an 8% increment of HC emissions and a 95% reduction of CO emissions was observed at 2000 rpm at the optimum lambda value of 1.32. In the case of 3000 rpm, a 13% reduction of  $NO_x$  emissions, an 19% increment of HC emissions and a 94% reduction of CO emissions occur at the optimum lambda value of 1.39.

### 5.3.2.2 Lean burn and cooled EGR synergy influence on a GTDI engine

In this section a study of the synergy and optimization between cooled EGR and a lean burn strategy is going to be presented. A common in-cylinder dilution factor is introduced in order to help with the comparison and analysis process of both strategies. In this section a DoE approach was used to perform the test plan because the final objective was to also find the optimum conditions that could minimize the fuel consumption. The DoE test plan was already explained and presented before in the Methodology Section 5.2.1. The tests were performed at iso-fuel mass flow and iso-intake temperature for 2000 rpm and 10 bar of BMEP and 3000 rpm and 10 bar of BMEP.

#### 5.3.2.2.1 In-cylinder dilution factor

External EGR and lean burn have similar dilution effect on the intake mixture of the engine. In order to compare the EGR and lean burn effect at different operating points, a new term, the in-cylinder dilution factor “ $\alpha$ ” is introduced. It is defined as the total gas mass trapped in the cylinder at the end of the gas exchange process, divided by the air mass required to operate under stoichiometric condition:

$$\alpha = \frac{m_{cyl}}{AFR_0 \cdot m_{fuel}} \quad (5.1)$$

After some arranging, Equation 5.1 can be expressed as [18]:

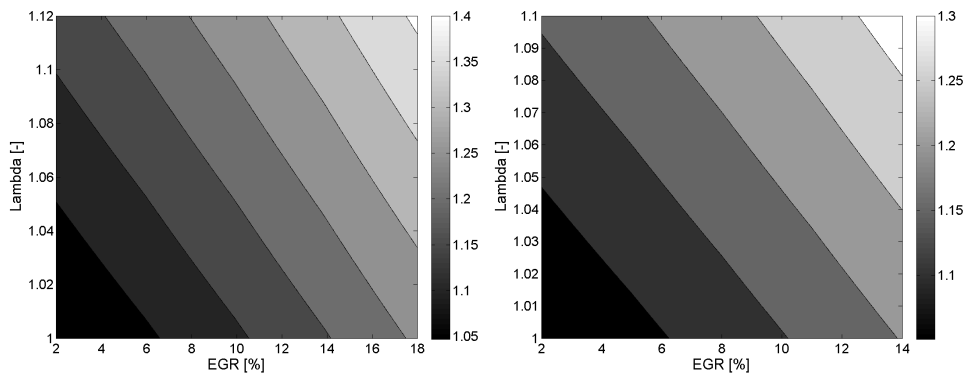
$$\alpha = \frac{\lambda}{1 - IGRF} \quad (5.2)$$

where  $IGRF$  is the internal gas residual fraction. The dilution factor reflects the overall in-cylinder dilution by only lean burn (when  $\lambda > 1$  and  $EGR = 0$ ), or by only EGR (when  $\lambda = 1$  and  $EGR > 0$ ), or the combination of both (when  $\lambda > 1$  and  $EGR > 0$ ). Because there always exists internal gas recirculation, ( $IGR > 0$ ), even when there is not EGR, thus the in-cylinder dilution factor is always greater than  $\lambda$ .

#### 5.3.2.2.2 Combustion and engine performance

In this part of the section the influence of cooled EGR operating with lean burn on the combustion and engine performance is presented. As mention

before, a dilution factor is used to account for the dilution phenomena of both used strategies. The observed possible maximum dilution factor achieved at 2000 rpm is higher than at 3000 rpm, as expected, and is observed in Figure 5.47. At 2000 rpm the maximum conditions of 18% of EGR and 1.12 lambda are achieved (1.4 of dilution factor) while at 3000 rpm only 14% of EGR and 1.1 lambda (1.3 of dilution factor) are attained. Increasing the engine speed increases the ignition advance needed to phase the combustion around the optimum crank angle and therefore increases the volume on the cylinder where the start of the combustion is placed, reducing the mixture inflammability which limits the maximum possible achievable dilution factor. The IGR is maintained under the same value for the different tests at iso-engine speed, since the variable valve timing settings are the same during the tests. The intake and exhaust pressure observed during the tests verily changed compared to the original values, this verily modifies the IGR value across the entire map.

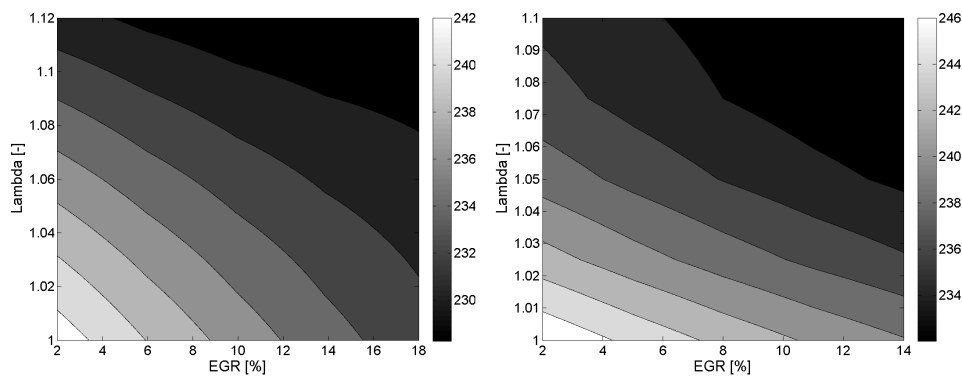


**Figure 5.47.** Dilution factor in % at 2000 rpm and 50% load (left graph) and at 3000 rpm and 50% (right graph) for different lambda and EGR values.

Introducing cooled EGR helped reduced the BSFC 2.5% or 6 g/kWh at 2000 rpm and 2.9% or 7 g/kWh at 3000 rpm, as can be seen in Figure 5.48. The EGR reduces the fuel consumption by reducing the pumping losses, heat transfer and improving the combustion phasing as found by Alger et al. [1]. Operating with lean burn also reduces the fuel consumption, which is represented in Figure 5.48, in 4.2% or 10 g/kWh at 2000 rpm and 4.3% or 10.5 g/kWh at 3000 rpm. The lean burn reduces the consumption by reducing the pumping losses and increasing the combustion efficiency, found by Tang et al. [18].



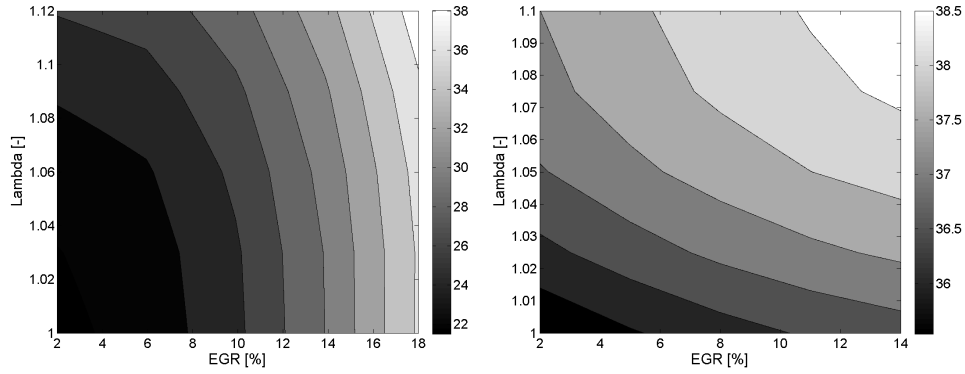
When combining these two strategies a further reduction on the BSFC is confirmed. Almost 5.8% or 14 g/kWh at 2000 rpm and 5.7% or 14 g/kWh at 3000 rpm of reduction are achieved compared to the original values. Although the reduction in fuel consumption is nearly the same at 2000 rpm and 3000 rpm, it must be taken into account that the observed fuel consumption reduction at 3000 rpm is obtained with a lower dilution factor than at 2000 rpm.



**Figure 5.48.** BSFC in g/kWh at 2000 rpm and 50% load (left graph) and at 3000 rpm and 50% (right graph) for different lambda and EGR values.

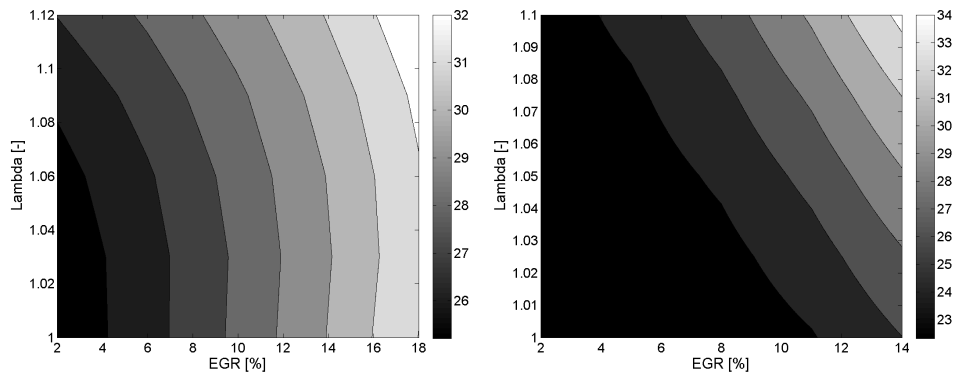
The observed reduction of BSFC combining both strategies increases the indicated efficiency of the engine. Figure 5.49 shows the evolution of the indicated efficiency when increasing lambda and EGR rate. The indicated efficiency at 2000 rpm increases from 35.5% to 39% with a BSFC of 228.1 g/kWh. And at 3000 rpm the indicated efficiency increases from 35.6% to 38.5% with a BSFC of 232.2 g/kWh.

The addition of cooled EGR and lean mixture operation also influence the combustion process. In Figure 5.50 the augmentation of the combustion duration when adding EGR and operating with lean burn can be observed. This increase in the combustion duration is due to the dilution effect, in the case of the EGR produced by the exhaust gases, and in the lean burn case by the excess of oxygen. The operation with high dilution factor values increases the combustion duration: at 2000 rpm a 32 CAD combustion duration is observed at 1.4 of dilution factor, which is almost 8 CAD more than the original combustion duration; and at 3000 rpm a 34 CAD combustion duration is confirmed at the highest dilution factor, being almost 12 CAD more than the original combustion duration.



**Figure 5.49.** Indicated efficiency in % at 2000 rpm and 50% load (left graph) and at 3000 rpm and 50% (right graph) for different lambda and EGR values.

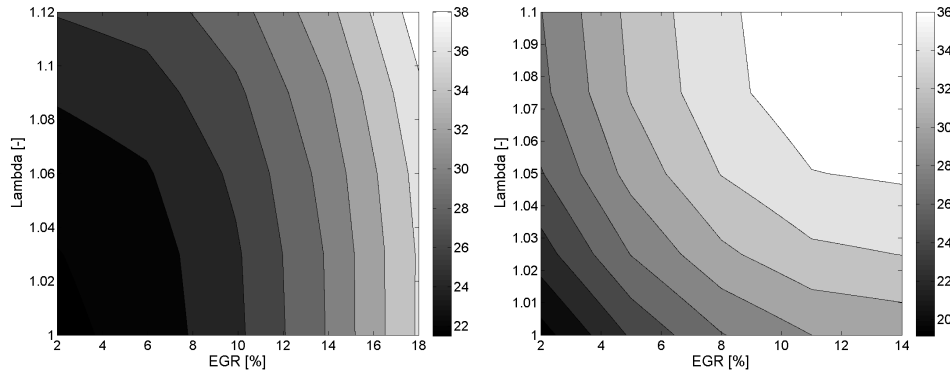
The combustion duration augmentation is more important at 3000 rpm, 4 CAD more than at 2000 rpm, despite the lower dilution factor at 3000 rpm compared to the 2000 rpm operating conditions. Higher engine speeds increase the combustion duration in CAD for the same combustion time.



**Figure 5.50.** Combustion duration in CAD at 2000 rpm and 50% load (left graph) and at 3000 rpm and 50% (right graph) for different lambda and EGR values.

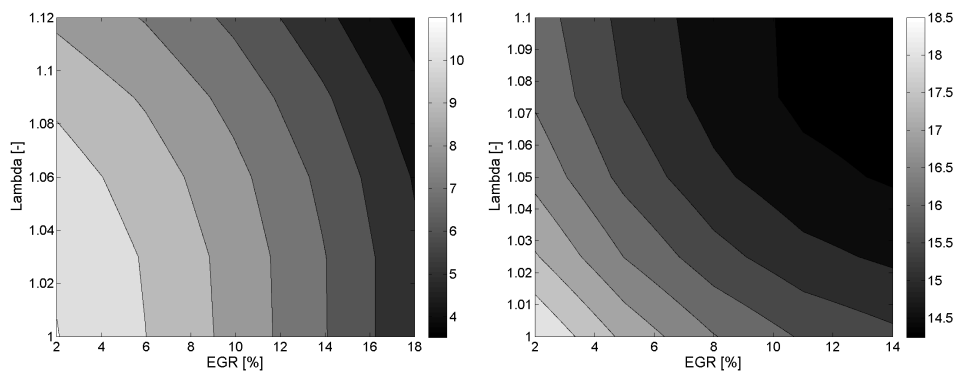
As mentioned before, increasing the combustion duration also increases the ignition advance needed in order to phase the combustion at the optimum crank angle. The spark timing evolution can be observed in Figure 5.51 for the different lambda and EGR rate conditions. It is observed that more ignition advance is needed when adding EGR or working with leaner mixtures in order

to phase the combustion process. The increase in the combustion duration, consequence of the dilution effect, leads to a higher value in the ignition advance.



**Figure 5.51.** Ignition advance in CADBTDC at 2000 rpm and 50% load (left graph) and at 3000 rpm and 50% (right graph) for different lambda and EGR values.

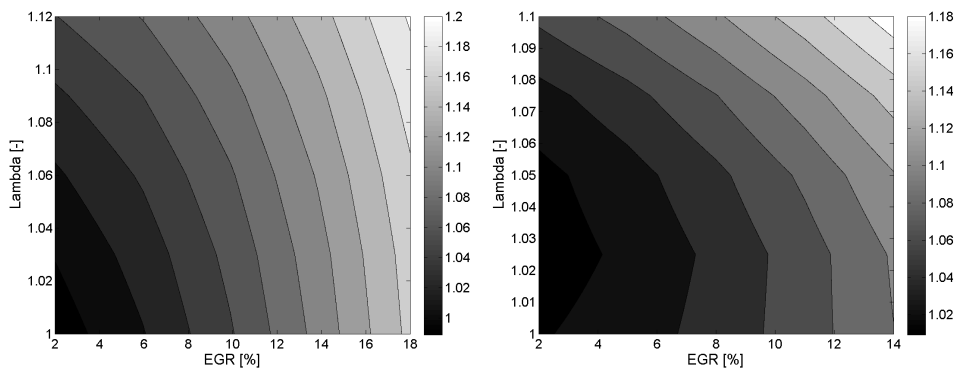
Analyzing the pumping losses, a reduction can be seen for both operating conditions when the EGR rate and lambda values are increased as can be seen in Figure 5.52. At 2000 rpm the pumping losses were reduced in more than 50% at 1.4 of dilution factor and at 3000 rpm were reduced in more than 25% at 1.3 of dilution factor.



**Figure 5.52.** Pumping losses in J at 2000 rpm and 50% load (left graph) and at 3000 rpm and 50% (right graph) for different lambda and EGR values.

The decrease in pumping losses is consequence of the intake manifold pressure increase. When increasing the dilution factor more mass is needed into the engine to maintain the conditions at iso-fuel and therefore more mass in the same intake manifold volume increases the pressure reducing the pumping losses. The original pumping losses represent around 3% of the BMEP in both cases.

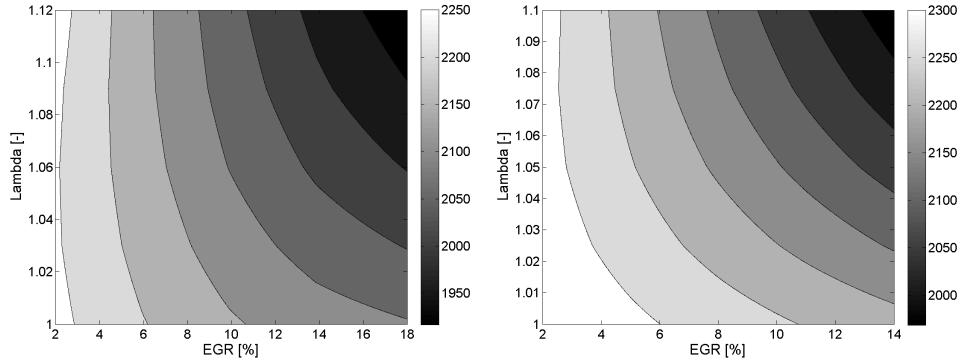
The increase on the intake pressure when introducing cooled EGR or operating with lean burn is represented in Figure 5.53 for 2000 rpm and 3000 rpm. The intake pressure gain is achieved by opening the throttle body, since the compressor outlet pressure is higher than the intake pressure no compressor outlet pressure increase is needed. Therefore the turbocharged speed and turbine working conditions did not changed significantly, maintaining at the same value the exhaust pressure.



**Figure 5.53.** Intake manifold pressure in bar at 2000 rpm and 50% load (left graph) and at 3000 rpm and 50% (right graph) for different lambda and EGR values.

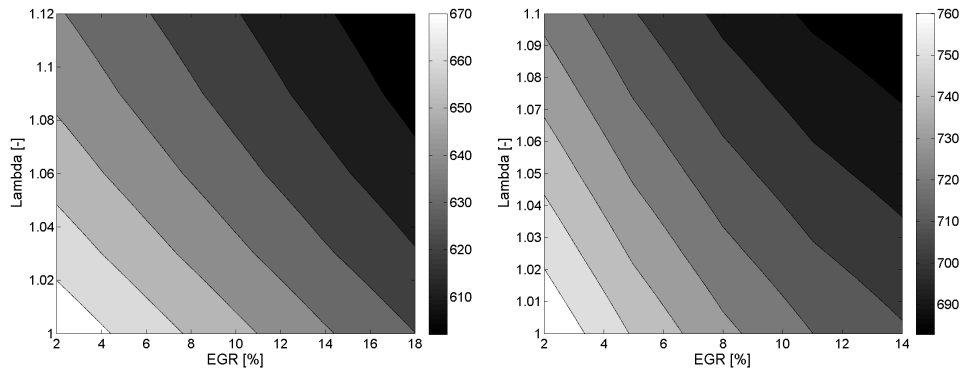
The reduction on the reactivity of the mixture while increasing the dilution factor leads to lower combustion temperatures and lower exhaust gas temperatures. In Figure 5.54 the combustion temperature is plotted for the different lambda and EGR rate values. As expected when the lambda value increases the combustion temperature decreases because of the dilution effect. The same phenomena occur when adding cooled EGR. The decrease on the combustion temperature reduces the heat losses which also helps reduce the BSFC, as stated before, and increases the thermal efficiency of the engine.

The exhaust temperature was also reduced when both strategies were used, due to the decrease of the combustion temperature and the new phasing of the combustion. In Figure 5.55 the temperature upstream the turbine can be



**Figure 5.54.** Combustion temperature in  $^{\circ}\text{C}$  at 2000 rpm and 50% load (left graph) and at 3000 rpm and 50% (right graph) for different lambda and EGR values.

seen for different EGR and lambda conditions, where at 2000 rpm a decrease of  $65^{\circ}\text{C}$  is observed when operating with a dilution factor of 1.4 and at 3000 rpm a decrease of  $75^{\circ}\text{C}$  is detected when running in the maximum dilution factor.

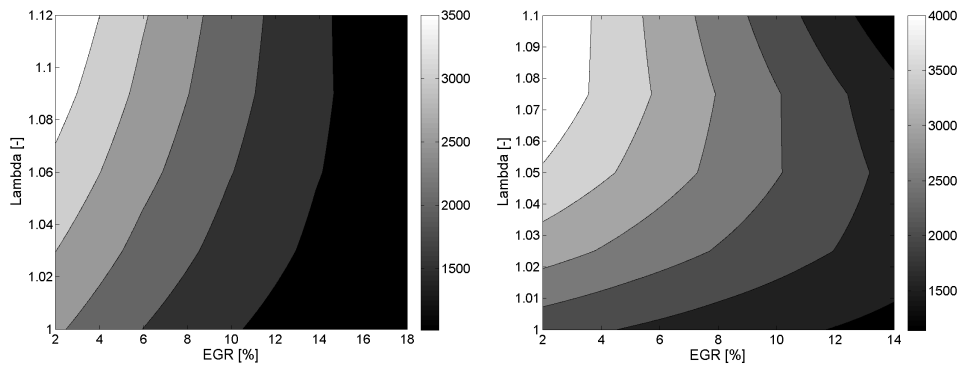


**Figure 5.55.** Exhaust manifold temperature in  $^{\circ}\text{C}$  at 2000 rpm and 50% load (left graph) and at 3000 rpm and 50% (right graph) for different lambda and EGR values.

### 5.3.2.2.3 Exhaust raw emissions

In the case of the exhaust raw emissions, a reduction is obtained on the  $\text{NO}_x$  raw emissions when the EGR rate was increased. The reduction in

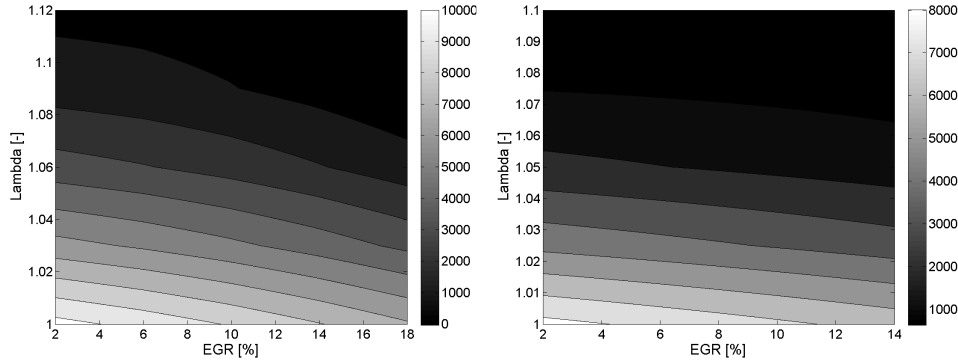
$NO_x$  emissions is caused by the reduction of the reactivity of the mixture or the increase of the dilution factor, which reduces the combustion temperature and the oxygen concentration [1, 3]. On the other hand, as soon as the engine starts to operate in lean burn the  $NO_x$  augmented with the increasing of the lambda value. Leading to higher lambda values tends to raise the oxygen concentration which increases the  $NO_x$  emissions while the combustion temperature is high enough to form them. These results can be seen in Figure 5.56, showing the  $NO_x$  emissions in parts per million (ppm). The reduction on  $NO_x$  raw emissions were around 56% at 2000 rpm and 35% at 3000 rpm for the highest dilution factor associated at each operating conditions.



**Figure 5.56.**  $NO_x$  raw exhaust emissions in ppm at 2000 rpm and 50% load (left graph) and at 3000 rpm and 50% (right graph) for different lambda and EGR values.

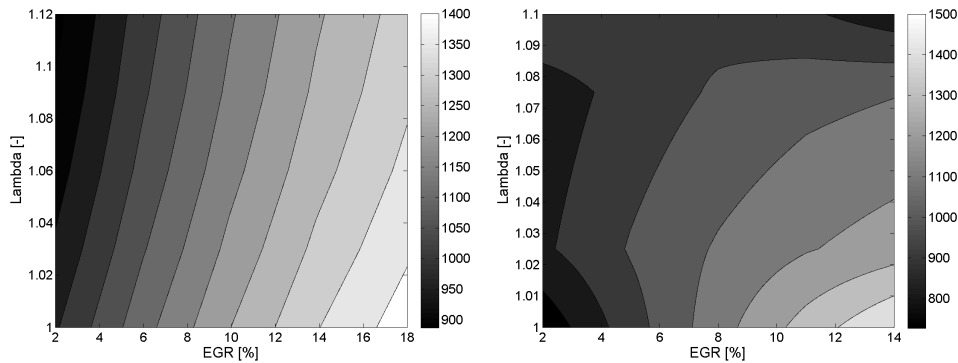
The observed  $CO$  emissions decrease when increasing the EGR rate and lambda values, as can be observed in Figure 5.57, where the  $CO$  emissions are represented in ppm for both operating conditions. This reduction in  $CO$ , when adding cooled EGR, is because of the reduction in the level of dissociation of  $CO_2$  due to the flame temperature decrease effect of the dilution of the mixture. When increasing the lambda value the  $CO$  was also reduced, due to the higher oxygen concentration which is used to form more  $CO_2$ , since the temperature is still enough to form it. The reduction on  $CO$  raw emissions was around 98% at 2000 rpm and 88% at 3000 rpm for the highest dilution factor associated at each operating conditions.

In the case of the  $HC$  emissions, an increase occurs when the cooled EGR rate is increased, due to the decrease on the combustion temperature and longer combustion duration. However, when increasing the lambda value



**Figure 5.57.** *CO raw exhaust emissions in ppm at 2000 rpm and 50% load (left graph) and at 3000 rpm and 50% (right graph) for different lambda and EGR values.*

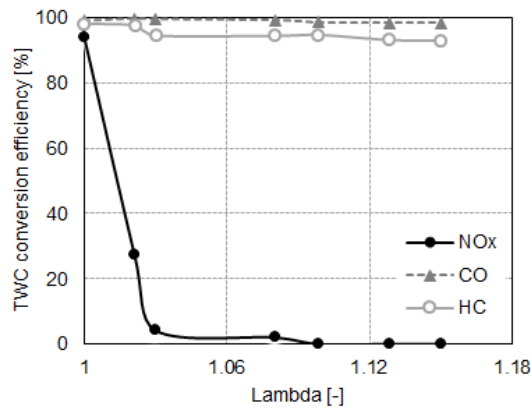
a *HC* emissions decrease is observed, due to the increase of the oxygen concentration while the combustion temperature is high enough to oxidize them, which leads to less unburned fuel and better combustion efficiency. The *HC* raw emissions increased by 30% at 2000 rpm and 20% at 3000 rpm as can be seen in Figure 5.58.



**Figure 5.58.** *HC raw exhaust emissions in ppm at 2000 rpm and 50% load (left graph) and at 3000 rpm and 50% (right graph) for different lambda and EGR values.*

When analyzing the exhaust emissions after the TWC, the total  $NO_x$ , *CO* and *HC* emissions are completely different and they mainly depend on the TWC conversion efficiency. The TWC conversion efficiency depends directly on the lambda value and exhaust gas temperature. When the engine starts

to operate in lean burn conditions the TWC  $NO_x$  conversion efficiency drops from 95% to 0%, as expected. This is detected in Figure 5.59 where the  $NO_x$ ,  $HC$  and  $CO$  emissions TWC conversion efficiency is presented in percentage. In the case of the  $HC$  emissions the conversion efficiency is reduced but not as much as observed with the  $NO_x$  emissions. The reduction in  $HC$  raw emissions before the catalyst using lean burn does not compensate the reduction on the TWC conversion efficiency and this leads to measure more  $HC$  emissions after the TWC than with the operating conditions on stoichiometric mixture. On the other hand the  $CO$  conversion efficiency was maintained at almost the same value through the entire lambda operating conditions range. The reduction in  $CO$  emissions, using cooled EGR and lean burn, before the catalyst also reduces the measured  $CO$  emissions after the catalyst.



**Figure 5.59.** Three way catalyst exhaust emissions conversion efficiency at 2000 rpm and 50% load for different lambda values and EGR values.

## 5.4 Summary and conclusions

During the development of this chapter, an optimization of the engine calibration was performed in order to minimize the engine fuel consumption when it was operated with cooled EGR. The VVT and injection timing settings were optimized using 1D simulation and DoE, and parametric approach, respectively. In addition, a variety of strategies to reduce further the engine fuel consumption were explored. In these different strategies, multi-injections, coolant temperature variation and induced swirl motion were analyzed and tested.



It was observed how difficult and time consuming can be to optimize the VVT settings in order to minimize the engine fuel consumption. This was the main cause to the simulation methodology development in order to reduce the time and amount of tests during the optimization process. The simulation optimization process requires 3 times less tests than a DoE approach and around 6 to 7 times less tests than a parametric testing approach. In the case of the VVT settings optimization, a reduction of the engine fuel consumption was observed basically due to the pumping losses and IGR reduction that lead to a reduction of CoV of the IMEP. Also the effect of IGR reduction on the exhaust emissions and combustion was observed and analyzed. Showing the same trend as observed in Chapter 4,  $NO_x$  emissions decrease with the EGR rate increase and despite the reduction in IGR,  $NO_x$  emissions did not change compared to the original VVT settings at maximum EGR rate tested, 15%.  $HC$  emissions were also the same compared with the original VVT setting at 15% of EGR rate. In the case of  $CO$  emissions, a reduction of 15% was observed at 2000 rpm and an increase of 7.5% was observed at 3000 rpm compared to the original VVT settings at maximum EGR rate tested also at 15%.

In general, the optimization of VVT settings reduced the engine fuel consumption in 1.4% at 2000 rpm and 1.8% at 3000 rpm at 15% of EGR rate compared with the original VVT settings conditions, having low impact on exhaust emissions as it was discussed before.

After the VVT setting optimization, the injection timing optimization based on a parametric approach testing was performed. The parametric study was used to fully analyze the impact of the injection timing on the engine performance and exhaust emissions, and also because it was only one variable to study. It was observed how optimizing the injection timing can reduce the fuel consumption mainly by reducing the CoV of the IMEP, increasing the combustion efficiency and reducing in a low percentage the pumping losses. Regarding the exhaust emissions,  $NO_x$  emissions were increased in 211% (still lower than the original conditions without EGR),  $HC$  emissions were increased 40% and  $CO$  emissions were reduced by 51% compared to the original injection timing conditions with EGR. The optimization of injection timing reduced in 1.7% the engine fuel consumption at 2000 rpm but increased  $NO_x$  emissions and  $HC$  emissions.

Regarding the other three strategies tested after the optimization process of VVT settings and injection timing, it was seen that a multi-injection strategy did not improve the fuel consumption compared to the original optimized VVT settings at the same EGR rate of 17.5%. The parametric approach for this

strategy could not have been the best approach since there were four variables to be optimized and therefore a DoE could have been a better approach, after seeing the difficulties of finding a better configuration than the original injection strategy. In the case of the induced swirl motion, also no reduction of the engine fuel consumption was observed due to mainly hardware limitations because the original design and turbulence were specifically designed to work in harmony with the original cylinder head turbulence motion.

And finally, the increase of the coolant temperature operation showed a reduction of 1.3% on the engine fuel consumption at 2000 rpm compared to the original coolant temperature operating conditions. The impact on exhaust emissions was fairly low with an increase of  $NO_x$  emissions by 13% and  $CO$  emissions by 1.6%, and a reduction of  $HC$  emissions by 11%. On the other hand, this strategy will increase the knocking risk because of the higher mean temperature of the cycle but the impact on emissions is advantageous compared to optimizing the injection timing, because the mixing process and wall wetting it is not changed, so  $PM$  emissions are going to be maintained at the same concentration or even reduced, and the impact on the rest of exhaust emissions is much lower. In addition, the optimization process for the injection timing consumes more time and shows a similar fuel consumption advantage.

Once the optimization process and the different strategies were analyzed, it was seen that at 2000 rpm and 10 bar of BMEP the BSFC could be reduced from 247.4 g/kWh of the original condition without EGR to 231.1 g/kWh with an optimized VVT setting using 17.5% of EGR rate and operating at 100°C of coolant temperature. In the case of 3000 rpm and 10 bar of BMEP there was not possible to perform the tests with higher coolant temperature or injection optimization but despite this issue, the BSFC was reduced from 247.5 g/kWh of original conditions without EGR to 234 g/kWh with the optimized VVT settings setup and using 15% of EGR rate.

The analysis and results shown in this chapter helped to understand the potential to reduce the engine fuel consumption, of each step of possible optimization modifying the calibration of the engine by using the original hardware. In addition, some strategies to reduce the engine fuel consumption were also evaluated modifying some-how the hardware or engine original operating conditions, in order to be carried out. These strategies are more complex and the engine should had been designed from the beginning in order to operate with multi-injections, swirl motion or higher coolant temperature, to fully show the potential of these strategies.

In the tested operating conditions, the use of lean burn and both technologies at the same time was also studied. The BSFC reduction was

caused by the improvement on the combustion phasing and the reduction on heat and pumping losses. The exhaust gas temperature decrease was due to the decrease on the combustion temperature, and the new combustion duration and phasing.

The observed reduction in  $NO_x$  raw emissions, despite the lean mixture, was due to the EGR dilution effect and therefore reduction of the combustion temperature, despite the increase on the oxygen concentration, compared to the original operating conditions. In the case of the conditions where no cooled EGR was used, the  $NO_x$  emissions were also reduced but mainly by the dilution effect of the extra oxygen and the reduction in combustion temperature, forming less  $NO_x$  emissions. On the  $HC$  raw emissions, an increase was seen due to the EGR dilution effect which decreases the combustion temperature compared to the original operating conditions, despite the increase of oxygen concentration, which helps the oxidation when operating with lean burn. In the case where only lean burn was used,  $HC$  also increase, despite the excess of oxygen, due to the reduction of combustion temperature and therefore the increase of quenching of the flame at the end of the combustion, similar reasons as when cooled EGR is added.

The reduction on  $CO$  raw emissions was detected because of the reduction in the level of dissociation of  $CO_2$  due to the combustion temperature decrease and, in addition, the oxidation of the  $CO$  when more oxygen was available operating with lean burn. In the case where only lean burn is used, the reduction in  $CO$  emissions is only caused by the oxidation process of  $CO$  emissions after the combustion.

The exhaust emissions after the catalyst showed that only a  $CO$  emissions reduction was achieved because of the TWC conversion efficiency decrease on the  $NO_x$  and  $HC$  emissions due to the lean mixture operating conditions. In the case where cooled EGR and lean burn was used, the decrease on  $NO_x$  emissions before the TWC did not compensate the TWC conversion efficiency decrease.

The lean burn strategy seems to have a big potential to reduce the fuel consumption but the TWC cannot be used if this strategy is used. Therefore, a proper  $NO_x$  conversion post-treatment system needs to be implemented in order to comply with the homologation regulations. This can be address by adding a  $NO_x$  trap or SCR to the exhaust after-treatment system to reduce the  $NO_x$  emissions and working in synergy with an oxidation catalyst to reduce the  $HC$  and  $CO$  emissions.

Cooled EGR and lean burn technologies have a big potential to reduce the BSFC as it was seen in this research work, but it was observed that working

in synergy a trade-off for  $NO_x$  emissions was not found when operating in lean burn conditions and cooled EGR was added. In addition, the benefits on fuel consumption are lower at 3000 rpm compared to only using a lean burn strategy, and at 2000 rpm the fuel consumption was the same due to knocking limitation when only using lean burn. Therefore, adding cooled EGR allowed a better combustion phasing at 2000 rpm, but the fuel consumption is the same for both cases. It was observed that, in order to obtain the maximum fuel consumption reduction, only one of the strategies should be used at once, either lean burn or cooled EGR. However, at the same time, there are no further benefits in fuel consumption and, in the case of cooled EGR, the main advantage of only using a TWC as post-treatment system is lost and, in the case of lean burn, the full potential to lower fuel consumption is reduced.

## Bibliography

- [1] Alger T., Chauvet T. and Dimitrova Z. “Synergies between High EGR Operation and GDI Systems”. *SAE Int. J. Engines*, Vol. 1 n° 1, pp. 101–114, 2008. 2008-01-0134.
- [2] Alger Terrence, Gingrich Jess, Khalek Imad A. and Mangold Barrett. “The Role of EGR in PM Emissions from Gasoline Engines”. *SAE Int. J. Fuels Lubr.*, Vol. 3 n° 1, pp. 85–98, 2010. 2010-01-0353.
- [3] Cairns A., Blaxill H. and Irlam G. “Exhaust Gas Recirculation for Improved Part and Full Load Fuel Economy in a Turbocharged Gasoline Engine”. In *SAE Technical Paper*, 2006. 2006-01-0047.
- [4] Lujan Jose Manuel, Climent Hector, Novella Ricardo and Rivas-Perea Manuel Eduardo. “Influence of a low pressure EGR loop on a gasoline turbocharged direct injection engine”. *Applied Thermal Engineering*, Vol. 89, pp. 432–443, 2015.
- [5] Vitek O., Macek J. and Polasek M. “New Approach to Turbocharger Optimization using 1-D Simulation Tools”. In *SAE Technical Paper*, 2006. 2006-01-0438.
- [6] Bozza F., Gimelli A. and Tuccillo R. “The Control of a VVA-Equipped SI Engine Operation by Means of 1D Simulation and Mathematical Optimization”. In *SAE Technical Paper*, 2002. 2002-01-1107.
- [7] Bozza F. and Torella E. “The Employment of a 1D Simulation Model for A/F Ratio Control in a VVT Engine”. In *SAE Technical Paper*, 2003. 2003-01-0027.
- [8] Lujan J., Pastor J., Climent H. and Rivas M. “Experimental Characterization and Modelling of a Turbocharger Gasoline Engine Compressor By-Pass Valve in Transient Operation”. In *SAE Technical Paper*, 2015. 2015-24-2524.
- [9] Jiang S., Nutter D. and Gullitti A. “Implementation of Model-Based Calibration for a Gasoline Engine”. In *SAE Technical Paper*, 2012. 2012-01-0722.
- [10] Vijayaraghavan K., Lindhjem C., DenBleyker A., Nopmongcol U., Grant J., Tai E. and Yarwood G. “Effects of light duty gasoline vehicle emission standards in the United States on ozone and particulate matter”. *Atmospheric Environment*, Vol. 60, pp. 109–120, 2012.

- 
- [11] Bandel W., Fraidl G. K., Kapus P. E., Sikinger H. and Cowland C. N. “The Turbocharged GDI Engine: Boosted Synergies for High Fuel Economy Plus Ultra-low Emission”. In *SAE Technical Paper*, 2006. 2006-01-1266.
- [12] Yang Jialin and Kenney Thomas. “Some Concepts of DISI Engine for High Fuel Efficiency and Low Emissions”. In *SAE Technical Paper*. SAE International, 2002. 2002-01-2747.
- [13] Hacohen J., Ashcroft S. J. and Belmont M. R. “Lean Burn Versus EGR S. I. Engine”. In *SAE Technical Paper*, 1995. 951902.
- [14] Lumsden G., Eddleston D. and Sykes R. “Comparing Lean Burn and EGR”. In *SAE Technical Paper*, 1997. 970505.
- [15] Grandin B. and Angstrom H. E. “Replacing Fuel Enrichment in a Turbo Charged SI Engine: Lean Burn or Cooled EGR”. In *SAE Technical Paper*, 1999. 1999-01-3505.
- [16] Ward Michael A. V. “High-Energy Spark-Flow Coupling in an IC Engine for Ultra-Lean and High EGR Mixtures”. In *SAE Technical Paper*. SAE International, 2001. 2001-01-0548.
- [17] Gukelberger Raphael, Alger Terrence, Mangold Barrett, Boehler Jeff and Eiden Corey. “Effects of EGR Dilution and Fuels on Spark Plug Temperatures in Gasoline Engines”. *SAE Int. J. Engines*, Vol. 6 n° 1, pp. 447–455, 2013. 2013-01-1632.
- [18] Tang Qijun, Liu Jingping, Zhan Zhangsong and Hu Tiegang. “Influences on Combustion Characteristics and Performances of EGR vs. Lean Burn in a Gasoline Engine”. In *SAE Technical Paper*, 2013. 2013-01-1125.
- [19] Bourhis Guillaume, Chauvin Jonathan, Gautrot Xavier and de Francqueville Loic. “LP EGR and IGR Compromise on a GDI Engine at Middle Load”. *SAE Int. J. Engines*, Vol. 6 n° 1, pp. 67–77, 2013. 2013-01-0256.
- [20] Wyszynski L., Stone C. and Kalghatgi G. “The Volumetric Efficiency of Direct and Port Injection Gasoline Engines with Different Fuels”. In *SAE Technical Paper*, 2002. 2002-01-0839.
- [21] Stevens E. and Steeper R. “Piston Wetting in an Optical DISI Engine: Fuel Films, Pool Fires, and Soot Generation”. In *SAE Technical Paper*, 2001. 2001-01-1203.
- [22] Yu C., Kim T., Yi Y., Lee J., Seokhong N. and Kyuhoon C. “Development of KMC 2.4L Lean Burn Engine”. In *SAE Technical Paper*, 1995. 950685.



# Chapter 6

## Conclusions and future works

### Contents

---

<b>6.1</b>	<b>Introduction</b> .....	<b>245</b>
<b>6.2</b>	<b>Conclusions</b> .....	<b>245</b>
<b>6.3</b>	<b>Future works</b> .....	<b>257</b>

---

### 6.1 Introduction

In this final chapter, the main objective is to gather the different contributions provided by this research work with their corresponding analysis. An exhaustive review of results and the relation with the objectives proposed at the beginning of the work will be presented in the first section of this chapter.

Clearly, this research work does not intend to address all the issues of gasoline turbocharged direct injection engines. Therefore, a proposal of future works is presented in the second section of this chapter. These proposals are based on suggestions that have emerged during the testing and analysis processes of this research work.

### 6.2 Conclusions

In order to fully understand and have a broader view of the contributions brought by this research work, a summary of Chapter 1 is necessary, to

remind the global framework and the initial objectives established. As it was presented, this research work has been developed in a difficult context market by both important energy and environmental issues. These are manifested respectively by the depletion of fossil resources, the energetic needs growth and despite the constant reduction of exhaust emissions due to new stringent pollution regulations. The constant increase of the car population offers a difficult situation to reduce these contaminant matters in the atmosphere. In this presented environment, the engine development must be focused on the reduction of fuel consumption and exhaust emissions at the same time. In this case, the presented research work focuses on the engine fuel efficiency improvement and main impact on exhaust emissions, using cooled EGR and lean burn as main strategies to achieve an engine fuel consumption reduction. An optimization needed to be developed in order to adjust the base calibration and setup of the engine to operate with cooled EGR and fully understand its potential. In addition, some additional strategies were planned to be used in order to increase the cooled EGR operation range at different engine conditions.

The current knowledge and latest strategies used to reduce the fuel consumption on SI gasoline engines were reviewed in Chapter 2 by including a detailed description of current development phase of SI gasoline engines: the strategies that are been used nowadays to reduce the fuel consumption and the ones that are under-development. The relative recent implementation of downsized SI gasoline engines increases the usage of turbochargers on these engines, therefore original limitations were worsened by increasing the engine load. In order to mitigate these SI gasoline limitations some strategies are being developed. One of these is cooled EGR which was already used in the past in some atmospheric gasoline engines, as it was described in Chapter 2 as strategy to reduce fuel consumption and exhaust emissions. In the case of lean burn, this is a strategy that has been also implemented in the past but that it has not been implemented in a full operational range of a SI gasoline engine because of its limitations on  $NO_x$  emissions.

From the literature review performed in Chapter 2, a clear approach for future gasoline engines was observed. Smaller engines with turbochargers is going to be the main recipe, reducing number of cylinders and increasing the engine load operation in normal driving conditions. This future approach arises new problems that have to be solved in order to further increase engine load and continue the path of development observed lately in SI gasoline engines. Cooled EGR has the potential to mitigate some of these problems and therefore further development in this area has to be done. This is the main reason why this research work shows a detailed analysis of this technology



effects on GTDI engines and its synergy with other strategies that could also further improve the EGR operational range or the engine thermal efficiency. It was observed that some work had to be performed to deeply analyze the cooled EGR effect on a GTDI engine using a LP EGR loop and further optimize the engine calibration in order to operate in synergy with cooled EGR. Additionally, a study of the lean burn potential operating in synergy with cooled EGR was necessary in order to show if  $NO_x$  exhaust emissions problems could be mitigated by using cooled EGR.

In consequence an experimental methodology had to be designed and developed from scratch in order to fulfill all the different objectives presented before. In Chapter 3, an experimental methodology, to perform that required test during this research work, was presented. This methodology had to be implemented from scratch with special care, since it was the first turbocharged multi-cylinder gasoline engine research work performed at CMT-Motores Térmicos and it could potentially be applied for later studies of the same kind:

- Prior to the start of the measurements, an analysis of the fuel that was going to be used during the research work was performed. Right after, an analysis of the engine base performance and exhaust emissions was performed in order to characterize it and correctly setup the engine test bench cell.
- The experimental setup and measurement procedure was basically improved during the characterization process of the engine: cooling power needed, fuel balance measurements accuracy (because of gasoline been used), sensors signals, test bench cell temperature and exhaust gases condensation affecting pressure measurements, and more obstacles that had to be solved in order to have an engine tests bench cell with the conditions required to perform good quality tests and provide accurate results.
- The characterization process of the engine served also to develop some of the theoretical tools and measurement procedure. Regarding the theoretical tools used in this research work, they were entirely developed at CMT-Motores Térmicos and, because of this research work, improved their use with SI gasoline engines. It is the case of Calmec, the combustion diagnosis tool, and OpenWam, the tool used to build the 1D engine model.
- A new theoretical tool, internally at CMT-Motores Térmicos, was implemented in this research work for the optimization process of the

VVT settings to minimize the fuel consumption. The model based calibration tool found in Matlab was used to create the DoE test plan and perform the optimization process. This MBC tool was also used to study the synergy between lean burn and cooled EGR presented at the end of Chapter 5.

- A parametric, DoE and simulation methodologies approach was used during the development of this research work in order to produce the results. For the initial basic study of the influence of a LP cooled EGR strategy on the performance and exhaust emissions of a GTDI engine, a parametric approach was used in order to analyze the effect of EGR rate on the different parameters of engine performance, combustion, air management and exhaust emissions. This parametric approach simplifies the process and it can be used when a single variable is changed or needs to be analyzed. In the case of the VVT optimization for 2000 rpm and 3000 rpm part load engine conditions, a more sophisticated approach was needed. In this case, a DoE approach was followed in order to optimize the VVT settings and in parallel a simulation methodology using a 1D engine model was developed and validated with the DoE approach results. After the optimization process, a parametric study was followed in order to compare the results of this new optimized VVT setting compared to the original setup for different EGR rates. Then, for the injection timing optimization and analysis of other strategies to increase the EGR operational range, a parametric approach was followed since only one variable was changed for each case. And as last, the synergy study between lean burn and cooled EGR was performed using also a DoE approach because an optimization process was also needed in order to fully understand the potential of using both strategies in combination.
- The experimental setup to measure the exhaust emissions  $NO_x$ ,  $HC$  and  $CO$  emissions was one of the setups already used in other engine test cells. But for the  $PM$  measurements, this research work contributed to the development of the  $PM$  measurement setup for gasoline engines.

After briefly describing the methodology approach for the different chapters of this research work and the experimental setup used to perform the tests, the main conclusions of the results presented in Chapter 4 regarding the influence of a LP cooled EGR loop on the engine performance, combustion, air management and exhaust emissions in steady state and transient conditions in NEDC cycles using a GTDI engine are listed below:

- The effect of cooled EGR on the combustion, engine performance and exhaust emissions was observed by performing a EGR rate sweep at 2000 rpm and 10 bar of BMEP and 3000 rpm and 10 of BMEP without optimizing the combustion phasing. It was observed that cooled EGR increased the engine BSFC by 9.8% at 2000 rpm and by 9% at 3000 rpm. The increased in BSFC is mainly due to the combustion retard caused by the mixture reactivity decrease. Cooled EGR has a dilution effect in the mixture and reduces the oxygen concentration, reducing the overall mixture reactivity, which causes a slower flame propagation and therefore a longer combustion. This is the main cause of the exhaust temperature increase of 15°C at 2000 rpm and 17°C at 3000 rpm both at 15% of EGR rate. Regarding the exhaust emissions, a decrease in  $NO_x$  emissions of 88.2% and  $CO$  emissions of 19.5% at 2000 rpm was observed, mainly due to the combustion temperature decrease as it was explained later in the chapter, product of the dilution effect of cooled EGR. The same reason was the cause of  $HC$  emissions increase of 49% at 2000 rpm. The trend was similar at 3000 rpm, observing a decrease on  $NO_x$  emissions and  $CO$  emissions of 90% and 26.4% respectively, and an increase on  $HC$  emissions of 18%.
- After a basic analysis of the cooled EGR impact on the combustion, engine performance and exhaust emissions, an optimization of the combustion phasing was performed for each EGR rate in order to fully observe the advantages and disadvantages with an optimized combustion phasing to minimize fuel consumption. This analysis was performed in 5 steady state operating points, 2000 rpm low, part and full engine load conditions, and 3000 rpm part and full engine load conditions. Part engine load conditions were the first part of the analysis, 2000 rpm and 10 bar of BMEP and 3000 rpm and 10 bar of BMEP, showing an improvement on BSFC of 3.8% at 2000 rpm and 3% at 3000 rpm using 15% of cooled EGR rate. This reduction in BSFC comes basically from the reduction of pumping and heat losses, the increase of the specific heat ratio of the mixture, and in the case of 2000 rpm due to the improvement in the combustion phasing by reducing the risk of knocking at this engine conditions. The reduction in pumping losses was obtained because of the increase of intake manifold pressure in order to maintain a constant air mass flow during the EGR rate sweep, although a smaller increase on the exhaust manifold pressure appeared. A pumping losses reduction of 19.5% at 2000 rpm and 8% at 3000 rpm was observed. In addition, heat losses were reduced due to the combustion reduction observed during the increase of EGR rate, a reduction of 230°C at 2000

rpm and 320°C at 3000 rpm was observed at 15% of EGR rate. This reduction of combustion temperature and new optimized combustion phasing reduced the exhaust manifold temperature by 46°C at 2000 rpm and by 76°C at 3000 rpm.

- An improvement on the combustion and engine performance was shown before after the optimization of the combustion phasing for both part load engine speed conditions using the maximum EGR rate tested, 15%. The impact on the exhaust emissions was also presented in Chapter 4, showing a decrease of  $NO_x$  and  $CO$  emissions of 54% and 8.5% at 2000 rpm and 71.4% and 22.7% at 3000 rpm. An increase of  $HC$  emissions was observed at 2000 rpm of 65% and at 3000 rpm of 55%. Regarding  $PM$  emissions, a reduction of number was observed when increasing the EGR rate. At 2000 rpm, the  $PM$  with a diameter between 7 and 22 nm were reduced from an average value of  $2.5E+4$  to  $2E+4$ . In the case of the  $PM$  with a diameter between 22 and 100 nm were reduced from an average values of  $4E+4$  to  $2E+4$ . The trend at 3000 rpm was similar, with a reduction of small  $PM$  from  $3E+4$  to  $1.5E+4$  and for bigger  $PM$  from  $4.5E+4$  to  $2.5E+4$ . The exhaust emissions had a similar trend as it was observed in the previous study performed without optimizing the combustion phasing but with a smaller reduction of  $NO_x$  and  $CO$  emissions, and a bigger increase in  $HC$  emissions, for the same engine conditions and same EGR rate.
- During the analysis at full engine load conditions, similar results were obtained as those already described in the part load engine conditions analysis, although the advantages are even higher when cooled EGR is introduced. An engine BSFC improvement of 12% at 2000 rpm with 14% of EGR rate and 11.5% at 3000 rpm with 10% of EGR rate was observed after optimizing the combustion phasing at trace knock for both engine speed conditions. At full engine load conditions, it is almost standard for every GTDI engine to have knocking limitations to phase the combustion phasing in its optimum position and an enrichment strategy in order to control the exhaust temperature at the turbine inlet in order to warranty the reliability of the components. Cooled EGR allowed the combustion phase to be advanced because of the reduction of the mixture reactivity also reducing the combustion temperature, as explained in part load conditions, decreasing the combustion exhaust temperature and making possible the elimination of the enrichment strategy. At 2000 rpm the enrichment strategy could be eliminated by just adding 5% of EGR rate, in the case of 3000 rpm 10% of EGR rate was enough to eliminate

the enrichment strategy. The main contributors for the engine BSFC reduction at high load are: the elimination of enrichment strategy, the advance of the combustion phasing, the reduction of heat losses and the increase of specific heat ratio of the mixture.

- At full load engine conditions the impact on exhaust emissions when cooled EGR is added is different because of the enrichment strategy elimination. The reduction of  $CO$  emissions is massive compared to partial load: a reduction of 83% at 2000 rpm and 85% at 3000 rpm was observed. The  $NO_x$  emissions were not reduced as in partial load conditions. In the case of 2000 rpm the  $NO_x$  emissions were maintained at the same value as the original condition without EGR but at 3000 rpm  $NO_x$  emissions were increased in 77%. This is mainly due to the elimination of the enrichment strategy which had a lower oxygen concentration than the conditions with 10% of EGR rate. The  $HC$  emissions were increased in 22% at 2000 rpm and reduced in 16.5% at 3000 rpm. In the case of  $PM$  emissions, a reduction was also observed at these engine conditions using cooled EGR, following the same trend as in part load conditions but with a higher reduction because of the enrichment strategy elimination. At 2000 rpm, the  $PM$  emissions were reduced from an average value of  $12E+4$  to  $3E+4$ . The trend at 3000 rpm was similar, with a reduction of  $PM$  from  $11E+4$  to  $4E+4$ . The main advantage at these engine conditions is that the TWC can be used to convert the exhaust emissions because the mixture is at stoichiometric conditions reducing all tailpipe emissions drastically.
- When cooled EGR was introduced at low engine load conditions, it was observed that the benefits were smaller than at part and full engine conditions. The engine BSFC improvement was 2.2% at 2000 rpm and 5 bar of BMEP using 15% of EGR rate and with an optimized VVT settings because with original settings only an improvement of 1% was observed. At these conditions the engine uses IGR in order to decrease engine exhaust emissions and fuel consumption and therefore the addition of cooled EGR did not change too much the conditions. However, when VVT settings were optimized to reduce the amount of IGR, a further improvement using the same amount of cooled EGR rate was observed. With cooled EGR replacing IGR a lower combustion temperature is obtained, reducing the heat losses. Although IGR was mostly replaced by cooled EGR,  $NO_x$  and  $CO$  emissions were reduced by 61% and 9.5% respectively.  $HC$  emissions were increased by 55.5%. The main reason for this increase is the combustion temperature reduction as

already mentioned before at part load conditions. At low loads the benefit was within the measurement error accuracy and therefore it was concluded that no further study was going to be performed later during the development of this research work. It seems that a good trade-off can be obtained between BSFC and exhaust emissions by optimizing the amount of IGR, and it would be easier to implement compared to a LP EGR loop which in terms of controls is more complicated offering similar results. This research work offers a broader view at low engine load conditions that it is missing in the literature.

- With all engine load conditions already analyzed, it is clear to mention that cooled EGR offers a big improvement in engine BSFC value from part load to full load engine conditions (10 to 18 – 20 bar BMEP). Regarding exhaust emissions, no significant change is observed at part load because the TWC will reduce the difference at the tailpipe to almost 0 in the *HC* emissions increase. But at full load, the possibility of using the TWC to convert the exhaust emissions, because of the enrichment strategy elimination, is a huge advantage and, therefore, also offers a significant reduction of all exhaust emissions at the tailpipe.
- The main disadvantages observed during the study were: (i) the increase of the compressor inlet temperature that for higher compression ratios could represent a limitation due to reliability issues, (ii) the water condensation at the inter-cooler placed after the compressor, that had to be removed periodically to prevent the engine to suck it in and (iii) the turbocharger limitation at 2000 rpm, because it was not possible to achieve the original engine torque due to limitation on the boost pressure that could be produced at that engine speed. Maybe complex turbocharging systems or variable geometry turbines are needed to achieve the required low end torque. In this case the control of cooled EGR was not necessary because all the tests were performed at steady state conditions but it could represent a problem during transient engine operation.
- It was observed how all advantages and disadvantages of cooled EGR were similar between the transient and the steady state conditions. The spark advance was not optimized for different EGR rates in transient conditions and, therefore, the improvement observed in fuel consumption could not be achieved. However, regarding the exhaust emissions, similar results were observed, reducing total accumulated  $NO_x$  in 48% and *CO* emissions in 14.4%, and increasing *HC* emissions in 15%. It was also observed that the reduction of *CO* emissions because of

the reduction of  $CO_2$  dissociation due to the combustion temperature reduction when cooled EGR was introduced and possible small increase in fuel consumption, not being able to detect by the fuel balance, caused an increase in 8.6% of  $CO_2$  emissions. It was observed that, in order to control the amount of EGR rate, a sophisticated control strategy using some simple engine model has to be use in order to anticipate the delay of this strategy during transient conditions. That was the main reason to perform the transient conditions with a fixed EGR valve opening for all the cycle.

With a broader view of the benefits of introducing cooled EGR into a GTDI engine, an optimization process to further reduce the engine fuel consumption was necessary in order to fully explore the maximum potential of this technology. In Chapter 5, an optimization process of the VVT settings and injection timing to further reduce the engine fuel consumption. The exploration of other strategies to further increase the operational range with EGR and the detailed study of the lean burn strategy operating in synergy with cooled EGR were presented. A summary and principal conclusions are listed below:

- For the optimization process only two operating points were selected, in this case part load engine conditions, 2000 rpm and 10 bar of BMEP and 3000 rpm and 10bar of BMEP. For the optimization of the VVT settings, a DoE approach was followed and in parallel a methodology using 1D model simulations was developed in order to reduce the amount of tests. It was observed how difficult and time consuming can be to optimize the VVT settings in order to minimize the engine fuel consumption. This was the main cause to the simulation methodology development in order to reduce the time and amount of tests during the optimization process. The simulation optimization process requires 3 times less tests than a DoE approach and around 6 to 7 times less tests than a parametric testing approach. In the case of the VVT setting optimization a reduction of the fuel consumption was observed basically due to the pumping losses and IGR reduction. Also the effect of IGR reduction on the exhaust emissions and combustion was observed and analyzed, showing the same trend as observed in last chapter.  $NO_x$  emissions decrease with the EGR rate increase and despite the reduction in IGR.  $NO_x$  emissions did not change compared to the original VVT setting both at maximum EGR rate tested, 15%.  $HC$  emissions were also the same compared with the original VVT setting at 15% of EGR rate. In

the case of  $CO$  emissions, a reduction of 15% was observed at 2000 rpm and an increase of 7.5% was observed at 3000 rpm compared to the original VVT setting both tested at 15% of EGR rate. In general, the optimization of VVT settings reduced the engine fuel consumption in 1.4% at 2000 rpm and 1.8% at 3000 rpm at 15% of EGR rate compared with the original VVT settings conditions, having low impact on exhaust emissions as it was discussed in Chapter 5.

- After the optimization of VVT settings, the injection timing optimization, using the optimum setup found before, was performed in order to further minimize the engine fuel consumption only at 2000 rpm and 10 bar of BMEP. A parametric approach in this part of the optimization was followed, as described in Chapter 5. The parametric study was used to fully analyze the impact of the injection timing on the engine performance and exhaust emissions, and also because it was only one variable to study. It was observed how optimizing the injection timing can reduce the fuel consumption mainly by reducing the CoV of the IMEP, increasing the combustion efficiency and reducing in a low percentage the pumping losses. Regarding the exhaust emissions,  $NO_x$  emissions were increased in 211% (still lower than the original conditions without EGR),  $HC$  emissions were increased 40% and  $CO$  emissions were reduced by 51% compared to the original injection timing conditions with EGR, using the optimum VVT settings and EGR rate setup, as analyzed in Chapter 5. Comparing with the original conditions without EGR, the  $NO_x$  emissions were reduced in 9%,  $CO$  emissions in 62% and  $HC$  emissions were increased in 239%. The optimization of injection timing reduced in 1.7% the engine fuel consumption at 2000 rpm but increased  $NO_x$  emissions and  $HC$  emissions. In this case maybe the injection optimization process and fuel saving does not compensate the increase of  $NO_x$  and  $HC$  emissions.
- A simple parametric approach was also followed for the testing of the three strategies to increase the operational range of EGR or at least improve the engine BSFC at the same EGR rate conditions. Strategies of multi-injection, higher coolant temperature and induced swirl motion were tested at 2000 rpm and 10 bar of BMEP, and later compared to the original condition at 17.5% EGR with the optimized VVT settings setup. Using a multi-injection strategy did not improve the fuel consumption compared to the original optimized VVT settings both at the same EGR rate of 17.5%. The parametric approach for this strategy could not have been the best approach since there were four variables to be optimized.



Therefore, a DoE could have been a better approach, after seeing the difficulties of finding a better configuration than the original injection strategy. In the case of the induced swirl motion, also no reduction of the engine fuel consumption was observed due to mainly hardware limitations because the design and turbulence was specifically designed to work in harmony with the original cylinder head produced turbulence motion. And finally the increase of the coolant temperature operation showed a reduction of 1.3% on the engine fuel consumption at 2000 rpm compared to the original coolant temperature operating conditions. The impact on exhaust emissions was fairly low with an increase of  $NO_x$  by 13% and  $CO$  emissions by 1.6%, and also reduction of  $HC$  emissions by 11%. On the other hand this strategy will increase the knocking risk because of the higher mean temperature of the cycle but the impact on emissions is advantageous compared to optimizing the injection timing because the mixing process and wall wetting it is not changed. Therefore,  $PM$  emissions are going to be maintained at least or even reduced and the impact on the rest of exhaust emissions is much lower. In addition, the optimization process for the injection timing consumes more time and shows a similar fuel consumption advantage.

- Once the optimization process and the different strategies were analyzed, it was seen that at 2000 rpm and 10 bar of BMEP the BSFC could be reduced from 247.4 g/kWh of the original condition without EGR to 231.1 g/kWh with an optimized VVT setting using 17.5% of EGR rate and operating at 100°C of coolant temperature. In the case of 3000 rpm and 10 bar of BMEP there was not possible to perform the tests with higher coolant temperature or injection optimization but despite this issue, the BSFC was reduced from 247.5 g/kWh of original conditions without EGR to 234 g/kWh with the optimized VVT settings setup and using 15% of EGR rate. This research work shows the potential of cooled EGR operating in synergy with other technologies already implemented in modern GTDI engines, such as VVT or direct injection, and also with other strategies that are being developed nowadays to further decrease the fuel consumption of SI gasoline engines.
- An experimental study on the potential of using only lean burn and using cooled EGR with lean burn in a SI gasoline turbocharged direct injection engine has been carried out following parametric and DoE approach respectively. The lean burn strategy showed an engine BSFC improvement of 10% at 2000 rpm and 10 bar of BMEP and 8.1% at 3000 rpm and 10 bar of BMEP. The potential to reduce  $CO$  emissions was

also confirmed, 94% at 2000 rpm and 95% at 3000 rpm. The exhaust temperature was also reduced. But, as it was seen for the optimum lambda values,  $NO_x$  emissions and  $HC$  emissions were increased at 2000 rpm by 14% and 8% respectively, and at 3000 rpm only  $HC$  emissions were increased by 18.5%. The increment in  $HC$  emissions it is not a main problem because an oxidation catalyst could convert this excess; the main drawback is the reduction of  $NO_x$  emissions conversion efficiency of the TWC when the mixture is lean.

- In the tested operating conditions the use of lean burn and cooled EGR at the same time were also studied. The observed BSFC reduction was 9.5% at 2000 rpm and 6% at 3000 rpm at the maximum dilution factor taking into account the dilution from the lean mixture and EGR. The reduction in BSFC was caused mainly by the improvement on the combustion phasing and the reduction on heat and pumping losses. The exhaust gas temperature decrease was due to the decrease on the combustion temperature, and the new combustion duration and phasing. The reduction on  $NO_x$  raw emissions were around 56% at 2000 rpm and 35% at 3000 rpm for the highest dilution factor associated at each operating conditions. The reduction on  $CO$  raw emissions was around 98% at 2000 rpm and 88% at 3000 rpm for the highest dilution factor associated at each operating conditions. In the case of the  $HC$  emissions, they were increased by 30% at 2000 rpm and 20% at 3000 rpm. When analyzing the exhaust emissions after the TWC, the total  $NO_x$ ,  $CO$  and  $HC$  emissions are completely different and they mainly depend on the TWC conversion efficiency. When the engine starts to operate in lean burn conditions the TWC  $NO_x$  conversion efficiency drops from 95% to 0%, and this is the main concern when the engine is operating with lean mixture. The exhaust emissions after the catalyst showed that only a  $CO$  emissions reduction was achieved, because of the TWC conversion efficiency decrease on the  $NO_x$  and  $HC$  emissions due to the lean mixture operating conditions. In the case where cooled EGR and lean burn was used the decrease on  $NO_x$  emissions before the TWC did not compensate the TWC conversion efficiency decrease.
- Cooled EGR and lean burn technologies have a big potential to reduce the engine BSFC, as it was seen in this research work, but it was observed that working in synergy a trade-off for  $NO_x$  emissions was not found when operating in lean burn conditions and cooled EGR was added. In addition, the benefits on fuel consumption are lower at 3000 rpm compared to only using a lean burn strategy, and at 2000 rpm

the fuel consumption was almost the same due to knocking limitation when only using lean burn. Therefore, adding cooled EGR allowed a better combustion phasing at 2000 rpm, although the fuel consumption is the same for both cases. It was observed that, in order to obtain the maximum fuel consumption reduction, only one of the strategies should be used because, when combined, there is no further benefit in fuel consumption. In the case of cooled EGR, the main advantage of only using a TWC as post-treatment system is lost when is operated with lean burn and, in the case of lean burn, the full potential to lower fuel consumption is reduced when is operated with cooled EGR.

### 6.3 Future works

Throughout the development of this PhD-Thesis, diverse remarks and suggestions about future works were brought into consideration because of the limitations of the hardware, budget and time constraints. These could potentially provide the basis for future studies that would further increase the knowledge about new technologies to reduce the fuel consumption in SI gasoline engines or methodologies of optimization that could also help to improve the thermal efficiency of the engine using technologies already developed and operating in synergy. The main remarks and suggestions are listed below:

- Further study should be performed using a multi-injection strategy in synergy with cooled EGR, in order to fully understand and obtain a configuration that could possibly increase the operational range of EGR on the entire engine map. This study should be performed using a DoE approach in order to use the output maps to also find an optimum configuration that could further decrease the fuel consumption with some CFD simulations in order to understand the mixing process. It does not have to be limited to two injections; a third or fourth injection can be added to the study. The developed methodology and results could help understand new strategies of injection and mixture formation. In this research work the software could not perform more than two injections and in addition no DoE approach was followed.
- The study of the dilution limit of this engine with a higher power ignition coils. This would increase the dilution limit of the engine and therefore further reduction on exhaust emissions can be achieved using a lean burn strategy that could require a high  $NO_x$  conversion efficiency SCR

or  $NO_x$  trap in order to comply with the exhaust emissions regulations. It would also help understand the effect of increasing the cooled EGR rate and its full potential with a particular hardware.

- In order to minimize the fuel consumption when cooled EGR is introduced, the engine must be designed with certain characteristics and therefore it would be beneficial to improve mixture ignitability under the operation of cooled EGR by designing and matching the proper injector, piston and cylinder head, to reproduce the optimum condition around the spark plug, but also taking into consideration the formation of  $PM$  emissions. This is an important field of study, since it would improve the kernel formation and therefore increase the dilution limit of the engine.
- It can be interesting to perform a study of the impact of new strategies of multi-injections and new injector, piston and cylinder head designs to operate with cooled EGR on  $PM$  emissions. Since new homologation regulations are being stricter about  $PM$  emissions on SI gasoline engines, this is also an important field of study since cooled EGR could offer a direct solution to this problem.
- Development of control strategies for transient conditions in order to use a LP EGR loop and HP EGR loop, because of their different benefits and possible solutions that could bring to the control strategy. The improvement and development of control strategies are the main limitation for this strategy to be implemented in a mass production engine.
- More efficient and compact EGR coolers are needed in order to decrease the package volume and improve the transient response of the EGR loop. This would also simplify the control strategies and models needed in order to control the amount of EGR rate during transient conditions.
- Implementation and analysis of a two-stage turbocharged gasoline engine using LP EGR loop and HP EGR loop in order to fully understand the limitations of these technologies when are introduced in a two-stage turbocharged engine.
- The development of a variable compression ratio engine that could operate in synergy with cooled EGR in order to analyze the impact and potential on engine performance, combustion and exhaust emissions of both technologies operating at the same time. Obviously the control

strategy at this stage plays an important role and transient operation evaluation should also be the main target of this study.

- Further studies with different compression ratios using cooled EGR and a more retarded intake valve closure in order to reduce as much as possible the compression stroke to expansion stroke ratio. An optimization process and, therefore, a methodology has to be developed in order to study the interaction of compression to expansion stroke ratio, compression ratio, EGR rate and injection strategies.

As it was observed, the list of future works can be infinite at this stage of development in the SI gasoline engines area. It would basically get more and more complex as the development of new technologies and control strategies for these technologies come into the light. SI gasoline engines are going to continue its journey to higher thermal efficiency, and as this journey progress, more complicated interaction and higher amount of variables related to these new technologies are going to come into the scene. That is the main reason why optimization methodologies and control strategies are going to play a big role in the future development of SI gasoline engines.

As downsizing keeps progressing, there is still no clear recipe that it is being followed, but an immense amount of possible technologies can be implemented in order to increase the thermal efficiency of the SI gasoline engine.



# Bibliography

*TSI 2006 Model 3090: engine exhaust particle sizer spectrometer. Operation and service manual (Shoreview, MN: TSI).*  
2006. (cited in pp. 94, 95)

*Energy Technology Perspectives 2012. Pathways to a Clean Energy System.*  
International Energy Agency IEA Publications, 2012. (cited in p. 20)

*D-Optimal Designs, Mathworks help guide,* 2016. (cited in p. 109)

**Aakko P. and Nylund N.**

Particle Emissions at Moderate and Cold Temperatures Using Different Fuels.  
In *SAE Technical Paper*, 2003.  
2003-01-3285. (cited in p. 34)

**Abdul-Khalek I., Kittelson D. and Brear F.**

The Influence of Dilution Conditions on Diesel Exhaust Particle Size Distribution Measurements.  
In *SAE Technical Paper*, 1999.  
1999-01-1142. (cited in p. 93)

**Akihisa D. and Daisaku S.**

Research on Improving Thermal Efficiency through Variable Super-High Expansion Ratio Cycle.  
In *SAE Technical Paper*, 2010.  
2010-01-0174. (cited in p. 48)

**Alger T., Chauvet T. and Dimitrova Z.**

Synergies between High EGR Operation and GDI Systems.  
*SAE Int. J. Engines*, Vol. 1 n° 1, pp. 101–114, 2008.  
2008-01-0134. (cited in pp. 34, 59, 60, 125, 139, 174, 230, 236)

**Alger Terrence, Gingrich Jess, Khalek Imad A. and Mangold Barrett.**

The Role of EGR in PM Emissions from Gasoline Engines.  
*SAE Int. J. Fuels Lubr.*, Vol. 3 n° 1, pp. 85–98, 2010.  
2010-01-0353. (cited in pp. 60, 136, 152, 174)

**Alger Terry and Mangold Barrett.**

Dedicated EGR: A New Concept in High Efficiency Engines.  
*SAE Int. J. Engines*, Vol. 2 n° 1, pp. 620–631, 2009.  
2009-01-0694. (cited in p. 117)

**Andersen, J. and Karlsson E. and Gawell A.**

Variable Turbine Geometry on SI Engines.

In *SAE Technical Paper*, 2006.

2006-01-0020.

(cited in p. 47)

**Armas O.**

*Diagnostico experimental del proceso de combustion en motores Diesel de inyeccion directa.*

Tesis Doctoral, PhD-Thesis. Universitat Politecnica de Valencia, Departamento de Maquinas

y Motores Termicos, 1998.

(cited in p. 101)

**Bandel W., Fraidl G. K., Kapus P. E., Sikinger H. and Cowland C. N.**

The Turbocharged GDI Engine: Boosted Synergies for High Fuel Economy Plus Ultra-low Emission.

In *SAE Technical Paper*, 2006.

2006-01-1266.

(cited in pp. 15, 114, 139, 175)

**Battistoni M., Foschini L., Postriotti L. and Cristiani M.**

Development of an Electro-Hydraulic Camless VVA System.

In *SAE Technical Paper*, 2007.

2007-24-0088.

(cited in p. 43)

**Benajes J. V., Lopez J. J., Novella R. and Garcia A.**

Advanced Methodology for improving testing efficiency in a single-cylinder research diesel engine.

*Experimental Techniques*, Vol. 32 n° 6, pp. 41–47, 2008.

(cited in p. 102)

**Benajes Jesus, Bermudez Vicente, Climent Hector and Rivas-Perea Manuel Eduardo.**

Instantaneous pressure measurement in pulsating high temperature internal flow in ducts.

*Applied Thermal Engineering*, Vol. 61 n° 2, pp. 48–54, 2013.

(cited in p. 89)

**Benajes Jesus, Olmeda Pablo, Martin Jaime and Carreno Ricardo.**

A new methodology for uncertainties characterization in combustion diagnosis and thermodynamic modelling.

*Applied Thermal Engineering*, Vol. 71 n° 1, pp. 389–399, 2014.

(cited in p. 90)

**Beretta G. P., Rashidi M. and Keck J. C.**

Turbulent flame propagation and combustion in spark ignition engines.

*Combustion and Flame*, Vol. 52 n° 0, pp. 217–245, 1983.

(cited in p. 24)

**Bermudez V., Lujan J. M., Climent H. and Campos D.**

Assessment of pollutants emission and aftertreatment efficiency in a GTDi engine including cooled LP-EGR system under different steady-state operating conditions.

*Applied Energy*, Vol. 158, pp. 459–473, 2015.

(cited in pp. 8, 59, 137, 156)

**Bourhis Guillaume, Chauvin Jonathan, Gautrot Xavier and de Franco Loic.**

LP EGR and IGR Compromise on a GDI Engine at Middle Load.

*SAE Int. J. Engines*, Vol. 6 n° 1, pp. 67–77, 2013.

2013-01-0256.

(cited in p. 182)

**Bozza F., Gimelli A. and Tuccillo R.**

The Control of a VVA-Equipped SI Engine Operation by Means of 1D Simulation and Mathematical Optimization.

In *SAE Technical Paper*, 2002.

2002-01-1107.

(cited in p. 174)



**Bozza F. and Torella E.**

The Employment of a 1D Simulation Model for A/F Ratio Control in a VVT Engine.  
In *SAE Technical Paper*, 2003.  
2003-01-0027. (cited in p. 174)

**Braisher M., Stone R. and Price P.**

Particle Number Emissions from a Range of European Vehicles.  
In *SAE Technical Paper*, 2010.  
2010-01-0786. (cited in p. 34)

**Cairns A., Blaxill H. and Irlam G.**

Exhaust Gas Recirculation for Improved Part and Full Load Fuel Economy in a Turbocharged Gasoline Engine.  
In *SAE Technical Paper*, 2006.  
2006-01-0047. (cited in pp. 59, 65, 114, 139, 174, 236)

**Cairns Alasdair, Fraser Neil and Blaxill Hugh.**

Pre Versus Post Compressor Supply of Cooled EGR for Full Load Fuel Economy in Turbocharged Gasoline Engines.  
In *SAE Technical Paper*, 2008.  
2008-01-0425. (cited in p. 115)

**Carvalho Leonardo, Melo Tadeu and Neto Rubelmar.**

Investigation on the Fuel and Engine Parameters that Affect the Half Mass Fraction Burned, CA50, Optimum Crank Angle.  
In *SAE Technical Paper*, 2012.  
2012-36-0498. (cited in p. 129)

**Chan T., Meloche E., Kubsh J., Rosenblatt D., Brezny R. and Rideout G.**

Evaluation of a Gasoline Particulate Filter to Reduce Particle Emissions from a Gasoline Direct Injection Vehicle.  
*SAE Int. J. Fuels Lubr.*, Vol. 5 n° 3, pp. 1277–1290, 2012. (cited in p. 41)

**Climent H.**

*Contribucion al modelado unidimensional de motores de dos tiempos de pequena cilindrada.*  
Tesis Doctoral, Ph.D-Thesis. Universitat Politecnica de Valencia, Departamento de Maquinas y Motores Termicos, 2002. (cited in p. 98)

**Coltman D., Turner J. W. G., Curtis R., Blake D., Holland B., Pearson R. J., Arden A. and Nuglisch H.**

Project Sabre: A Close-Spaced Direct Injection 3-Cylinder Engine with Synergistic Technologies to Achieve Low CO<sub>2</sub> Output.  
*SAE Int. J. Engines*, Vol. 1 n° 1, pp. 129–146, 2008.  
2008-01-0138. (cited in pp. 7, 46)

**Daugherty R.L. and Franzini J.B.**

*Fluid Mechanics.*  
McGraw-Hill, New York, 1965. (cited in p. 98)

**De Bortoli Cassiani M., Bittencourt M., Galli L. and Villalva S.**

Variable Compression Ratio Engines.  
In *SAE Technical Paper*, 2009.  
2009-36-0245. (cited in p. 54)

**Degraeuwe B.**

*Contribution to the thermal management of DI Diesel engines.*

Tesis Doctoral, PhD thesis. Universitat Politecnica de Valencia, Departamento de Maquinas y Motores Termicos, 2007. (cited in p. 103)

**Desantes J.M., Berm dez V., Molina S. and Linares W.**

Methodology for measuring exhaust aerosol size distributions using an engine test under transient operating conditions.

*Measurement Science and Technology*, Vol. 22 n  11, pp. 115101, 2011. (cited in p. 93)

**Eichenberger D. A. and Roberts W. L.**

Effect of unsteady stretch on spark-ignited flame kernel survival.

*Combustion and Flame*, Vol. 118 n  3, pp. 469–478, 1999. (cited in p. 23)

**França O.**

Impact of the Miller Cycle in the Efficiency of an FVVT (Fully Variable Valve Train) Engine During Part Load Operation.

In *SAE Technical Paper*, 2009.

2009-36-0081. (cited in p. 52)

**Fraser Neil, Blaxill Hugh, Lumsden Grant and Bassett Mike.**

Challenges for Increased Efficiency through Gasoline Engine Downsizing.

*SAE Int. J. Engines*, Vol. 2 n  1, pp. 991–1008, 2009.

2009-01-1053. (cited in p. 114)

**Galindo J., Lujan J. M., Serrano J. R., Dolz V. and Guilain S.**

Design of an exhaust manifold to improve transient performance of a high-speed turbocharged diesel engine.

*Experimental Thermal and Fluid Science*, Vol. 28 n  8, pp. 863–875, 2004.

(cited in p. 104)

**Galindo J., Serrano J. R., Guardiola C. and Cervello C.**

Surge limit definition in a specific test bench for the characterization of automotive turbochargers.

*Experimental Thermal and Fluid Science*, Vol. 30 n  5, pp. 449–462, 2006.

(cited in p. 98)

**George S., Morris G., Dixon J., Pearce D. and Heslop G.**

Optimal Boost Control for an Electrical Supercharging Application.

In *SAE Technical Paper*, 2004.

2004-01-0523. (cited in p. 47)

**Glahn C., Kluin M., Konigstein A. and Cloos L.K.**

Cooled External EGR - System Optimization of the Cooling and Charging System on a 3-Cylinder Gasoline DI T/C Engine.

In *24th Aachen Colloquium Automobile and Engine Technology*, pp. 189–204, 2015.

(cited in pp. 39, 47, 63, 64, 65, 66, 67)

**Gomez A. and Reinke P.**

Lean burn: A Review of Incentives, Methods, and Tradeoffs.

In *SAE Technical Paper*, 1988.

880291. (cited in pp. 13, 55)

**Goto Satoru and Fukuda Takahiro.**

Study on NOx formation and reduction of lean-burn spark ignition gas engine.

*JSAE Review*, Vol. 19 n  4, pp. 351–354, 1998.

(cited in p. 31)

**Grandin B. and Angstrom H. E.**

Replacing Fuel Enrichment in a Turbo Charged SI Engine: Lean Burn or Cooled EGR.  
In *SAE Technical Paper*, 1999.  
1999-01-3505. (cited in pp. 56, 59, 176)

**Grandin B., Angstrom H. E., Stalhammar P. and Olofsson E.**

Knock Suppression in a Turbocharged SI Engine by Using Cooled EGR.  
In *SAE Technical Paper*, 1998.  
982476. (cited in pp. 58, 59, 60, 114, 129)

**Guillemot P.**

*Les émissions de polluants des moteurs à allumage commandé.*  
École du Pétrole et des Moteurs, 2008. (cited in p. 33)

**Gukelberger Raphael, Alger Terrence, Mangold Barrett, Boehler Jeff and Eiden Corey.**

Effects of EGR Dilution and Fuels on Spark Plug Temperatures in Gasoline Engines.  
*SAE Int. J. Engines*, Vol. 6 n° 1, pp. 447–455, 2013.  
2013-01-1632. (cited in pp. 60, 61, 176)

**Gurupatham Anand and Teraji Atsushi.**

A Study of Rich Flame Propagation in Gasoline SI Engine Based on 3D Numerical Simulations.  
In *SAE Technical Paper*. The Automotive Research Association of India, 2011.  
2011-28-0125. (cited in p. 141)

**Hacohen J., Ashcroft S. J. and Belmont M. R.**

Lean Burn Versus EGR S. I. Engine.  
In *SAE Technical Paper*, 1995.  
951902. (cited in pp. 57, 58, 176)

**Happer W.**

The Truth About Greenhouse Gases.  
In *The Global Warming Policy Foundation*, pp. 57–61, 2011.  
Briefing Paper No 3. (cited in pp. 6, 7)

**Hara S., Suga S., Watanabe S. and Nakamura M.**

Variable valve actuation systems for environmentally friendly engines.  
*Hitachi Review*, Vol. 58 n° 7, pp. 319–324, 2009. (cited in p. 44)

**He Y.**

Development and Application of a Lean NOX Trap Model.  
In *SAE Technical Paper*, 2006.  
2006-01-0686. (cited in p. 40)

**Hepburn J., Patel K., Meneghel M. and Gandhi H.**

Development of Pd-only Three Way Catalyst Technology.  
In *SAE Technical Paper*, 1994.  
941058. (cited in p. 9)

**Herbst F., Staber-Schmidt C., Eilts P., Sextro T., Kammeyer J., Natkaniec C., Seume J., Porzig D. and Schwarze H.**

The Potential of Variable Compressor Geometry for Highly Boosted Gasoline Engines.  
In *SAE Technical Paper*, 2011.  
2011-01-0376. (cited in p. 47)

**Hermann, F. Zeuch T. and Klingmann J.**

The Effect of Diluents on the Formation Rate of Nitrogen Oxide in a Premixed Laminar Flame.

In *ASME 2004 Proceedings Combustion and Fuels*, Vienna, Austria, 2004.

(cited in pp. 31, 153)

**Hettinger A. and Kulzer A.**

A New Method to Detect Knocking Zones.

*SAE Int. J. Engines*, Vol. 2 n° 1, pp. 645–665, 2009.

(cited in p. 11)

**Heywood J. B.**

*Internal combustion engine fundamentals*.

Ed. McGraw-Hill Science/Engineering/Math, 1988.

(cited in p. 35)

**Hill P. G. and Zhang D.**

The effects of swirl and tumble on combustion in spark-ignition engines.

*Progress in Energy and Combustion Science*, Vol. 20 n° 5, pp. 373–429, 1994.

(cited in p. 25)

**Hiroyuki Oda, Yasuyuki Morita, Toshimitsu Fujishima and Masashi Marubara.**

Investigation of High-Compression Lean Burn Engine.

In *SAE Technical Paper*, 1987.

871215.

(cited in p. 55)

**Hoegh-Guldberg O., Mumby P. J., Hooten A. J., Steneck R. S., Greenfield P., Gomez E., Harvell C. D. and Sale P. F.**

Coral Reefs Under Rapid Climate Change and Ocean Acidification.

*Science*, Vol. 318 n° 5857, pp. 1737–1742, 2007.

(cited in p. 7)

**Hohenberg G.**

Definition und Eigenschaften des thermodynamischen Verlustwinkels von Kolbenmaschinen.

*Automobile Index 4*, pp. 15–21, 1976.

(cited in p. 90)

**Hosaka T. and Hamazaki M.**

Development of the Variable Valve Timing and Lift (VTEC) Engine for the Honda NSX.

In *SAE Technical Paper*, 1991.

910008.

(cited in p. 43)

**Jiang S., Nutter D. and Gullitti A.**

Implementation of Model-Based Calibration for a Gasoline Engine.

In *SAE Technical Paper*, 2012.

2012-01-0722.

(cited in p. 175)

**John J.**

Lean Burn Engine Concepts-Emissions and Economy.

In *SAE Technical Paper*, 1975.

750930.

(cited in p. 55)

**Kaiser M., Krueger U., Harris R. and Cruff L.**

Doing More with Less - The Fuel Economy Benefits of Cooled EGR on a Direct Injected Spark Ignited Boosted Engine.

In *SAE Technical Paper*, 2010.

2010-01-0589.

(cited in pp. 59, 104)

**Kalghatgi Gautam T.**

Spark Ignition, Early Flame Development and Cyclic Variation in I.C. Engines.  
In *SAE Technical Paper*, 1987.  
870163. (cited in p. 23)

**Karjalainen Panu, Pirjola Liisa, Heikkilä Juha, Lahde Tero, Tzamkiozis Theodoros, Ntziachristos Leonidas, Keskinen Jorma and Ronkko Topi.**

Exhaust particles of modern gasoline vehicles: A laboratory and an on-road study.  
*Atmospheric Environment*, Vol. 97, pp. 262–270, 2014. (cited in p. 49)

**Kawamoto M., Honda T., Katashiba H., Sumida M., Fukutomi N. and Kawajiri K.**

A Study of Center and Side Injection in Spray Guided DISI Concept.  
In *SAE Technical Paper*, 2005.  
2005-01-0106. (cited in p. 9)

**Kiga S., Mae Y., Akasaka Y. and Tomogane K.**

Development of Innovative Variable Valve Event and Lift (VVVEL) System.  
In *SAE Technical Paper*, 2007.  
2007-01-3548. (cited in p. 43)

**Kinoshita K., Ueda K., Ito F., Shinojima Y., Yanagizawa T., Sakaguchi T. and Yamazaki T.**

Development of a Custom Integrated Circuit for Continuously Variable Valve Lift Mechanism System Control.  
In *SAE Technical Paper*, 2008.  
2008-01-0913. (cited in p. 43)

**Kleeberg Henning, Tomazic Dean, Dohmen J<sub>Ä</sub><sup>1</sup>/<sub>4</sub>rgen, Wittek Karsten and Balazs Andreas.**

Increasing Efficiency in Gasoline Powertrains with a Two-Stage Variable Compression Ratio (VCR) System.  
In *SAE Technical Paper*, 2013.  
2013-01-0288. (cited in p. 54)

**Knop V. and Essayem E.**

Comparison of PFI and DI Operation in a Downsized Gasoline Engine.  
*SAE Int. J. Engines*, Vol. 6 n<sup>o</sup> 2, pp. 941–952, 2013. (cited in p. 48)

**Ko Y., Arpacı V. S. and Anderson R. W.**

Spark ignition of propane-air mixtures near the minimum ignition energy: Part II. A model development.  
*Combustion and Flame*, Vol. 83 n<sup>o</sup> 1-2, pp. 88–105, 1991. (cited in p. 23)

**Kumano K. and Yamaoka S.**

Analysis of Knocking Suppression Effect of Cooled EGR in Turbo-Charged Gasoline Engine.  
In *SAE Technical Paper*, 2014.  
2014-01-1217. (cited in pp. 60, 114)

**Ladommatos N., Abdelhalim S. and Zhao H.**

Control of oxides of nitrogen from diesel engines using diluents while minimising the impact on particulate pollutants.  
*Applied Thermal Engineering*, Vol. 18 n<sup>o</sup> 11, pp. 963–980, 1998. (cited in p. 32)

- Lancaster David R., Krieger Roger B., Sorenson Spencer C. and Hull William L.**  
Effects of Turbulence on Spark-Ignition Engine Combustion.  
In *SAE Technical Paper*, 1976. (cited in p. 21)
- Lapuerta M.**  
*Un modelo de combustion fenomenologico para un motor Diesel de inyeccion directa rapido.*  
Tesis Doctoral, PhD-Thesis. Universitat Politecnica de Valencia, Departamento de Maquinas y Motores Termicos, 1988. (cited in p. 101)
- Lapuerta M., Armas O. and Hernandez J. J.**  
Diagnosis of DI Diesel combustion from in-cylinder pressure signal by estimation of mean thermodynamic properties of the gas.  
*Applied Thermal Engineering*, Vol. 19 n<sup>o</sup> 5, pp. 513–529, 1999. (cited in pp. 101, 102)
- Lecoite B. and Monnier G.**  
Downsizing a Gasoline Engine Using Turbocharging with Direct Injection.  
In *SAE Technical Paper*, 2003.  
2003-01-0542. (cited in p. 11)
- Li Y., Zhao H., Stansfield P. and Freeland P.**  
Synergy between Boost and Valve Timings in a Highly Boosted Direct Injection Gasoline Engine Operating with Miller Cycle.  
In *SAE Technical Paper*, 2015.  
2015-01-1262. (cited in p. 52)
- Liu F., Pfeiffer J., Caudle R., Marshall P. and Olin P.**  
Low Pressure Cooled EGR Transient Estimation and Measurement for an Turbocharged SI Engine.  
In *SAE Technical Paper*, 2016.  
2016-01-0618. (cited in p. 117)
- Lou Z., Wen S, Qian J., Xu H., Zhu G. and Sun M.**  
Camless Variable Valve Actuator with Two Discrete Lifts.  
In *SAE Technical Paper*, 2015.  
2015-01-0324. (cited in p. 43)
- Lujan J., Bermudez V., Serrano J. and Cervello C.**  
Test bench for turbocharger groups characterization.  
In *SAE Technical Paper*, 2002.  
2002-01-0163. (cited in p. 98)
- Lujan J., Pastor J., Climent H. and Rivas M.**  
Experimental Characterization and Modelling of a Turbocharger Gasoline Engine Compressor By-Pass Valve in Transient Operation.  
In *SAE Technical Paper*, 2015.  
2015-24-2524. (cited in p. 174)
- Lujan Jose Manuel, Climent Hector, Novella Ricardo and Rivas-Perea Manuel Eduardo.**  
Influence of a low pressure EGR loop on a gasoline turbocharged direct injection engine.  
*Applied Thermal Engineering*, Vol. 89, pp. 432–443, 2015. (cited in pp. 60, 64, 174)

**Lujan Jose Manuel, Climent Hector, Pla Benjamin, Rivas-Perea Manuel Eduardo, Francois Nicolas-Yoan, Borges-Alejo Jose and Soukeur Zoulikha.**

Exhaust gas recirculation dispersion analysis using in-cylinder pressure measurements in automotive diesel engines.

*Applied Thermal Engineering*, Vol. 89, pp. 459–468, 2015. (cited in p. 39)

**Lumsden G., Eddleston D. and Sykes R.**

Comparing Lean Burn and EGR.

In *SAE Technical Paper*, 1997.

970505. (cited in pp. 56, 114, 176)

**Luttermann C., Schunemann E. and Klauer N.**

Enhanced VALVETRONIC Technology for Meeting SULEV Emission Requirements.

In *SAE Technical Paper*, 2006.

2006-01-0849. (cited in p. 43)

**Makarow M., Ceulemans R. and Horn L.**

Impacts of Ocean Acidification.

In Foundation European Science, editor, *Science Policy Briefing*, 2009. (cited in p. 7)

**Maly R.**

*Initiation and Propagation of Flame Fronts in Lean CH<sub>4</sub>-Air Mixtures by the Three Modes of Ignition Spark in Fuel Economy in Road Vehicles Powered by Spark-Ignition Engines.*

Hilliard, J. C. and Springer, G. S. Plenum Press, New York, 1984. (cited in p. 22)

**Maly R.**

*Spark Ignition: Its Physics and Effect on the Internal Combustion Engine in Fuel Economy in Road Vehicles Powered by Spark-Ignition Engines.*

Hilliard, J. C. and Springer, G. S. Plenum Press, New York, 1984. (cited in p. 22)

**Mathis U., Mohr M. and Zenobi R.**

Effect of organic compounds on nanoparticle formation in diluted diesel exhaust.

*Atmospheric Chemistry and Physics Discussions*, 2004. (cited in p. 93)

**Mathis Urs, Mohr Martin and Forss Anna-Maria.**

Comprehensive particle characterization of modern gasoline and diesel passenger cars at low ambient temperatures.

*Atmospheric Environment*, Vol. 39 n<sup>o</sup> 1, pp. 107–117, 2005. (cited in p. 34)

**Michaels H. C. and Fulper B. K.**

Nitrous oxide emission factors for mobile sources US EPA.

In *AWMA emissions inventory conference*, New Orleans, USA, 1998. (cited in p. 32)

**Michel C. and Eckard H.**

Critical evaluation of the European diesel car boom - global comparison, environmental effects and various national strategies.

In *Environmental Sciences Europe*, 2013. (cited in pp. 4, 20)

**Miklanek L., Vitek O., Gotfryd O. and Klir V.**

Study of Unconventional Cycles (Atkinson and Miller) with Mixture Heating as a Means for the Fuel Economy Improvement of a Throttled SI Engine at Part Load.

*SAE Int. J. Engines*, Vol. 5 n<sup>o</sup> 4, pp. 1624–1636, 2012. (cited in p. 52)

**Mohr M., Forss A.N. and Lehmann U.**

Particle Emissions from Diesel Passenger Cars Equipped with a Particle Trap in Comparison to Other Technologies.

*Environmental Science & Technology*, Vol. 40 n° 7, pp. 2375–2383, 2006.

PMID: 16646477.

(cited in p. 34)

**Molenkamp H.**

Zur Genauigkeit der Brenngesetzrechnung eines Dieselmotors mit Nichtunterteiltem Brennraum.

*MTZ Motortechnische Zeitschrift*, Vol. 37 n° 7-8, pp. 285–291, 1976.

(cited in p. 102)

**Montajir R., Kawai T., Goto Y. and Odaka M.**

Thermal Conditioning of Exhaust Gas: Potential for Stabilizing Diesel Nano-Particles.

In *SAE Technical Paper*, 2005.

2005-01-0187.

(cited in p. 93)

**Mori S. and Shimizu R.**

Analysis of EGR Cyclic Variations in a Direct Injection Gasoline Engine by Using Raman Scattering Method.

In *SAE Technical Paper*, 2002.

2002-01-1646.

(cited in pp. 48, 49, 62)

**Ntziachristos L., Amanatidis S., Samaras Z., Janka K. and Tikkanen J.**

Application of the Pegasor Particle Sensor for the Measurement of Mass and Particle Number Emissions.

*SAE Int. J. Fuels Lubr.*, Vol. 6 n° 2, pp. 521–531, 2013.

2013-01-1561.

(cited in p. 8)

**O'Dell P. R.**

Why carbon fuels will dominate.

In *The 21st Century's Global Energy Economy Conference*. Brentwood, Multi-Science, 2004.

(cited in p. 32)

**Ouellette, P. Douville B. Hill P. G. and Ursu B.**

NOx reduction in a directly injected natural gas engine.

In *Proceedings of the ASME 1998 Internal Combustion Engine Division Fall Technical Conference*, September 2008.

(cited in p. 32)

**Pallotti P., Torella E., New J., Criddle M. and Brown J.**

Application of an Electric Boosting System to a Small, Four-Cylinder S.I. Engine.

In *SAE Technical Paper*, 2003.

2003-32-0039.

(cited in p. 47)

**Patterson Donald J.**

Cylinder Pressure Variations, A Fundamental Combustion Problem.

In *SAE Technical Paper*, volume 660129, 1966.

660129.

(cited in p. 24)

**Payri F., Benajes J., Galindo J. and Serrano J. R.**

Modelling of turbocharged diesel engines in transient operation. Part 2: Wave action models for calculating the transient operation in a high speed direct injection engine.

*Proceedings of the Institution of Mechanical Engineers, Part D: Journal of Automobile Engineering*, Vol. 216 n° 6, pp. 479–493, 2002.

10.1243/09544070260137507.

(cited in p. 104)



**Payri F., Lujan J., Climent H. and Pla B.**

Effects of the Intake Charge Distribution in HSDI Engines.

In *SAE Technical Paper*, 2010.

2010-01-1119.

(cited in pp. 92, 121)

**Payri F., Margot X., Gil A. and Martin J.**

Computational Study of Heat Transfer to the Walls of a DI Diesel Engine.

In *SAE Technical Paper*, 2005.

2005-01-0210.

(cited in p. 103)

**Payri F., Molina S., Martin J. and Armas O.**

Influence of measurement errors and estimated parameters on combustion diagnosis.

*Applied Thermal Engineering*, Vol. 26 n° 23, pp. 226–236, 2006.

(cited in p. 102)

**Payri F., Reyes E. and Galindo J.**

Analysis and Modeling of the Fluid-Dynamic Effects in Branched Exhaust Junctions of ICE.

*Journal of Engineering for Gas Turbines and Power*, Vol. 123 n° 1, pp. 197–203, 2000.

10.1115/1.1339988.

(cited in p. 104)

**Payri Francisco, Olmeda Pablo, Martin Jaime and Carreno Ricardo.**

A New Tool to Perform Global Energy Balances in DI Diesel Engines.

*SAE Int. J. Engines*, Vol. 7 n° 1, pp. 43–59, 2014.

2014-01-0665.

(cited in p. 102)

**Peters N.**

Laminar flamelet concepts in turbulent combustion.

*Symposium (International) on Combustion*, Vol. 21 n° 1, pp. 1231–1250, 1988.

(cited in p. 24)

**Peters N. and Williams F. A.**

Premixed combustion in a vortex.

*Symposium (International) on Combustion*, Vol. 22 n° 1, pp. 495–503, 1989.**Potteau S., Lutz P., Leroux S., Moroz S. and Tomas E.**

Cooled EGR for a Turbo SI Engine to Reduce Knocking and Fuel Consumption.

In *SAE Technical Paper*, 2007.

2007-01-3978.

(cited in pp. 14, 59, 60, 114, 127, 139)

**Price P., Stone R., OudeNijeweme D. and Chen X.**

Cold Start Particulate Emissions from a Second Generation DI Gasoline Engine.

In *SAE Technical Paper*, 2007.

2007-01-1931.

(cited in pp. 48, 49)

**Pulkrabek Willard W.***Engineering Fundamentals of the Internal Combustion Engine*.

Upper Saddle River, New Jersey 07548, 1997.

(cited in pp. 22, 26)

**Raimann J., Arndt S., Grzeszik R., Ruthenberg and Worner P.**

Optical Investigations in Stratified Gasoline Combustion Systems with Central Injector Position Leading to Optimized Spark Locations for Different Injector Designs.

In *SAE Technical Paper*, 2003.

2003-01-3152.

(cited in p. 13)

**Ridgwell A. and Zeebe R. E.**

The role of the global carbonate cycle in the regulation and evolution of the Earth system.

*Earth Planet. Sci. Lett.*, Vol. 234, pp. 299–315, 2005.

(cited in p. 7)

**Roberts M.**

Benefits and Challenges of Variable Compression Ratio (VCR).

In *SAE Technical Paper*, 2003.

2003-01-0398.

(cited in p. 54)

**Saito C., Nakatani T., Miyairi Y., Yuuki K., Makino M., Kurachi H., Heuss W., Kuki T., Furuta Y., Kattouah P. and Vogt C.D.**

New Particulate Filter Concept to Reduce Particle Number Emissions.

In *SAE Technical Paper*, 2011.

2011-01-0814.

(cited in p. 41)

**Saito H., Shirasuna T. and Nomura T.**

Extension of Lean Burn Range by Intake Valve Offset.

*SAE Int. J. Engines*, Vol. 6 n° 4, pp. 2072–2084, 2013.

2013-32-9032.

(cited in p. 56)

**Sarlashkar J., Rengarajan S. and Roecker R.**

Transient Control of a Dedicated EGR Engine.

In *SAE Technical Paper*, 2016.

2016-01-0616.

(cited in p. 117)

**Schwaderlapp M., Habermann K. and Yapici K.**

Variable Compression Ratio - A Design Solution for Fuel Economy Concepts.

In *SAE Technical Paper*, 2002.

2002-01-1103.

(cited in p. 54)

**Serrano Jose, Climent Hector, Dolz Vicente and Rivas Manuel Eduardo.**

Analysis of Variable Geometry Turbine and Variable Valve Timing Combined Potential in a GTDI Engine Using 1D Simulation.

In *SIA Congress*, 2011.

(cited in pp. 104, 105)

**Shahed S. M. and Bauer Karl-Heinz.**

Parametric Studies of the Impact of Turbocharging on Gasoline Engine Downsizing.

In *SAE Technical Paper*. SAE International, 2009.

2009-01-1472.

(cited in p. 114)

**Sher Eran and Keck James C.**

Spark ignition of combustible gas mixtures.

*Combustion and Flame*, Vol. 66 n° 1, pp. 17–25, 1986.

(cited in p. 22)

**Soltic P. and Hausberger S.**

On-Road Emission Measurements and emission modeling results for a tractor-semi trailer in Trans-Alpine operation.

*13th International Scientific Symposium Transport and Air Pollution Boulder*, September 13-15, 2004.

(cited in p. 32)

**Steven A.**

Attacking GDI engine particulate emissions.

In *Automotive Engineering Magazine*, 2014.

13624.

(cited in pp. 36, 38)

**Stevens E. and Steeper R.**

Piston Wetting in an Optical DISI Engine: Fuel Films, Pool Fires, and Soot Generation.

In *SAE Technical Paper*, 2001.

2001-01-1203.

(cited in pp. 35, 36, 37, 201)

**Stone R.**

*Introduction to Internal Combustion Engines.*

Palgrave Macmillan, England, 4th edition edition, 2012. (cited in p. 43)

**Szczepanski D.**

*Factors influencing NOx emissions at Tarong and Stanwell power stations.*

Tesis Doctoral, PhD-Thesis. The University of Queensland, 1998. (cited in p. 32)

**Takaki D., Tsuchida H., Kobara T., Akagi M., Tsuyuki T. and Nagamine M.**

Study of an EGR System for Downsizing Turbocharged Gasoline Engine to Improve Fuel Economy.

In *SAE Technical Paper*, 2014.

2014-01-1199. (cited in pp. 62, 65, 66, 115, 116)

**Tang Qijun, Liu Jingping, Zhan Zhangsong and Hu Tiegang.**

Influences on Combustion Characteristics and Performances of EGR vs. Lean Burn in a Gasoline Engine.

In *SAE Technical Paper*, 2013.

2013-01-1125. (cited in pp. 176, 229, 230)

**Thirouard M. and Pacaud P.**

Increasing Power Density in HSDI Engines as an Approach for Engine Downsizing.

*SAE Int. J. Engines*, Vol. 3 n° 2, pp. 56–71, 2010. (cited in p. 11)

**Torregrosa A., Olmeda P., Degraeuwe B. and Reyes M.**

A concise wall temperature model for DI Diesel engines.

*Applied Thermal Engineering*, Vol. 26 n° 11-12, pp. 1320–1327, 2006. (cited in p. 103)

**Torregrosa A. J., Galindo J., Guardiola C. and Varnier O.**

Combined experimental and modeling methodology for intake line evaluation in turbocharged diesel engines.

*International Journal of Automotive Technology*, Vol. 12 n° 3, pp. 359–367, 2011.

(cited in p. 104)

**Turner, J. W. Popplewell A. Patel R. Johnson T. R. Darnton N. J. Richardson S. Bredda S. W. Tudor R. J. Bithell C. I. Jackson R. Remmert S. M. Cracknell R. F. Fernandes J. X. Lewis A. G. J. Akehurst S. Brace C. J. Copeland C. Martinez-Botas R. Romagnoli A. and Burluka A. A.**

Ultra Boost for Economy: Extending the Limits of Extreme Engine Downsizing.

*SAE Int. J. Engines*, Vol. 7 n° 1, pp. 387–417, 2014.

2014-01-1185. (cited in p. 46)

**Varnier O.**

*Trends and Limits of Two-Stage Boosting Systems for Automotive Diesel Engines.*

Tesis Doctoral, Ph.D-Thesis. Universitat Politècnica de València, Departamento de

Maquinas y Motores Termicos, 2012. (cited in p. 45)

**Verhoeven Dean.**

Spark Heat Transfer Measurements in Flowing Gases.

In *SAE Technical Paper*, 1995.

952450. (cited in p. 23)

**Vijayaraghavan K., Lindhjem C., DenBleyker A., Nopmongcol U., Grant J., Tai E. and Yarwood G.**

Effects of light duty gasoline vehicle emission standards in the United States on ozone and particulate matter.

*Atmospheric Environment*, Vol. 60, pp. 109–120, 2012. (cited in pp. 5, 175)

**Vitek O., Macek J. and Polasek M.**

New Approach to Turbocharger Optimization using 1-D Simulation Tools.

In *SAE Technical Paper*, 2006.

2006-01-0438.

(cited in p. 174)

**Vitek O., Macek J., Polasek M., Schmerbeck S. and Kammerdiener T.**

Comparison of Different EGR Solutions.

In *SAE Technical Paper*, 2008.

2008-01-0206.

(cited in p. 114)

**Wang B., Monasbach S., Schmutzhard S., Shuai S., Huang Y. and Kraft M.**

Modelling soot formation from wall films in a gasoline direct injection engine using a detailed population balance model.

In *Preprint Article. Department of Chemical Engineering and Biotechnology, University of Cambridge*, 2015. (cited in p. 31)

**Wang C., Daniel R. and Ma X.**

Comparison of Gasoline (ULG), 2,5-Dimethylfuran (DMF) and Bio-Ethanol in a DISI Miller Cycle with Late Inlet Valve Closing Time.

In *SAE Technical Paper*, 2012.

2012-01-1147.

(cited in p. 53)

**Ward Michael A. V.**

High-Energy Spark-Flow Coupling in an IC Engine for Ultra-Lean and High EGR Mixtures.

In *SAE Technical Paper*. SAE International, 2001.

2001-01-0548.

(cited in p. 176)

**Warey A., Huang Y., Matthews R., Hall M. and Ng H.**

Effects of Piston Wetting on Size and Mass of Particulate Matter Emissions in a DISI Engine.

In *SAE Technical Paper*, 2002.

2002-01-1140.

(cited in p. 9)

**Watanabe I., Kawai T., Yonezawa K and Ogawa T.**

The New Toyota 2.0-Liter Inline 4-Cylinder ESTEC D-4ST Engine - Turbocharged Direct Injection Gasoline Engine -.

In *23rd Aachen Colloquium Automobile and Engine Technology*, 2014.

(cited in pp. 11, 43, 48)

**Weernink W.O.**

*Europeans, Japanese intensify hybrid, diesel debate*, volume 8.

Europe: Automotive News, 2003.

(cited in p. 20)

**Wei Haiqiao, Zhu Tianyu, Shu Gequn, Tan Linlin and Wang Yuesen.**

Gasoline engine exhaust gas recirculation - A review.

*Applied Energy*, Vol. 99 n° 0, pp. 534–544, 2012.

(cited in p. 114)

**Wei L., Ying W., Longbao Z. and Su L.**

Study on improvement of fuel economy and reduction in emissions for stoichiometric gasoline engines.

*Applied Thermal Engineering*, Vol. 27 n° 17-18, pp. 2919–2923, 2007. (cited in p. 59)

**Werner S. and Ulrich A.**

Lung cancer due to diesel soot particles in ambient air.

*International Archives of Occupational and Environmental Health*, Vol. 68 n° 1, pp. S3–S61, 1996. (cited in p. 8)

**Wheeler J., Polovina D., Ramanathan S., Roth K., Manning D. and Stein J.**

Increasing EGR Tolerance using High Tumble in a Modern GTDI Engine for Improved Low-Speed Performance.

In *SAE Technical Paper*, 2013.

2013-01-1123. (cited in p. 60)

**Whitaker P., Kapus P., Ogris M. and Hollerer P.**

Measures to Reduce Particulate Emissions from Gasoline DI engines.

*SAE Int. J. Engines*, Vol. 4 n° 1, pp. 1498–1512, 2011. (cited in pp. 48, 49)

**Williams F. A.**

An approach to turbulent flame theory.

*Journal of Fluid Mechanics*, Vol. 40, pp. 401–421, 2 1970. (cited in p. 24)

**Witze P. and Green R.**

LIF and Flame-Emission Imaging of Liquid Fuel Films and Pool Fires in an SI Engine During a Simulated Cold Start.

In *SAE Technical Paper*, 1997.

970866. (cited in pp. 26, 35)

**Woschni G.**

A Universally Applicable Equation for the Instantaneous Heat Transfer Coefficient in the Internal Combustion Engine.

In *SAE Technical Paper*, 1967.

670931. (cited in p. 103)

**Woschni G.**

Die Berechnung der Wandverluste und der thermischen Belastung der Bauteile von Dieselmotoren.

*MTZ Motortechnische Zeitschrift*, Vol. 31 n° 12, pp. 491–499, 1970. (cited in p. 103)

**Wyszynski L., Stone C. and Kalghatgi G.**

The Volumetric Efficiency of Direct and Port Injection Gasoline Engines with Different Fuels.

In *SAE Technical Paper*, 2002.

2002-01-0839. (cited in p. 199)

**Xiong Y., Roberts W. L., Drake M. C. and Fansler T. D.**

Investigation of pre-mixed flame-kernel/vortex interactions via high-speed imaging.

*Combustion and Flame*, Vol. 126 n° 4, pp. 1827–1844, 2001.

**Yang Jialin and Kenney Thomas.**

Some Concepts of DISI Engine for High Fuel Efficiency and Low Emissions.

In *SAE Technical Paper*. SAE International, 2002.

2002-01-2747. (cited in p. 175)

**Yu C., Kim T., Yi Y., Lee J., Seokhong N. and Kyuhoon C.**

Development of KMC 2.4L Lean Burn Engine.

In *SAE Technical Paper*, 1995.  
950685.

(cited in pp. 56, 227)

**Zhao F., Lai M. C. and Harrington D. L.**

Automotive spark-ignited direct-injection gasoline engines.

*Progress in Energy and Combustion Science*, Vol. 25 n° 5, pp. 437–562, 1999.

(cited in p. 35)

**Zhong L., Musial M., Reese R. and Black G.**

EGR Systems Evaluation in Turbocharged Engines.

In *SAE Technical Paper*, 2013.

2013-01-0936.

(cited in pp. 63, 65, 67, 115, 139)